Optimal Battery Energy Storage System Sizing and Placement in Low Voltage Distribution Network

Emerging robust electric vehicle charging using photovoltaics

Tubagus Fakhri Muhammad

4592506

TU Delft

Optimal Battery Energy Storage System Sizing and Placement in Low Voltage Distribution Network

Emerging robust electric vehicle charging using photovoltaics

by

Tubagus Fakhri Muhammad

in partial fulfilment of the requirements for the degree of

Master of Science

in Sustainable Energy Technology

at the Delft University of Technology,

to be defended publicly on Wednesday, October 31th 2018 at 15:00 PM.

Supervisor:	Prof. dr. ir. Pavol Bauer,	TU Delft
Advisor:	Dr. ir. Gautham Ram Chandra Mouli,	TU Delft
	Dr. Seyedmahdi Izadkhast,	TU Delft
Thesis committee :	Prof. dr. ir. Pavol Bauer,	TU Delft
	Prof. dr. Arno Smets,	TU Delft
	Dr. ir. Laura Ramirez Elizondo,	TU Delft

TU Delft

Abstract

Electric Vehicles (EVs) provide a promising sustainable clean mode of transportation with much fewer emissions compared to the traditional Internal Combustion Engine (ICE) vehicles. However, this can only be considered true if the energy sources used for charging EVs are also from clean energy form. Various Renewable Energy Sources (RES) are available to provide the EVs charging demand. Nevertheless, due to intermittency power generation characteristic of RES, there is a high risk of supply and demand power mismatch. A grid-connected topology system is commonly used as a backup for lack or over power supply from RES generation. Even though, this configuration may lead to new problems of under/over voltage issues and maximum transformer/lines loading capacity due to RES fluctuation power production. The storage system is considered necessary to be installed in the system as a buffer of the power mismatch and also reducing the grid stress. Excellent approximation of storage sizing and placement is mandatory to provide satisfactory influence to the overall system technically and economically.

This study proposes optimization strategy for optimal battery sizing and placement with optimal power management system in the EVs charging station using photovoltaics (PV) power in a low voltage distribution network using Mixed Integer Linear Programming (MINLP) algorithm. The lithium-ion battery is considered in this project because of its relatively high power and energy density characteristic along with low self-discharging. The radial low voltage CIGRE benchmark is adopted as a model topology to evaluate the performance of the proposed optimization strategy. Dynamic daily electricity price, residential load, and PV power profile of the Netherlands are taken into account in this project. Furthermore, the research project implements several case studies using DICOPT (Discrete and Continuous OPTimizer) solver in GAMS (General Algebraic Modelling System) software with MATLAB interfacing. As the main result, proper EVs charging strategy with optimal battery sizing and placement with the appropriate power management system is successfully maintaining the system away from the grid violation while at the same time reducing the total cost of the system.

Keywords: EV-PV charging, optimal battery sizing and placement, MINLP

Acknowledgements

Alhamdulillahirabbil'alamiin …

This master thesis project document represents the result of my findings during graduation project period in Sustainable Energy Technology Master Programme at DC System, Energy Conversion and Storage Research Group of Delft University of Technology. It has been a year of ups and downs, through many challenges and obstacles to accomplish the research goals. I would like to express my gratitude to all who have supported me during the process.

First of all, my biggest gratitude to Allah SWT for giving me strength and patience so that I can finish my study at TU Delft. I would like to thank my thesis supervisor, Prof. dr. Pavol Bauer for giving me the opportunity to work on very interesting topic of storage system. My gratitude is also for Prof. dr. Arno Smets and Dr. ir. Laura Ramirez Elizondo as my thesis committees for sparing the time to give evaluation on this work. Moreover, I am also very grateful and honoured to have a chance working on this project with my mentors Dr. ir. Gautham Ram Chandra Mouli and Dr. Seyedmahdi Izadkhast. I would like to give high appreciation for their countless patience and generosity to give very helpful guidance and insights for the development of this thesis project.

Special thanks to my lovely life partner, Fitriadita Wulandari for her limitless patience and support, accompanying me through joys and hard moments, also always pushing and making me believe that I can pass through all the struggles. I am also very blessed to have very supportive parents, always asking my condition and pray for me all the time. I would like to thank all my Indonesian friends during study period in Delft as my second family and place to release my stress. Huge thanks are also for Om Tri's family for accepting me as a family member during life in Delft. Last but not least, I would like to acknowledge LPDP (Indonesia Endowment Fund for Education) for trusting and funding me as a scholar to accomplish my Master's Degree at TU Delft.

Laa hawla wa laa quwwata illa Billaah …

Delft, October 21st 2018

Tubagus Fakhri Muhammad

Table of Contents

List of Figures

List of Tables

1. Introduction

Transportation has been the main sector of global final energy consumption and energy-related CO_2 emission besides industry and buildings sector, contributing 28% and 22% to the final energy share and carbon dioxide emission respectively as shown in **Figure 1.1** [1]. Nowadays, Electric Vehicles (EVs) are increasingly developed and encouraged to reduce the gas emissions from transportation sector. However, EVs are only considered as clean transportation mode if the energy source of EV charging is also from clean energy form. Photovoltaics (PV) power is a promising energy source for EV charging application as it does not produce direct emission and has free abundant power source of sun irradiance. Even though, due to PV intermittency, storage is needed as a backup power. Battery is regarded as one of the most developed storage technology. In this chapter, recent developments regarding EVs, PV, and battery energy storage system are presented to give a big picture of the main domains in this research project.

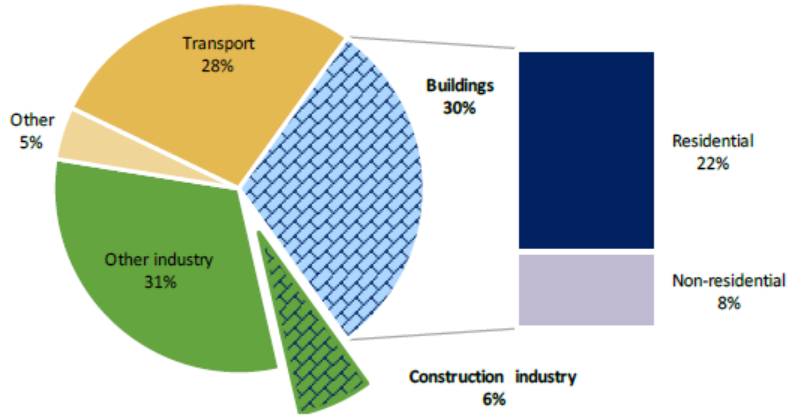

(a)

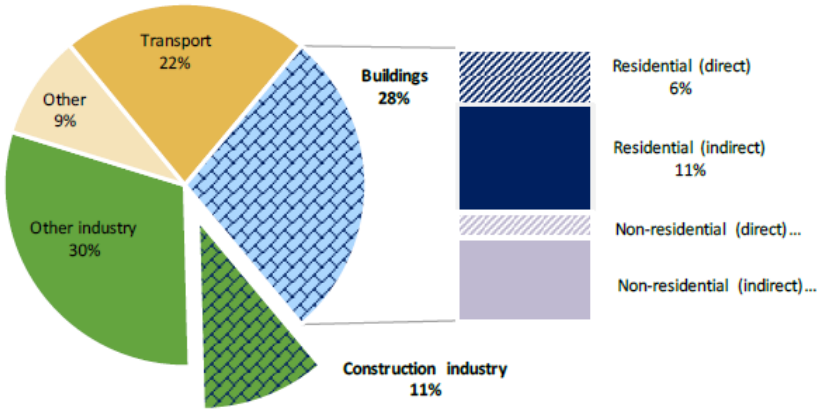

(b)

Figure 1.1 (a) Global Final Energy Consumption per Sector (b) Global energy-related CO_2 emission per Sector [1]

1.1 Electric Vehicles Movements

Electric vehicles were initiated in 1837 by Robert Davidson of Aberdeen in Scotland, powered by galvanic cells. EVs were then growing at the early of the 19th century from 1890 until 1924 and were having peak production in 1912 as they were considered more comfortable, quiet, and clean compared with 1900s gasoline cars which were well known as noisy, dirty, and unreliable cars. However, due to limited EVs travel range because of inadequate battery capacity and also the massive development of oil refinery to support gasoline cars, EVs were then slowly abandoned until the 1970s when there were oil embargoes and gasoline shortages. Engineers started building hybrid cars, combining good features of both gasoline and electric cars. Lately, in this past five years, research and re-introduction of pure EVs are significantly increasing to replace conventional Internal Combustion Engine Vehicles (ICEVs) as they are considered not directly polluting to the environment [2].

In general, there are four types of EVs derivatives based on power source used to drive [3]:

1. Hybrid Electric Vehicles (HEVs): use gasoline and electric motors, batteries are charged with regenerative braking, cannot be plugged in to the external charger
2. Plug-In Hybrid Electric Vehicles (PHEVs): use electric and internal combustion engine, batteries can be charged using an external charger
3. Battery Electric Vehicles (BEVs): use only electric motor and can be plugged in to charge the batteries
4. Fuel Cell Electric Vehicles (FCEVs): generate electricity to electric power motor from hydrogen processed in a fuel cell.

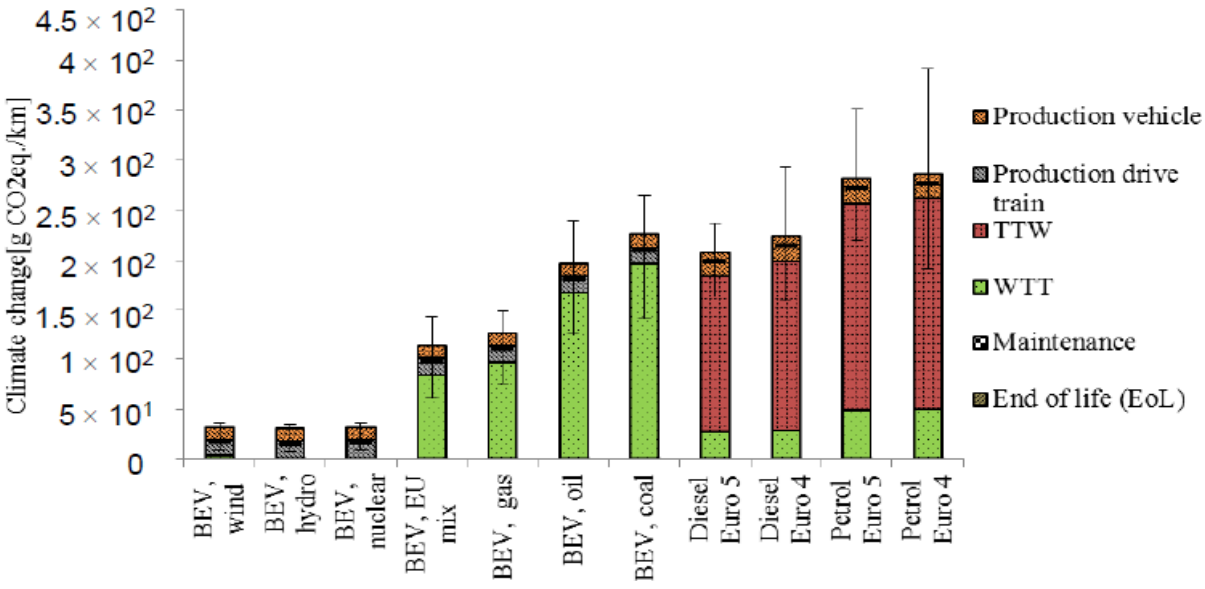

Figure 1.2 Comparison of carbon dioxide produced by different vehicle technologies and fuels [4]

Although EVs do not pollute direct emission, there is significant difference of overall emission produced when taking into account the whole process from the production, electricity power generation source, and end of life. **Figure 1.2** shows the comparison of carbon dioxide produced by EVs and ICEVs with various fuels and electricity production source. Significant emission reduction occurs when EVs are charged from clean energy form. Nevertheless, when EVs are still charged from fossil based electricity power plant, the total emission is still comparable with the ICEVs. This fact emphasizes the necessity of clean energy form to charge EVs as a true solution for less harmful environmental effect.

1.1.1 Global Electric Vehicles Trends

The number of global EVs has been exponentially increased, more than six times over the last five years as shown in **Figure 1.3**. China dominates by owning almost half of the total global EVs. Besides, in the last three years, BEV has been favoured more than PHEV [3]. There are several reasons that make more people are using EVs. Besides the growing of people awareness about the environment, governments of most countries are also supporting by giving incentives to the EVs users as presented in **Figure 1.4**. For example, in most EU countries, significant tax reduction is given to EVs user to promote more people switching from conventional ICEVs to EVs [5]. **Figure 1.5** shows the proportion of public EV charger station compared to the EV number.

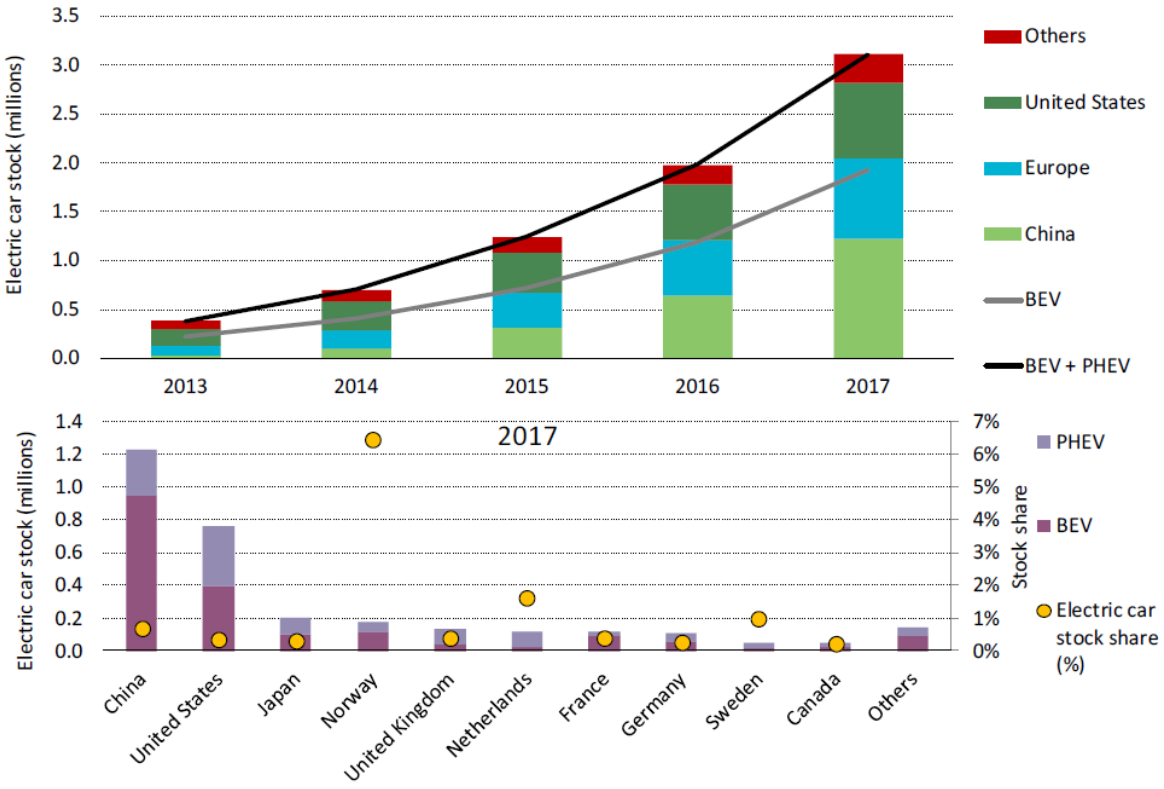

Figure 1.3 Global EVs number in the last five years [3]

The Netherlands has the highest ratio of public EV charger to the total EV number and has already exceeded the EU 2020 target. However, slow EV chargers still highly outnumber the fast EV chargers which give less flexibility for the EV users due to long charging time [3].

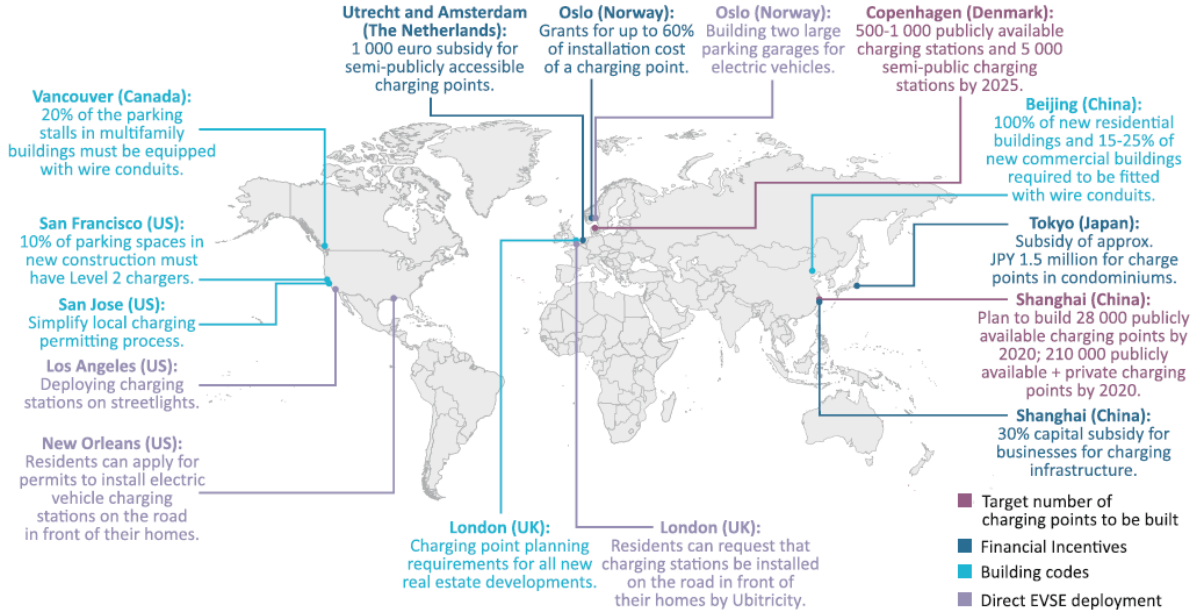

Figure 1.4 Electric Vehicle Policies Around the World [3]

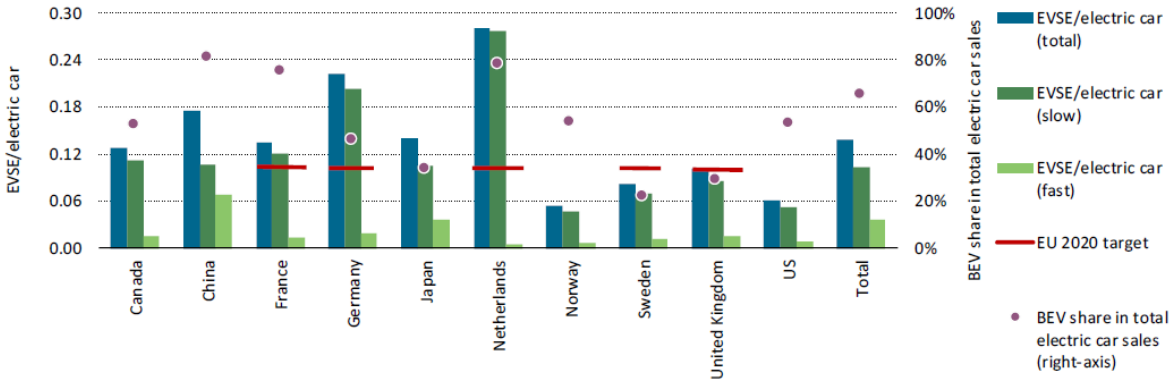

Figure 1.5 Ratio of public EV charging station to EV number [3]

1.1.2 Electric Vehicles in the Netherlands

The Netherlands is considered as a country with most electric vehicle users. Over 120,000 electric passenger vehicles are registered by the end of 2017, proving that the Netherlands is one of the EV pioneers in Europe as illustrated in **Figure 1.6.** This situation appears because of the high ambition of the Dutch Government. Only zero-emission cars will be retailed by 2030 in the Netherlands as the government's commitment to a more sustainable environment. The electric mobility is promoted by *Rijksdienst Voor Ondernemend* (RVO), the Netherlands Enterprise Agency as representative of the Ministry of Infrastructure and Water Management [6].

In the last five years, significant EV number increase happens in the Netherlands as illustrated in **Figure 1.7**. PHEVs are more widely used, compared to the BEVs due to limited range. However, stagnancy of PHEVs number occurs in the last two years, while BEVs keep growing because of higher battery capacity and more incentives are introduced. Moreover, in line with the highly EV number growth, the total number of charging points are also amplified to support the limited range of EV and convince more people to use EV [7].

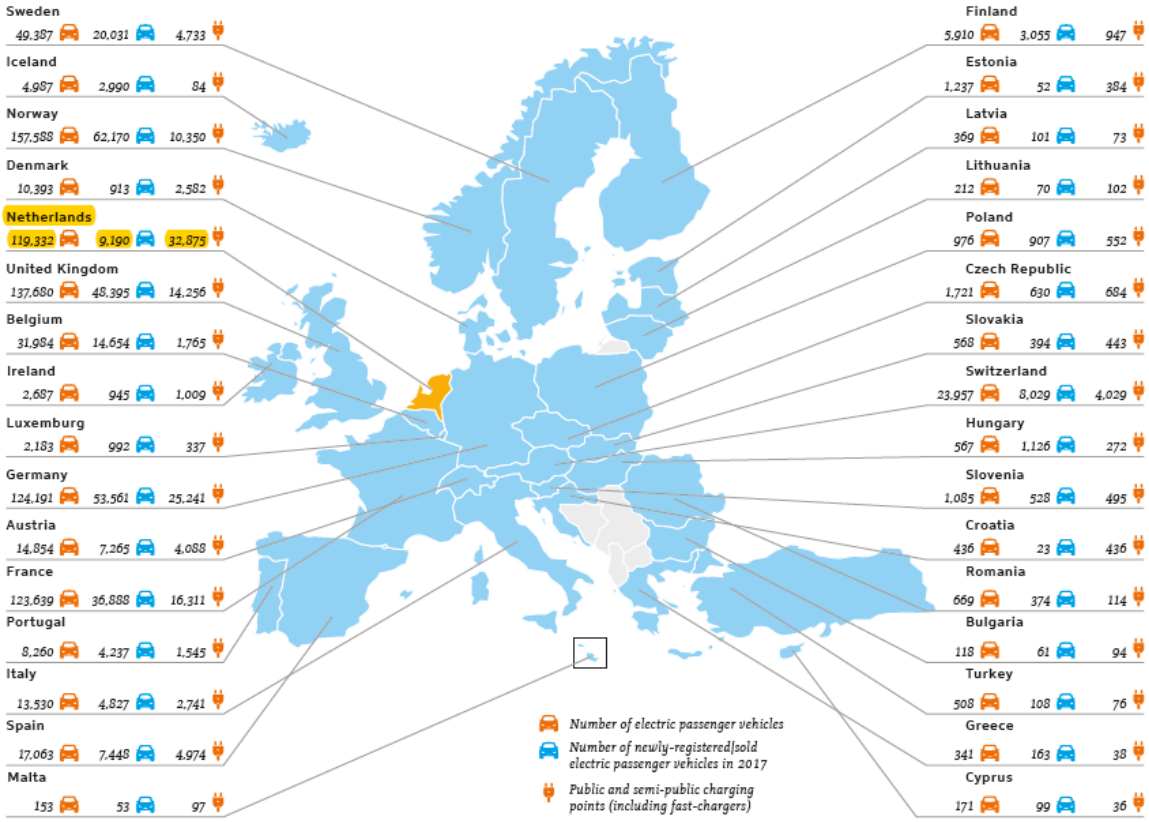

Figure 1.6 EV Share in Europe [6]

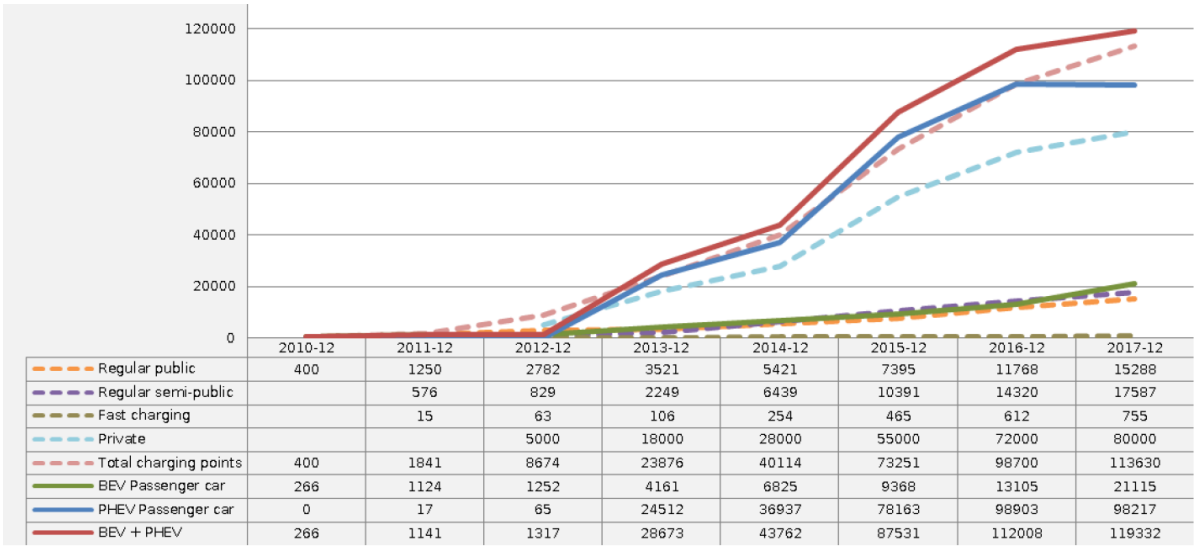

	2010-12	2011-12	2012-12	2013-12	2014-12	2015-12	2016-12	2017-12
Regular public	400	1250	2782	3521	5421	7395	11768	15288
Regular semi-public		576	829	2249	6439	10391	14320	17587
Fast charging		15	63	106	254	465	612	755
Private			5000	18000	28000	55000	72000	80000
Total charging points	400	1841	8674	23876	40114	73251	98700	113630
BEV Passenger car	266	1124	1252	4161	6825	9368	13105	21115
PHEV Passenger car	0	17	65	24512	36937	78163	98903	98217
BEV + PHEV	266	1141	1317	28673	43762	87531	112008	119332

Figure 1.7 EVs Fleet and Charging Station Development in the Netherlands [7]

1.2 Photovoltaic Trends

Solar power generation has been proven itself as the most preferred energy sources at the present. In 2017, global PV capacities installed is more than other power generation technology as presented in **Figure 1.8**. Even the solar investment alone is still higher than the fossil fuels and nuclear based power plants combined [8]. The total solar PV power capacity significantly increased by 32% from 360.4 GW in 2016 to 404.5 GW in 2017. The world's cumulative PV capacity has an increase of more than 4300% only in the last ten years from 9.2 GW in 2007. Currently, China dominates the world's solar power generation by operating nearly 1/3 of the total capacity as illustrated in **Figure 1.9** [8]. The Europe region is ranked third after China and Asia-Pacific region with total capacity of 114 GW.

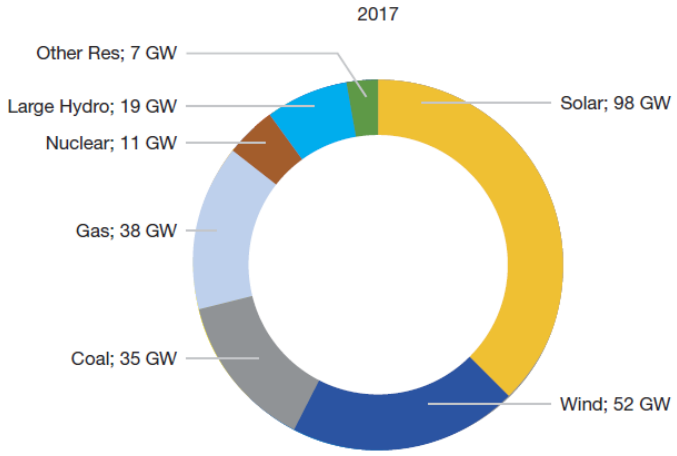

Figure 1.8 Power Capacity Addition in 2017 [8]

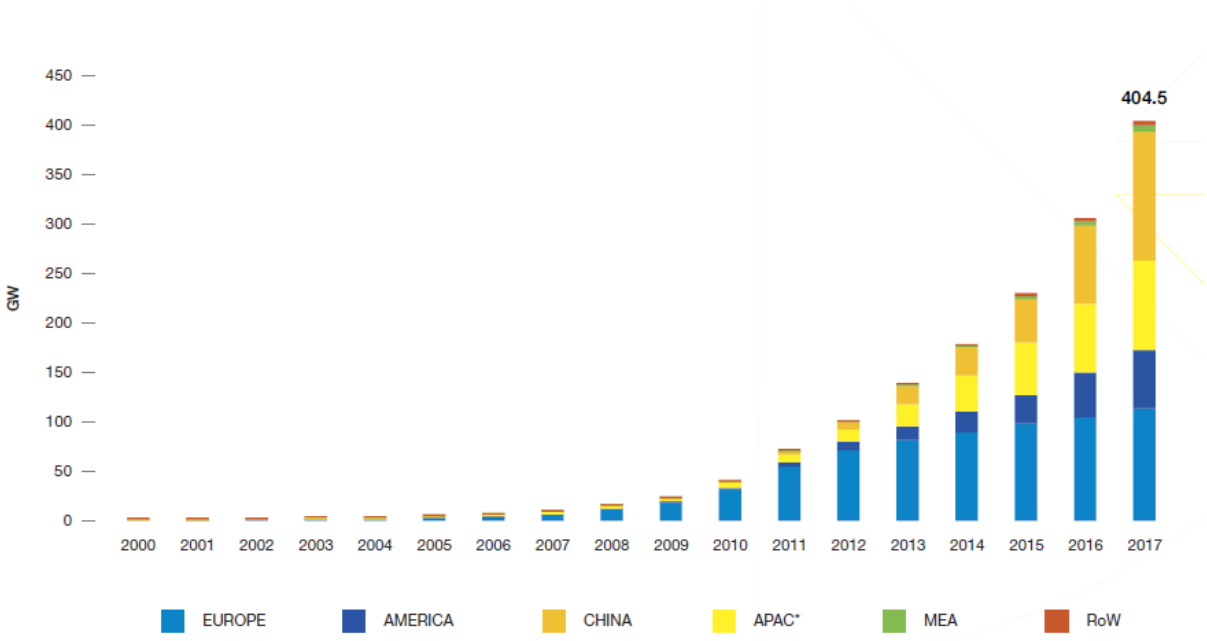

Figure 1.9 Total Global PV Power Installed Capacity During 2000-2017 [8]

Figure 1.10 illustrates the solar power generation by country in the European region. Germany leads the PV installed capacity by 37.7%, then followed by Italy and the UK with 17% and 11.1% respectively. The Netherlands itself has a total capacity of 2,681 MW by 2017 [8]. Currently, the PV power capacity in the Netherlands contributes to 8% of the total power generation as shown in **Figure 1.11**. More than half of the total power generation is obtained from the fossil gas based power plant. However, in the next five years, the annual PV Power capacity growth rate of 34% is expected and results in a total capacity of 11,430 MW by 2022 [9]. All in all, this ambition gives a bright prospect for mass EV-PV charging installation in the future.

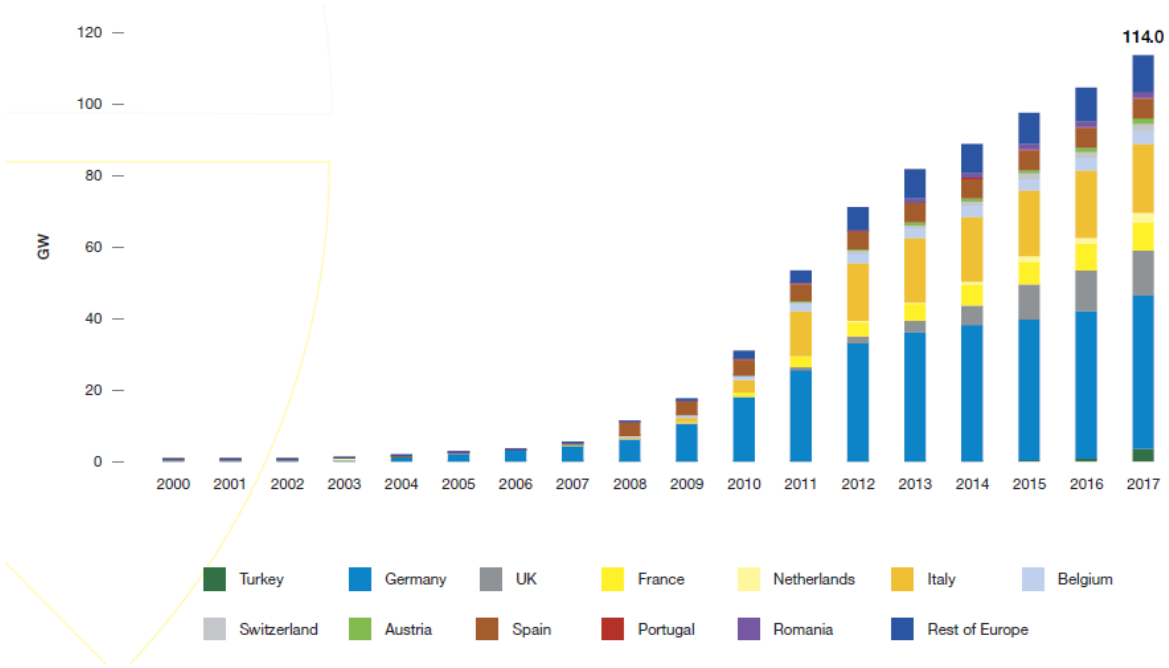

Figure 1.10 PV Power Capacity in Europe During 2000-2017 [8]

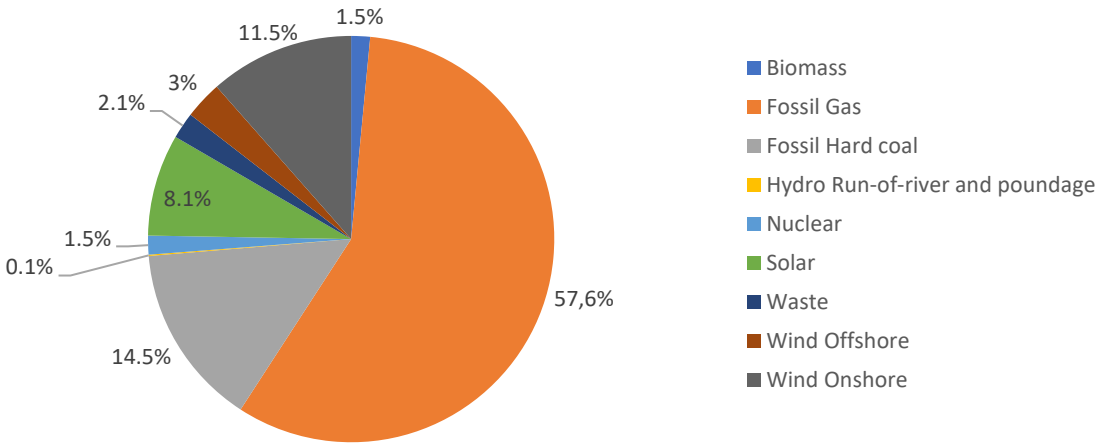

Figure 1.11 Electrical Power Generation Share by Energy Sources in the Netherlands (2018) [9]

1.3 Battery Energy Storage System Development

The increasing trend of renewable energy sources gives the new challenge of balancing the power demand and supply due to the intermittency issue. Energy storage plays a crucial role as a buffer of generation and consumption mismatch. **Figure 1.12** shows the electrical energy storage Currently, pumped hydro storage has the highest share with 176 GW installed capacity which corresponds to 96% of the total global storage. Other technologies have much lower percentage with thermal storage as the second highest with 3.3 GW (1.9%), followed by batteries with 1.9 GW (1.1%) and other mechanical storage with 1.6 GW (0.9%) [10].

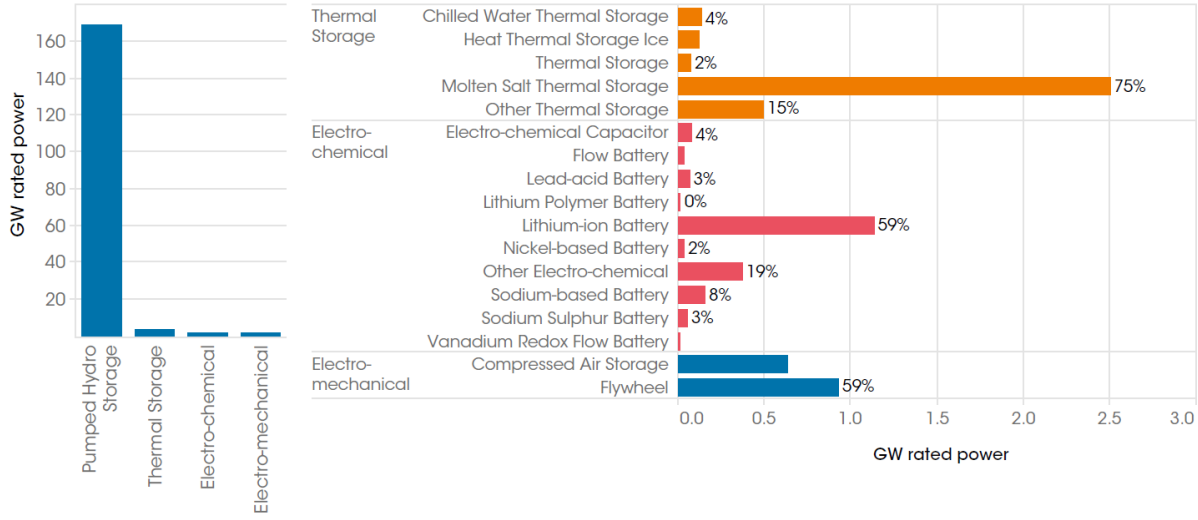

Figure 1.12 Global Share of Electrical Energy Storage Power by Technology [10]

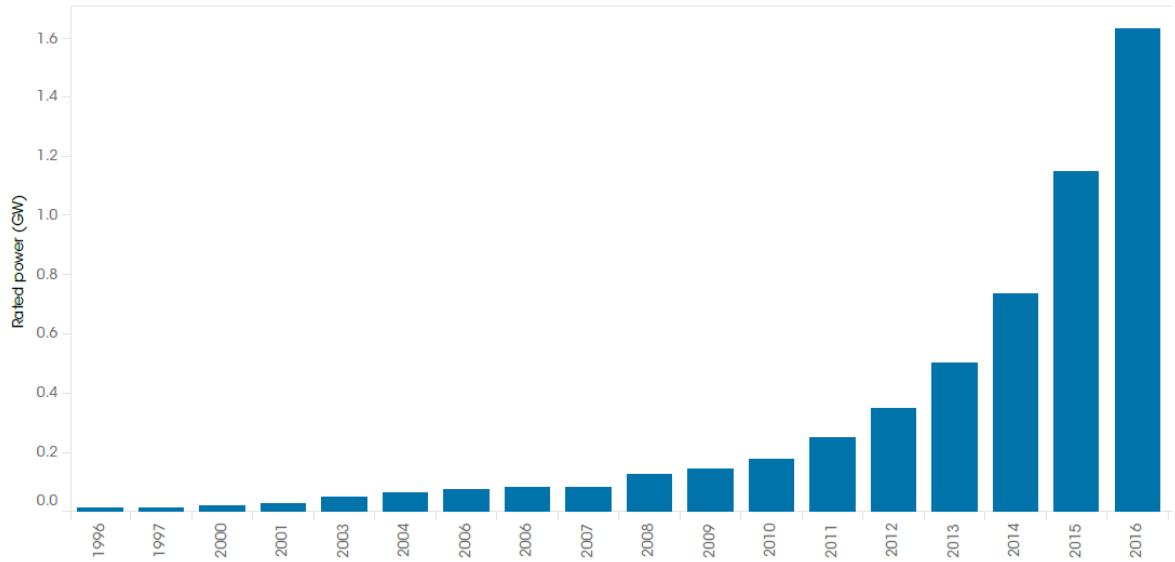

Figure 1.13 Development of global electro-chemical storage capacity [10]

Although the battery installed capacity is still considerably very low at present, the recent development of the battery shows a bright future. Global installation of battery storage has been exponentially increased in the last 20 years as indicated in **Figure 1.13** [10]. This situation occurs because of declining trend of the production cost, for example in Li-ion battery as shown in **Figure 1.14**. With more competitive price, the battery is expected to play a bigger role in the future renewable based electricity, decreasing dependency on the fossil based power plant [11].

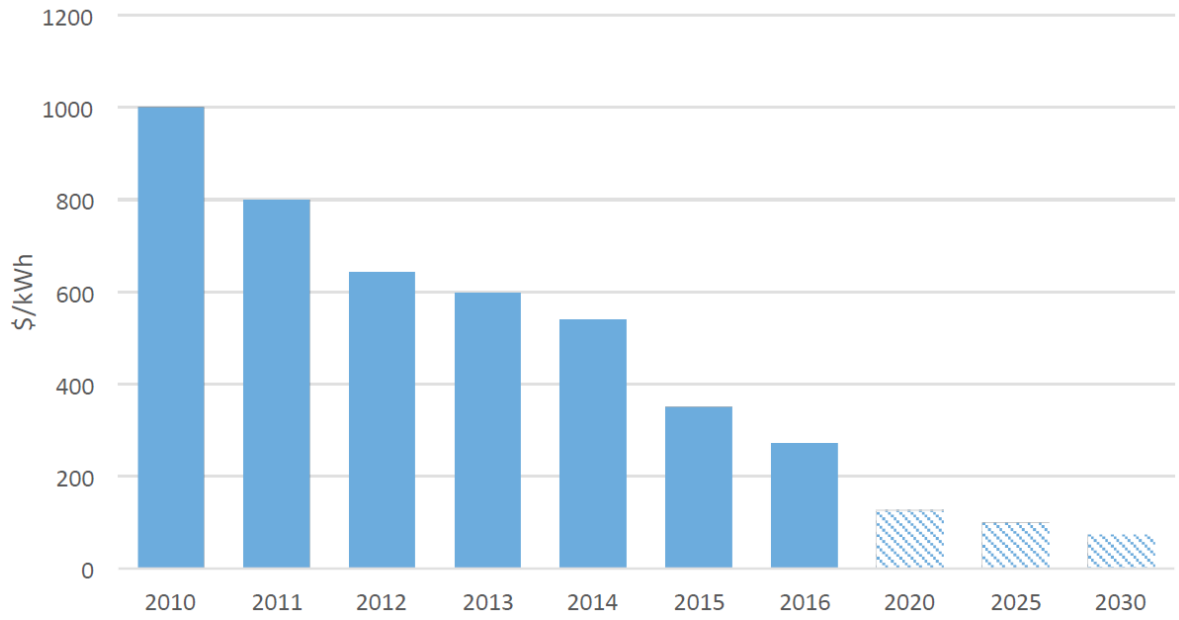

Figure 1.14 Past and Projection Cost of Li-ion Battery Production Cost [11]

1.4 Thesis Project

1.4.1 Thesis Motivation

Rapid EV development gives a bright future for more sustainable transportation with less harmful emission. However, EV can only be considered as a green solution if the energy sources of charging are also from clean energy form. In this study, solar power is chosen as the primary source to fulfil the EV charging power demand. Nevertheless, the sun irradiance fluctuation leads to unwanted intermittent power production. The easiest solution is by connecting the EV-PV charging system to the grid network as backup support. Even so, the variable power generation of PV may lead to harmful overvoltage and undervoltage condition due to excess and lack of power production respectively. Furthermore, there is also a chance when the maximum transformer loading capacity is exceeded when the PV power generation is extremely low. To tackle these issues, battery energy storage system (BESS) instalment at the EV-PV charging station is proposed to balance the mismatch

power and help to keep the system from grid violations at the same time. The battery needs to be sized and located properly to achieve the desired grid parameters while also maintains the total cost low. This study is aimed to bridge the technical and economic issue of the EV-PV charging system with BESS support in a Distribution System Operator (DSO) point of view, by formulating the optimal battery sizing and location optimization strategy along with the optimal power management system.

1.4.2 Research Objectives

1.4.2.1 Main Research Goal

Developing optimal battery sizing and location strategy in the scope of technical and economic, together with the optimal power management system, supporting EV-PV charging distribution networks to achieve minimum charging cost without grid violations.

1.4.2.2 Research Questions

1. How to formulate the optimal battery sizing and location optimization along with the power management system of the EV-PV charging system in a low voltage distribution network?
   (a) How are the EVs properties modeled in the system?
   (b) How is the BESS characteristic modeled in the system?
   (c) How is the low voltage distribution network model formed?
   (d) What is the objective function of the proposed optimization strategy?

2. How does the proposed optimization react with different EV number penetration and allocation?
   (a) How does different EV number penetration affect the battery sizing and location along with the exchange power profile?
   (b) How does asymmetrical EV allocation at the charger station affect the battery sizing and location along with the exchange power profile?

3. What is the impact of decentralized BESS instalment compared to the centralized BESS placement?

4. How does different EV charging strategy affect the battery sizing and location along with the exchange power profile?

1.4.3 Thesis Outline

This thesis project consists of six chapters as described below.

- **Chapter 1: Introduction**
  This chapter presents recent development of Electric Vehicles, Photovoltaics, and Battery Energy Storage System as the main research domains. The research motivation and objectives are also elaborated as a guideline for this study.

- **Chapter 2: Literature Review**
  This chapter provides details of the Battery Energy Storage System work principle and integration with grid application. Previous literature studies on optimal battery sizing and location are also discussed.

- **Chapter 3: Network Model and Data Characteristics**
  This chapter describes the configuration of the simulation model and the input parameters of EV properties, PV power profile, residential load data, and daily electricity price trend.

- **Chapter 4: Model Formulation**
  This chapter delivers the formulation of the optimization model in equations form. The characteristic and interaction between EVs, BESS, PV, and grid are formulated together with the objective functions.

- **Chapter 5: Case Studies Simulation Results**
  This chapter evaluates the proposed optimization strategy for optimal battery sizing and location along with the power management system. Technical and economic analysis are discussed for every case studies.

- **Chapter 6: Conclusions and Future Works**
  This chapter compiles the overall work of this study. Answer of the research questions is presented together with several recommendations for next improvements of this study.

2. Literature Review

In this chapter, the research state of the art is comprehensively discussed. First, a comparison of energy storage technology is provided. Then, details of the battery energy storage system design and the integration with grid operation are elaborated. Last, several approaches on the optimal battery sizing and location are compared.

2.1 Energy Storage Comparison

Energy storage plays an important role in the renewable based power system. There is various type of energy storage technologies available. In general, energy storage is categorized into five classifications according to the main source as illustrated in **Figure 2.1** [12]:

1. Chemical energy storage: energy is stored in gaseous, liquid, or solid form and released through chemical reactions. Generally, it has high energy density and variation of storage and transport form.
2. Electrochemical energy storage: energy is stored in chemical form and then converted to electrical energy, commonly called as a battery. Various electrode and electrolyte materials determine the battery properties which is customized depends on the application.
3. Electrical energy storage: energy is stored in the electrostatic field between electrodes for the capacitor, while in superconducting magnetic energy storage (SMES), energy is stored in the magnetic field of the coil. Typically, it has high power, efficiency, and fast reaction time, but limited energy capacity.
4. Mechanical energy storage: energy is stored in several mechanical philosophies, for example utilizing potential energy of water, pressure work in compressed air, and rotational energy in a flywheel.
5. Thermal energy storage: energy is stored in the heat of materials, determined by the temperature difference and the heat capacity.

Energy storage technologies differ in various size. **Figure 2.2** presents the power and energy density characteristic of different energy storage type. It is observed that the fuel cell has the highest energy density, while capacitor possesses the highest power density compared to the other technologies. Although the pumped hydro storage is the most applied storage application, in fact, it has the lowest power and energy density. The pumped hydro

storage requires a larger area to store the energy which makes it not suitable for small applications. On the other hand, the lithium-ion battery energy and power density are considered high which fits wider operations, such as portable utilization, electromobility, and also stationary storage as grid support. However, in a real application, these power and energy density values are not the only factor determining the storage application. In larger stationary application, storage lifetime and cost are frequently more important because of less volumetric and weight constrained compared to the portable application [13].

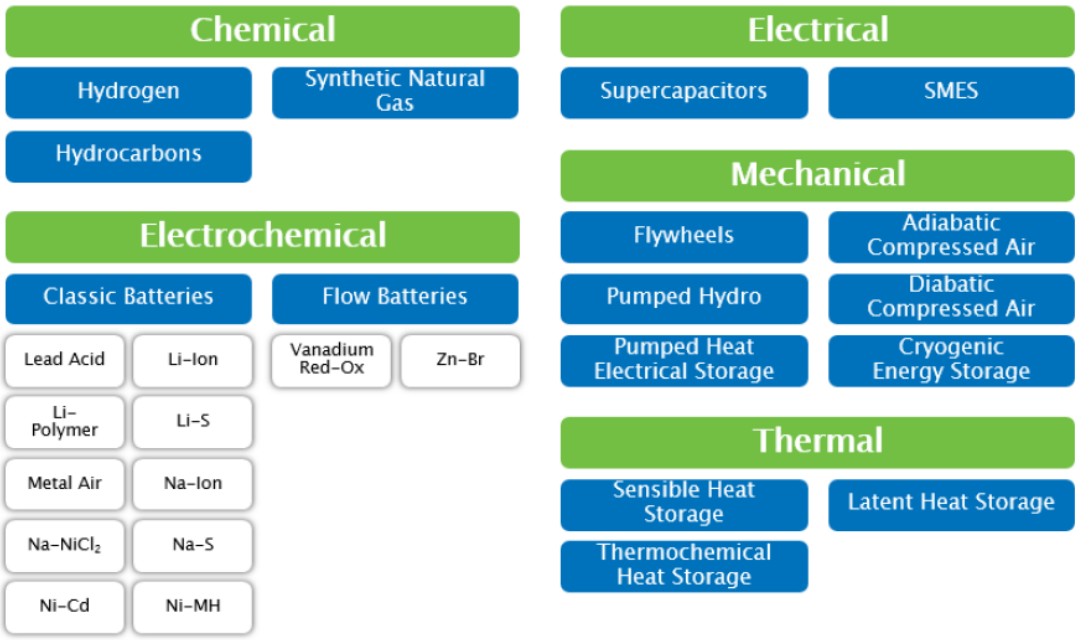

Figure 2.1 Classification of Electrical Energy Storage Technologies [12]

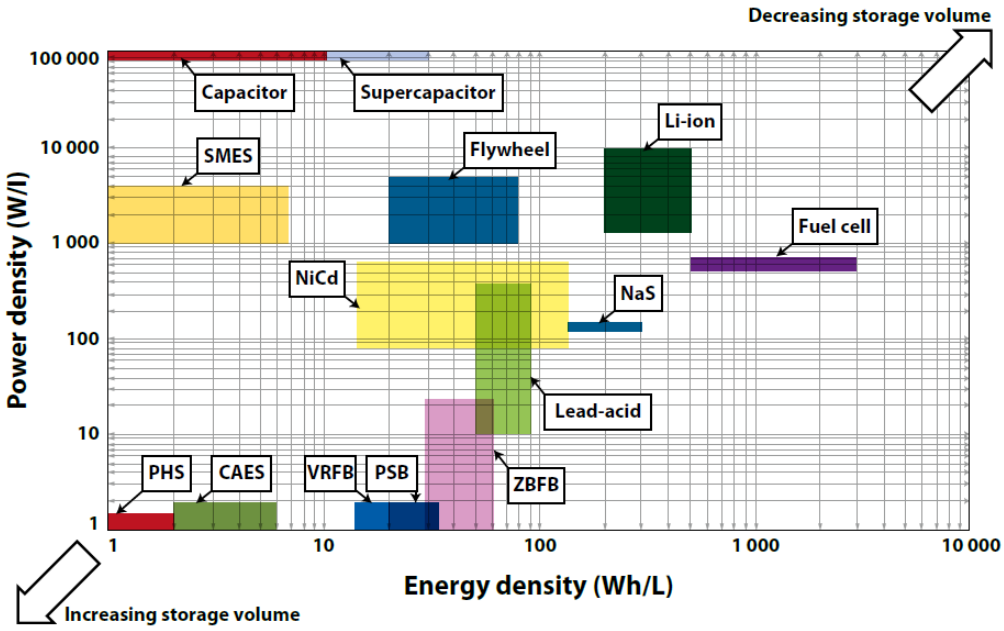

Figure 2.2 Power and Energy Density Comparison of the Energy Storage [14]

Moreover, energy storage implementation is also determined by the working period. **Figure 2.3** shows the suitable operation of energy storage based on discharging time at rated power. Storage technology with lower power capability under 100 kW and shorter discharge time in order of seconds to minutes is more suitable as an uninterruptible power supply or to increase the power quality of the system. Supercapacitors and flywheels are categorized into this classification. In opposite, high rated power and discharging period storage fits to bulk power management, such as pumped hydro and compressed air energy storage which usually have enormous energy container. In the middle range, various batteries technologies are available with diverse discharge time from an order of minutes to hours application. These form of storage is advisable to support transmission and distribution grid along with load shifting. More details on suitable energy storage applications are illustrated in **Figure 2.4**.

2.2 Lithium-ion Battery Technology

In general, it can be concluded from the previous section that the Lithium-Ion battery energy storage has the fittest characteristics as the energy storage technology for electric vehicles charging using photovoltaics power system. The Li-ion batteries have considerable high power and energy density which allow the compact size, also reasonable discharge time and power capability for EV charger station application. Besides, they have a relative long lifetime, low self-discharge, and high round-trip efficiency. Detail look of Li-ion battery components and operating scheme in a cell unit is illustrated in **Figure 2.5**. Lithium ions (Li^+) exchange occurs between the anode and cathode. Commonly, the Li-ion batteries cathode is made from a lithium metal oxide ($LiMO_2$), while the anode is manufactured from graphite [15].

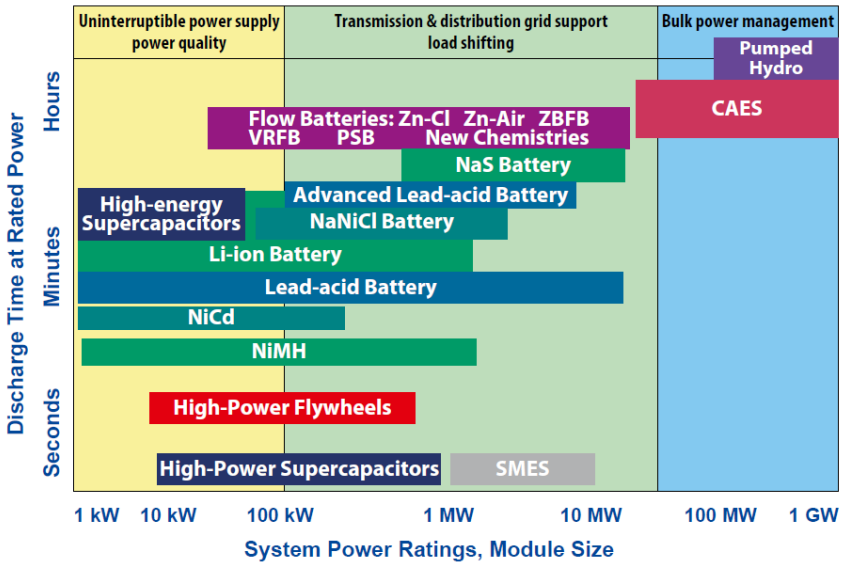

Figure 2.3 Power Rating and Typical Discharge Time of Diverse Energy Storage Technologies [16]

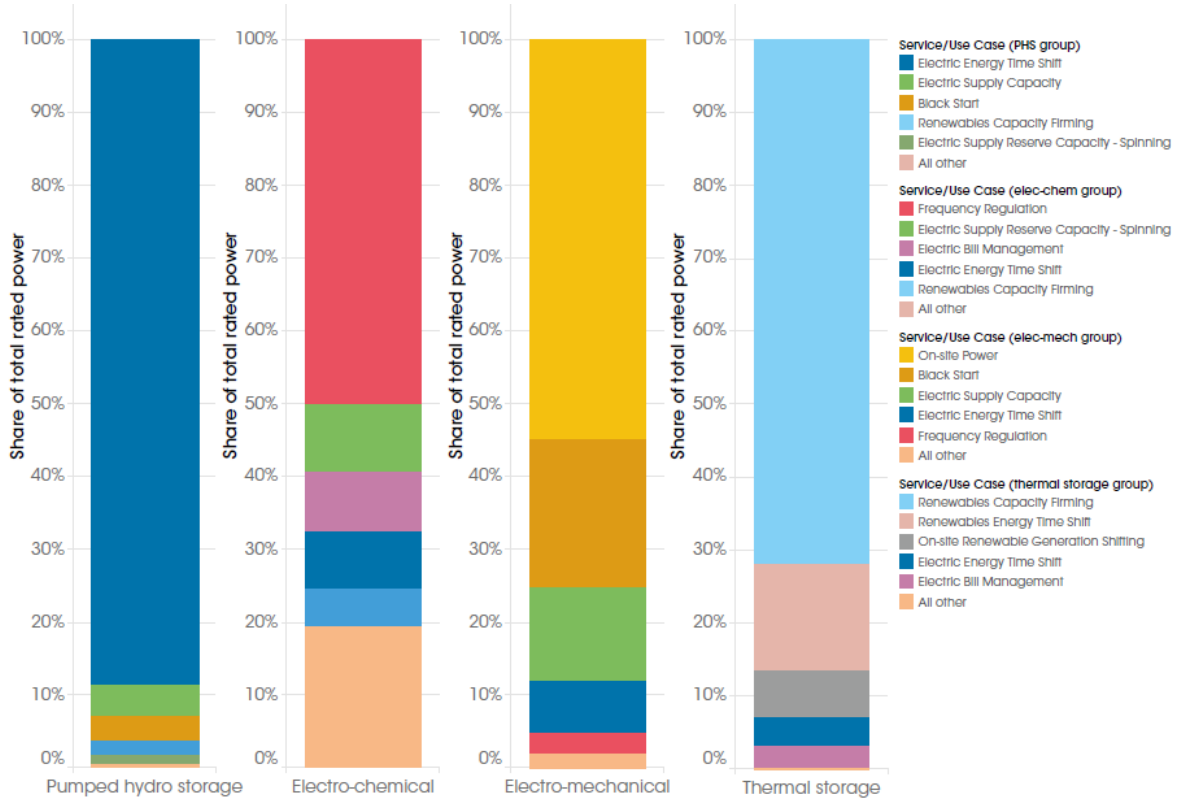

Figure 2.4 Main-Use Case of Global Energy Storage Power Capacity Shares [17]

The diverse material combinations of lithium ion battery energy storage results to a particular performance, cost, and safety characteristics. The various operational application and performance determine chemistry choice of the Li-ion battery. There are five most common Li-ion material compositions used in the stationary storage application as presented in **Figure 2.6** and **Figure 2.7**. The material combinations are as follows:

1. Lithium Nickel Manganese Cobalt Oxide (NMC): common choice for stationary and electromobility application. The equal composition of nickel, cobalt, and manganese is contained in a crystal-structured material layered. The NMC material delivers a good combination of power, energy, cycle life, and thermal stability [18].
2. Lithium Manganese Oxide (LMO): has high power capabilities due to the LMO cells in three-dimensional spinel crystal structure. Besides, it is less expensive than cobalt because of relying on manganese. Nevertheless, the drawback is that the battery has low energy performance and moderate life cycle properties which makes it less attractive for stationary implementation.
3. Lithium Nickel Cobalt Aluminium (NCA): addition of aluminium in lithium nickel oxide based battery improves the thermal and electrochemical stability while keeping maintaining high energy density and lower cost compared to the cobalt based [19]. However, the higher voltage operation of NCA causes worse electrolytes degradation [20].

4. Lithium Iron Phosphate (LFP): has better thermal stability compared to other Li-ion materials and still possess relatively high power capability. Furthermore, the cathode material is non-toxic and has a long lifetime with relative low discharge rate makes this battery type favourable for stationary application. The disadvantage of using the material is the lower rated cell voltage and energy density due to the lower electrical and ionic conductivity of the material [21].
5. Lithium Titanate (LTO): replaces graphite with spinel structure of LTO. The increased ion agility leads to thermal stability and allows fast charging with high rate operation [22]. However, the cell voltage is reduced due to the higher potential of titanate compared to graphite which lowering the energy density [23]. On the other hand, this condition avoids the issue of electrolyte decomposition even at high rates and make LTO become the most durable Li-ion technology at present [24]. Yet, the battery price is still high because of low production volume.

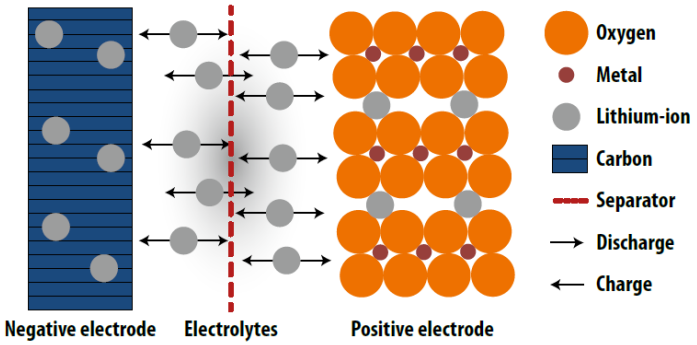

Figure 2.5 Lithium-ion Battery Cell Main Components and Working Principle [25]

Key active material	lithium nickel manganese cobalt oxide	lithium manganese oxide	lithium nickel cobalt aluminium	lithium iron phosphate	lithium titanate
Technology short name	NMC	LMO	NCA	LFP	LTO
Cathode	$LiNi_xMn_yCo_{1-x-y}O_2$	$LiMn_2O_4$ (spinel)	$LiNiCoAlO_2$	$LiFePO_4$	variable
Anode	C (graphite)	C (graphite)	C (graphite)	C (graphite)	$Li_4Ti_5O_{12}$
Safety					
Power density					
Energy denisty					
Cell costs advantage					
Lifetime					
BES system performance					
Advantages	-good properties combination -can be tailored for high power or high energy -stable thermal profile -can operate at high voltages	-low cost due to manganese abundance -very good thermal stability -very good power capability	-very good energy and good power capability -good cycle life in newer systems -long storage calendar life	-very good thermal stability -very good cycle life -very good power capability -low costs	-very good thermal stability -long cycle lifetime -high rate discharge capability -no solid electrolyte interphase issues
Disadvantages	-patent issues in some countries	-moderate cycle life insufficient for some applications -low energy performance	-moderate charged state thermal stability which can reduce safety -capacity can fade at temperature 40-70°C	-lower energy density due to lower cell voltage	-high cost of titanium -reduced cell voltage -low energy density

Figure 2.6 Most common Li-ion batteries technology properties comparison [26]

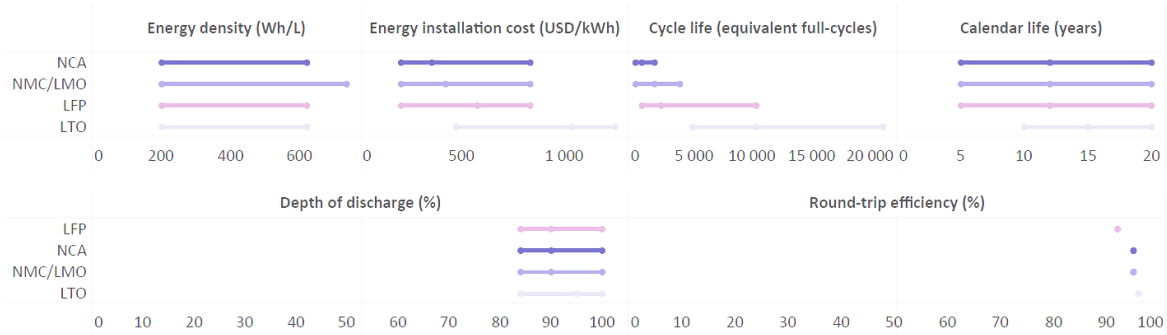

Figure 2.7 Technical properties comparison of most common Li-ion batteries technology [10]

2.3 Battery Energy Storage System Design

The battery energy storage system requires several supporting components besides the battery itself. A typical configuration of the system is illustrated in **Figure 2.8**.

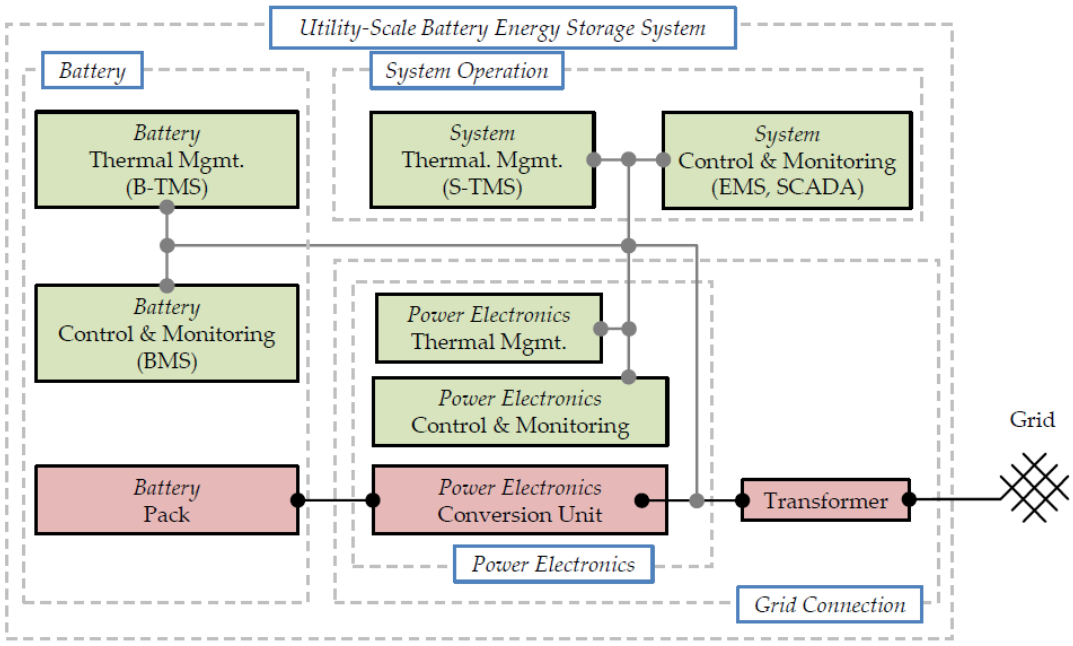

Figure 2.8 Common Stationary Battery Energy Storage System Design [27]

The system components are categorized into four main sections as follows [27]:

1. The battery consists of three main parts:
   a) Battery Pack, derived from a combination of series-parallel connection to achieve a desired voltage and capacity value.
   b) Battery Control and Monitoring also called as Battery Management System (BMS). The function is to maintain the reliable and safe battery operation by managing the cell voltage, temperature, and balancing cell state of charge in a serial connection.
   c) Battery Thermal Management System controls the cell temperature within the safe margin.

2. System Operation consists of two main components:
   a) System Thermal Management System regulates the overall temperature system by managing all functions of air conditioning, ventilation, and heating of the system containment.
   b) System Control and Monitoring, the main 'brain' of the system, derived to Supervisory Control and Data Acquisition (SCADA) and Energy Management System (EMS) which is responsible for controlling overall power management.
3. Power Electronics consists of three main parts:
   a) Power Electronics Thermal Management System controls the heat management of the power converter in the safe region.
   b) Power Electronics Control and Monitoring System, regulates the operation of the power converter to be in line with the energy management system.
   c) Power Electronics Conversion Unit, the power converter hardware that connects the battery pack to the grid connection.
4. Grid Connection, represented by the step up transformer.

There are three common configurations of the power converter in the PV-BESS system, as illustrated in **Figure 2.9** [27]:

1. AC-coupled configuration (Figure 2.9a): the battery is connected to the battery inverter through the DC/DC converter. Then, the battery inverter is connected to the PV inverter via electrical power lines. This topology provides high flexibility to fit the existing PV system.
2. DC-coupled configuration (Figure 2.9b): the battery is connected to the DC/DC converter before linked to the high voltage DC bus between PV Maximum Power Point Tracker (MPPT) and inverter to the grid. The advantage of this topology is a reduction of battery inverter which gains the higher efficiency compared to the AC-coupled configuration for power flow from PV to BESS.
3. Generator-coupled configuration (Figure 2.9c): the battery DC/DC converter is coupled with the PV output through the MPPT DC/DC converter. With a shorter path between battery and PV, this topology allows higher efficiency for the power flow from PV to BESS. On the other hand, this configuration requires a precise and fast communication connection between the battery and AC-grid link to fulfil the load demand from PV and/or battery. Moreover, the topology cannot be easily fitted to the existing PV system. However, due to only one inverter is required, less cost needs to be spent.

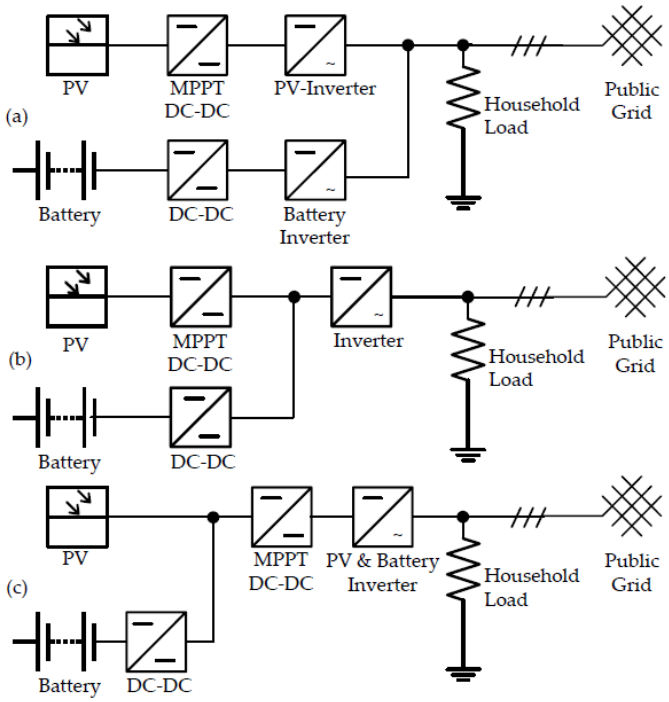

Figure 2.9 Different topologies approach for PV-BESS application [28]

2.4 Grid-Connected Application

In the modern power grids, the stationary battery energy storage system can be applied to various task application. Figure 2.10 gives an illustration of the possible integration of BESS with the grid. There are two common voltage level connections, mostly in low voltage level and less frequently in medium voltage level, interconnected through the transformer.

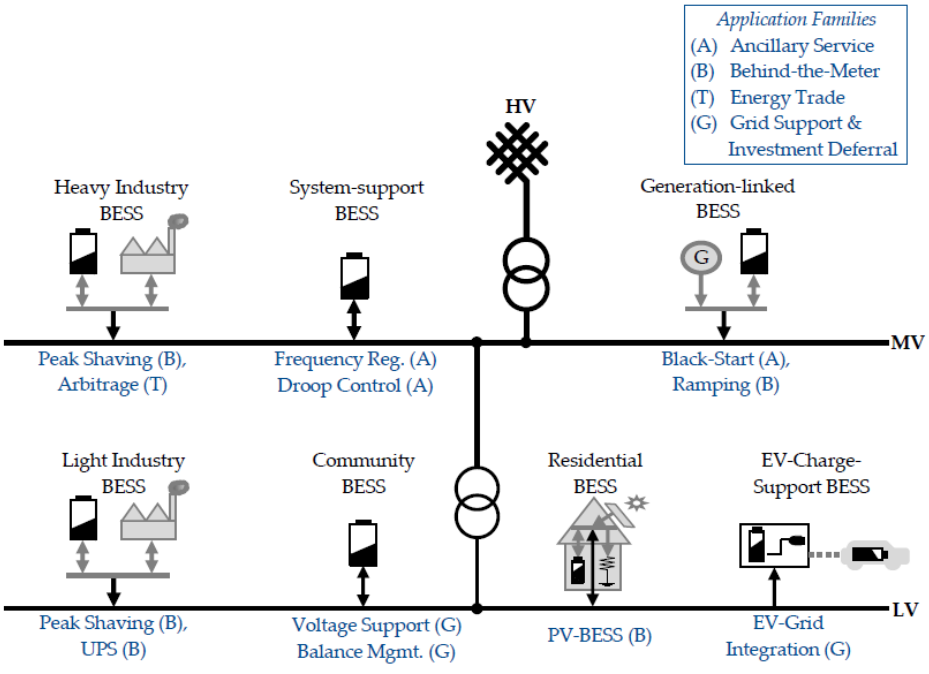

Figure 2.10 Various Grid Connected Application of Battery Energy Storage System [27]

Overview of the BESS classification according to implementation in grid level is presented in **Table 2.1**. The grid applications are usually involving several stakeholders and grid operators. Based on the work region, grid system operators are categorized as Distribution System Operator (DSO) and Independent System Operator (ISO) which handle regional and over-regional area.

Table 2.1 Classification of Battery Energy Storage Applications in The Grid Level [27]

Application Family	Application	Revenue Stream	Stakeholder
Ancillary Service (A)	Frequency Regulation Black-Start Droop control	Auction Profit ISO Contract DSO/ISO Contract	Enterprise Electric Utility All Feeders
Behind-the-Meter (B)	PV-BESS Peak-Shaving UPS Ramping	Retail Tariff Savings Peak Tariff Reduction Reliability Value Enhancement DSO/ISO Regulation Compliance	Private Sector Industry Industry RES Feeders
Energy Trade (T)	Arbitrage	Energy Exchange Markets	Enterprise
Grid Support and Investment Deferral (G)	Voltage Support EV-Grid Integration Balance Management	Red. Utility Cost Red. Power Link Cost ISO contract	DSO/Enterprise Enterprise DSO
Combined Applications	Multiple Appl. Island-/Micro-Grid V2G	Value Stacking Reduced Fuel Cost Value Stacking	Various Grid Operator Various

In general, there are five categories of BESS-grid interconnection as follows [27]:

1. Ancillary Service, consists of three common functions:
   (a) Frequency regulation: BESS is capable of delivering power to balance the frequency fluctuation in the power system on the millisecond timescale . BESS has the potential of economically and technically beneficial to be served as Primary Control Reserve (PCR) for short term power fluctuation compensation, supervised on the ISO level.
   (b) Black start: BESS can accommodate system restore by helping a restart of power generation units in a blackout condition. The lithium-ion BESS can fit this implementation because of relatively high power and low self-discharge.
   (c) Droop control: BESS also can be adopted as a secondary and tertiary control reserve in the timescale of a minute to an hour. However, this application is less favorable since BESS is less useful and location dependent.
2. Behind the Meter, consists of four common functions:
   (a) PV-BESS: a combination of PV power and battery may increase power self-consumption and save the overall cost. Besides, BESS addition also gives less stress to the grid. The lithium-ion battery is suitable because of its high energy and power density as well as cycle life characteristic.

(b) Peak shaving: industrial consumers can reduce the electricity bill by reducing energy bought from the grid during peak electricity tariff and drawn energy from the battery during that period.

(c) Uninterruptible Power Supply (UPS): BESS can rely on as a backup power supply when there is a failure in the power system. Lithium-ion BESS has longer battery lifetime compared to the common lead-acid based UPS.

(d) Ramping control: BESS is utilized to refine the output power of the power plant with high intermittencies such as wind and PV power. However, this application is still only rewarded in small regions and dependent on the regulation standard made by the system operators.

3. Energy Trade, Lithium-ion based BESS can be economically worthwhile for dealing short time fluctuations market price arbitrage because of fast reaction characteristic.
4. Grid Support and Investment Deferral consists of three common functions:

(a) Voltage support: BESS can help to reduce the voltage fluctuations through coordinated active and reactive power control on a level of community scale. Unfortunately, there is still no clear regulation and market for reimbursement for serving as voltage support.

(b) EV-grid integration: BESS can serve as an alternative power addition for electric vehicle charging necessity which draws a lot of power from the grid causing severe stress in the grid.

(c) Balance management: BESS can be utilized to balance the load demand and supply generation in the power system.

5. Combined Application, consists of three common functions:

(a) Multiple application: BESS is utilized for more than a single use case. In most cases, the profit increase is more than the enlarged degradation cycle cost. However, it is still a challenge to serve different tasks simultaneously and meet the regulation constraints when different stakeholders are involved.

(b) Microgrid: In a rural area, BESS can drastically decrease the traditional diesel fuel consumption and at the same time lower the emissions level. With a proper energy management system, BESS can simultaneously operate for various tasks such as frequency control, voltage stabilization, and balancing the supply and demand mismatch.

(c) Vehicle to the grid: Utilization of EV battery for grid connected application beside as EV propulsion may help to relive the grid stress. Nonetheless, the regulation and involvement of multiple stakeholders standards are still the challenges for applying the vehicle to grid concept.

2.5 Battery Sizing and Placement Optimization Technique

Optimal size and position of the battery are crucial things to be considered during the feasibility study of BESS integration with the grid, local loads and power generator. Oversizing of battery capacity may lead to the unnecessarily increased investment, while undersizing results to unachieved technical constraints. Complementary to the battery size, the wrong decision of battery location could lead to an undesired technical influence to the system and at the end, more battery capacity needs to be installed as the compensation for suboptimal positioning. The batteries are commonly sized regarding power and energy capacity. The battery size differs according to the application. **Figure 2.11** presents the power and energy size of several existing storage projects in the world.

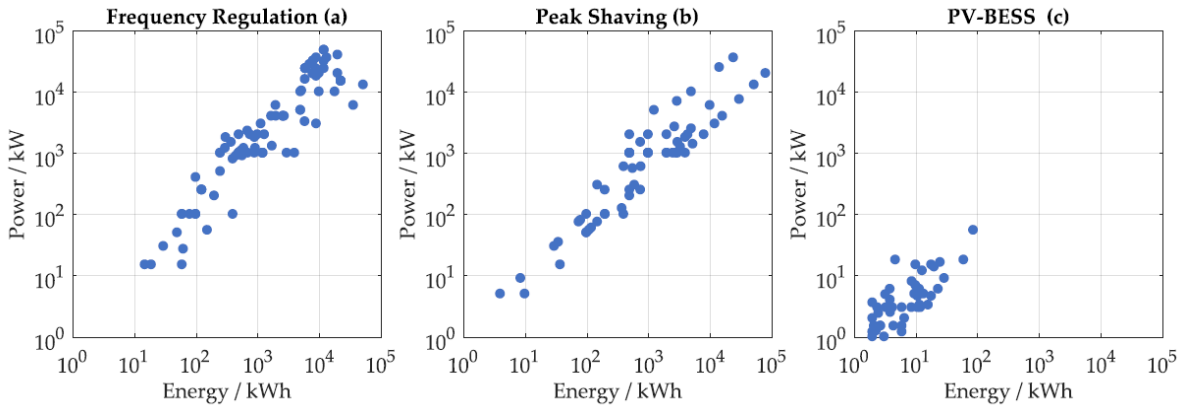

Figure 2.11 Statistics of Power to Energy Ratio in several real world-wide storage projects based on the application in the grid/system (a) Frequency regulation (b) Peak shaving (c) Photovoltaics with battery energy storage system [27]

It is observed that frequency regulation application exhibits the highest storage size. Most projects have nominal power of more than 1 MW to have a significant impact to the system frequency. Commonly, there is a minimum size of the storage to participate in the power application market depends on the local regulation. However, requirements of high power capability and fast speed reaction are still challenging for the existing Lithium-ion BESS. For peak shaving applications, the storage size ranges between tens kWh to several MWh order. Typically, the peak shaving storage works in a short term load fluctuations during the average time window of 15 minutes to 1 hour as specified by DSO. In PV-BESS implementation, much lower battery power and energy capacity are required due to smaller scope of the residential load. The battery size varies between 1 to tens kWh. The battery size requirement is highly influenced by the PV system size and local loads energy consumption.

Various optimization techniques are available for optimal sizing and placement of the storage. **Table 2.2** presents several relevant literature reviews of various optimal storage sizing and placement studies that have been done. In general, various algorithm principles for optimal storage sizing and location can be categorized as follows [29]:

1. Probabilistic methods: a combination of renewable energy sources production, load demand, and net present cost are stochastically developed into several predefined probable scenarios, (e.g. Monte Carlo).
2. Iterative methods: performance assessment of system is made in each iteration until the optimum design is achieved. (e.g. (Mixed Integer) Linear / Non Linear Programming (LP/NLP/MILP/MINLP)).
3. Analytical methods: computational models are used for describing components which affect the optimization, such as weather information and battery energy storage. This algorithm may remove the necessity of long time series by simulating different configurations of study case.
4. Multi-objective methods: all individual objectives are merged to form a single objective and the pareto solution is calculated. Pareto introduces a set of optimal solutions and only can deviate when at least one objective is deteriorated.
5. Artificial Intelligence (AI) methods: the creation of smart machine learning which able to handle non-linear or stochastic problems, moreover it can lead to satisfactory results without weather information which is useful in a remote area. (e.g. Artificial Neural Network (ANN), Ant Colony Optimization (ACO), Genetic Algorithm (GA), Particle Swarm Optimization (PSO)).
6. Intuitive method: calculation is conducted by average information on load, generation, weather, used when there is no exact data on the system. It is less used primarily because current computers technology allows researches are doing a numerical simulation by using exact information on the system.

Table 2.2 Overview of optimal storage sizing and placement literature reviews

Authors	Objectives	Optimization Technique	Features	Test System
R. Tisseur et al. [30]	Minimize grid energy exchange, maximize revenue	Ant Colony Optimization (ACO)	Optimal operation scheduling with load and RES forecast	House with three kWp PV (3300 kWh), load 2300 kWh
D.Q. Hung et al. [31]	Energy losses reduction at peak load	Analytical Method	Optimal location, size, and power factor of the storage unit	(1) 15 bus radial distribution system, total load 1.23 MW & 1.25 MVAr (2) 69 bus, 3.8 MW & 2.69 MVAr
V. Kalkhambkar et al. [32]	Line losses and intermittency minimization	Analytical Method	Optimal sizing solar PV and battery in grid connected system	13 bus test system
T. Kerdphol et al. [33]	Loss reduction	Artificial Neural Network (ANN)	Optimum BESS size and location based on frequency and voltage regulation	13 bus, total 43 MVA (trafo capacity)
Y. Zhang et al. [34]	Maximize system's self-sufficiency ratio and net present value	Genetic Algorithm (GA)	Optimal PV and battery sizing with hybrid operation strategy and dynamic price	Apartment with PV 50-200 kWp, grid connected
Y. Zhang et al. [35]	Maximize system's net present value and self-sufficiency ratio	Genetic Algorithm (GA)	Optimal battery, PV, hydrogen sizing with hybrid operation strategy and dynamic price under grid power fluctuation	House complex with PV 200 kWp with storage, grid connected
J. Zhuang et al. [36]	Maximize life cost cycle, income by load shifting, and minimize line losses	Genetic Algorithm (GA)	Optimal battery location and sizing based on demand response	34 node microgrid with peak load 5000 kW

Authors	Objectives	Optimization Technique	Features	Test System
B.J. Abdelhaak et al. [37]	Minimize total cost	Fuzzy-Adaptive Genetic Algorithm (GA)	Optimal PV, wind turbines, storages size with battery's life consideration	Microgrid with max load 65 kW
K. K. Mehmood et al. [38]	Minimize energy losses in the system and total investment cost	Genetic Algorithm (GA)	Optimal location and size of BESS for voltage regulation and increase lifespan	The IEEE 906 bus European low-voltage (LV) test feeder
V. Kalkhambkar et al. [39]	Energy loss minimization	Grey Wolf Optimizer (GWO)	Optimal sizing energy storage and renewable distributed generation	34 bus radial system, peak load 5MW
M. Gitizadeh et al. [40]	Maximize battery life span	Mixed Integer Programming (MIP)	Optimal battery sizing considering battery degradation and dynamic price	Residential load
F. Marra et al. [41]	Minimize storage power needed for voltage support in the feeder	Mixed Integer Linear Programming (MILP)	Optimal battery sizing with bus voltage sensitivity	LV residential grid feeder with PV 43 kWp for EV charging
P. Fortenbacher et al. [42]	Maximize PV utilization and minimize battery degradation	Multi-objective function Optimal Power Flow (OPF) using Benders Decomposition	Optimal battery sizing and location considering total cost, voltage control, grid losses, PV and load forecast	CIGRE low voltage (LV) benchmark grid with 18 node
J. Hill et al. [43]	Minimize total cost of the system	Optimal Power Flow (OPF)	Optimal battery sizing and location considering voltage	Three buses with loads and two generators
P. Fortenbacher et al. [44]	Minimize system total cost and losses	Forward Backward Sweep Optimal Power Flow (FBS-OPF)	Optimal battery sizing and placement considering voltage and losses, and comparison centralized and decentralized	CIGRE low voltage (LV) benchmark grid with 18 nodes, load 5 kW 1 kVAr

Authors	Objectives	Optimization Technique	Features	Test System
A. K. Barnes et al. [45]	Maximizing the net present value of the system	Optimal Power Flow (OPF)	Optimal battery sizing and placement with voltage control and peak shaving services	Eleven node distribution feeder with total 6300 kW 3600 kVA
E.G. Silva et al. [46]	Minimize the system total cost and losses	Second Order Cone Program Optimal Power Flow (SOCP-OPF)	Optimal battery sizing and placement considering voltage and losses	69 nodes nominal voltage 12.66 kV peak load 5.9 MW (winter)
D. I. Karadimos et al. [47]	Maximization system profit	Optimal Power Flow (OPF)	Optimal battery sizing and placement with services voltage and ramping rate control	The IEEE 33-bus system with PV 500-800 kW
H. Nazaripouya et al. [48]	Minimize battery storage size with proper placement	Optimal Power Flow (OPF)	Optimal battery sizing and placement considering voltage control	The IEEE 14-bus benchmarks
Z. Qing et al. [49]	Maximize BESS participation in the system	Multi-objective Particle Swarm Optimization (PSO)	Optimal battery sizing and placement for voltage control and peak shaving	21 nodes with max load 324 kW 177 kVAr
S.B. Karanki et al. [50]	Minimize system losses	Particle Swarm Optimization (PSO) for sizing and loss sensitivity for placement	Optimal battery sizing and placement considering voltage and losses	The IEEE 13 and 34 bus distributed systems
S.B. Karanki et al. [51]	Minimize system total cost and losses	Particle Swarm Optimization (PSO) for sizing and loss sensitivity for placement	Optimal battery sizing and placement considering voltage and losses	Substation with 278 nodes and six buses
T. Kerdphol et al. [52]	Minimize the power of BESS	Particle Swarm Optimization (PSO)	Optimal battery sizing considering voltage control, frequency control, and load shedding scheme	Microgrid with 1.2 MW mini-hydro, 2 MW hydro, 3 MW PV, two critical loads 1.85 MW and 1.9 MW

Authors	Objectives	Optimization Technique	Features	Test System
I. Biswas et al. [53]	Minimize total system cost	Particle Swarm Optimization (PSO) and Extremal Optimization (EO)	Optimal storage size considering reliability constraint	Microgrid with PV, battery, fuel cell
C.D. R. Gallegos et al. [54]	Minimize total system cost	Double Particle Swarm Optimization (PSO)	Optimal storage sizing and location considering grid voltage and losses	Off grid system with a diesel generator, PV, and batteries

2.6 Mixed Integer Non Linear Programming Technique

In engineering applications, the problems frequently involve non linearity of system dynamics and discrete decisions which affect the final design. These problem constraints lead to the emergence of mixed integer linear programming (MINLP) technique which combines optimization over discrete variable and non-linear functions [55]. This technique suits the necessity of optimal battery sizing and placement. The battery size exhibits a non-linear constraint such as the battery state of charge, while the discrete variable is required to determine the optimal location of the battery. MINLP is derived from nonlinear programming (NLP) and mixed integer linear programming (MILP) subproblems. The general form of MINLP is commonly expressed as follows [56]:

$$minimize\ f(x,y) \tag{2.1}$$

subject to:

$$g(x,y) \leq 0$$

$$x \in X, y \in Y\ integer$$

The function f(x,y) and g(x,y) can be combination of linear and non-linear equation. The variables x and y are the decision variables, while X and Y are bounding box type restrictions on the variables. Function f(x,y) and g(x,y) are assumed to be convex and bounded over X and linear in y.

In general, there are five solution algorithms for the MINLP problem as follows [55]:

1. Non-linear Branch and Bound Method

   The algorithm starts by solving the NLP problem relaxation which is the root node, determined by relaxing the integrality of the integer variables. The MINLP becomes infeasible if the relaxation is infeasible. If the relaxation solution is an integer, then the MINLP can be solved. Otherwise, the branch and bound method will search a tree whose nodes corelates to NLP subproblems and whose edges corelates to the branching decision. Optimality and feasibility of NLP subproblems are used to prune nodes in the tree. The node problem is firstly defined before the branching and pruning operations before stating the algorithm as illustrated in **Figure 2.12**.

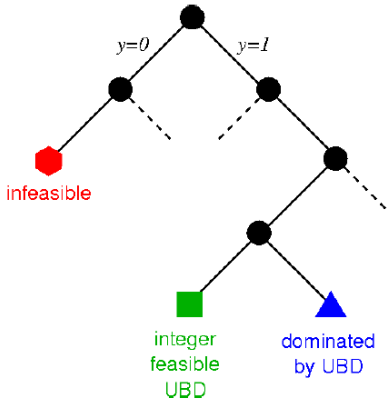

Figure 2.12 Tree traversing of the non-linear branch and bound algorithm by solving NLP problem at every node [55]

2. LP/NLP based Branch and Bound

   This method is considered as a powerful tool for solving convex MINLP problems. The algorithm avoids the time consuming of multiple MILP master problems. As a replacement, the algorithm solves the continuous relaxation and imposes integrality of the variables by branching. When the new integer solution is found, the tree search is interrupted, and the master MILP is updated with new outer approximation which is generated from the subproblem solution. **Figure 2.13** gives an illustration of LP/NLP based branch and bound optimization stage. First, two branches are introduced after the LP does not give an integer feasible solution. Then, the next LP produces an feasible integer solution as indicated by a box. Next, after the corresponding NLP subproblem is solved, all nodes on the heap are updated by adding linearization from the NLP subproblem. Lastly, the branch and the bound process keep continuing on the updated tree by solving the marked LP.

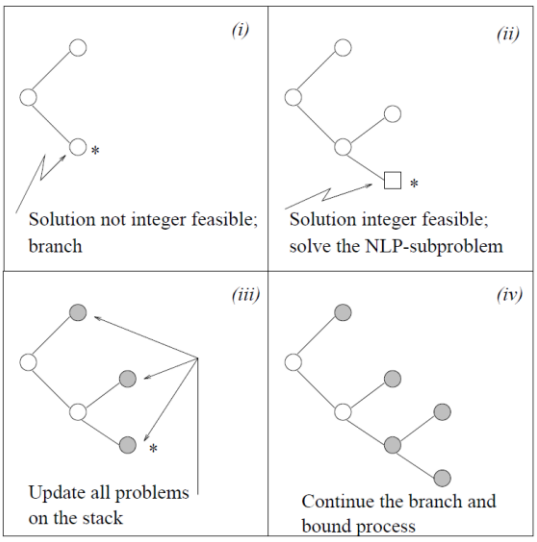

Figure 2.13 Chronological of LP/NLP based branch and bound [55]

3. Outer-Approximation

In this algorithm, the problem is firstly solved as an NLP with all integer variables relaxed as continues variables between their boundaries. Then, a linearization is conducted around the optimal solution, resulting add the resulting constraints to the linear constraint that are already present which is referred to as the master MIP problem and solved later. Next, the integer part of the optimal solution is temporarily fixed and the original MINLP problem with fixed integer variables is solved as a nonlinear problem. Later, a linearization is constructed around the optimal solution and the master MIP problem adds the new linear constraints. One or more constraints are added to cut off the previously found integer solution for preventing cycling. These steps are repeated when the master MIP problem becomes infeasible or stopped if the termination criteria are satisfied. Overall work flow of the algorithm is presented in **Figure 2.14**.

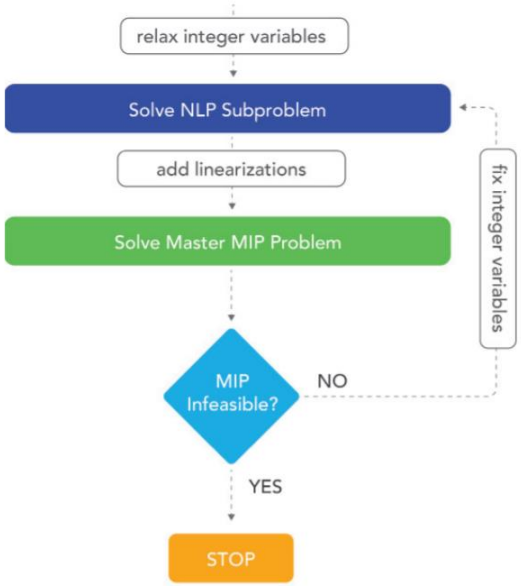

Figure 2.14 Flowchart of the Outer Approximation Algorithm [57]

4. Generalized Benders Decomposition

The Benders decomposition approach exploits mathematical programming problems structure with complicating variables which render remaining optimization problem more tractable when temporarily fixed. The algorithm finds the optimal value of the vector by employing a cutting plane for building up adequate representations of the linear program extremal value as a function of the parameterizing vector and values set of the parameterizing vector which linear program is feasible. Linear programming duality is deployed to derive the natural families of cuts characteristic representations. Last, the parameterized linear program is used to generate deepest cuts for building up the representations. In Generalized Benders Decomposition, the parameterized subproblem

is no longer needed to be a linear program. A nonlinear convex duality is employed to derive the natural cuts families related to the Bender's case. The algorithm flowchart is illustrated in **Figure 2.15**.

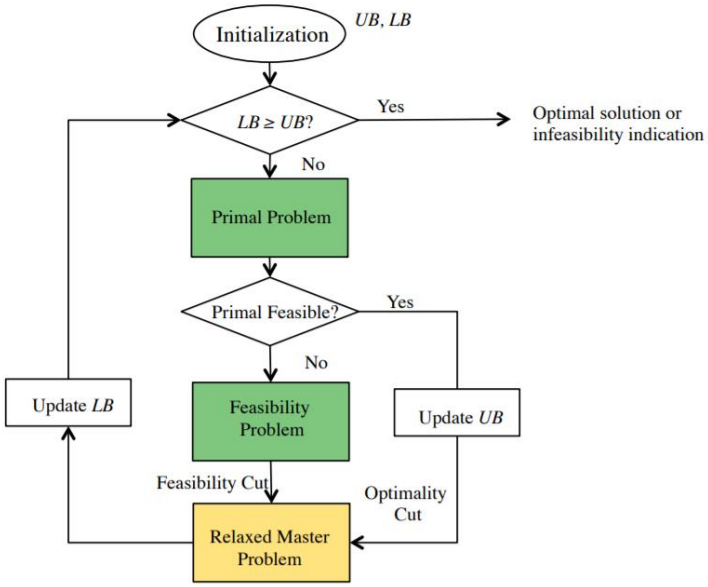

Figure 2.15 Algorithm Flowchart of Generalized Benders Decomposition [58]

5. Extended Cutting Plane

   This optimization method uses iterative Newton's method to refine the feasible area and solve the problem within tolerable error. The first differential approximation is utilized to cut the plane. Therefore, the extended cutting plane algorithm does not require nonlinear programming as outer approximation and branch and bound method. However, this strategy has a slower convergence compared to another algorithm which leads to more iterations are required. The algorithm is considered suitable for cases where the non-linear functions evaluation is time to consume [59].

In this study, the mixed integer non-linear programming problems are solved using software GAMS (General Algebraic Modeling System) with solver DICOPT (Discrete and Continuous OPTimizer). The solver is developed by the Engineering Design Research Center at Carnegie Mellon University. The program is based on the extensions of the outer approximation algorithm, equality relaxation strategy, and augmented penalty. In the algorithm, outer approximations are achieved by constructing linearization at each iteration and accumulating them to provide the improved linear approximations of nonlinear convex functions that overestimate the feasible region or underestimate the objective function. Augmented penalty corresponds to the introduction of non-negative slack variables on the inequality constraints right hand side and modification of the objective function when convexity assumptions do not hold [60].

The DICOPT algorithm initiates by solving the NLP problem in which the binary variables are relaxed. The search stops when the problem solution is an integer. Otherwise, the algorithm continues the search with an alternating sequence of NLP subproblems and MIP master problems. The NLP subproblems are solved for fixed variables that are predicted by the MIP master problem at each major iteration. In the convex problem case, the master problem also provides a lower bound for the objective function. In the minimization case, this lower bound increases monotonically as iterations continue due to linear approximation accumulation. In the maximization case, the upper bound is used. These bounds can be used as the stopping criterion. Besides, the heuristic approach also fits as the stopping criterion for convex and non-convex problems by forcing the iterations to stop when the NLP subproblems start worsening which means the current NLP subproblem has worse optimal objective function than the previous NLP subproblem. The augmented penalty approach is used as the basis of this stopping criterion [60].

In overall, there are two main principles of the DICOPT solver [60]:

1. Construct on existing modeling concepts and introduce a minimum extension of the existing modelling language. Besides, it also provides upward compatibility to ensure an easy transition to non-linear mixed integer formulations from existing modeling applications.
2. Utilize existing optimizers to solve the DICOPT subproblems. This enables the best algorithms to handle the problem and guarantees any new development and enhancement in NLP and MIP solvers become immediately available to DICOPT.

3. Network Model

In this chapter, the test model will be introduced with the input data of the component inside the network to evaluate the proposed optimization technique of optimal sizing and placement of BESS along with the power management system. Several cases are prepared to check the robustness of the technique to different input data of EV number, weather profile, and energy prices. Therefore, the input parameter data of EV characteristic, PV power profile, and daily electricity price trend will be presented.

3.1 Network Specification

This study adopts low voltage distribution network of CIGRE Benchmark in [61] to evaluate the proposed optimization method. The network consists of three buses connected in a straight line of radial architecture as shown in **Figure 3.1** The grid represents the medium voltage network which is connected to step down transformer 20/0.4 kV with the capacity of 400 kVA. Each bus consists of an EV charger station, residential load, PV system, and BESS that will be deployed in one of three buses.

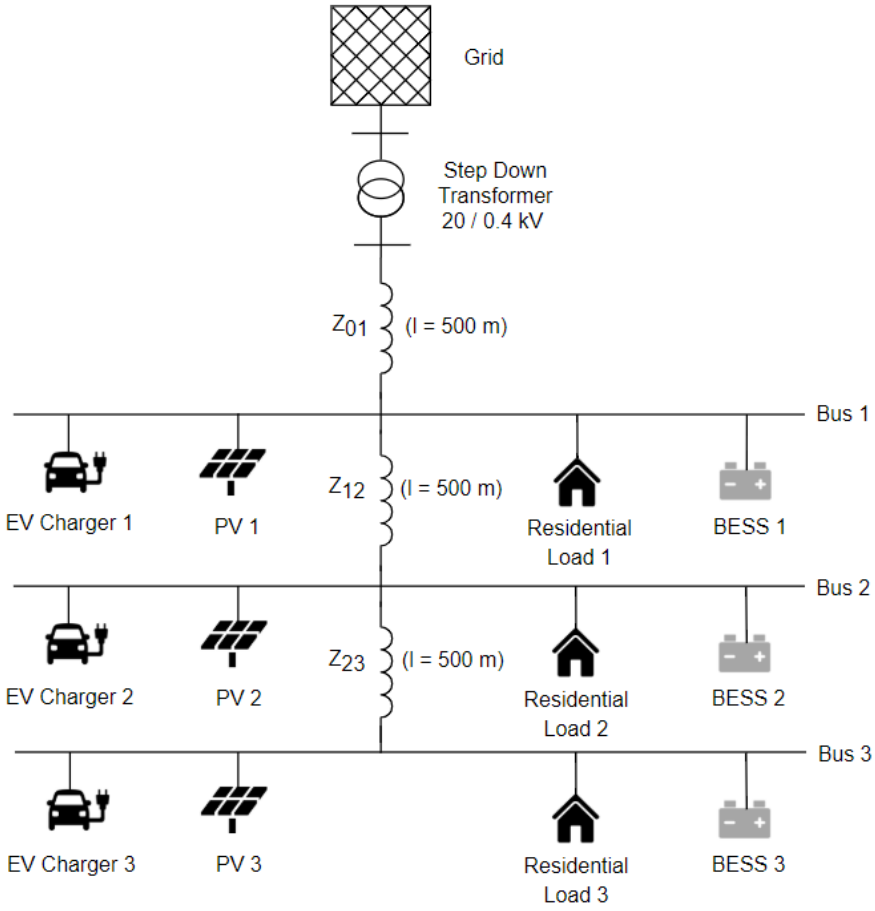

Figure 3.1 Network Model of The Test System

The transformer is connected to the first load bus via transmission line with a length of 500m and so are the connection of other two load buses. The line impedance is obtained from the impedance value of underground line given in CIGRE Benchmark as shown in **Table 3.1**. Furthermore, the line has maximum ampacity of 3 x 160 A.

Table 3.1 Line Impedance Characteristic of Transmission Line in Network Model, based on [61]

Resistance Specific (Ω/km)	Reactance Specific (Ω/km)	Line Length (m)	Line Resistance (Ω)	Line Reactance (Ω)	Line Impedance (Ω)
0.264	0.071	500	0.132	0.0355	0.1367

3.2 Battery Energy Storage System

Lithium-ion based battery is chosen as the storage used in this network model as it has a relatively long lifetime and high power density. In this study the charging and discharging efficiency of the battery is assumed to be 92% [10]. Optimal sizing and placement of battery will be conducted based on the investment cost and operational cost. Cost breakdown of the battery is given in **Table 3.2**.

Table 3.2 Cost breakdown of battery energy storage system [62], [63]

Specification	Cost Value
Module	0.61 €/W
Inverter	0.18 €/W
The balance of system equipment	0.49 €/W
Installation labour	0.13 €/W
Installer margin and overhead	0.65 €/W
Permitting	0.05 €/W
Operation and Maintenance	17.2 €/kW-yr
Battery	260 €/kWh
Efficiency	92%

3.3 Electric Vehicles

This study implements ten most used Battery Electric Vehicles (BEV) in the Netherlands [64]. Brands and their characteristic are shown in

Table 3.3. EVs are assumed to have State of Charge (SoC) 5-15% when arriving at the charger station and will be charged until full capacity. Arrival and departure time of the EVs to the charger station is set between 8.40 to 17.20 based on EV user study behaviour in the Netherlands during workdays as shown in Figure 3.2 with variation of ± 20 minutes [65].

Table 3.3 Ten most popular Battery Electric Vehicles in the Netherlands [64]

EV	Number in Netherlands	Percentage Share (%)	Battery Useable (kWh)
Tesla Model S 75D	9047	35.1	72.5
Nissan Leaf	3101	12	38
Renault Zoe R90	2836	11	37
BMW I3	2296	8.9	27.2
Volkswagen e-Golf	2275	8.8	32
Tesla Model X 75D	2234	8.7	72.5
Hyundai Ioniq	1668	6.5	28
Nissan E-NV200 Evalia	814	3.2	38
Renault Kangoo Maxi ZE 33	790	3.1	31
Opel Ampera-e	692	2.7	57

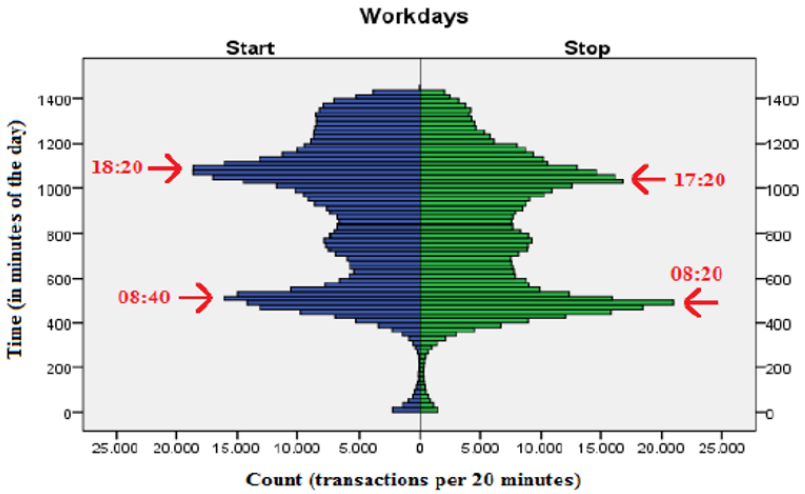

Figure 3.2 EV charging start and stop time pattern in the Netherlands [65]

3.4 PV Profile

PV systems are placed in every bus to support EV charger station and residential load. The size of PV is scalable with the energy requirement of EVs and residential loads. The average sun irradiance of Delft, Netherlands is taken into account with solar irradiation of 999 kWh/m^2 at horizontal plane and 1146 kWh/m^2 at optimal tilt plane of 36^0. When taking into account length of the year, those numbers are equivalent to sun hours of 2.7 and 3.1 hours for horizontal and optimal tilt respectively [66]. The peak power of the PV system is then obtained from the average energy required of the residential load, 279 kWh/day divided by the average sun hour of 3 hours, resulting to 93 kWp which will be applied during summer season. This study considers summer and winter weather profile as the two extreme conditions during a year and also autumn as a transitional season. The PV power generation profile of those three seasons are given in **Figure 3.3**.

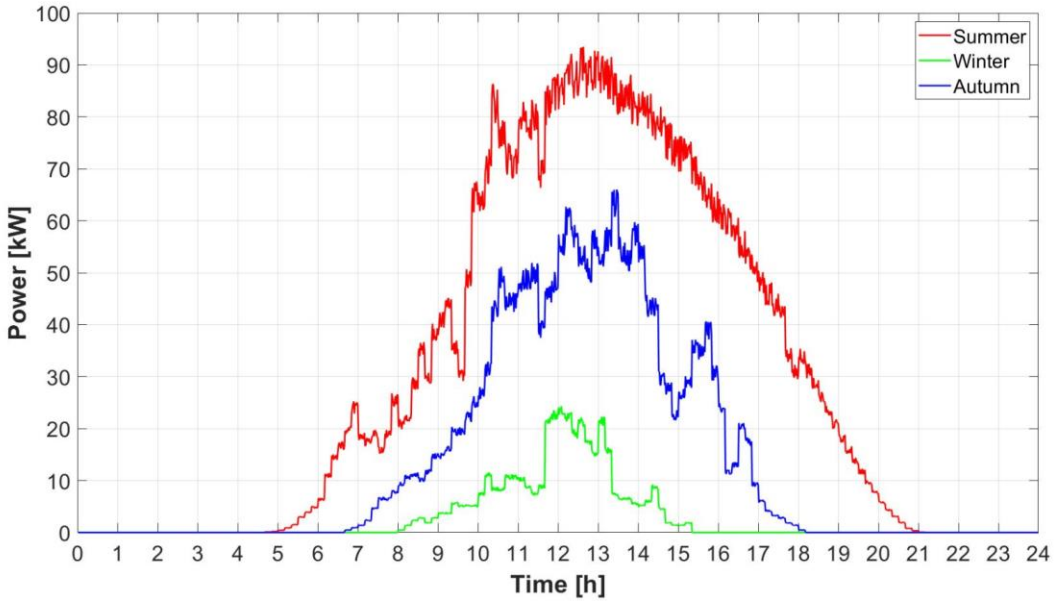

Figure 3.3 PV Power Generation Profile [67]

3.5 Residential Load Profile

Residential load of 30 houses are placed at every load bus in the network system. The power profile of residential load differs for every season as shown in **Figure 3.4**. It can be seen that winter has the highest power demand while summer has the lowest. In general, the residential load profile of the three seasons have similar pattern. The demand is low during dawn when people are resting. Then, the demand grows when people starts their activity during morning and afternoon. Peak period occurs during the evening when people are coming back home and extra lighting demand occurs.

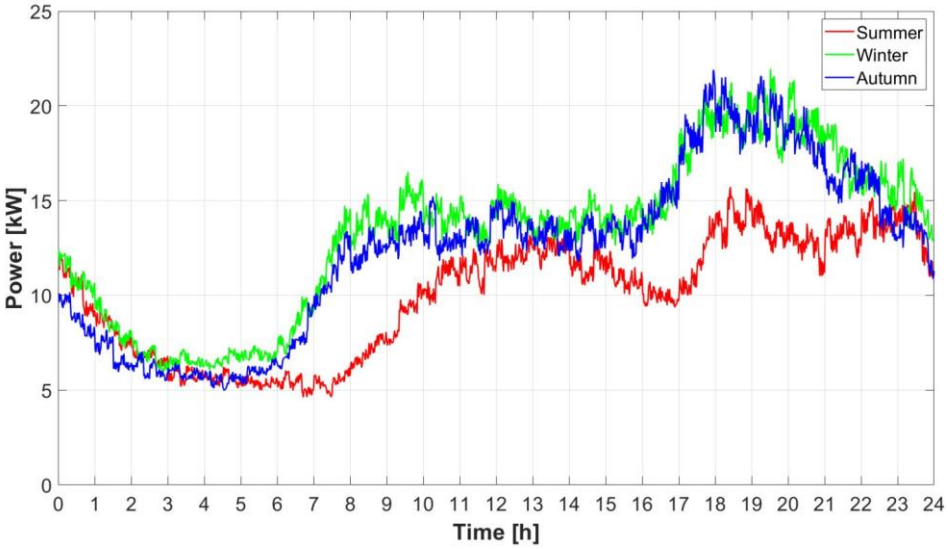

Figure 3.4 Residential Load Power Generation Profile [67]

3.6 Energy Prices

Dynamic electricity price is implemented in this study to evaluate the power management system in order to minimize the total cost. The tariff is obtained by averaging the hourly price of three months in a season as shown in **Figure 3.5**. It is noticeable that electricity price has the highest value during winter and the lowest during summer due to abundant power generation. In general, the electricity price of the three seasons have similar pattern. High and low price period alternately occurs during a day. The lowest electricity price period happens during the dawn when less electricity demand occurs. There are two peak price periods, first during morning when people start their activity and second at late afternoon when people arrive back to their home. There is also electricity price pattern shift from winter to summer because of the demand shift.

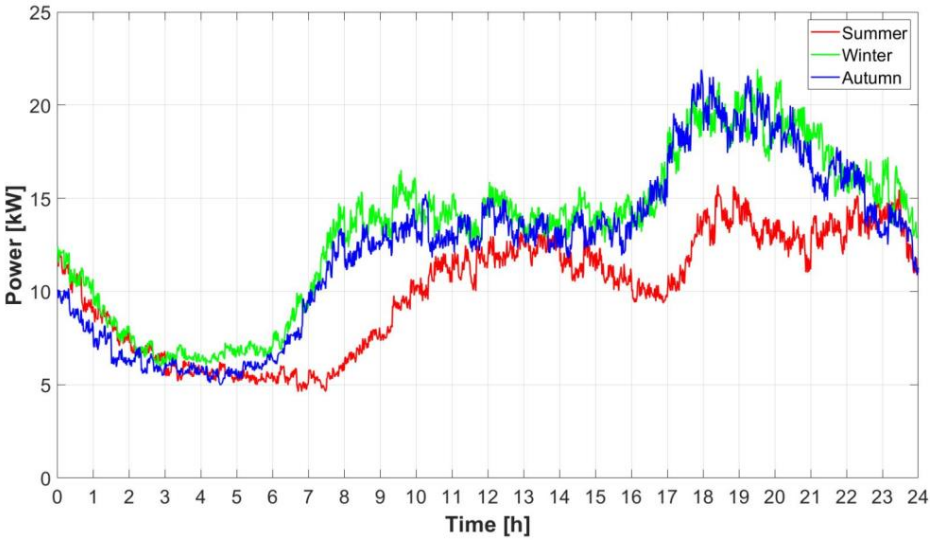

Figure 3.5 Daily Electricity Prices Profile [68]

4. Model Formulation

This chapter presents a formulation of the network model defined in the previous chapter. List of formulation parameters and variables are firstly presented. Then, sets of the equation describing characteristic and interaction between BESS, EV, PV, and distribution grid are defined. Lastly, the objective function of the system is expressed as the purpose of the power management system.

4.1 Nomenclatures

Indexes

v Electric vehicles, running from 1 to *V* vehicles.

n Nodes, running from 1 to *N* nodes.

t Time, running from 1 to *T* minutes.

Parameters

Battery Energy Storage System Parameters

η^b Charging and discharging efficiency of battery energy storage system (%).

$\lambda^{b,cap}$ Marginal investment cost of battery energy storage maximum capacity (€/kWh).

$\lambda^{b,pwr}$ Marginal investment cost of battery energy storage maximum power (€/kW).

N^b Number of battery energy storage system applied.

$S^{b,min}$ Minimum state of charge of battery energy storage system allowed (%).

$S^{b,max}$ Maximum state of charge of battery energy storage system allowed (%).

$S^{b,init}$ Initial state of charge of battery energy storage system (%).

$R^{b,max}$ Maximum C-rate of battery energy storage system allowed.

T^b Expected lifetime of battery energy storage system (days).

Electric Vehicles Parameters

$t_{n,v}^{arr}$ Arrival time of EV *v* at node *n* (min).

$t_{n,v}^{dep}$ Departure time of EV *v* at node *n* (min).

η^{v} Charging efficiency of EV's battery (%).

$E_{n,v}^{arr}$ Initial energy stored in battery of EV *v* at node *n* at arrival time (kWh).

$E_{n,v}^{max}$ Maximum energy stored in battery of EV *v* at node *n* (kWh).

$P^{v,ch}$ Charging power of EV (kW).

Photovoltaics Parameter

$P_{n,t}^{PV}$ PV system power at node *n* at time *t* (kW).

Grid Parameters

$B_{n,k}$ Imaginary part of Y matrix corresponding to row *n* and column *k* (1/Ω).

$G_{n,k}$ Real part of Y matrix corresponding to row *n* and column *k* (1/Ω).

$P_{n,t}^{load}$ Residential load power at node *n* at time *t* (kW).

$P^{tr,max}$ Maximum power capacity of the transformer (kVA).

V^{min} Minimum bus voltage allowed (V).

V^{max} Maximum bus voltage allowed (V).

$\lambda^{g,inv}$ Marginal investment cost of grid (€/kW/year).

$\lambda_{t}^{g,FiT}$ Marginal price revenue by supplying power to the grid (€/kWh).

$\lambda_{t}^{g,buy}$ Marginal price paid by drawing power from the grid (€/kWh).

Variables

Battery Energy Storage System Variables

$P_{n,t}^{b,ch}$ Charging power to battery energy storage system at node *n* at time *t* (kW).

$P_{n,t}^{b,dis}$ Discharging power from battery energy storage system at node *n* at time *t* (kW).

$P_{n,t}^{b,acc}$ Accumulated power of battery energy storage system at node *n* at time *t* (kW).

$P_{n}^{b,max}$ Maximum power of battery energy storage system at node *n* (kW).

$E_{n,t}^{b}$ Energy stored in battery energy storage system at node *n* at time *t* (kWh).

$E_{n}^{b,max}$ Capacity of battery energy storage system at node *n* (kWh).

$S_{n,t}^{b}$ State of charge of battery energy storage system at node *n* at time *t*.

$R_{n,t}^{b}$ C-rate of battery energy storage system at node *n* at time *t*.

$C^{b,inv}$ Total investment cost of battery energy storage system (€).

$C^{b,op}$ Operation cost of battery energy storage system (€).

o_{n}^{b} Binary variable which determine the location of battery energy storage system at node *n*.

Electric Vehicles Variables

$P_{v,n,t}$ Actual power delivered to EV *v* at node *n* at time *t* due to efficiency (kW).

$E_{v,n,t}$ Energy content of EV *v* at node *n* at time *t* (kWh).

Grid Variables

$P_{n,t}^{g,in}$ Power to the grid from node *n* at time *t* (kW).

$P_{n,t}^{g,out}$ Power from the grid to node *n* at time *t* (kW).

$P^{g,max}$ Maximum power exchange of the grid (kW).

$P_{n,t}^{line,loss}$ Losses power at the transmission line *n* at time *t* (kW).

$P_{n,t}^{line}$ Power at the transmission line *n* at time *t* (kW).

$C^{g,inv}$ Total investment cost of grid reinforcement (€).

$C^{g,op}$ Operation cost of grid power exchange (€).

C^{sys} Total cost involved in the system (€).

$V_{n,t}$ Voltage at node *n* at time *t* (V).

$\theta_{n,t}$ Phase angle at node *n* at time *t* (rad).

4.2 Mathematical Formulation

4.2.1 Battery Energy Storage System

In this system, Battery Energy Storage System (BESS) will be applied in one node of the distribution grid to ensure that the overall system is not breaking the grid code of voltage limit and maximum transformer peak power. Actual exchange power that flows in BESS is the difference between charging and discharging power plus the efficiency factor of the battery as shown in (4.1). Charging and discharging power of BESS is limited by the maximum power which will be defined by the solver. Binary variable o_n^b is introduced to decide the most optimal placement of BESS. The number of BESS installed in the system is set by the value of N^b. In normal case, N^b is set to be one which means only one BESS can be installed in the system.

$$P_{n,t}^{b,acc} = o_n^b \cdot \left(\eta^b \cdot P_{n,t}^{b,ch} - \frac{P_{n,t}^{b,dis}}{\eta^b} \right) \qquad \forall\, n,t \qquad (4.1)$$

subject to:

$$P_{n,t}^{b,ch} \leq P_n^{b,max} \qquad \forall\, n,t$$

$$P_{n,t}^{b,dis} \leq P_n^{b,max} \qquad \forall\, n,t$$

$$\sum_{n=1}^{N} o_n^b = N^b \qquad \forall\, n,t$$

The energy of BESS is calculated as shown in (4.2) with timestep (Δt) of one minute. The sum of BESS energy is set to be zero to ensure that the BESS State of Charge (SoC) comes back to its initial value at the end of the day. The SoC and C-rate of BESS is determined using (4.3) and (4.4). The initial BESS SoC is assumed to be 30% at the beginning of the day. The BESS SoC is kept between 10-90% while the C-rate is held under 0.5 to prolong the battery lifetime [62].

$$E_{n,t}^b = E_{n,t-1}^b + P_{n,t}^{b,acc} \cdot \Delta t \qquad \forall\, n,t \qquad (4.2)$$

subject to:

$$\sum_{t=1}^{T} \sum_{n=1}^{N} E_{n,t}^b = 0 \qquad \forall\, n,t$$

$$S_{n,t}^b = \frac{E_{n,t}^b}{E_n^{b,max}} \qquad \forall\, n,t \qquad (4.3)$$

subject to:

$$S_{n,t=0}^b = S^{b,init} = 30\%$$

$$S^{b,min} \leq S_{n,t}^b \leq S^{b,max} \qquad \forall\, n,t$$

$$10\% \leq S_{n,t}^b \leq 90\% \qquad \forall\, n,t$$

$$R_{n,t}^{b} = \frac{P_{n,t}^{b,acc}}{E_{n}^{b,max}} \qquad \forall\, n,t \qquad (4.4)$$

subject to:

$$R_{n,t}^{b} \leq R^{b,max} \qquad \forall\, n,t$$

$$R_{n,t}^{b} \leq 0.5 \qquad \forall\, n,t$$

4.2.2 Electric Vehicles

In normal case, EVs are assumed to be directly charged when they arrive at the charging station. The charging power of EV is set to be constant 11 kW. Charging connection is automatically cut off when EV is already fully charged. Power flow and energy content of EV are expressed in (4.5) and (4.6).

$$P_{v,n,t} = \begin{cases} \eta^{b} \cdot P_{v,n,t}^{ch} & if\ \ (t_{n,v}^{arr} < t < t_{n,v}^{dep}) \qquad \forall\, v,n \\ 0 & if\ (t < t_{n,v}^{arr} \vee t > t_{n,v}^{dep}) \qquad \forall\, v,n \end{cases} \qquad (4.5)$$

$$E_{v,n,t} = \begin{cases} 0 & if\ t < t_{n,v}^{arr} \qquad \forall\, v,n \\ E_{n,v}^{arr} + P_{v,n,t} \cdot \Delta t & if\ \left(t_{n,v}^{arr} < t < t_{n,v}^{dep}\right) \qquad \forall\, v,n \\ E_{n,v}^{max} & if\ t \geq t_{n,v}^{dep} \qquad \forall\, v,n \end{cases} \qquad (4.6)$$

4.2.3 Distribution Grid

The low voltage distribution grid is arranged in a radial network. Every charger station and residential load in each node are connected through the transmission line. The overall system can be equivalent presented in electrical circuit as shown in Figure 4.1. The grid is represented as a voltage source feeding to three branches of EV and residential load with BESS in one of the branches that will be defined by the solver. The grid power is transferred through a transmission line which is represented as a series connection of resistance and inductance.

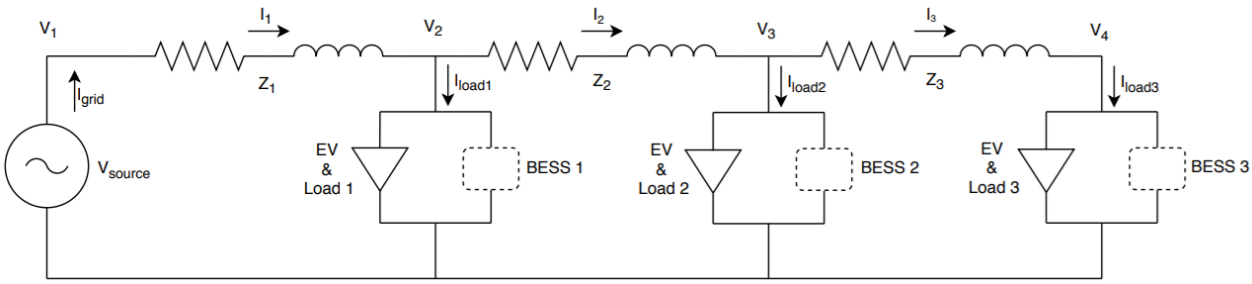

Figure 4.1 Electrical circuit of the network model

The network model is then expressed in admittance matrix form by applying Kirchoff current law in every node as follows:

$$I_{grid} = \frac{V_1 - V_2}{Z_1} \tag{4.7}$$

$$I_{load1} = \frac{V_1 - V_2}{Z_1} - \frac{V_2 - V_3}{Z_2} \tag{4.8}$$

$$I_{load2} = \frac{V_2 - V_3}{Z_2} - \frac{V_3 - V_4}{Z_3} \tag{4.9}$$

$$I_{load3} = \frac{V_3 - V_4}{Z_3} \tag{4.10}$$

Those four equations above are then reconstructed in matrix form as shown in **(4.11)** and has equivalent admittance matrix in **(4.12)**.

$$\begin{pmatrix} I_{grid} \\ I_{load1} \\ I_{load2} \\ I_{load3} \end{pmatrix} = \begin{pmatrix} \frac{1}{Z_1} & -\frac{1}{Z_1} & 0 & 0 \\ \frac{1}{Z_1} & -\frac{1}{Z_1} - \frac{1}{Z_2} & \frac{1}{Z_2} & 0 \\ 0 & \frac{1}{Z_2} & -\frac{1}{Z_2} - \frac{1}{Z_3} & \frac{1}{Z_3} \\ 0 & 0 & \frac{1}{Z_3} & -\frac{1}{Z_3} \end{pmatrix} \begin{pmatrix} V_1 \\ V_2 \\ V_3 \\ V_4 \end{pmatrix} \tag{4.11}$$

$$\begin{pmatrix} I_{grid} \\ I_{load1} \\ I_{load2} \\ I_{load3} \end{pmatrix} = \begin{pmatrix} Y_{11} & Y_{12} & Y_{13} & Y_{14} \\ Y_{21} & Y_{22} & Y_{23} & Y_{24} \\ Y_{31} & Y_{32} & Y_{33} & Y_{34} \\ Y_{41} & Y_{42} & Y_{43} & Y_{44} \end{pmatrix} \begin{pmatrix} V_1 \\ V_2 \\ V_3 \\ V_4 \end{pmatrix} \tag{4.12}$$

where the admittance matrix element consists of real and imaginary part.

$$Y_{n,k} = G_{n,k} + jB_{n,k} \tag{4.13}$$

In order to know the value of every bus voltage, an AC power flow is implemented in the network model to relate grid power exchange with the voltage as shown in **(4.14)** [69]. To reduce the harmful effect of under/overvoltage to the electrical appliances, the bus voltage is limited to a safe margin of 360 to 440 V, which is 10% deviation of nominal voltage of 400V, based on the European grid standard of EN50160 [70]. Besides, the power drawn from the grid is also controlled to not exceeding the maximum transformer power rating of 400 kVA. The line current is also kept below the ampacity limit of the transmission line.

$$P_{n,t}^{g} = P_{n,t}^{g,out} - P_{n,t}^{g,in} = \sum_{k=1}^{N} V_{n,t} \cdot V_{k,t} \cdot \left(G_{n,k} \cdot \cos\left(\theta_{n,t} - \theta_{k,t}\right) + B_{n,k} \cdot \sin\left(\theta_{n,t} - \theta_{k,t}\right)\right) \quad \forall\, n, t \quad (4.14)$$

subject to:

$$V^{min} \leq V_{n,t} \leq V^{max} \qquad \forall\, n, t$$

$$P_{n,t}^{g} \leq P^{tr,max} \qquad \forall\, n, t$$

$$I_{n,t}^{line} \leq I_{n}^{line,max} \qquad \forall n \neq 4, t$$

Losses power in the transmission line is determined by firstly calculate the current flowing in the line as the function of voltage different and line impedance in **(4.15)**. The line current is maintained below the maximum ampacity of the line. Then, the line losses can be directly calculated using **(4.16)**. Besides, the line power is obtained by using formulation in **(4.17)**.

$$I_{n,t}^{line} = \frac{V_{n,t} - V_{n+1,t}}{Z_n} \qquad \forall\, n \neq 4, t \qquad (4.15)$$

subject to:

$$I_{n,t}^{line} \leq I_{n}^{line,max} \qquad \forall n \neq 4, t$$

$$P_{n,t}^{line,loss} = {I_{n,t}}^{2} \cdot Re(Z_n) \qquad \forall n \neq 4, t \qquad (4.16)$$

$$P_{n,t}^{line} = V_{n,t} \cdot I_{n,t} \qquad \forall n \neq 4, t \qquad (4.17)$$

The grid power exchange gets its value from the power balance equation in every node of the system and overall power balance which also takes into account the losses of power as expressed in **(4.18)** and **(4.19)** respectively.

$$P_{n,t}^{g} + P_{n,t}^{b,dis} - P_{n,t}^{b,ch} + P_{n,t}^{PV} = P_{n,t}^{load} + \sum_{v=1}^{V} P_{v,n,t}^{ch} \qquad \forall\, n, t \qquad (4.18)$$

$$\sum_{n=1}^{N}\left(P_{n,t}^{g} + P_{n,t}^{b,dis} - P_{n,t}^{b,ch} + P_{n,t}^{PV}\right) = \sum_{n=1}^{N}\left(P_{n,t}^{load} + \sum_{v=1}^{V} P_{v,n,t}^{ch}\right) + \sum_{n=1}^{N-1} P_{n,t}^{line,loss} \qquad \forall\, v, n, t \qquad (4.19)$$

4.2.4 Objective Function

The purpose of the power management system is to minimize the total cost to fulfil the power demand from EV charging and residential load while also obeying the grid voltage allowed and maximum transformer power limit. Total cost involved can be broken down into two parts, investment and operational cost of BESS and distribution grid.

Due to time constraint, simulation is only done to simulate one day of the season in a year. Therefore, the investment cost of the system is stretched to one day cost instead of full period of expected lifetime of BESS. The investment cost is determined from the maximum energy of BESS obtained times marginal cost then divided with the expected BESS lifetime in days unit as shown in (4.20). In this study, the Lithium-ion based BESS is expected to be operated in 10 years which is equivalent to the 3650 days.

$$C^{b,inv} = \sum_{n=1}^{N} \frac{E_n^{b,max} \cdot \lambda^{b,cap} + P_n^{b,max} \cdot \lambda^{b,pwr}}{T^b} \tag{4.20}$$

In case of no BESS involved in the system, as the number of EV in the charger station is increasing, the grid power required to fulfil the power demand starts exceeding the maximum transformer power rating. Therefore the grid reinforcement is needed to tackle this issue. The reinforcement cost of the grid is formulated as shown in (4.21). Besides, there is also operational cost which needs to be paid by the aggregator from buying the electricity as expressed in (4.22). Finally, the total cost of the system which is the objective function is obtained from the summation of investment and operational cost as shown in (4.23) for case with BESS and (4.24) for case without BESS.

$$C^{g,inv} = \frac{(P^{g,max} - P^{tr,max}) \cdot \lambda^{g,inv}}{365} \tag{4.21}$$

$$C^{g,op} = \sum_{t=1}^{T} \sum_{n=1}^{N} (P_{n,t}^{g,out} \cdot \lambda_t^{g,buy} - P_{n,t}^{g,in} \cdot \lambda_t^{g,FiT}) \cdot \Delta t \tag{4.22}$$

$$\boldsymbol{Obj.function}: \ min \left[C^{sys} = C^{b,inv} + C^{g,op} \right] \tag{4.23}$$

$$\boldsymbol{Obj.function}: \ min \left[C^{sys} = C^{g,inv} + C^{g,op} \right] \tag{4.24}$$

4.2.5 Conclusion

An analytical method has been proposed to solve the optimization problem of the system. Optimal sizing and placement of BESS also with the optimum power management of the system will be defined by the optimization solver. The formulations consist a combination of linear, non-linear, and discrete equations. Hence, a Mixed Integer Non-Linear Programming (MINLP) optimization technique is proposed to overcome the optimization problem.

5. Simulation Results

In this chapter, several study cases are conducted to evaluate the performance of the proposed optimization problem. There are four main cases under three seasons to be tested in the model that has been developed. Overview of the simulations is shown in **Table 5.1**.

Table 5.1 List of Simulations

Case Name	Study Case	Specific Test	PV Profile	Number of EV
1A-1	Increasing EV Number	without BESS	Summer	5, 10, 15, 20
1A-2		with BESS		
1B-1		without BESS	Winter	
1B-2		with BESS		
1C-1		without BESS	Autumn	
1C-2		with BESS		
2A-1	Unbalance EV Number	10-15-20 EV	Summer	10, 15, 20
2A-2		20-15-10 EV		
2B-1		10-15-20 EV	Winter	
2B-2		20-15-10 EV		
2C-1		10-15-20 EV	Autumn	
2C-2		20-15-10 EV		
3A	Decentralized BESS Location	multiple batteries applied	Summer	15
3B			Winter	
3C			Autumn	
4A-1	Different EV Charging Strategy	shift charging time	Summer	15
4A-2		constant charging		
4A-3		dynamic charging		
4B-1		shift charging time	Winter	
4B-2		constant charging		
4B-3		dynamic charging		
4C-1		shift charging time	Autumn	
4C-2		constant charging		
4C-3		dynamic charging		

First, the effect of increasing EV number charged in every charger station is investigated for the case of providing power only from the grid and also with BESS. Second, the unsymmetrical number of EV deployed is analysed. Third, the impact of the decentralized battery is evaluated instead of the centralized battery. Last, different EV charging methods are tested into the model. Technical and economic analysis are elaborated to give an evaluation for every case.

5.1 Increasing EV Number

In this section, the effect of EV number being charged in the charger station is examined. Simulations are done for every multiple of five EVs placed in every bus until the maximum EV number that can be handled by one BESS in the system. This case is divided into two scenarios, first is the condition without applying BESS in the system, and second is the condition with BESS that will be placed in one of the bus in the system.

5.1.1 Case 1A-1 (Summer, without BESS)

In this case, PV power profile of season summer is adapted to the model. Power to charge EVs and electrify residential load are drawn from grid and PV. Compared to another season, summer has the longest sun period, starting from around 5 a.m. and ended at 9 p.m. with peak power at between 12-13 p.m. It is beneficial to the system since the PV can fulfil the power demand during the day and even give the excess power to the grid as revenue **Figure 5.1** shows the overall exchange power profile of case 5 EVs per node. Unsymmetrical EV charging profile is because there are variations of EV's battery capacity in this simulation as shown in

Table 3.3. Although all EVs are charged with same constant charging power of 11 kW, EVs with larger battery capacity will require longer charging time to reach their full capacity.

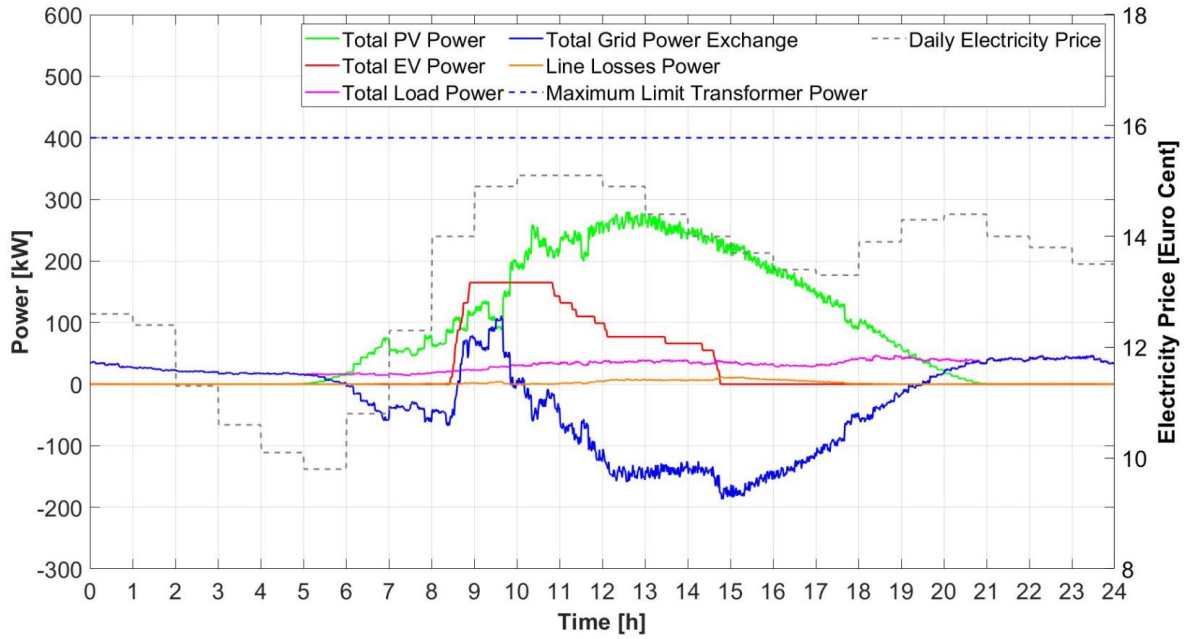

Figure 5.1 Power Exchange Profile of the System for Case 1A-1 (5 EV, Summer)

During the night, power is drawn only from the grid to meet the demand from residential load since there is no PV power generation. In the morning, PV starts to generate power and feeds the excess power to the grid until EVs arrive at the charger station at around 8.30 a.m.

and directly charged until their full capacity. Power is drawn from the grid until the time when PV power generation is enough to supply the load demand. Then, PV starts back giving excess power to the grid until starts of the evening around 7.30 a.m. when the sun goes down and the system is back rely on the grid power. The bus voltage profile in this case is shown in **Figure 5.2** It can be seen that the voltages are all in safe margin between 360 and 440V which is 10% deviation of nominal voltage 400V. In general, the voltage will rise when there is excess power given to the grid (negative power) and drop when power is drawn from the grid (positive power). Bus with further distance to the transformer has higher voltage drop or rise compared to the nearer bus due to line impedance.

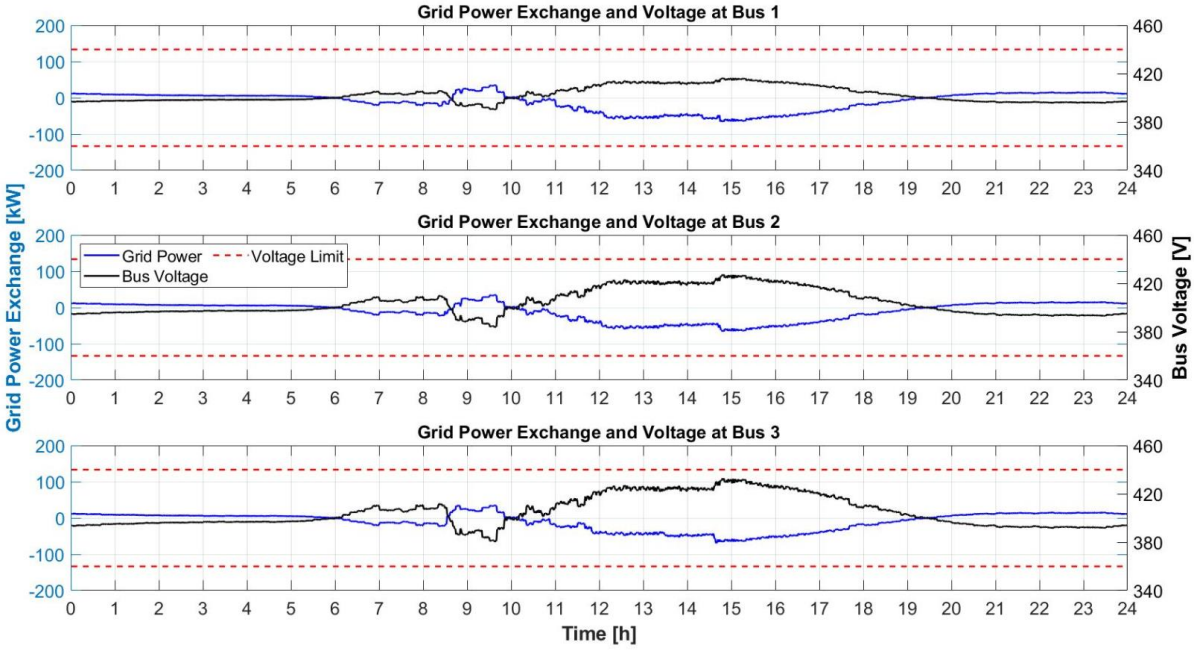

Figure 5.2 Voltage Profile at Different Bus of the System for Case 1A-1 (5 EV, Summer)

In case of 10 and 15 EVs, more power is drawn from the grid to charge the EVs as shown in **Figure 5.3** and **Figure 5.4** respectively. Moreover, in the case of 15 EVs, grid power drawn exceeds the maximum power of the transformer which is 400 kW due to low PV power production in the morning. Furthermore, with the higher EV penetration, higher line losses are generated due to the higher current flowing in the line. Besides exceeding peak transformer capacity, the bus voltage also drops lower than the minimum limit allowed as shown in **Figure 5.5** and **Figure 5.6** correspondingly. This condition occurs because of too many power drawn from the grid during the morning. To tackle these issues, BESS will be introduced to the system in case 1A-2 to reduce the peak power drawn from the grid.

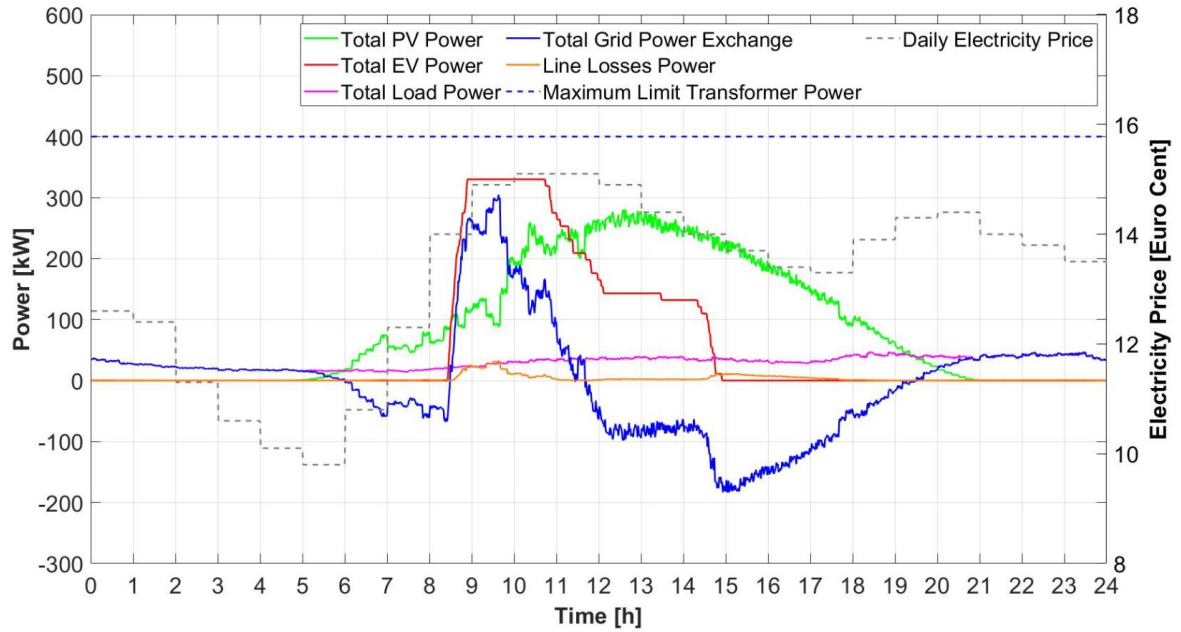

Figure 5.3 Power Exchange Profile of the System for Case 1A-1 (10 EV without BESS, Summer)

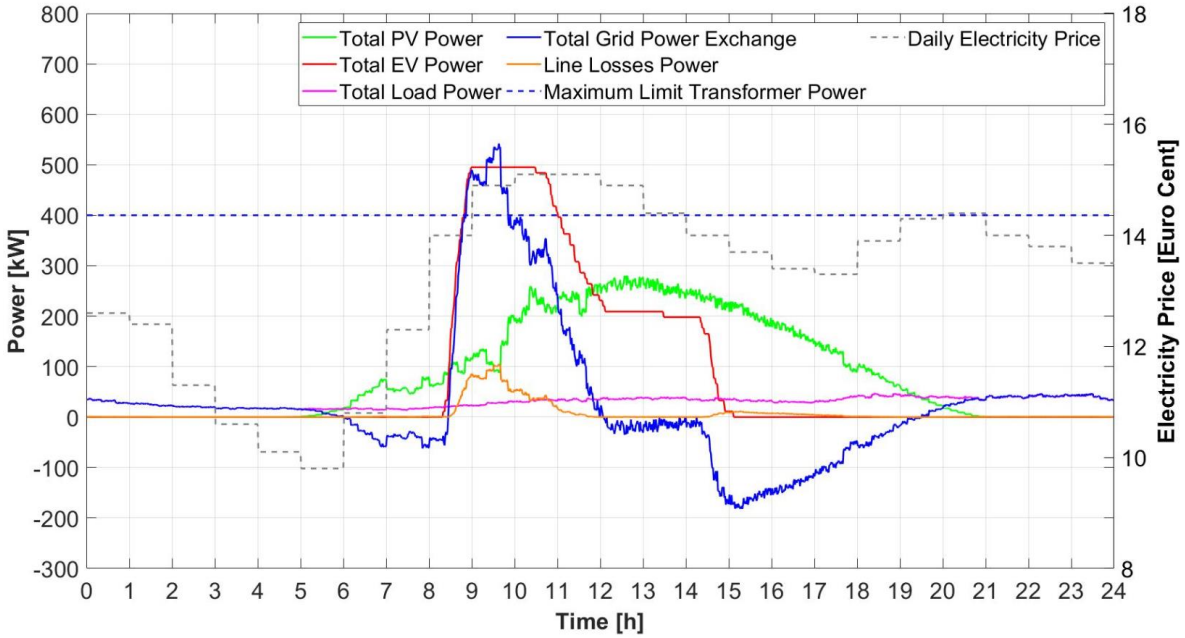

Figure 5.4 Power Exchange Profile of the Overall System for Case 1A-1 (15 EV without BESS, Summer)

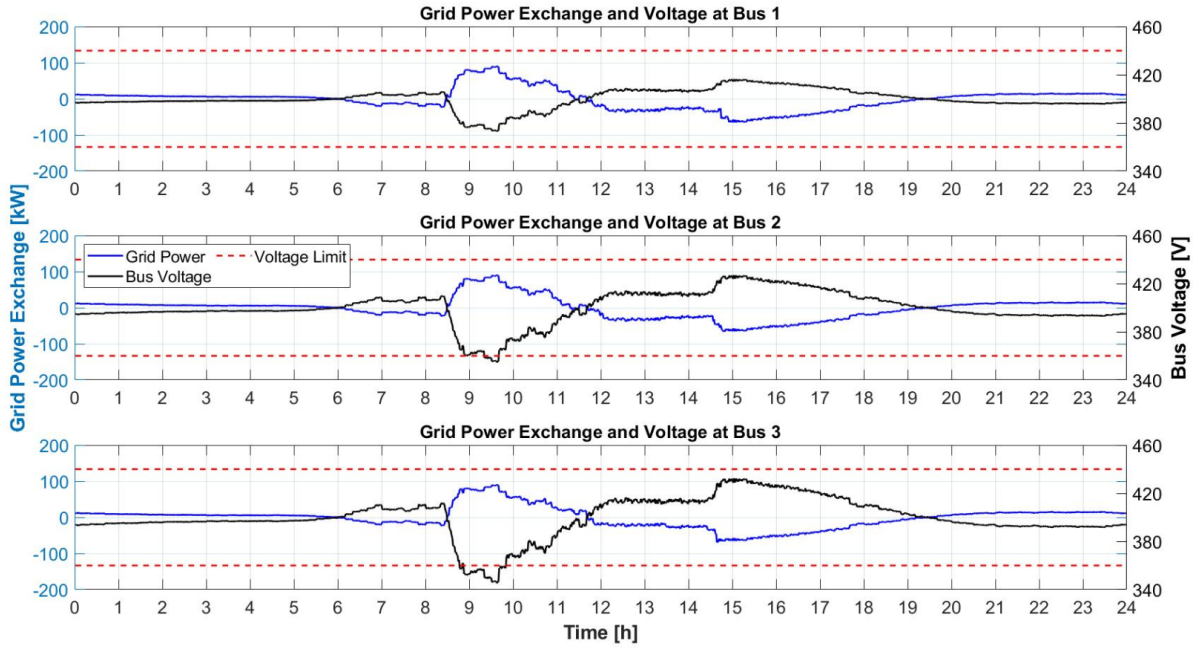

Figure 5.5 Voltage Profile at Different Bus of the System for Case 1A-1 (10 EV without BESS, Summer)

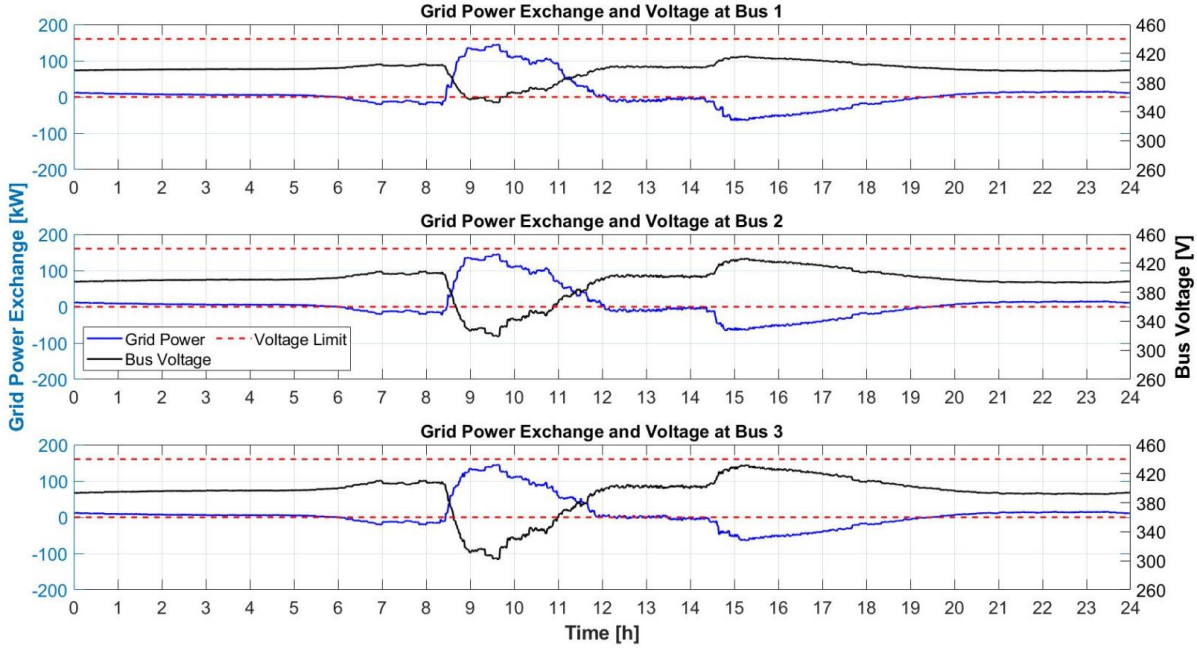

Figure 5.6 Voltage Profile at Different Bus of the System for Case 1A-1 (15 EV without BESS, Summer)

5.1.2 Case 1A-2 (Summer, with BESS)

In this scenario, BESS will be installed in one of the bus in the system to keep the transformer work under its maximum capacity and handle the bus voltage to be in the safe margin allowed. First, in the case of 5 EVs in every node, the same result is given as scenario of case 1A-1, which means no BESS is suggested to be placed in the system. This happens because of the relatively high price of BESS instalment. Since the system does not violate the maximum transformer power and voltage limit as seen in **Figure 5.1** and **Figure 5.2**, BESS will not be suggested to appear in the system, in order to minimize the total cost.

In case of 10 and 15 EVs, BESS is suggested to the system. BESS is assumed to have 30% state of charge remained from the previous day operation. The power management system controls the charging and discharging operation of BESS to satisfy the grid code and also minimize the total cost. **Figure 5.7** and **Figure 5.8** shows the overall exchange power profile for case 10 and 15 EVs with BESS. In the case of 10 EVs, it can be seen that BESS is charged during the lowest electricity price period at 5-6 a.m. The battery is then discharged when the EVs are at the beginning of charging process with spontaneous high power demand, but the PV power production is still considered low. This discharging operation of BESS helps to limit the peak grid power and keep the voltage not to drop lower than 360V as shown in **Figure 5.9** and **Figure 5.10**.

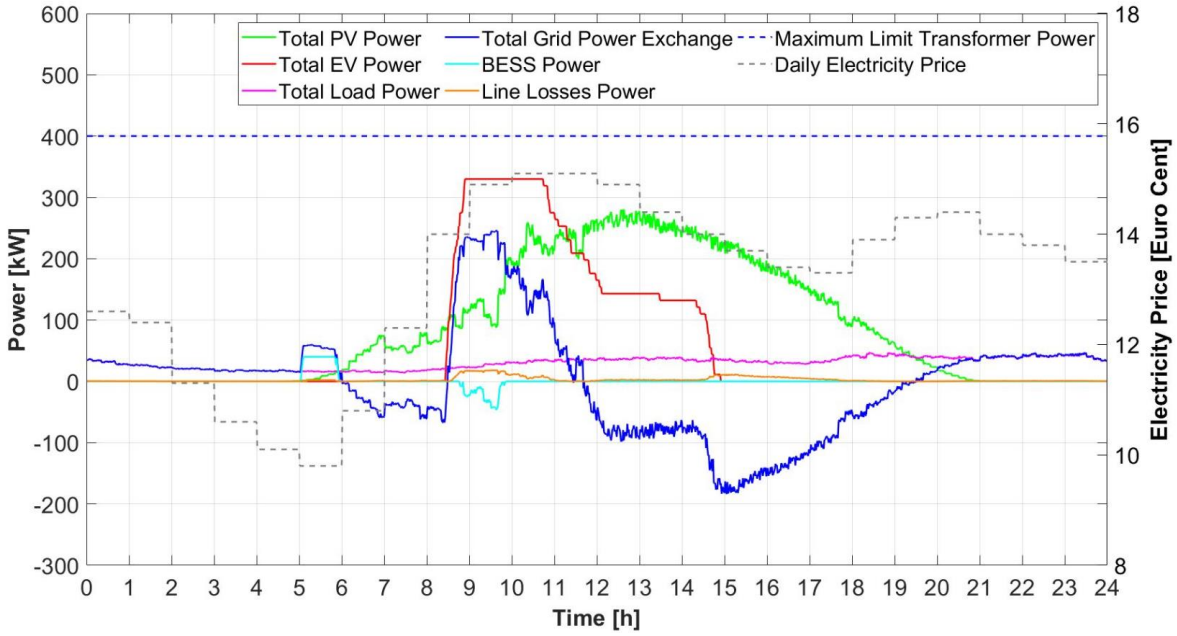

Figure 5.7 Power Exchange Profile of the System for Case 1A-2 (10 EV with BESS, Summer)

In the case of 15 EVs, charging and discharging power of BESS is higher than the case of 10 EVs due to higher power demand for EV charging. BESS spreads its charging time from 4-6 a.m. which are the two lowest electricity price period until it reaches the maximum state of charge allowed of 90%. BESS cannot be charged only during one period of the lowest electricity period (5-6 a.m.) because if this occurs can lead the bus voltage becomes lower than the minimum voltage limit. However, the power management system still manages the BESS to charge more power during the lowest price period to decrease the total cost. Then, BESS is being discharged during the peak power of EV charging until its lowest state of charge permitted of 10%. To maintain the sustainability of BESS operation for following day, BESS is then recharged during the lowest price period again at 5-6 p.m. until its state of charge gains back to 30%, same as the initial value. The BESS state of charge during a day is shown in **Figure 5.11** and **Figure 5.12**. For both 10 and 15 EVs cases, BESS is suggested to be placed in bus three by the solver, which is the furthest bus from the transformer. This is logical since the furthest bus will suffer the highest voltage drop so that the BESS is placed on this bus.

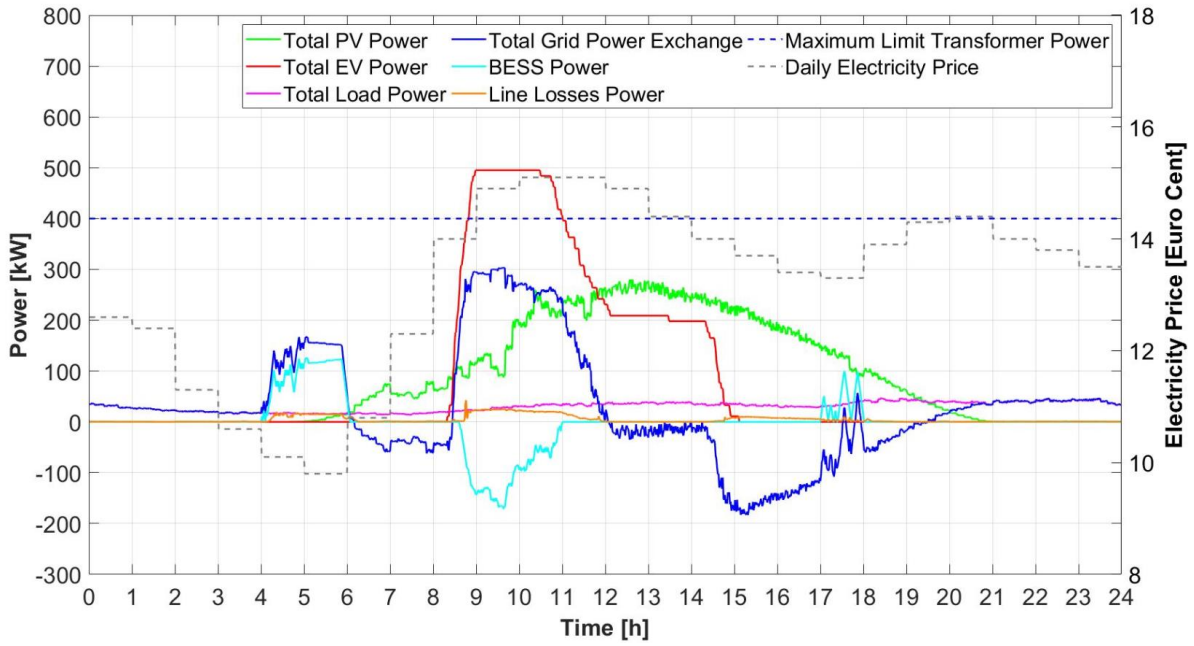

Figure 5.8 Power Exchange Profile of the Overall System for Case 1A-2 (15 EV with BESS, Summer)

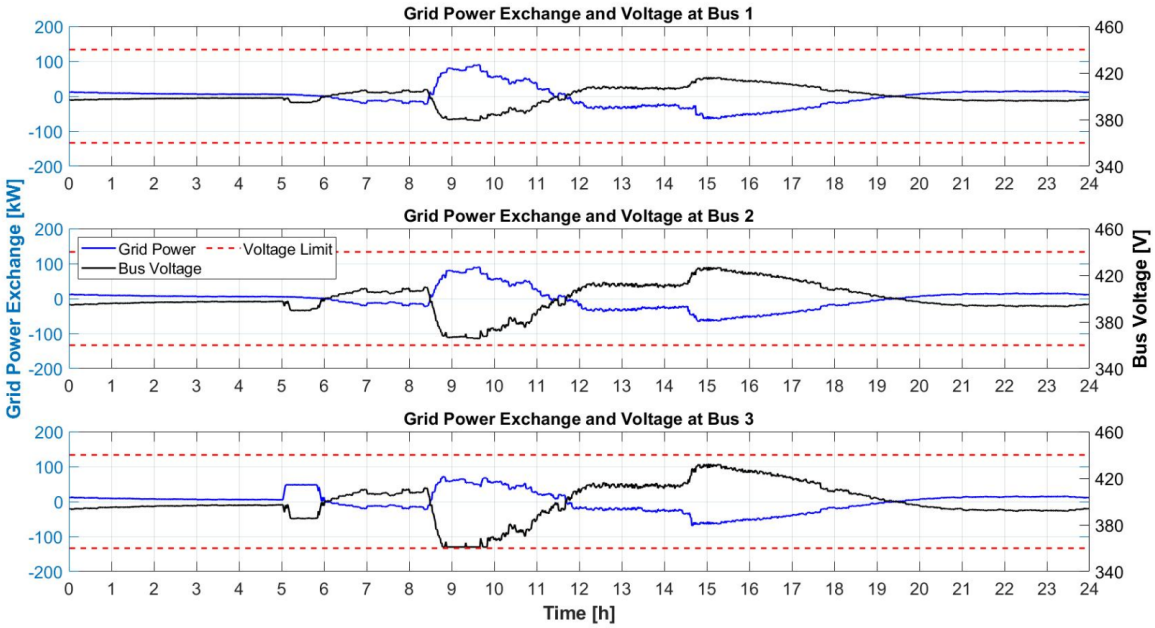

Figure 5.9 Voltage Profile at Different Bus of the System for Case 1A-2 (10 EV with BESS, Summer)

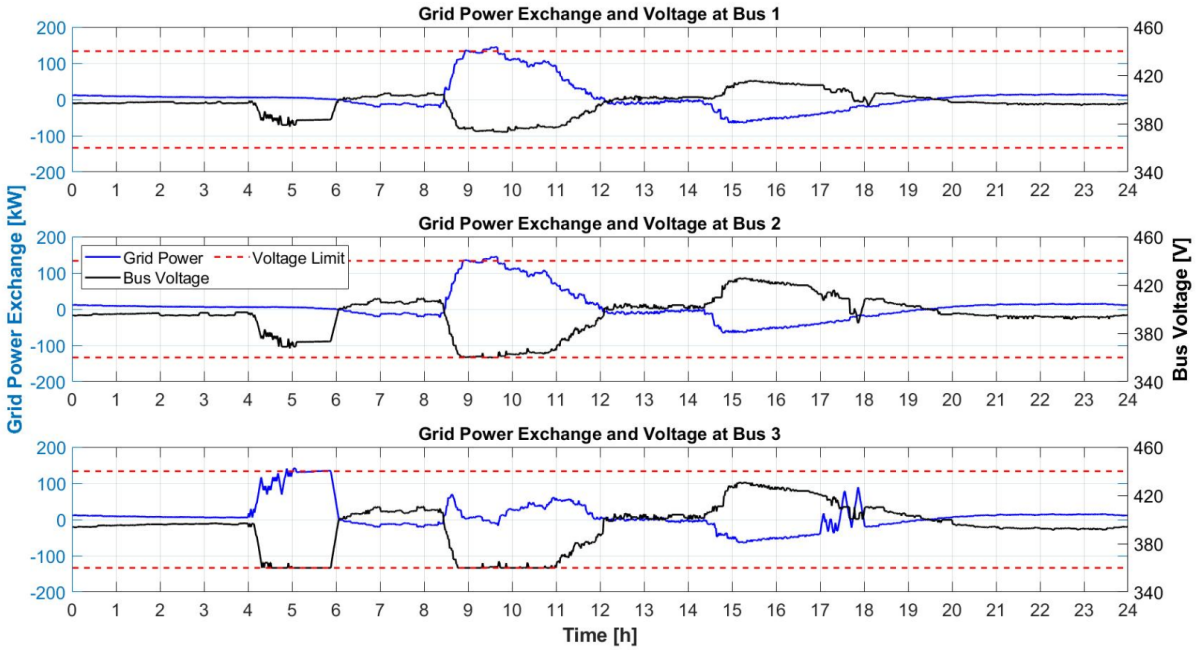

Figure 5.10 Voltage Profile at Different Bus of the System for Case 1A-2 (15 EV with BESS, Summer)

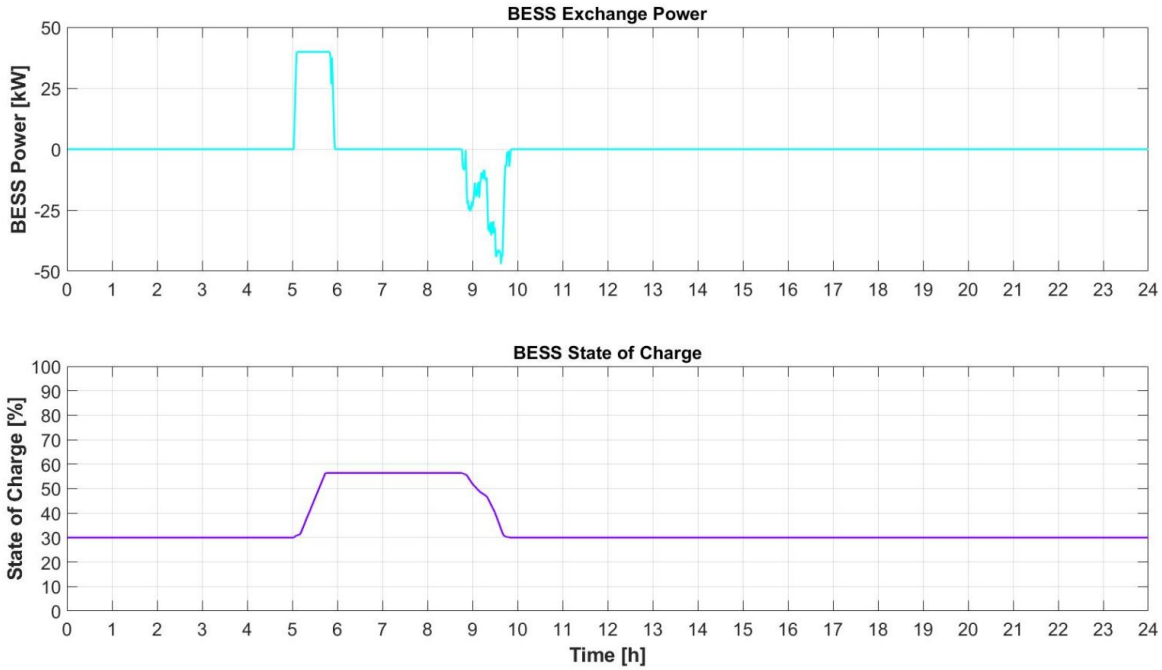

Figure 5.11 BESS Power and State of Charge Profile for Case 1A-2 (10 EV with BESS, Summer)

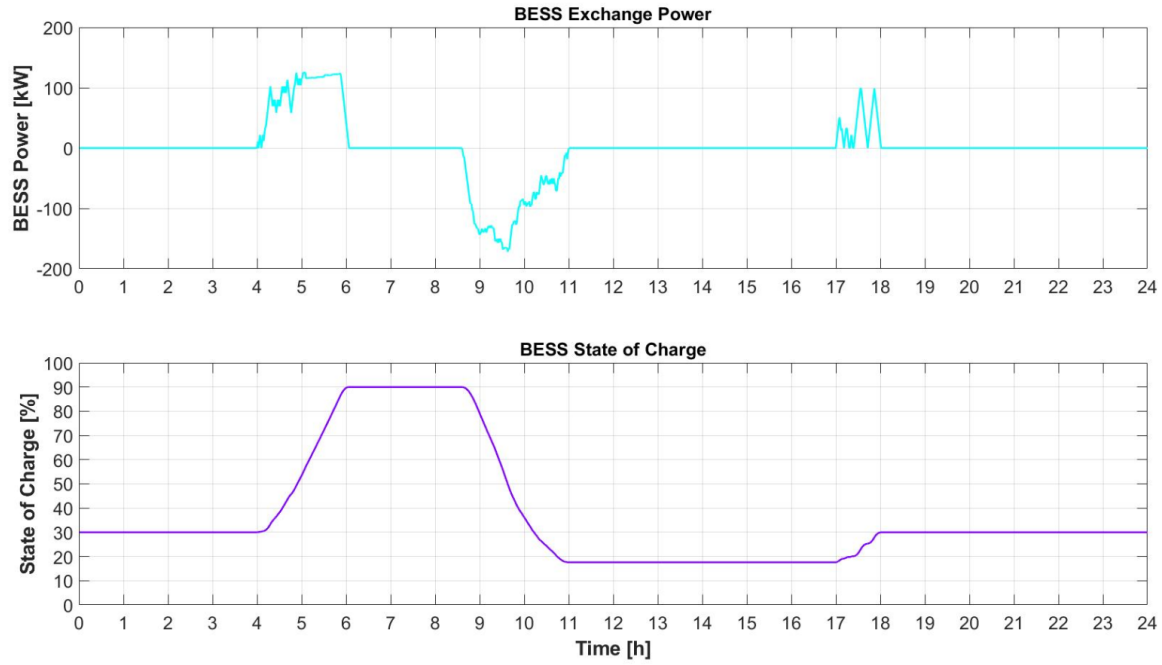

Figure 5.12 BESS Power and State of Charge Profile for Case 1A-2 (15 EV with BESS, Summer)

5.1.3 Case 1B-1 (Winter, without BESS)

During winter, PV power generation is extremely low and even cannot fulfil all the residential load demand during a day. PV produces power in a short period, only from around 8.a.m until 15 p.m. This leads to the excessive amount of grid power is drawn to match the peak EV charging power. However, in the case of 5 EVs per bus, the grid power is still under maximum transformer capacity and no voltage limit is violated as shown in **Figure 5.13** and **Figure 5.14** respectively.

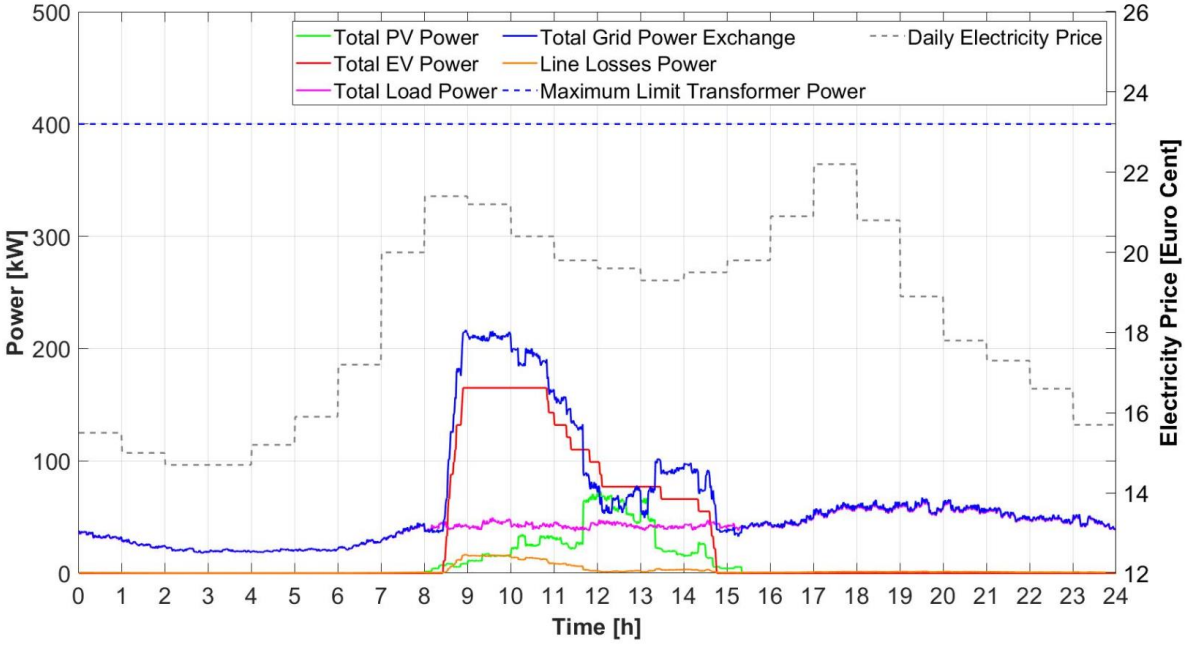

Figure 5.13 Power Exchange Profile of the System for Case 1B-1 (5 EV, Winter)

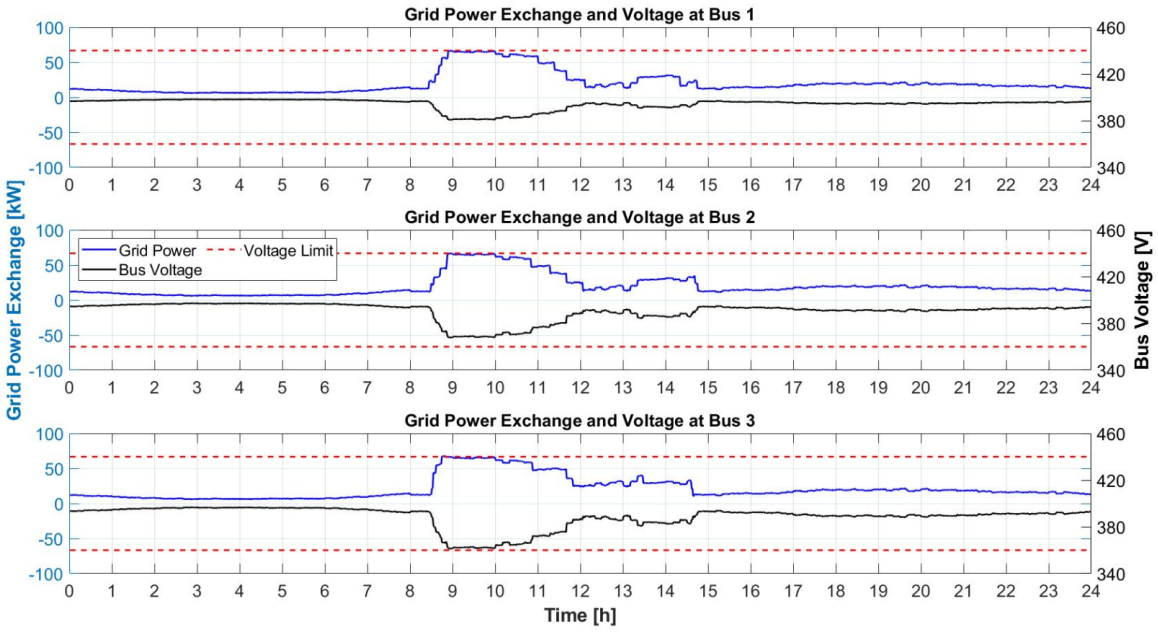

Figure 5.14 Voltage Profile at Different Bus of the System for Case 1B-1 (5 EV, Winter)

In the case of 10 EVs and 15 EVs in every charger station, the peak grid power surpass the transformer limit as illustrated in **Figure 5.15** and **Figure 5.16**. Inefficiency occurs during peak EV charging power period due to high line losses. The bus voltage also goes under minimum voltage allowed as shown in **Figure 5.17** and **Figure 5.18** due to lack of PV power production. Therefore, BESS should be placed to overcome these limitations.

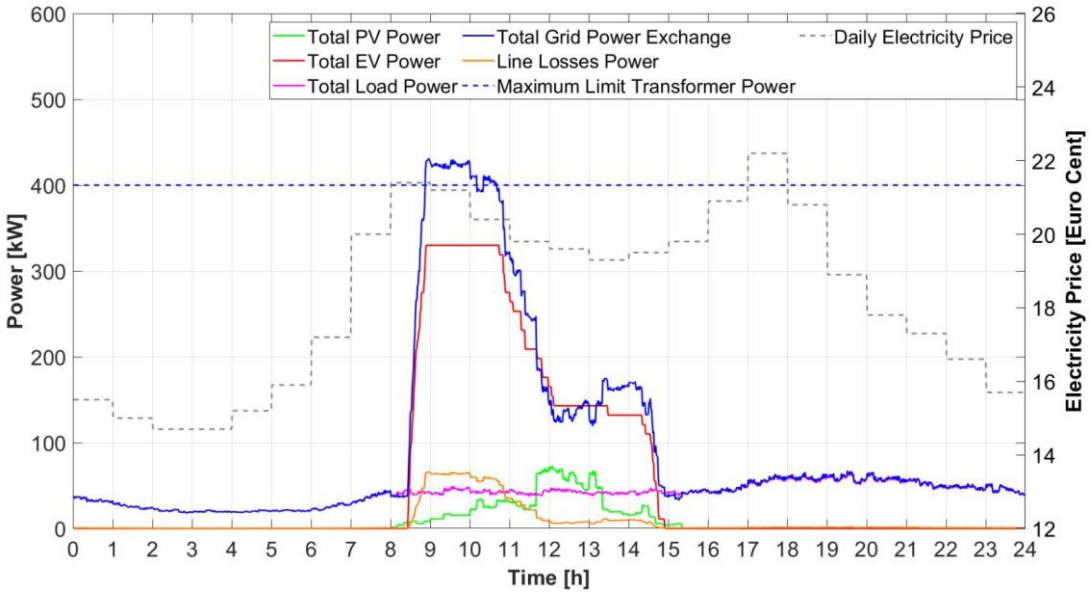

Figure 5.15 Power Exchange Profile of the System for Case 1B-1 (10 EV without BESS, Winter)

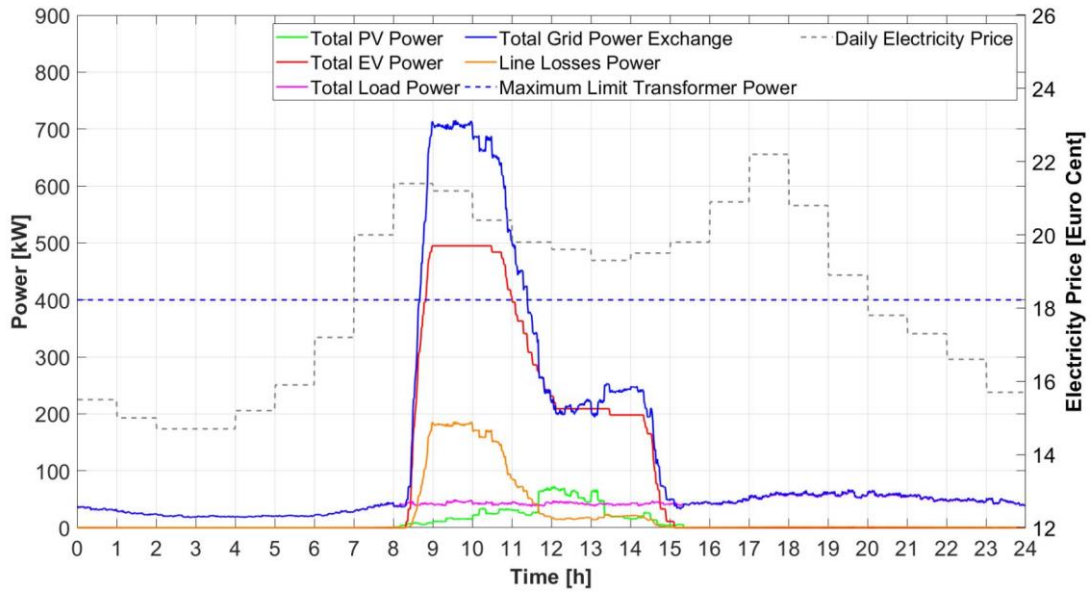

Figure 5.16 Power Exchange Profile of the Overall System for Case 1B-1 (15 EV without BESS, Winter)

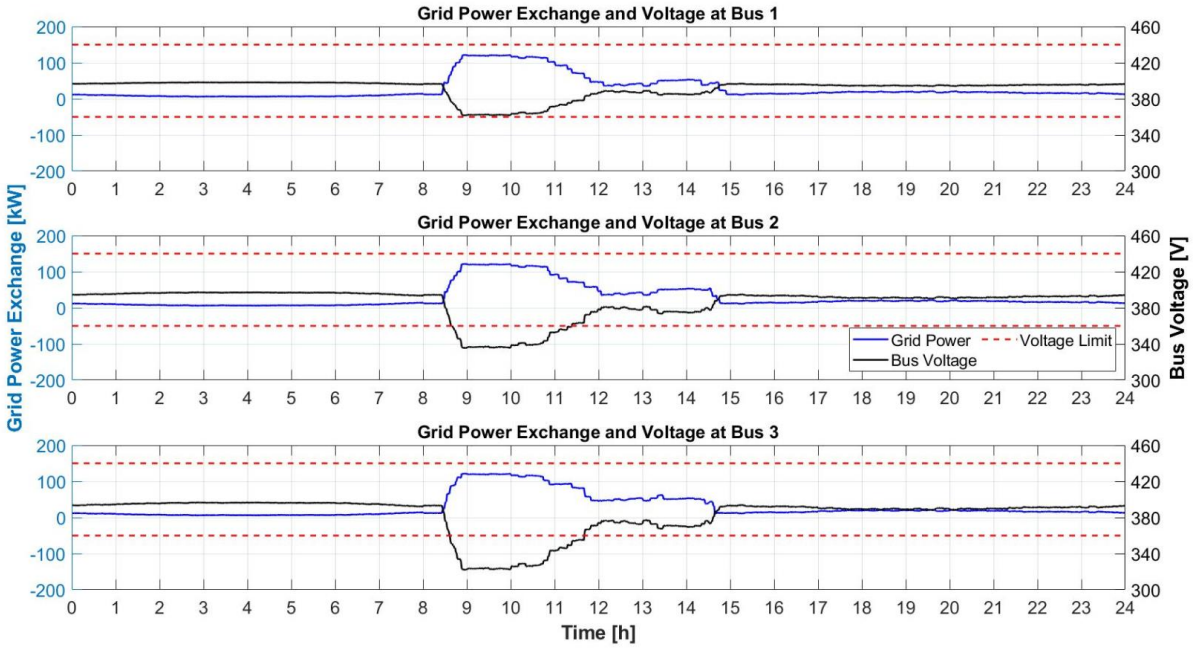

Figure 5.17 Voltage Profile at Different Bus of the System for Case 1B-1 (10 EV without BESS, Winter)

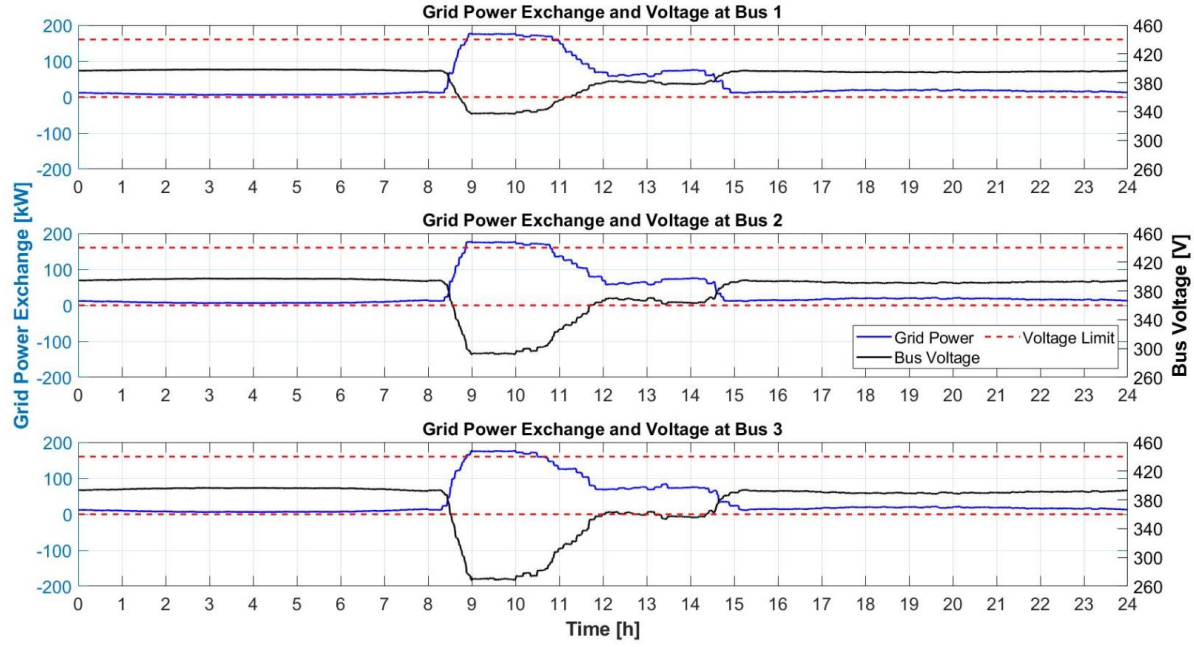

Figure 5.18 Voltage Profile at Different Bus of the System for Case 1B-1 (15 EV without BESS, Winter)

5.1.4 Case 1B-2 (Winter, with BESS)

Similar to case 1A-2, one BESS will be deployed in one of the bus to fix the transformer limit and bus voltage issues. For case only 5 EVs connected to the charger station, no BESS is needed to be installed since the system does not break any grid limitation. The result is the same with no BESS simulation as illustrated **Figure 5.13** and **Figure 5.14**. Different result happens for case 10 EVs where BESS is required by the system as shown in **Figure 5.19**. BESS is charged during the lowest electricity price period during a day which is from 2-4 a.m. until its maximum capacity. Then, BESS is discharged during peak EV charging period to do peak grid power shaving operation, so that the grid power is not exceeding the transformer limit and the bus voltage is not going under the limit as shown in **Figure 5.20**. Last, the power management will manage BESS to be charged during the next lowest electricity period, which is between 11-12 p.m., so the BESS bounces back to its initial state of charge as shown in **Figure 5.21.**

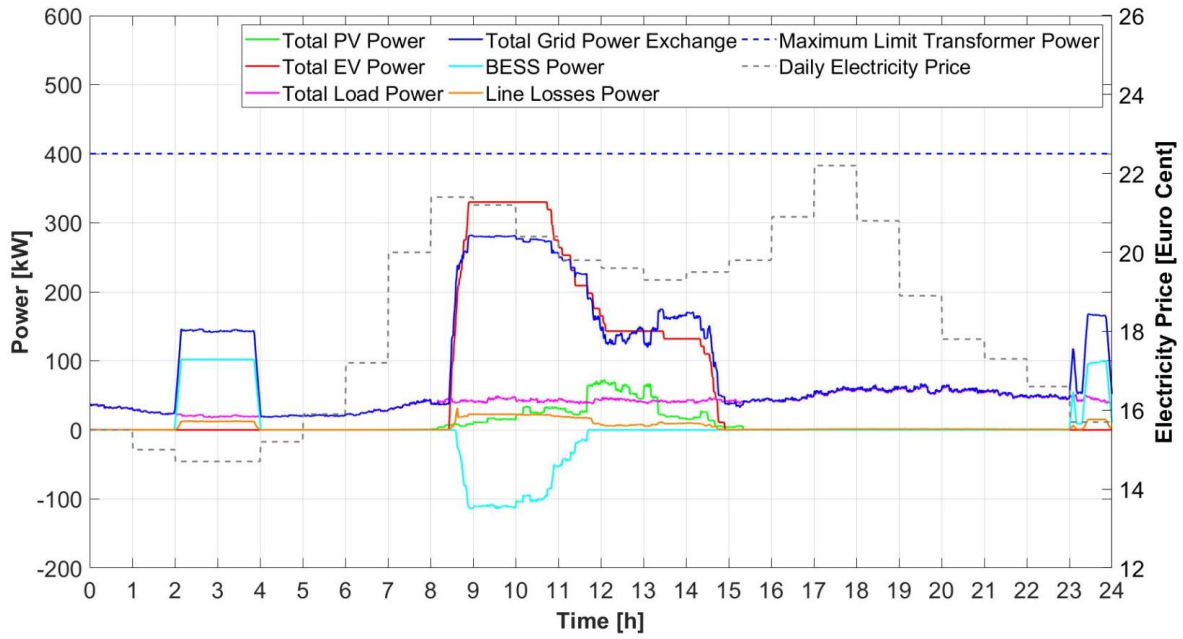

Figure 5.19 Power Exchange Profile of the System for Case 1B-2 (10 EV with BESS, Winter)

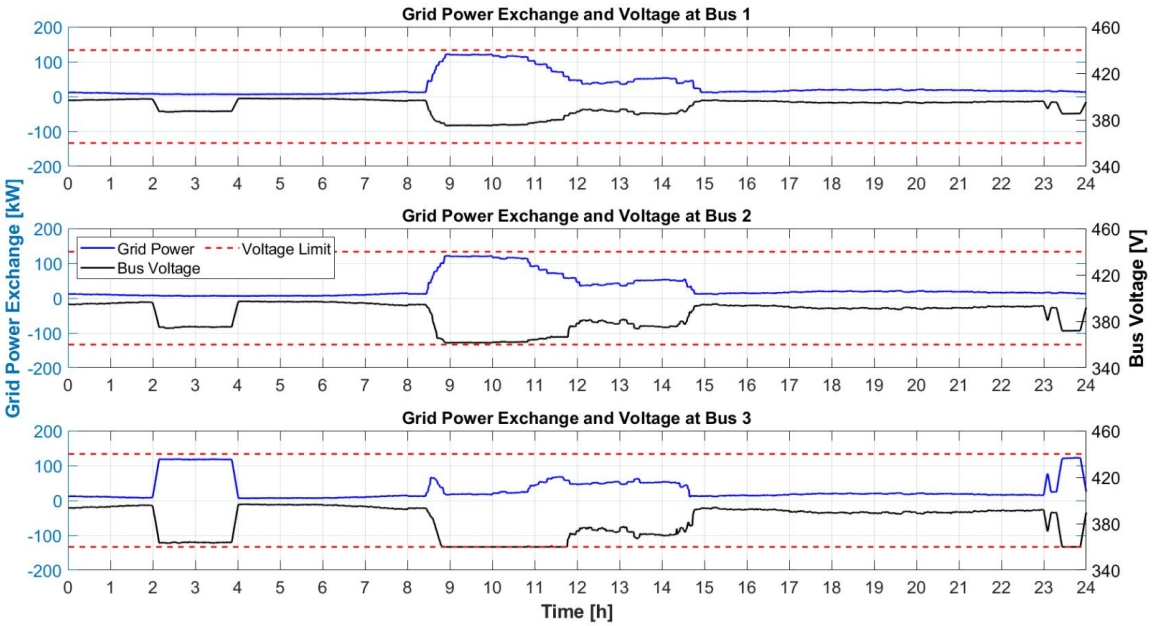

Figure 5.20 Voltage Profile at Different Bus of the System for Case 1B-2 (10 EV with BESS, Winter)

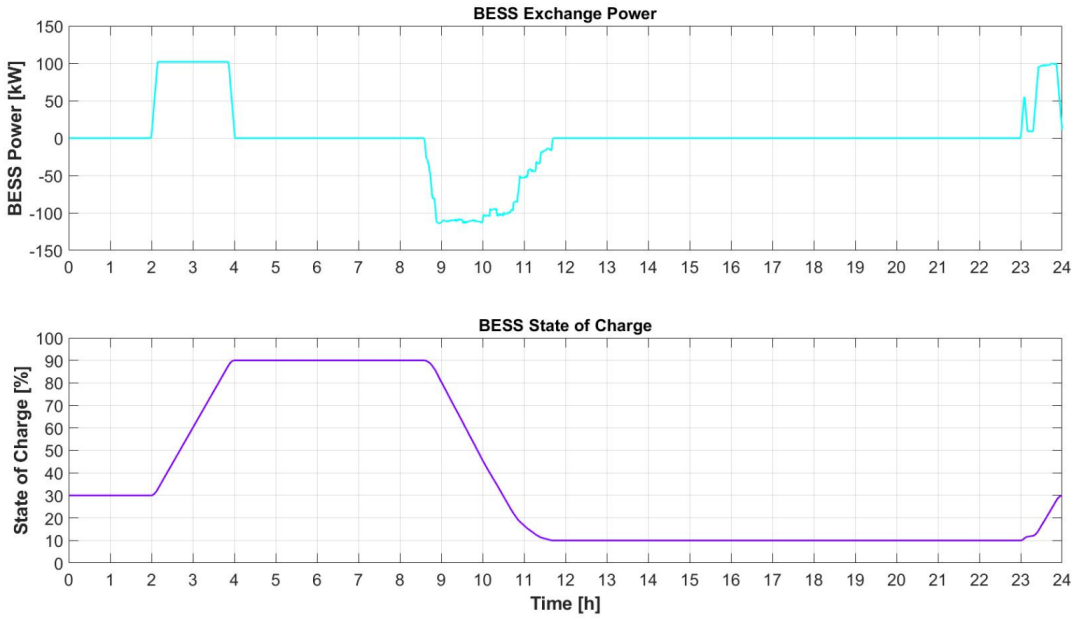

Figure 5.21 BESS Power and State of Charge Profile for Case 1B-2 (10 EV with BESS, Winter)

In the case of 15 EVs, the longer charging period is required by BESS to mitigate the grid violation during EV charging process as shown in **Figure 5.22**. BESS charging process expands from 12 a.m. to 5 a.m. which is the lowest price period to buy electricity from the grid. However, the power management system prioritizes BESS to be charged during the cheapest period and only take a small amount of power when the electricity price is slightly higher from 12 a.m. to 1 a.m. BESS is then being discharged at most all of the time during EV charging period due to very low PV power generation. Nevertheless, BESS still takes a

small amount of power to charge itself during the peak PV power period when the amount of required grid power does not lead to voltage violation. Then similar to the case of 10 EVs, BESS is charged again during the next low price period to prepare for the next day operation. Unlike the case of 10 EVs, BESS needs to spread its second charging time not only at the cheapest period, due to maximum grid power that can be drawn to ensure that the bus voltage limit is not surpassed. The bus voltage profile and BESS state of charge during a day are presented in **Figure 5.23** and **Figure 5.24.**

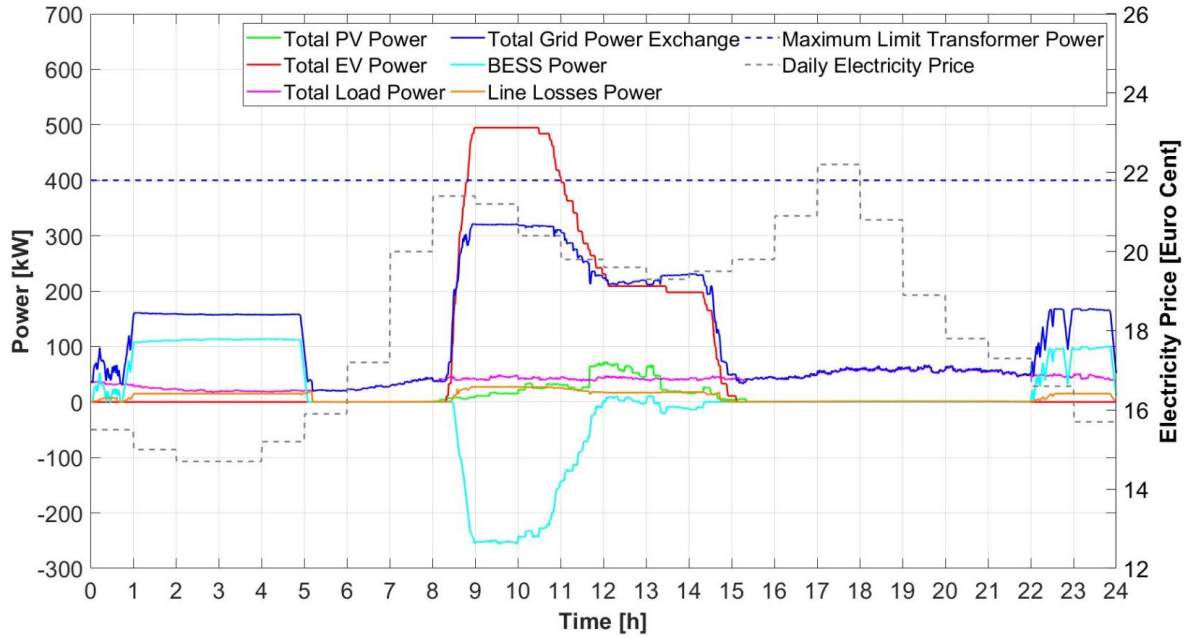

Figure 5.22 Power Exchange Profile of the Overall System for Case 1B-2 (15 EV with BESS, Winter)

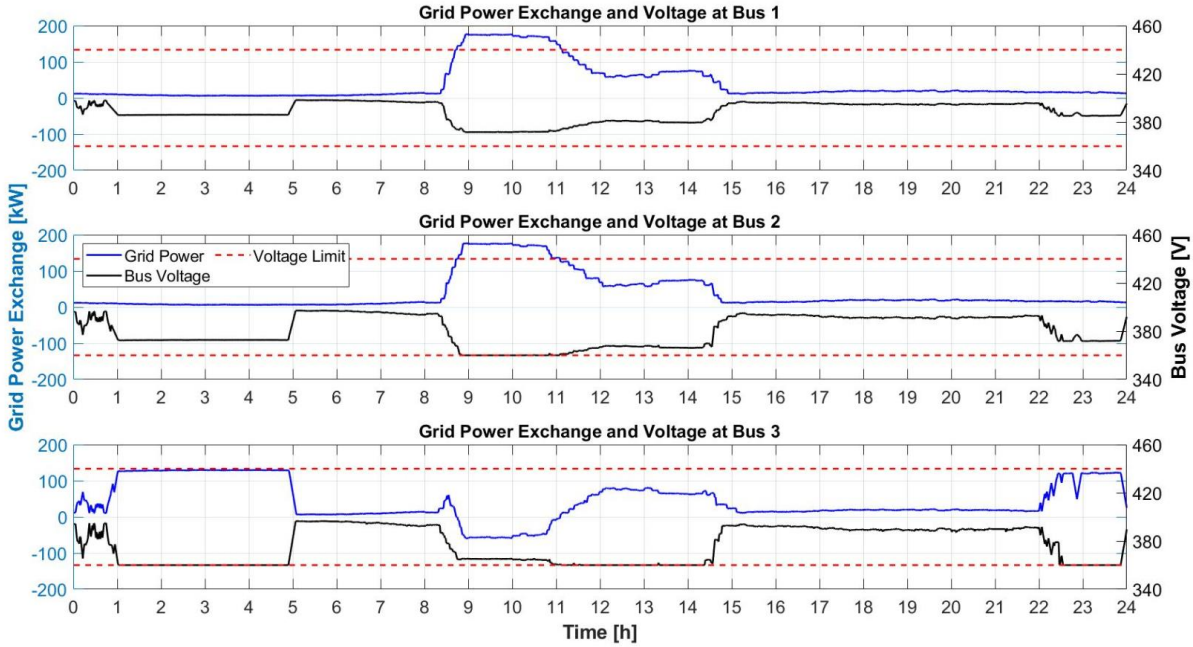

Figure 5.23 Voltage Profile at Different Bus of the System for Case 1B-2 (15 EV with BESS, Winter)

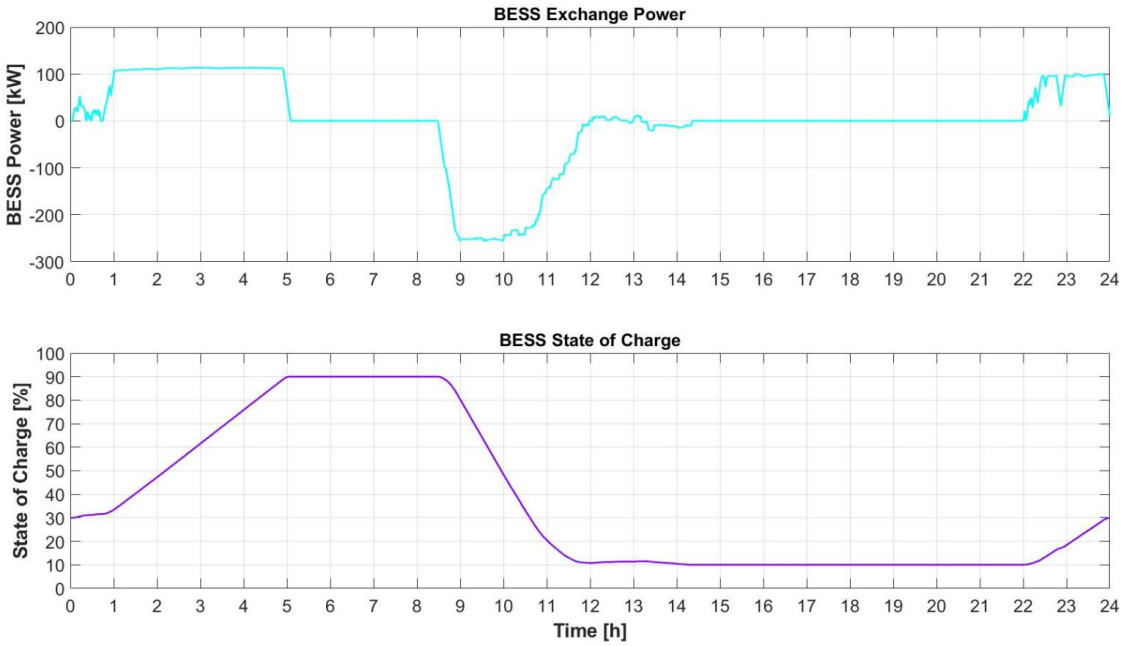

Figure 5.24 BESS Power and State of Charge Profile for Case 1B-2 (15 EV with BESS, Winter)

5.1.5 Case 1C-1 (Autumn, without BESS)

Performance of the proposed power management system is also examined during season autumn, which is transition from summer to the winter season. In general, PV power profile of autumn is around 60% compared to the PV power profile during summer. The sun power starts kick-in from around 7 a.m. to 6 p.m. Similar to summer condition, there is a mismatch between EV charging power profile with the peak of PV power period as shown in **Figure 5.25** for the case of 5 EVs per bus. Therefore, high amount of power is drawn from the grid during the morning when the PV power is still relatively low. Then PV starts feeding power to the grid when some EVs with lower battery capacity finish their charging duration until the PV power production goes down again at late afternoon. Similar to the case of 5 EVs in two previous seasons discussed before, the bus voltage is still in between the safe margin allowed during a day as shown in **Figure 5.26**.

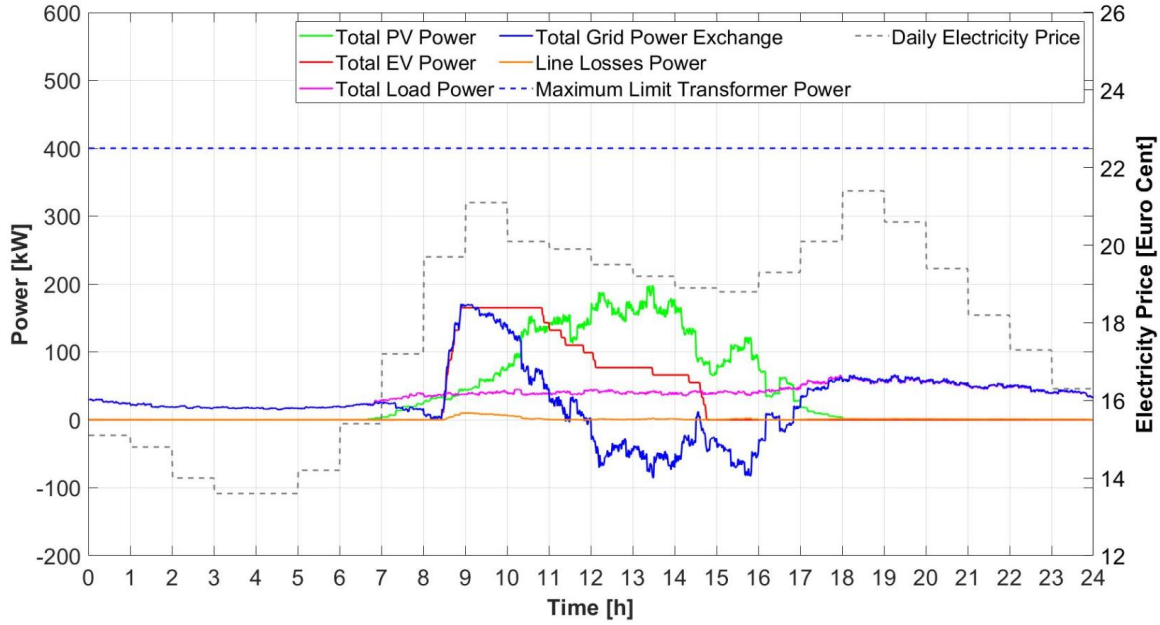

Figure 5.25 Power Exchange Profile of the System for Case 1C-1 (5 EV, Autumn)

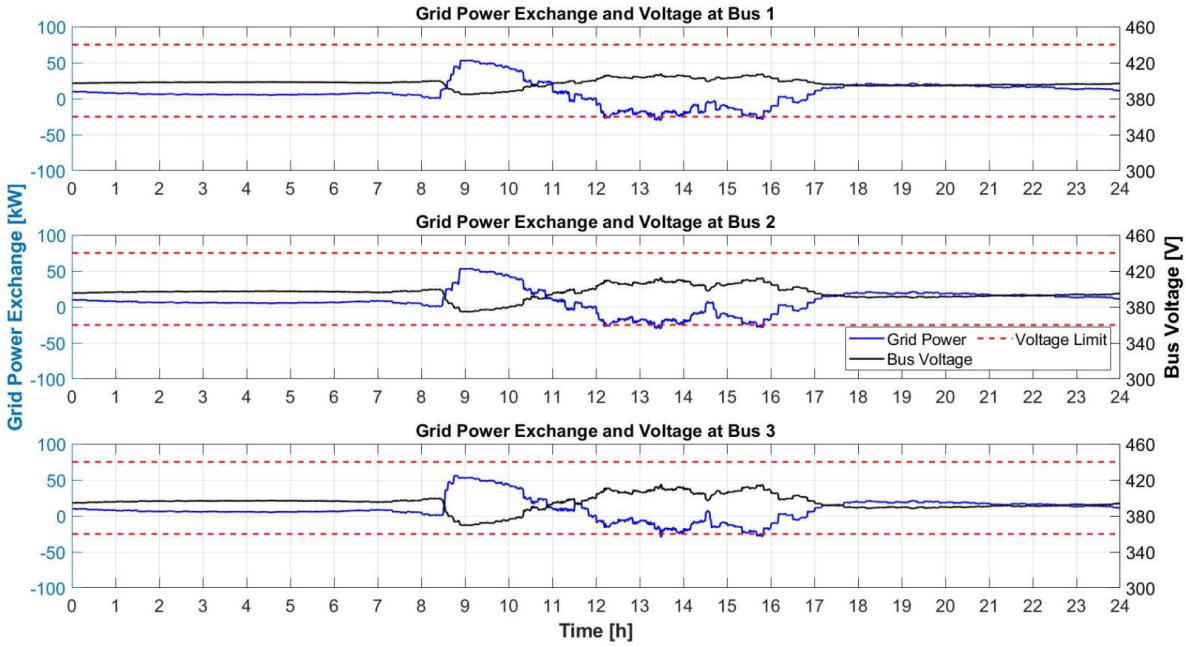

Figure 5.26 Voltage Profile at Different Bus of the System for Case 1C-1 (5 EV, Autumn)

For the scenario of 10 EVs, peak power drawn from the grid is still below maximum transformer capacity, while the bus voltage is already violated due to mismatch PV power production with EV charging period as shown in **Figure 5.27** and **Figure 5.28**. At the beginning of EV charging process, high amount of grid power is necessary to satisfy the load demand until some of EVs with large battery capacity remains. Then, after all, EVs are finished to be charged, PV gives extra power from residential load demand to the grid as revenue until the PV power is not enough to fulfil the load demand.

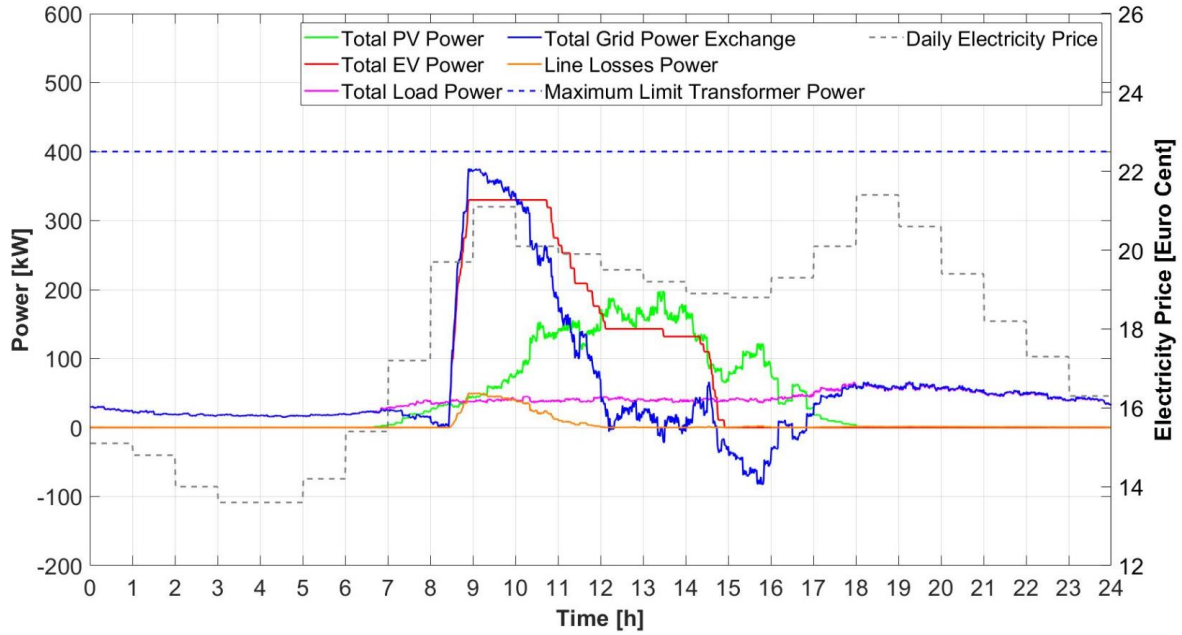

Figure 5.27 Power Exchange Profile of the System for Case 1C-1 (10 EV without BESS, Autumn)

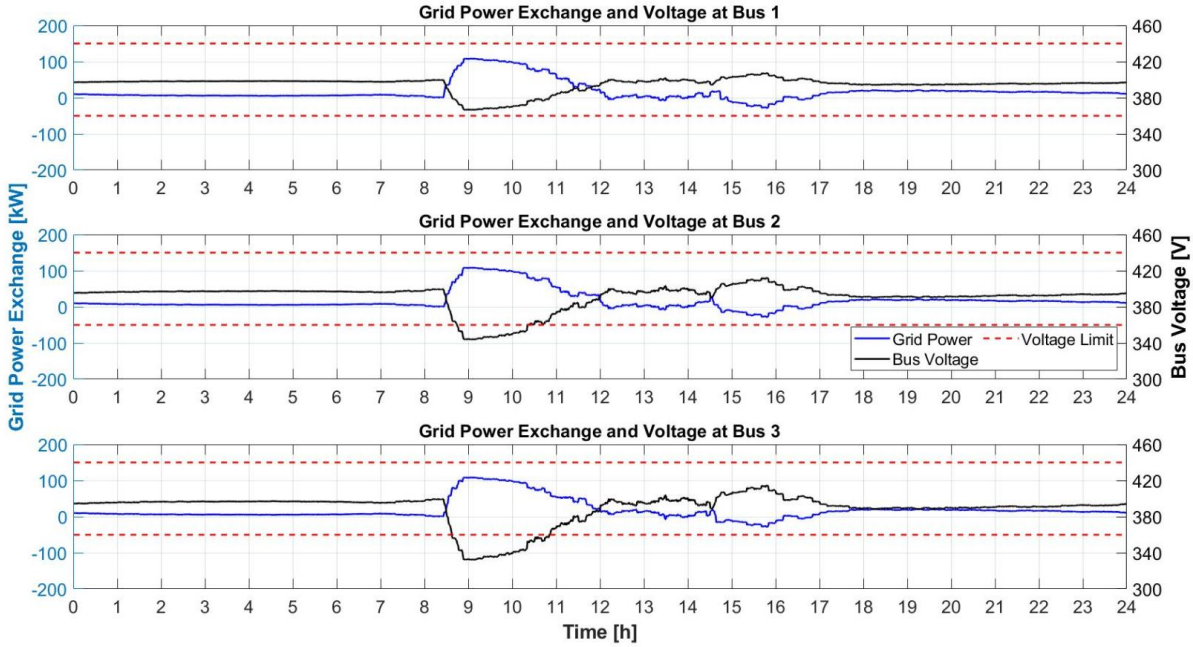

Figure 5.28 Voltage Profile at Different Bus of the System for Case 1C-1 (10 EV without BESS, Autumn)

In the case of 15 EVs per node, maximum power transformer capacity is exceeded during peak EV charging period as presented in **Figure 5.29**. Besides, high losses also occur due to a large amount of current is flowing in the transmission line to supply EV charging power needs. Furthermore, the bus voltage experience more severe condition compared to the case of 10 EVs due to larger power is drawn from the grid as shown in **Figure 5.30**. Similar to two previous seasons, these problems will be fixed by applying BESS which will be discussed in the next section.

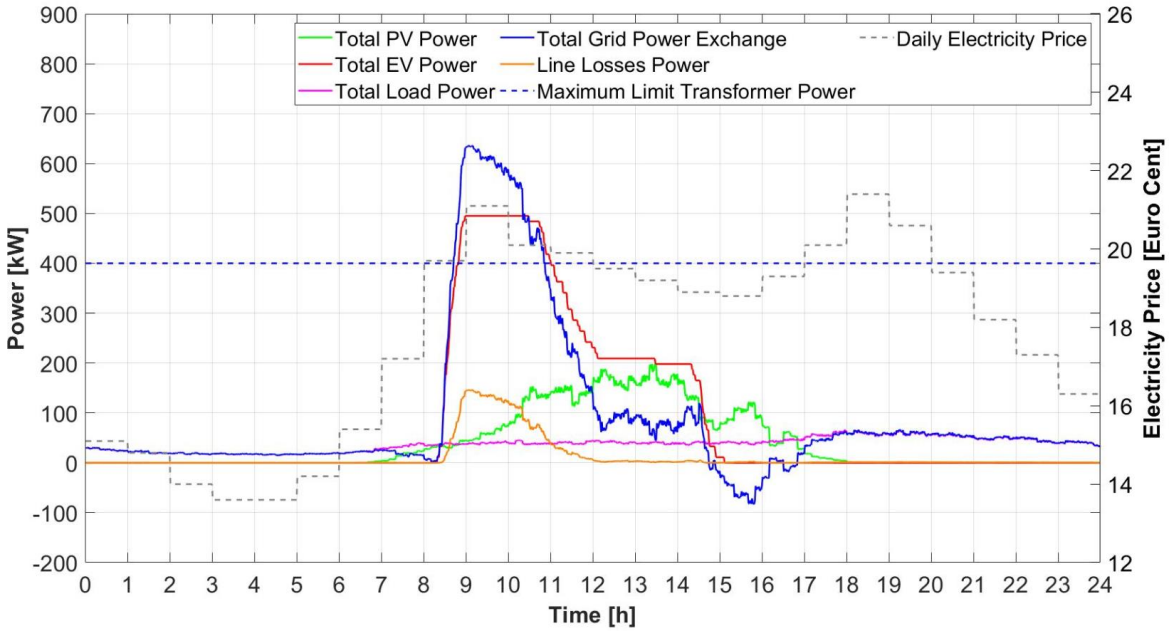

Figure 5.29 Power Exchange Profile of the Overall System for Case 1C-1 (15 EV without BESS, Autumn)

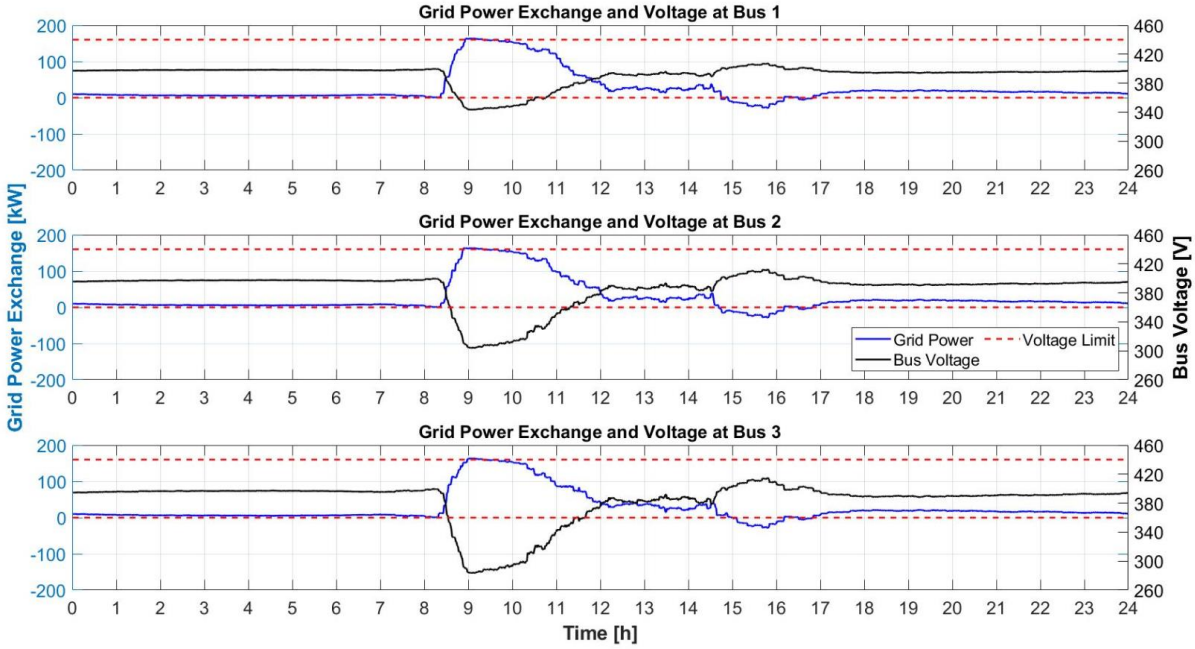

Figure 5.30 Voltage Profile at Different Bus of the System for Case 1C-1 (15 EV without BESS, Autumn)

5.1.6 Case 1C-2 (Autumn, with BESS)

In the case of 5 EVs, no BESS is suggested by the solver, alike with season summer and winter result. It proves that with the given value data of BESS characteristics, it is not economically beneficial to install BESS into the system when no violation occurs. Different from the case of 10 and 15 EVs per node, BESS needs to be installed to resolve the grid problems. Exchange power profile of case 10 EVs in every bus is presented in **Figure 5.31**. Similar to previous simulations of summer and winter, BESS will be charged during the period of lowest electricity price, between 3-5 a.m. until its maximum capacity Then, BESS will be discharged until its lowest capacity during the early period of EV charging, to reduce the grid power stress in the transformer. Last, BESS will be charged again during the next cheapest period until it reaches its initial state of charge. As a result, BESS is successfully managing the bus voltage beyond the minimum voltage limit as illustrated in **Figure 5.32**. Furthermore, the BESS state of charge is presented in **Figure 5.33**.

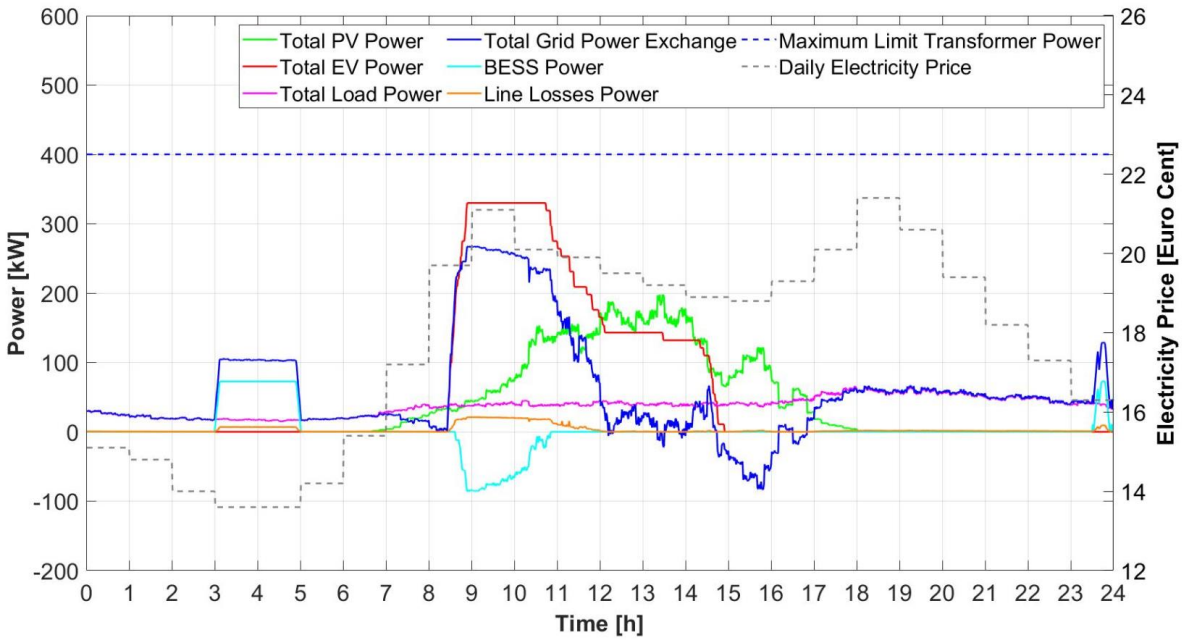

Figure 5.31 Power Exchange Profile of the System for Case 1C-2 (10 EV with BESS, Autumn)

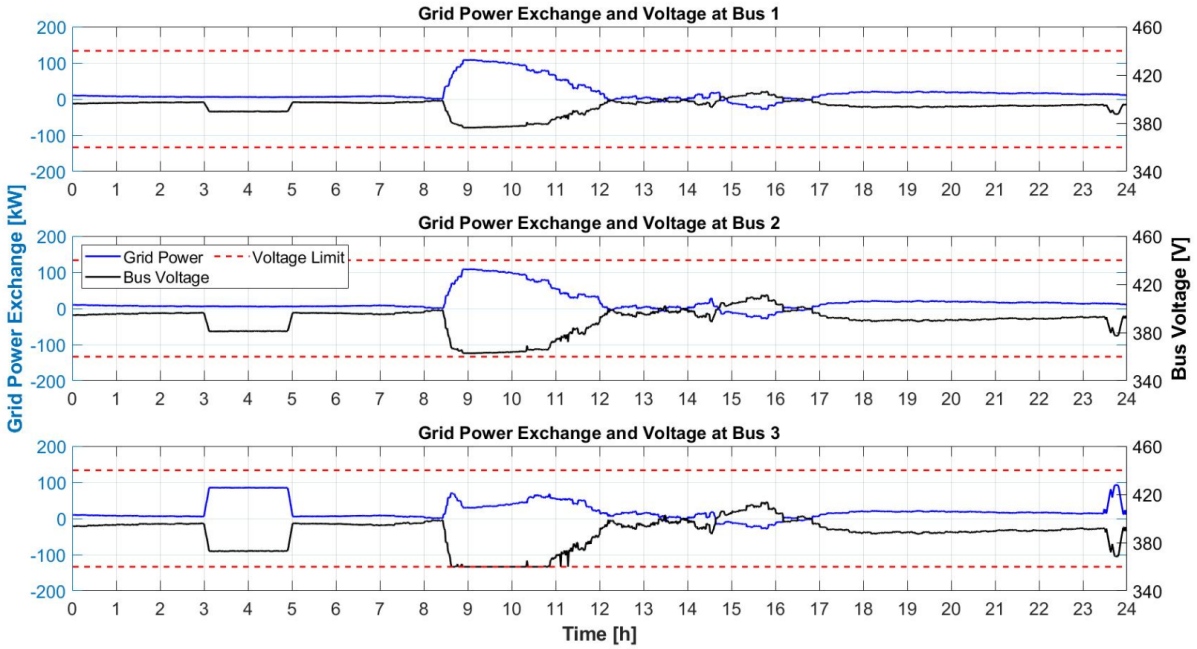

Figure 5.32 Voltage Profile at Different Bus of the System for Case 1C-2 (10 EV with BESS, Autumn)

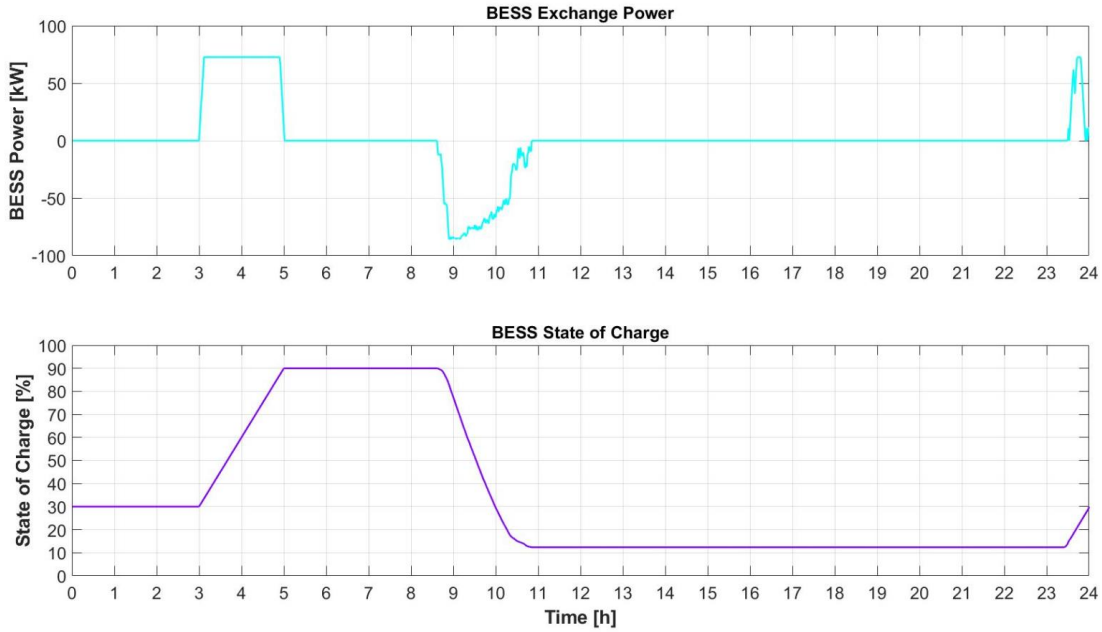

Figure 5.33 BESS Power and State of Charge Profile for Case 1C-2 (10 EV with BESS, Autumn)

In the case of 15 EVs, the same behaviour of BESS occurs in the system as shown in **Figure 5.34**. BESS is charged during low price period until its maximum capacity. Similar to the winter season case, BESS needs to spread its charging period to the second lowest electricity price due to minimum voltage limit. BESS is then discharged during peak EV charging power period to alleviate maximum power needs to be drawn from the grid. Finally, BESS is charged again at the end of the day, when the electricity price is low. The bus voltage and BESS state of charge during a day is presented in **Figure 5.35** and **Figure 5.36**.

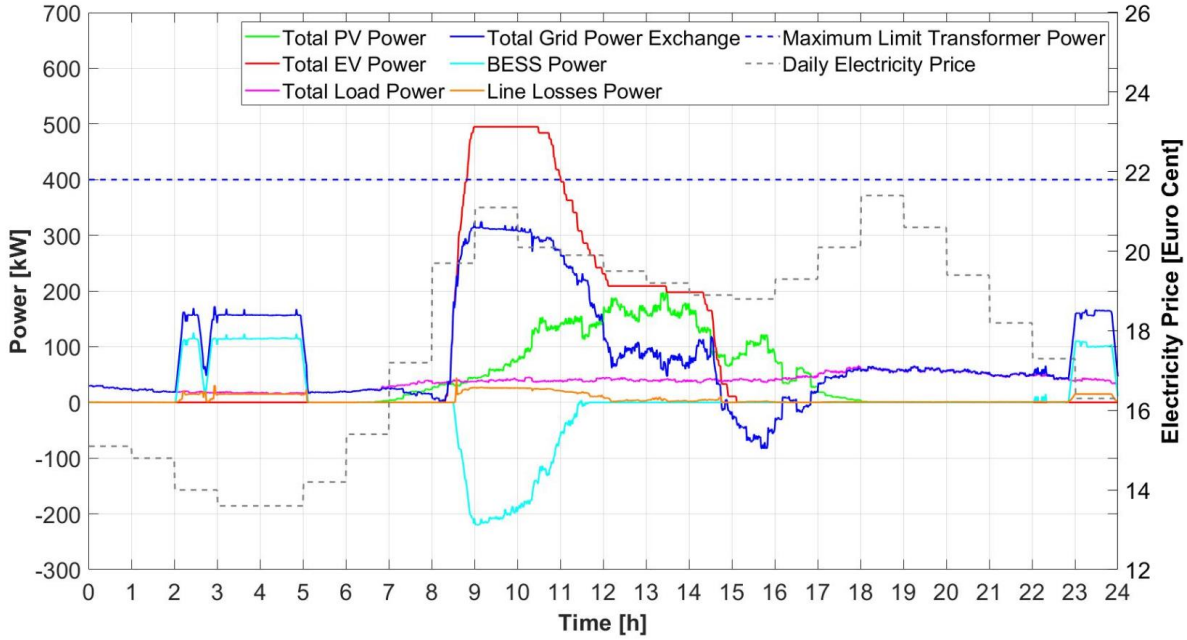

Figure 5.34 Power Exchange Profile of the Overall System for Case 1C-2 (15 EV with BESS, Autumn)

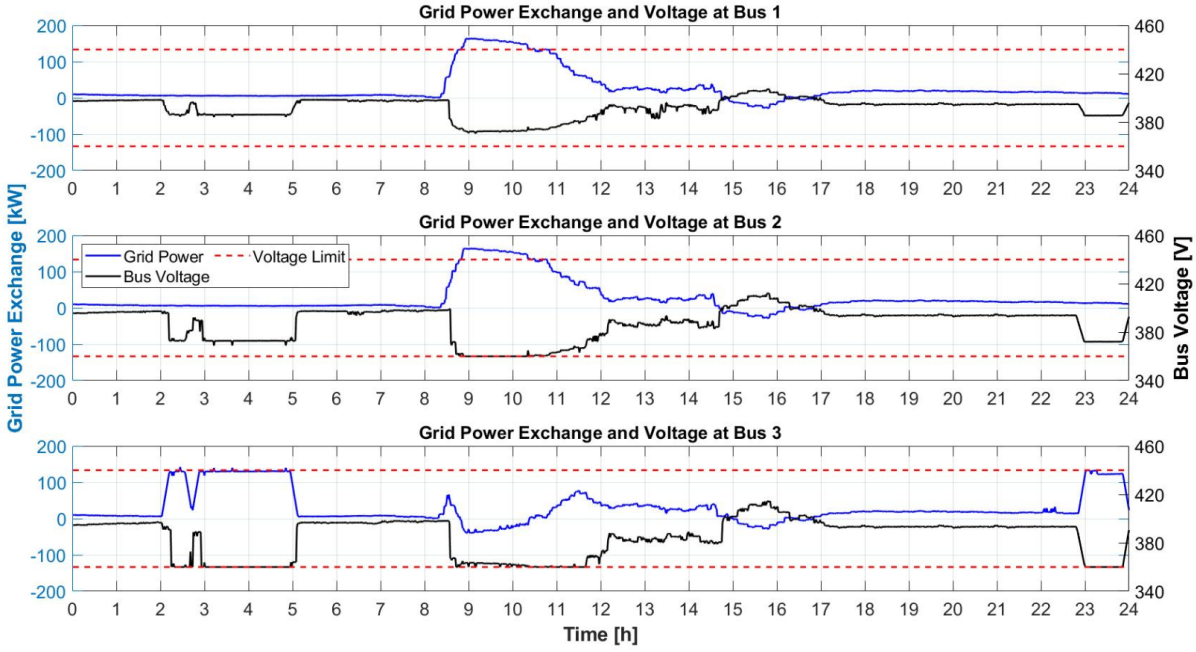

Figure 5.35 Voltage Profile at Different Bus of the System for Case 1C-2 (15 EV with BESS, Autumn)

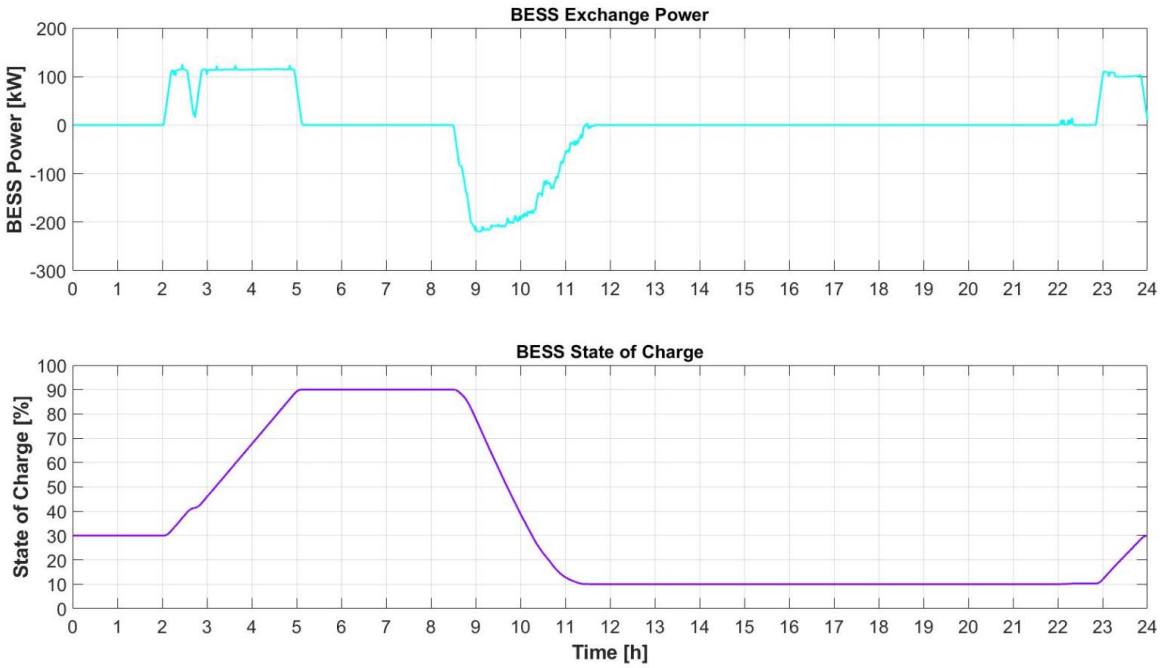

Figure 5.36 BESS Power and State of Charge Profile for Case 1C-2 (15 EV with BESS, Autumn)

5.1.7 Summary

In overall, the proposed power management system has been successfully removed the grid violations occur in the system. In case of low EV penetration, maximum transformer capacity and minimum voltage limit will not be breached and does not promote the urgency of BESS installation due to its relatively high investment cost. When more EVs are charged, more grid power needs to be drawn, and as a result, a high voltage drop occurs in the system. In this situation, BESS is needed to help to reduce the loading of the transformer and at once maintain the bus voltage to be in the safe margin allowed.

For all seasons, BESS has a similar daily operation. First, BESS is charged during the cheapest period which usually happens during the dawn. The period and charging power differ depending on the season and EV number that will be faced. The lower of PV power production and more EVs charged leads to longer and higher charging power of BESS and also with the capacity. Second, BESS is discharged in the beginning period of EV charging when power demand is the highest and PV power production is still relatively low. The discharging process occurs until some of EVs with lower battery capacity finish their charging period. In this time, EV charging power demand is going low, and the combination of PV and grid power is already enough to fulfil the power needs without violating the bus voltage and maximum transformer capacity. During summer and autumn, after all EVs are being charged, PV feeds excess power generation to the grid as revenue until the sun goes down. Last, BESS has recharged again to its initial state charge to prepare for the next day

operation. In winter and autumn, the BESS recharging process occurs at the end of the day when the electricity price is the lowest after discharging period. Different to those two seasons, during summer, the recharging process of BESS happens in the late afternoon, also when the electricity price is low.

Comparison of BESS maximum power and capacity for every seasons and EV penetration is presented in **Figure 5.37** and **Figure 5.38** consecutively. As consequent of very low PV production, operation during winter requires the largest BESS power and capacity to overcome the grid violations, followed by autumn and then summer. This condition leads to higher BESS investment cost as a function of BESS power and energy, illustrated in **Figure 5.39**. The BESS is suggested by the solver to be placed at the end of the feeder as illustrated in **Figure 5.40**. Placing BESS at the furthest bus enables BESS to give direct influence at the bus which suffers the most severe voltage drop. As a result, less BESS size is required compared than locating BESS at different bus.

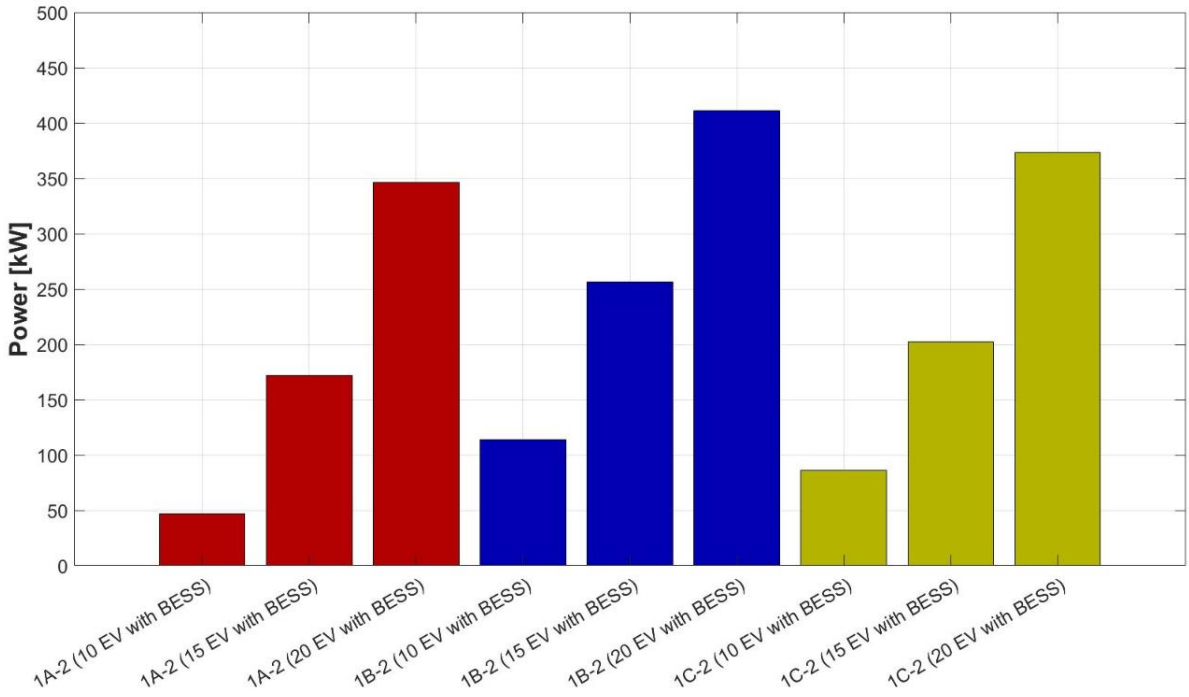

Figure 5.37 BESS Maximum Power for Case 1 (Increasing EV Number)

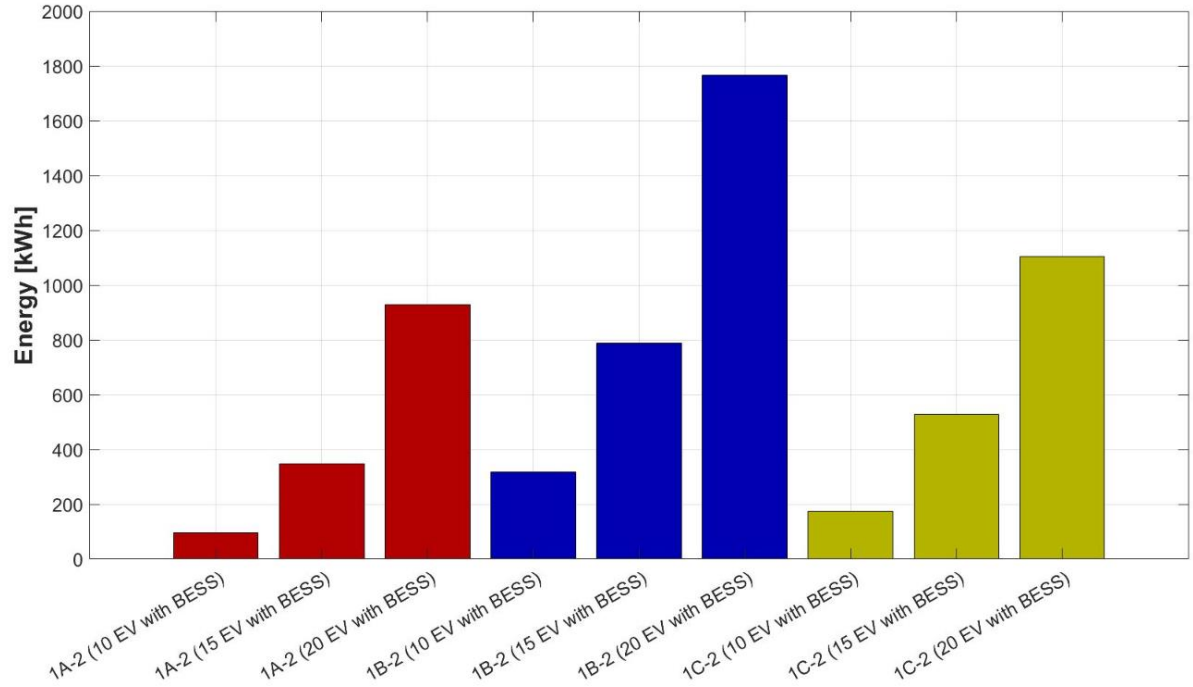

Figure 5.38 BESS Capacity Required for Case 1 (Increasing EV Number)

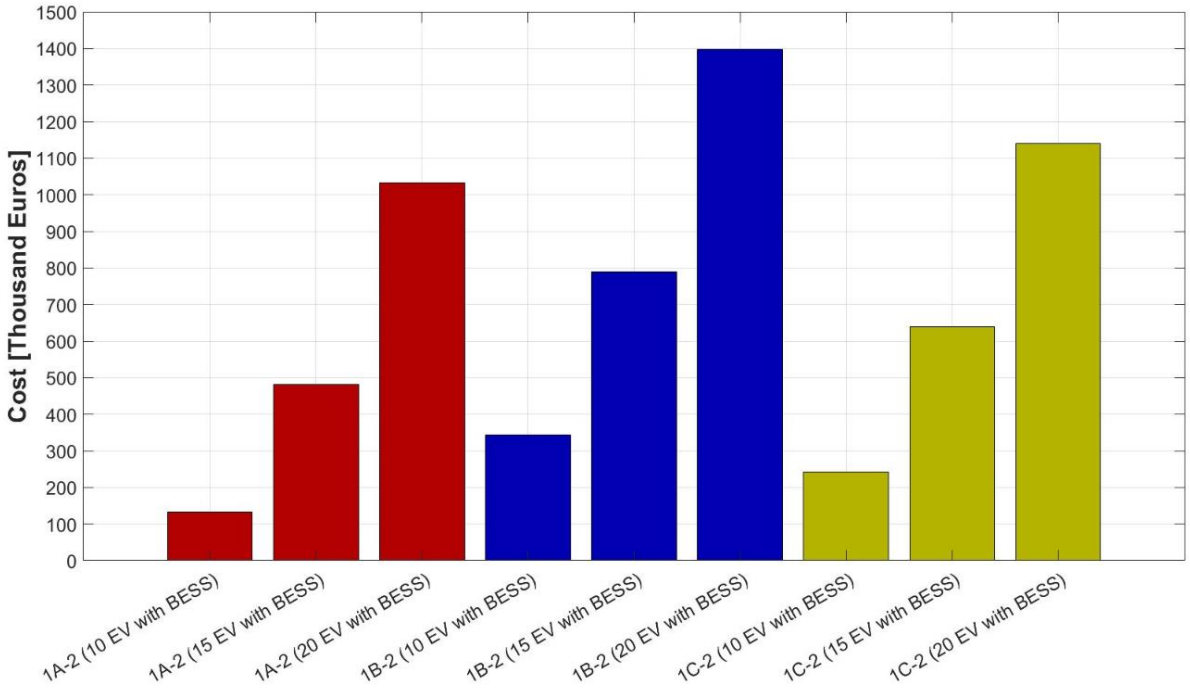

Figure 5.39 BESS Investment Cost for Case 1 (Increasing EV Number)

Furthermore, as mentioned before, one of the benefits of using BESS in the system is a significant reduction of maximum power drawn from the grid. **Figure 5.41** presents the comparison of the transformer loading for every case. By using BESS in the system, the loading of the transformer is maintained below 400 kW. Moreover, electricity bill needs to be paid by buying electricity from the grid is considerably decreased because of BESS installation as shown in **Figure 5.42**. Combination of BESS and optimal power management system manages to buy electricity during the cheapest period for charging process.

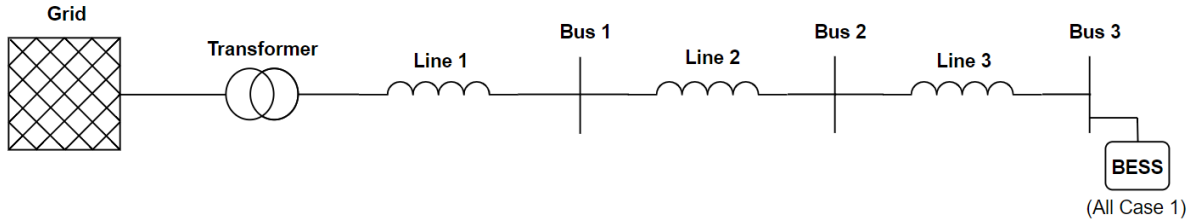

Figure 5.40 Optimal BESS Location for Case 1 (Increasing EV Number)

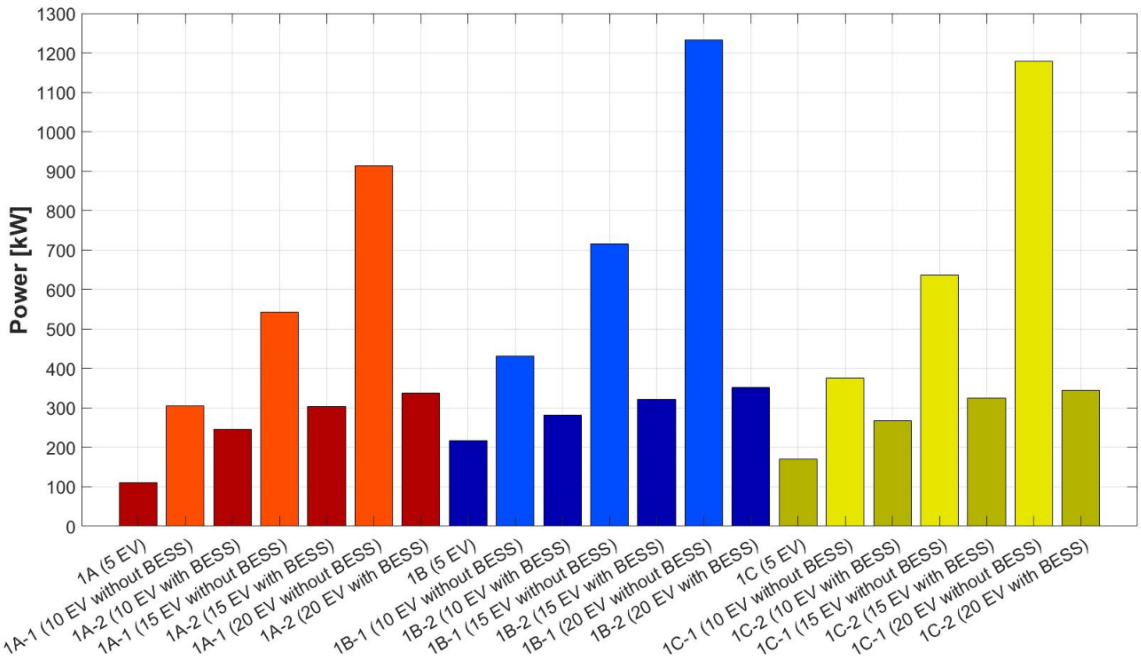

Figure 5.41 Maximum Transformer Loading Power for Case 1 (Increasing EV Number)

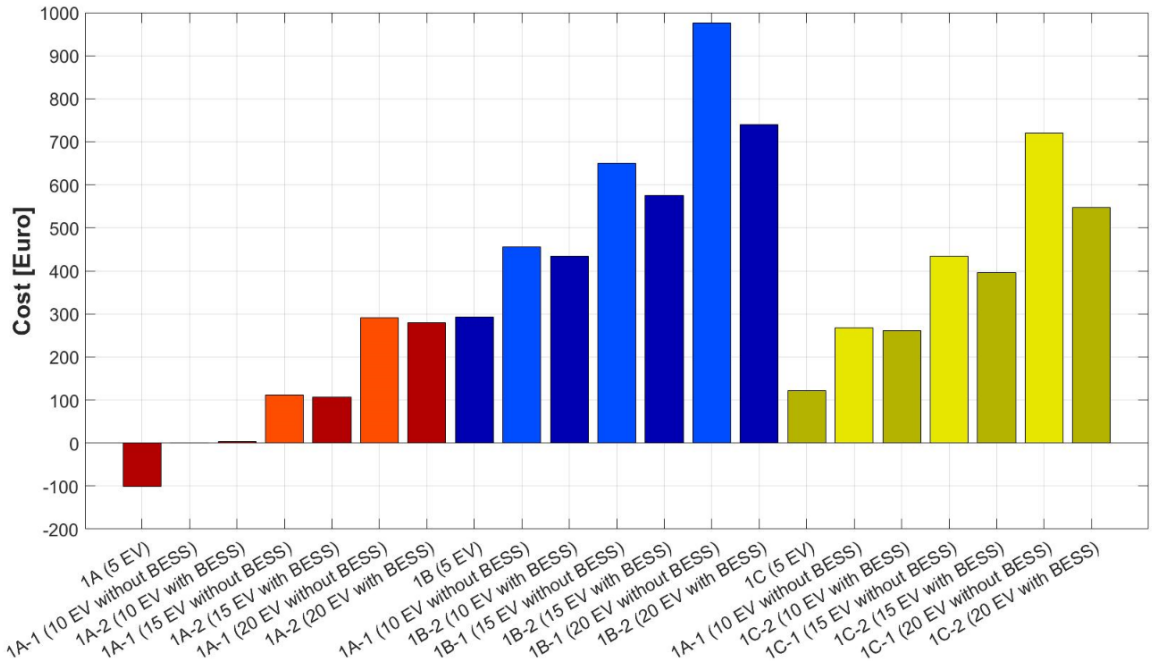

Figure 5.42 Electricity Cost for Case 1 (Increasing EV Number)

Nevertheless, when the electricity cost is combined with the BESS investment, the total cost of the system as illustrated in **Figure 5.43** becomes higher than the case of without BESS application. This condition shows that the gap in electricity cost is not enough to cover the BESS price. More investigation about different pricing scheme will be discussed in section **5.3**.

Furthermore, the comparison of maximum transformer power and bus voltage violation are presented in **Figure 5.44** and **Figure 5.45** respectively. It is noticeable that more violation occurs during season with lower PV power profile. The most important thing is that no violation happens by installing BESS in the system. Furthermore, when number of EVs in the charger station is added up, there is maximum EV number that can be held by installing one BESS in the system as shown in **Figure 5.46**. There is significant increase of EV number that can be held by the system by installing BESS. Besides, more EVs can be connected in the charger station during summer, without violating the grid code compared to autumn and winter because of more PV power is available to charge the EVs.

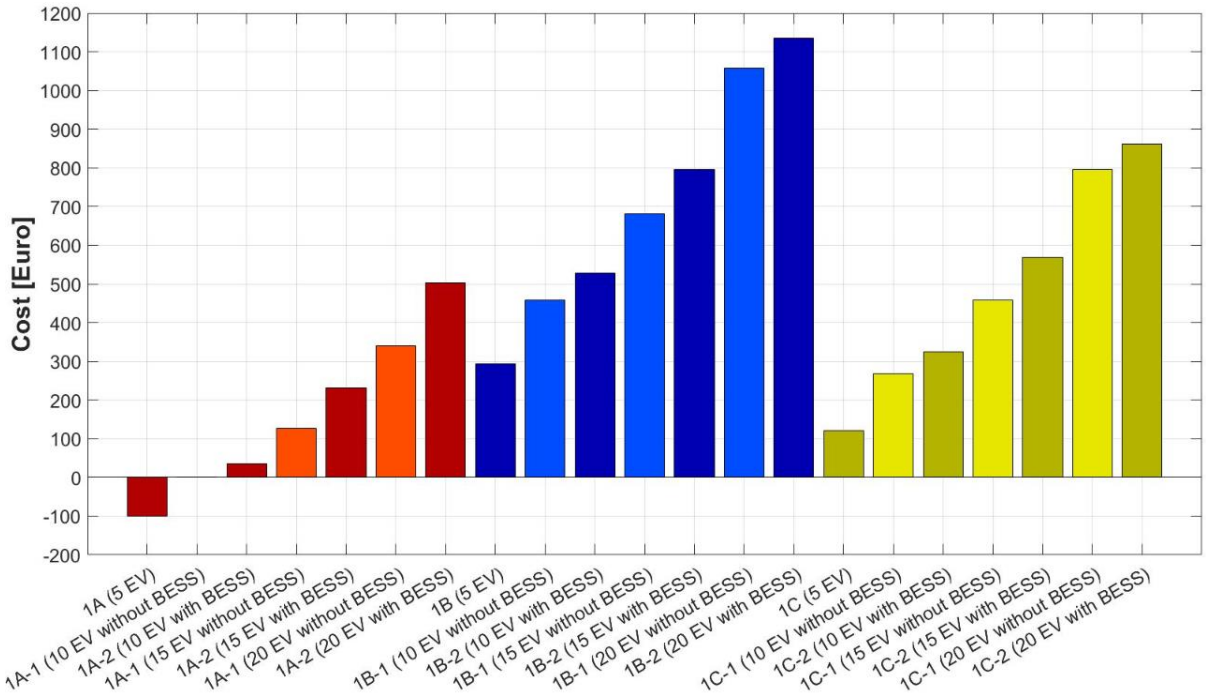

Figure 5.43 Total Cost for Case 1 (Increasing EV Number)

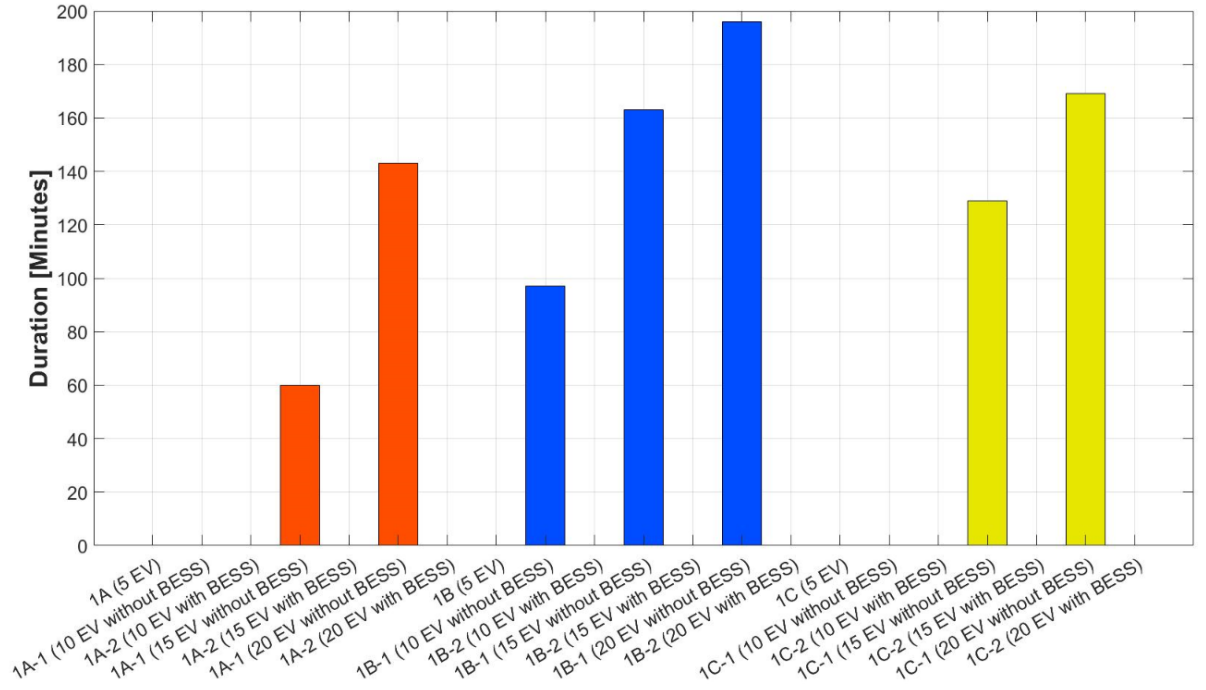

Figure 5.44 Duration of Maximum Transformer Loading Violation for Case 1 (Increasing EV Number)

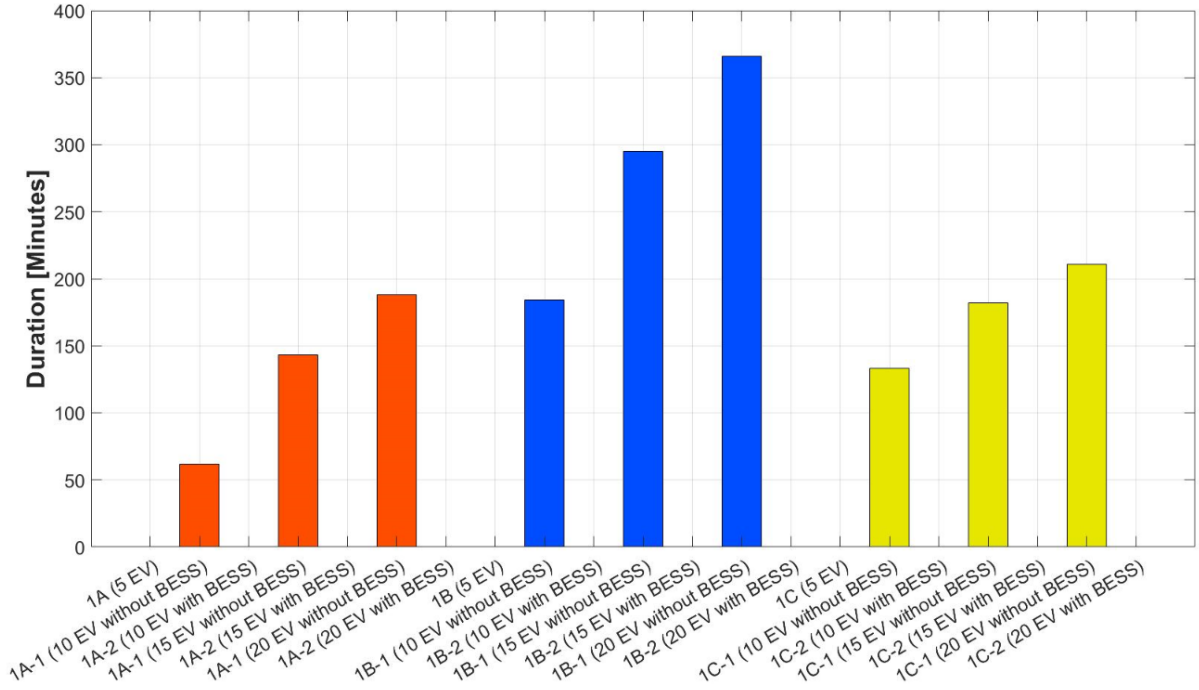

Figure 5.45 Duration of Bus Voltage Violation for Case 1 (Increasing EV Number)

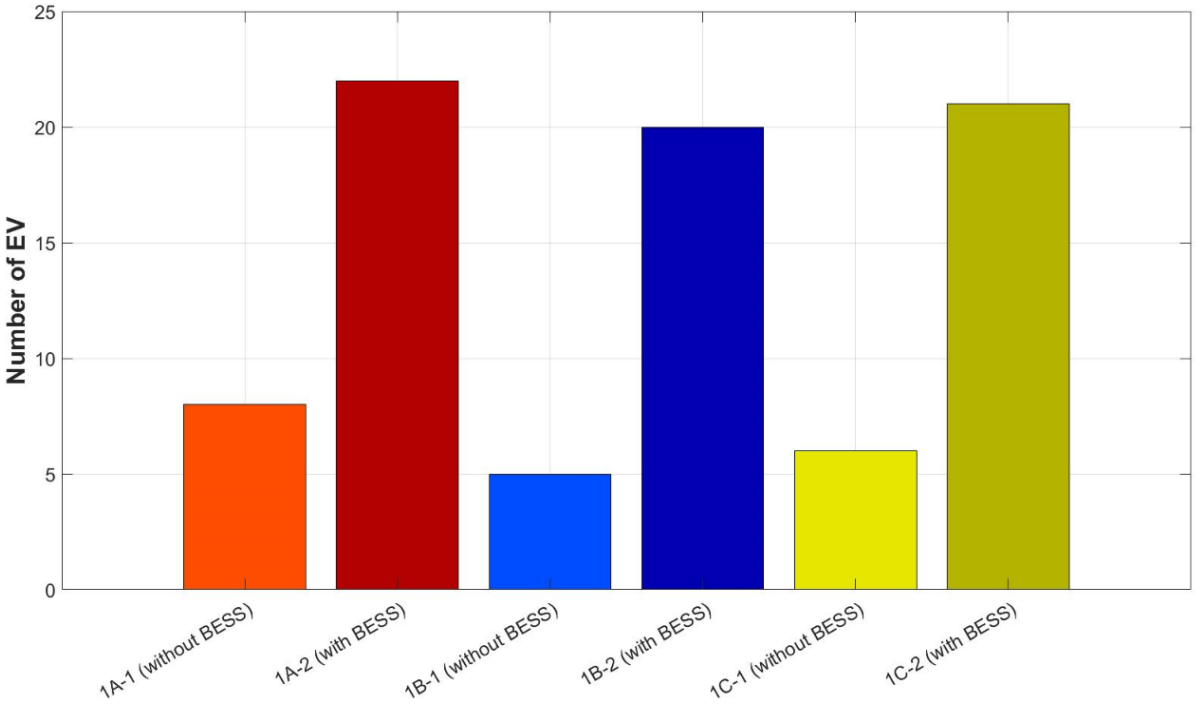

Figure 5.46 Maximum EV Number in the Charger Station for Case 1 (Increasing EV Number)

5.2 Unbalance EV Number

In this section, unsymmetrical EV penetration for every charger station is simulated. There are two asymmetrical conditions. First, the EV number placed is in increasing order, which means that the bus nearer to the transformer accommodate less EV compared than the further bus. Second, the decreasing order of EV will be deployed from the nearest to the furthest bus. Combination of 10, 15, and 20 EVs will be applied in the model to evaluate how the proposed power management system reacts to the unbalance load compared to the balance condition in Case 1.

5.2.1 Case 2A-1 (Summer, 10-15-20 EV)

In this case, increasing order of EV number will be applied from the front to back bus. Ten EVs are placed in the first bus, then the second bus receives 15 EVs, and last 20 EVs are charged in the third bus. The result of the overall exchange power in the system is shown in **Figure 5.47**. The same behaviour of BESS power flow still occurs, where BESS is charged during the cheapest period of buying electricity from the grid, then BESS is discharged during the peak EV charging power to keep the grid power below the transformer capacity and last, BESS is recharged until its initial state of charge. However, higher charging and discharging power are required to keep the system following the grid limitation compared to Case 1A-2 in **Figure 5.8** where the EVs number is balanced, 15 EVs in every bus. This condition happens due to more EVs are placed at the end of the feeder which gives more stress to the bus voltage. As a result, more BESS power is required to balance the overall system and keep the bus voltage in safe margin as presented in **Figure 5.48**. BESS state of charge during a day is illustrated in **Figure 5.49**.

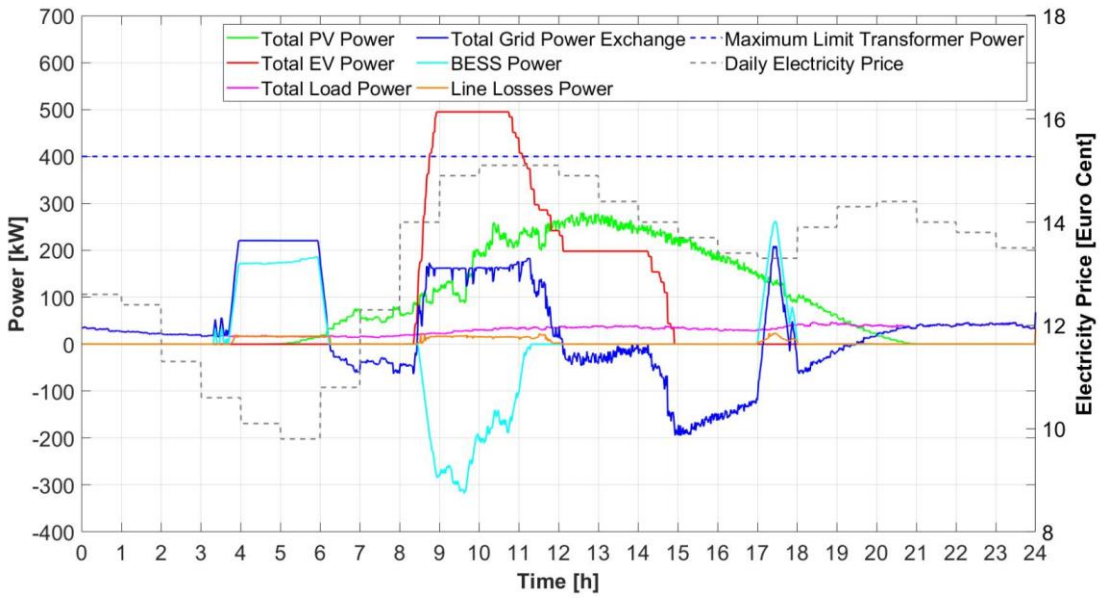

Figure 5.47 Power Exchange Profile of the Overall System for Case 2A-1 (10-15-20 EV, Summer)

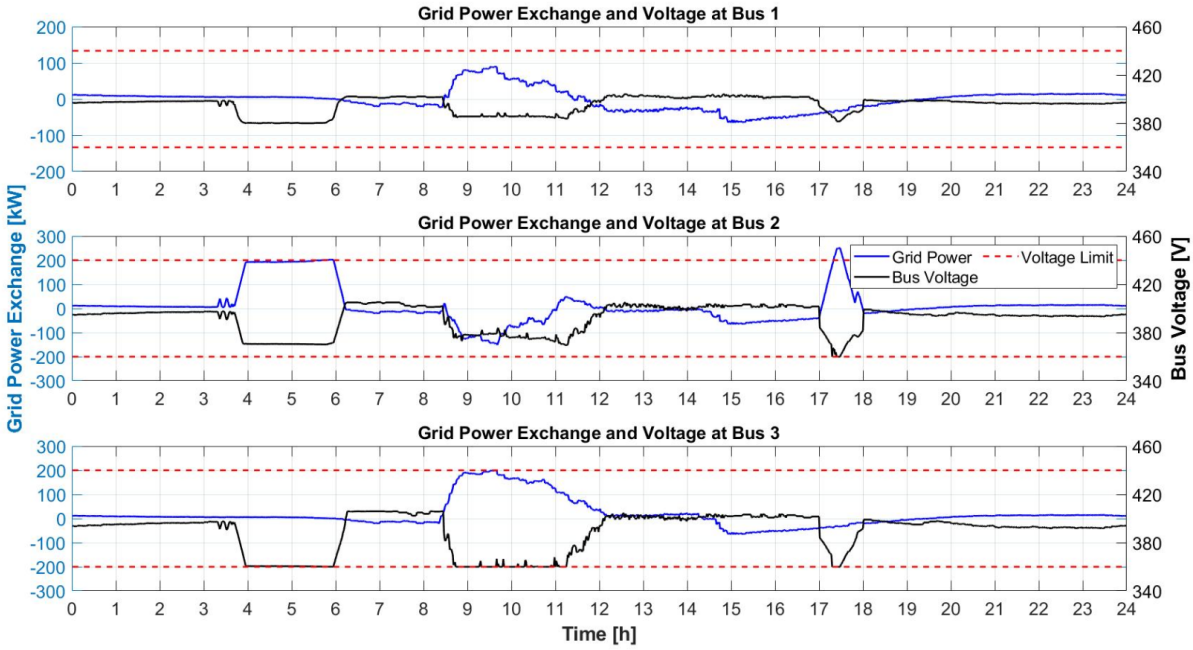

Figure 5.48 Voltage Profile at Different Bus of the System for Case 2A-1 (10-15-20 EV, Summer)

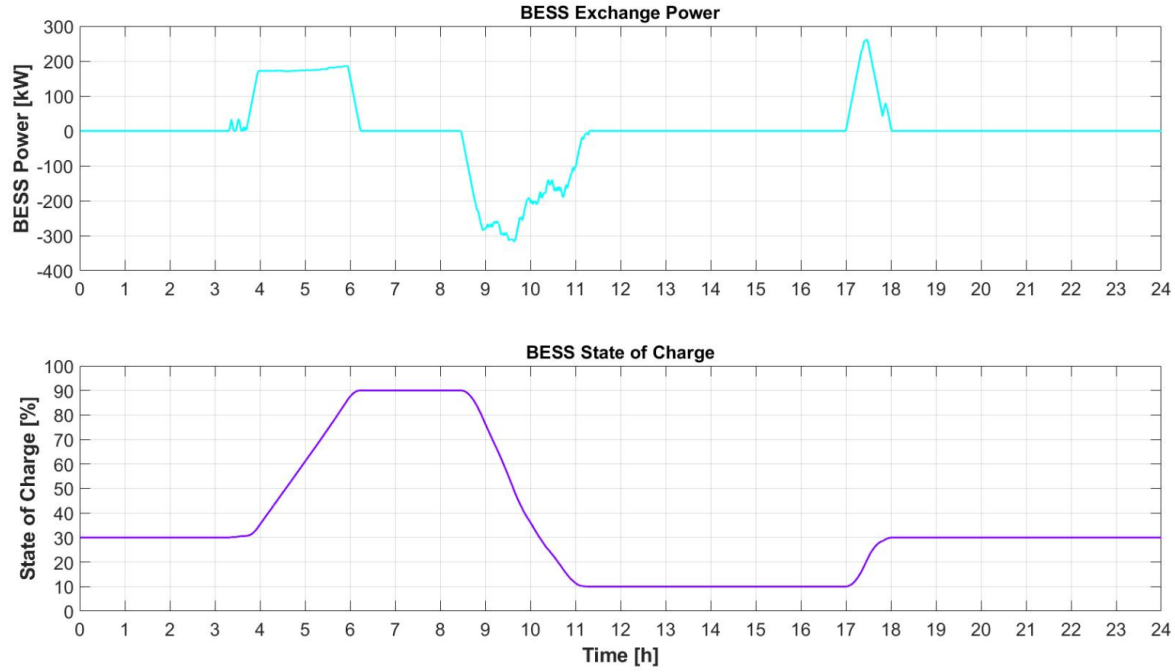

Figure 5.49 BESS Power and State of Charge Profile for Case 2A-1 (10-15-20 EV, Summer)

5.2.2 Case 2A-2 (Summer, 20-15-10 EV)

In this scenario, a decreasing order of EVs number is applied in the system. Exchange power profile of the system is shown in **Figure 5.50**. Compared to increasing EV number scenario in the previous section, a shorter period of BESS charging is needed before being discharge during initial EV charging period. Less BESS discharge power is also required to keep the bus voltage safe from the violation. This condition means that less BESS capacity is needed to neutralize the grid problems. Therefore, less charging power is also required to make the BESS state of charge gains back to initial value. This situation appears because more EVs are placed in front of the feeder where the bus voltage drop is not as severe as the end of the feeder. By placing less EVs in the last bus, less voltage stress occurs in the overall system, and as a result, less BESS intervention is required. Bus voltage and BESS state of charge are presented in **Figure 5.51** and **Figure 5.52**.

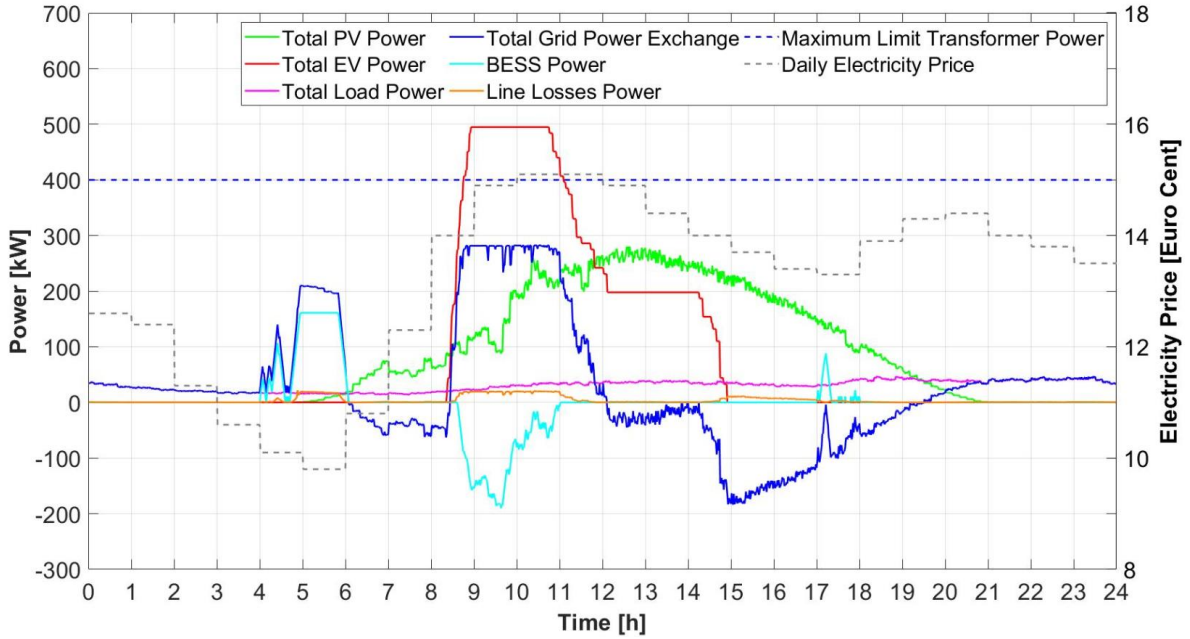

Figure 5.50 Power Exchange Profile of the Overall System for Case 2A-2 (20-15-10 EV, Summer)

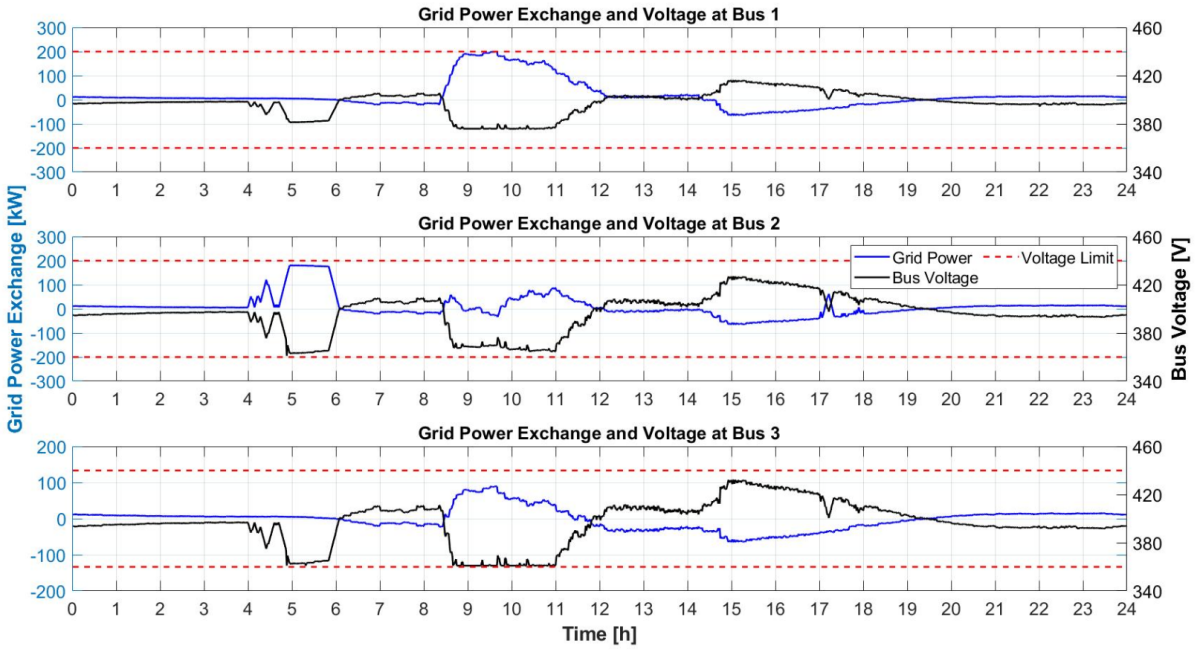

Figure 5.51 Voltage Profile at Different Bus of the System for Case 2A-2 (20-15-10 EV, Summer)

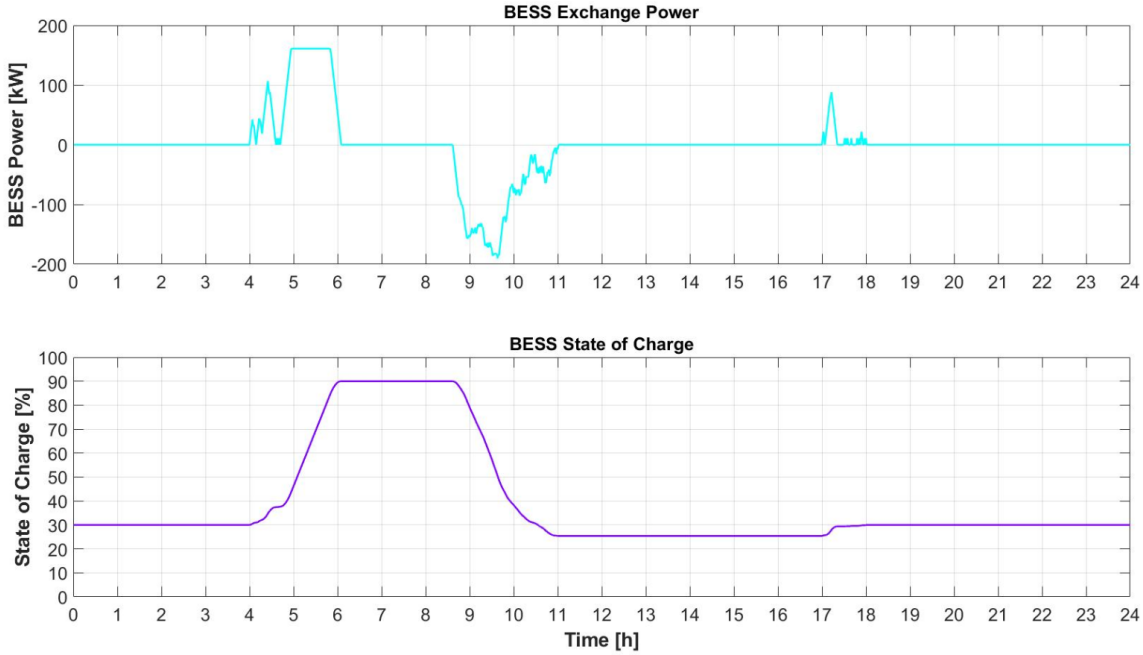

Figure 5.52 BESS Power and State of Charge Profile for Case 2A-2 (20-15-10 EV, Summer)

5.2.3 Case 2B-1 (Winter, 10-15-20 EV)

In this section, increasing EVs distribution is simulated using winter PV profile. Overall the power profile in the system is illustrated in **Figure 5.53**. It is noticeable that higher BESS power is required to stabilize the system compared to the balance EV placement, 15 EVs in every bus as simulated in previous Case 1B-2, presented in **Figure 5.22**. BESS is charged with high constant power during “valley” electricity price period until its maximum state of

charge allowed as preparation before high EV charging power demand during the day. Then, BESS is discharged with slightly higher peak power compared to balance EV distribution. Last, BESS is recharged to restore its state of charge as the initial value with high constant power. **Figure 5.54** shows that BESS operation successfully saves the bus voltage between the limit. The BESS state of charge during a day is illustrated in **Figure 5.55**.

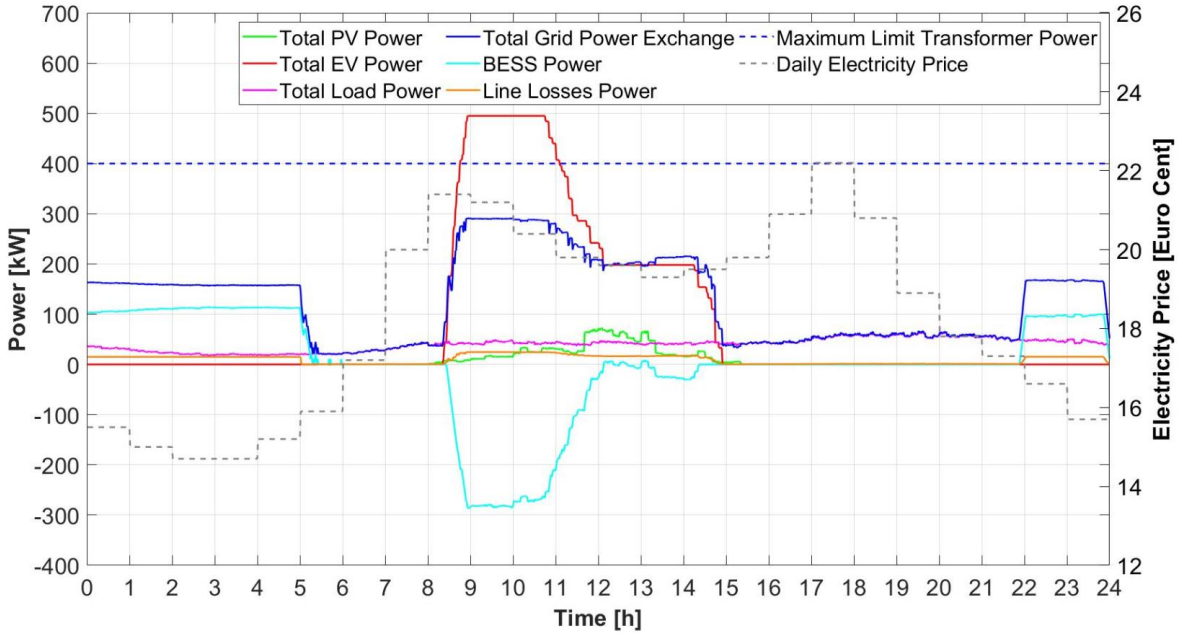

Figure 5.53 Power Exchange Profile of the Overall System for Case 2B-1 (10-15-20 EV, Winter)

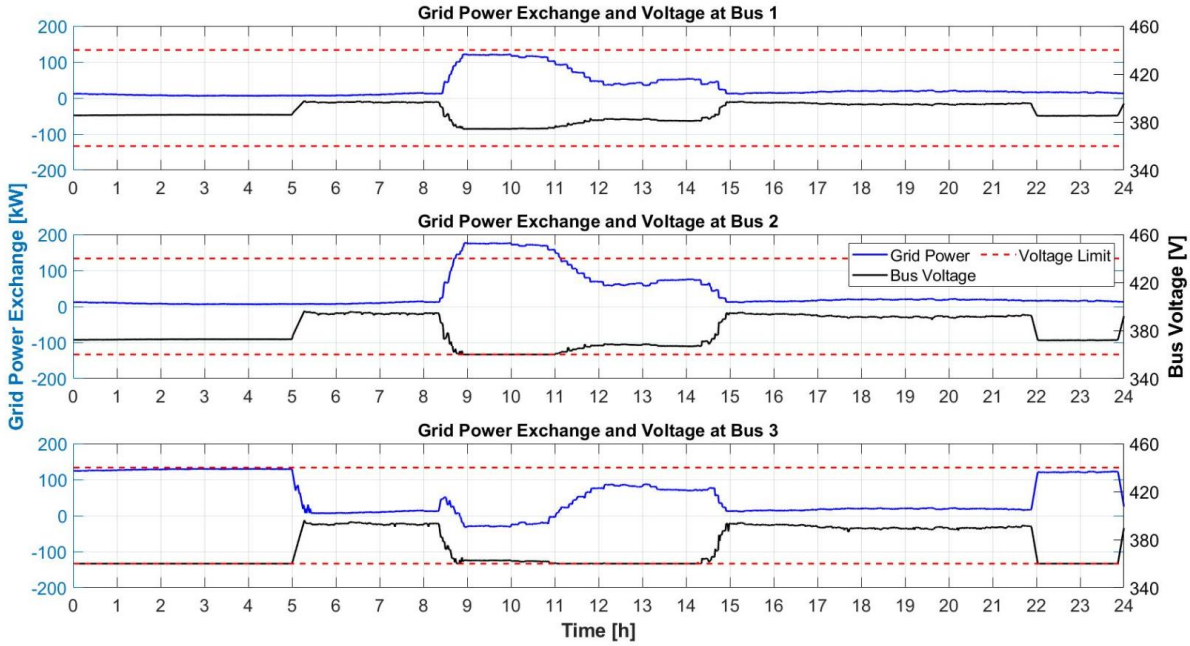

Figure 5.54 Voltage Profile at Different Bus of the System for Case 2B-1 (10-15-20 EV, Winter)

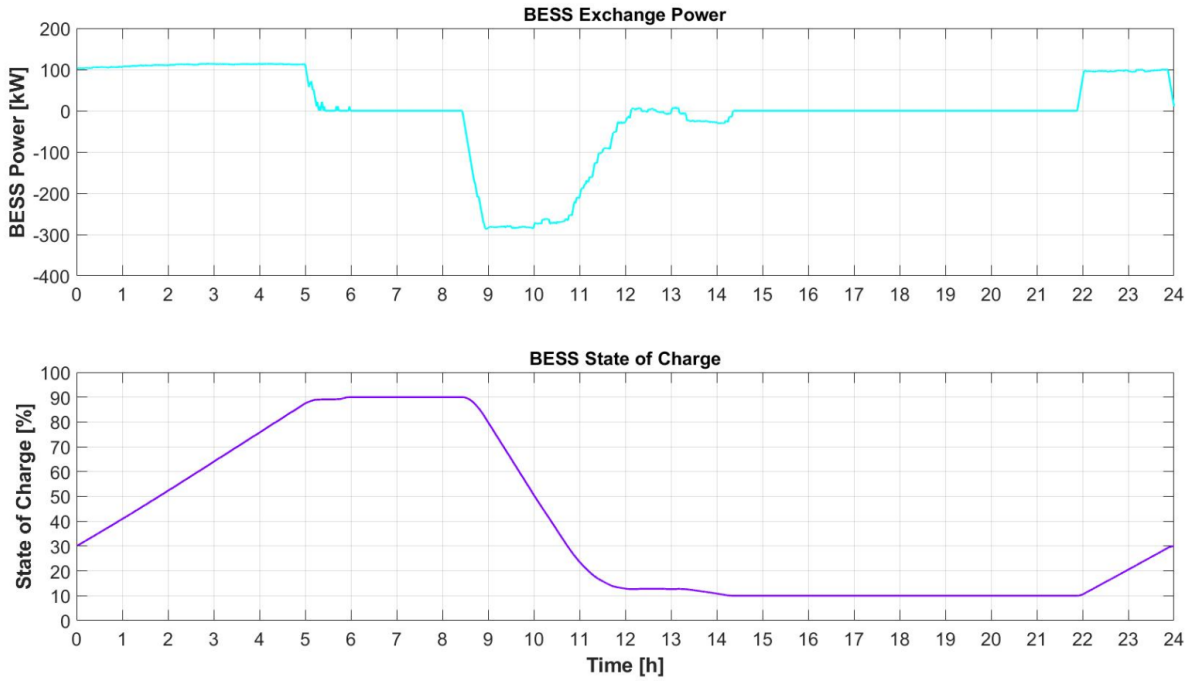

Figure 5.55 BESS Power and State of Charge Profile for Case 2B-1 (10-15-20 EV, Winter)

5.2.4 Case 2B-2 (Winter, 20-15-10 EV)

In this section, less EVs are placed in the further bus from the transformer. **Figure 5.56** illustrates the overall power profile of the system. The BESS charging power period is one hour shorter compared than the case of increasing EV number distribution. Besides, less peak BESS discharging power is required to reduce the maximum transformer power loading. Last, less energy required to recharge BESS during end of the day, as indicated from lower charging power during 10-11 p.m. To sum up, similar to the trend shown in summer, decreasing order of EV placement will be more beneficial because of less BESS power and capacity are needed to keep the system in the safe zone. Bus voltage is maintained beyond minimum voltage of 360 V during the day as shown in **Figure 5.57**. Furthermore, in line with previous simulations, BESS state of charge during a day occupies full allowable range from 10-90% as shown in **Figure 5.58**.

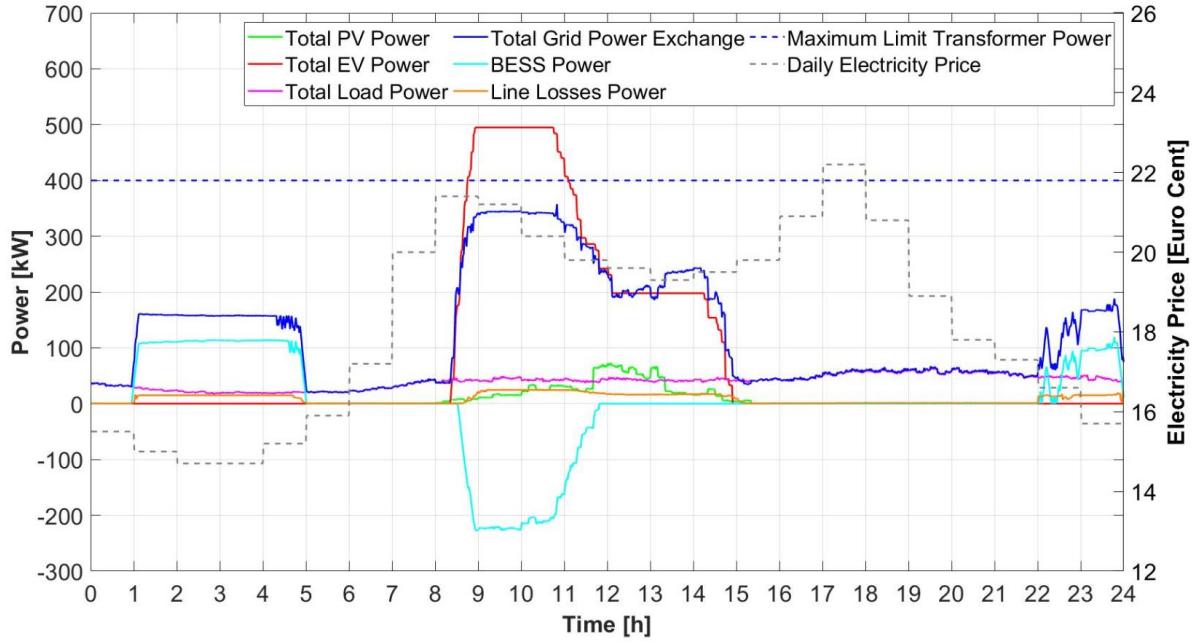

Figure 5.56 Power Exchange Profile of the Overall System for Case 2B-2 (20-15-10 EV, Winter)

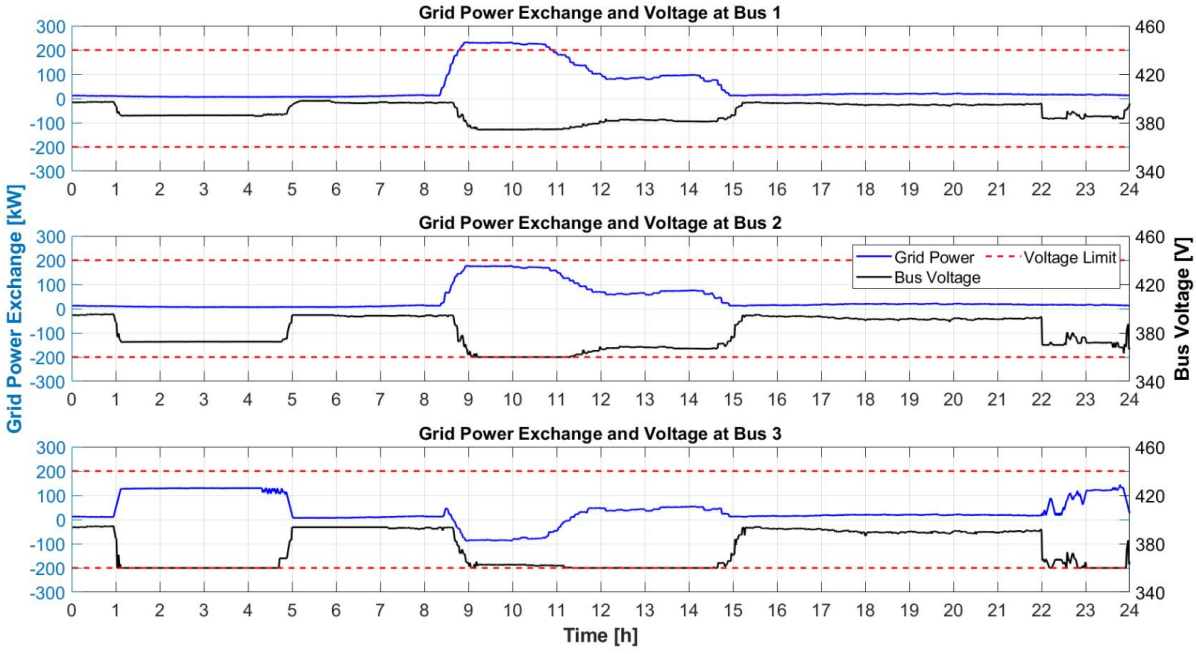

Figure 5.57 Voltage Profile at Different Bus of the System for Case 2B-2 (20-15-10 EV, Winter)

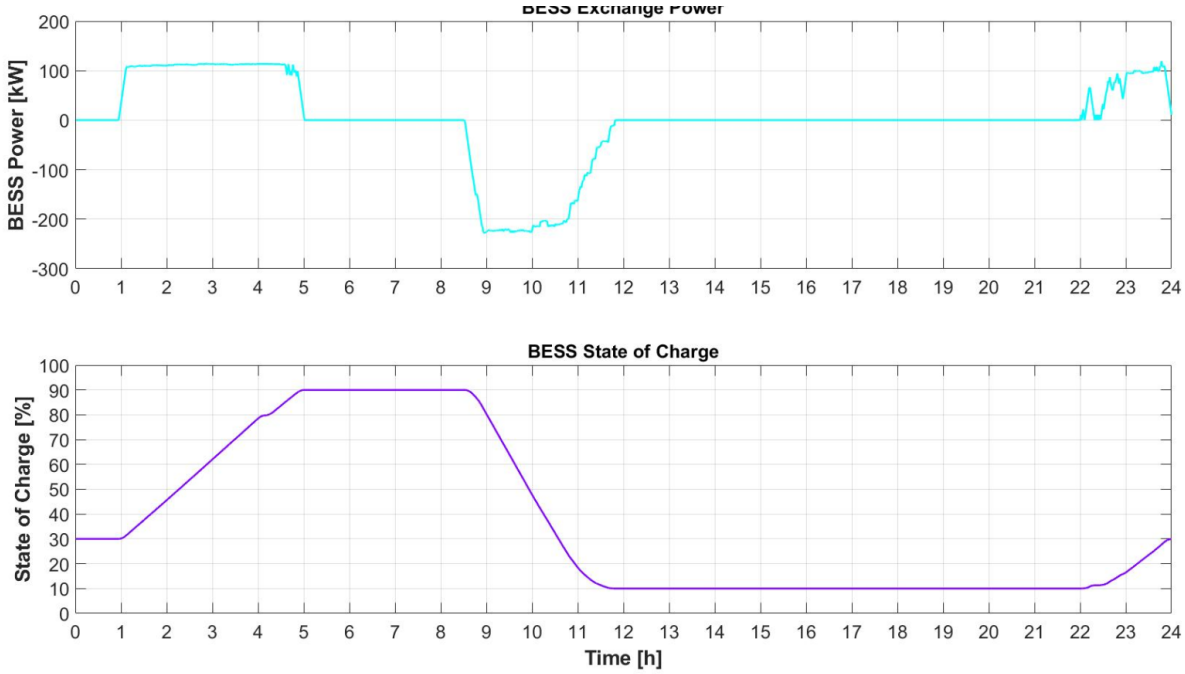

Figure 5.58 BESS Power and State of Charge Profile for Case 2B-2 (20-15-10 EV, Winter)

5.2.5 Case 2C-1 (Autumn, 10-15-20 EV)

In this section, the increasing order of EV number distribution simulation test is run using PV power profile of autumn. The general system power profile is illustrated in **Figure 5.59**. The main difference with the case of equally distributed EV number in Case 1C-2, which is presented in **Figure 5.34**, is that longer charging BESS power is performed as more energy required to hold the system voltage during highest EV charging power period. Moreover, similar to the previous test trend in season summer and winter, higher peak discharge power is required to keep the bus voltage not exceeding the minimum limit as presented in **Figure 5.60**. Last, as a consequence of larger BESS capacity, longer charging time needs to be done to bring back the BESS state of charge to its initial value. **Figure 5.61** shows the trend of BESS state of charge during the daily operation.

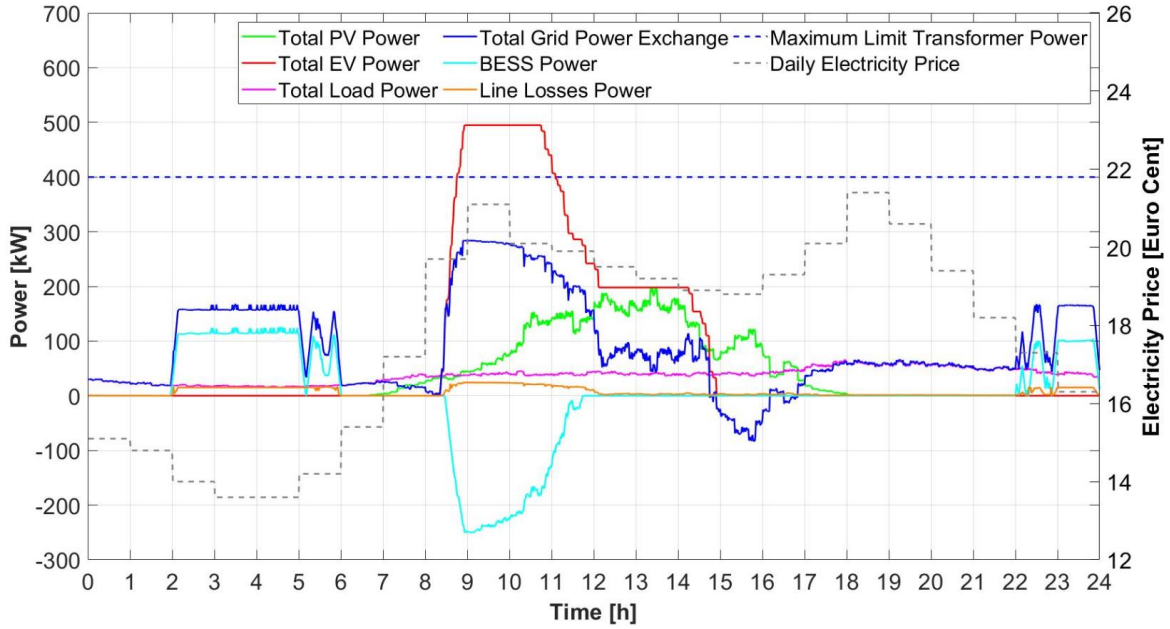

Figure 5.59 Power Exchange Profile of the Overall System for Case 2C-1 (10-15-20 EV, Autumn)

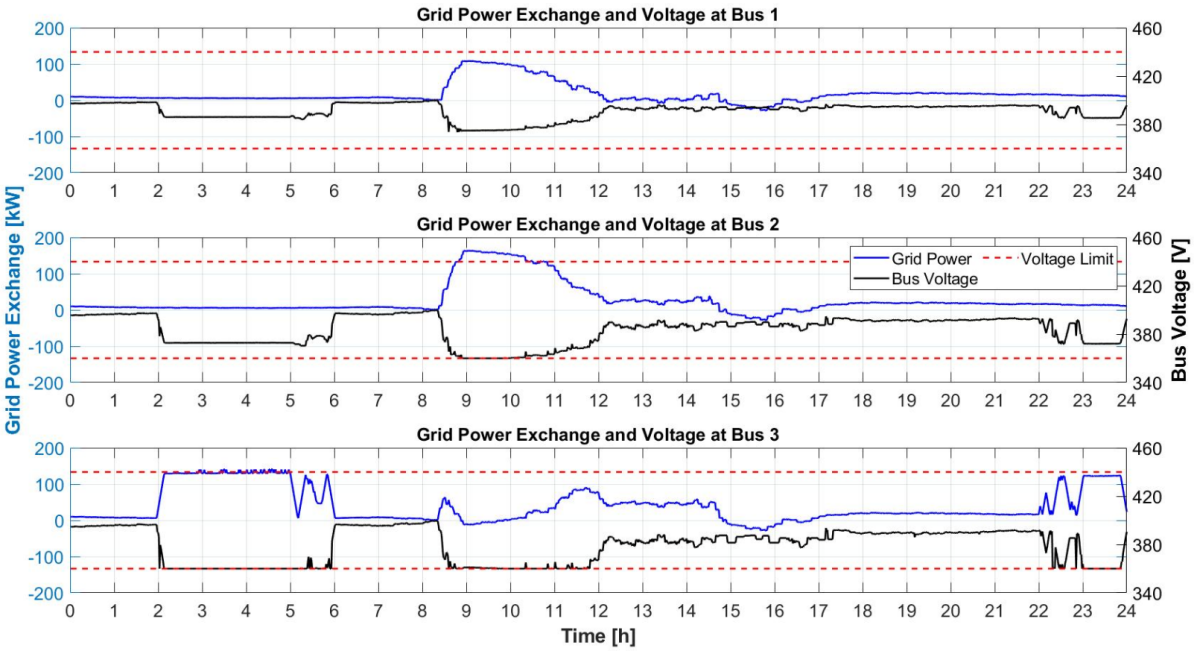

Figure 5.60 Voltage Profile at Different Bus of the System for Case 2C-1 (10-15-20 EV, Autumn)

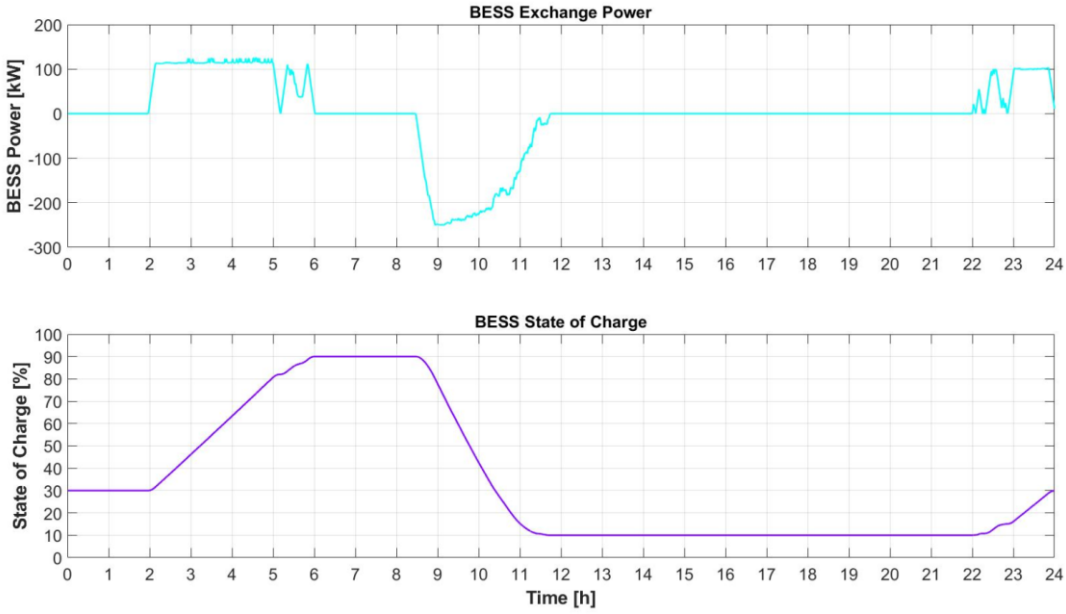

Figure 5.61 BESS Power and State of Charge Profile for Case 2C-1 (10-15-20 EV, Autumn)

5.2.6 Case 2C-2 (Autumn, 20-15-10 EV)

Decreasing order of asymmetrical EV number composition is simulated in this scenario. Figure 5.62 shows the global exchange of power in the system. It can be seen that the shorter BESS charging period is required to fulfil the energy needs for peak shaving operation during the day. More EV penetration in the front bus leads to a reduction of stress voltage in the overall system which causes less BESS power mitigation is needed during EV charging time. At the end of the day, BESS has recharged again to its initial state of charge value with shorter time because of lower BESS capacity. The bus voltage and BESS state of charge profile during a day are presented in Figure 5.63 and Figure 5.64 respectively.

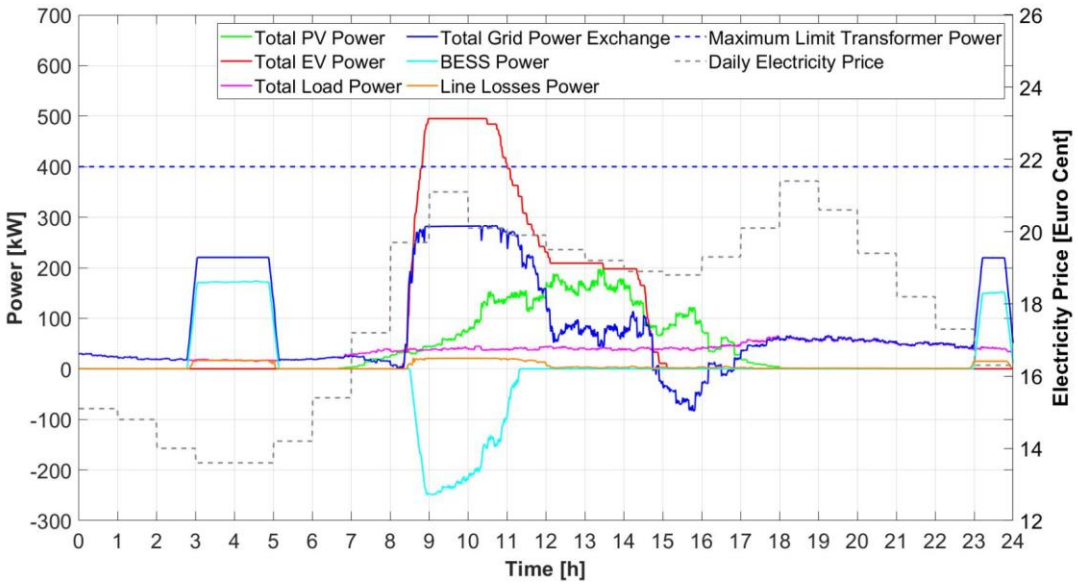

Figure 5.62 Power Exchange Profile of the Overall System for Case 2C-2 (20-15-10 EV, Autumn)

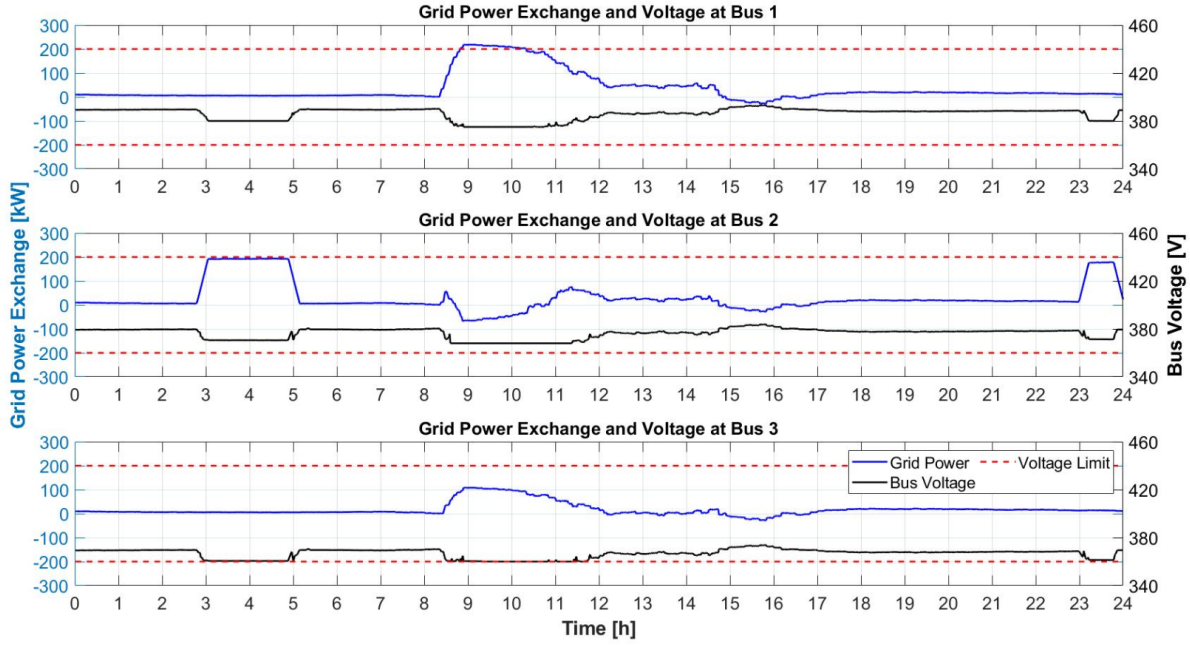

Figure 5.63 Voltage Profile at Different Bus of the System for Case 2C-2 (20-15-10 EV, Autumn)

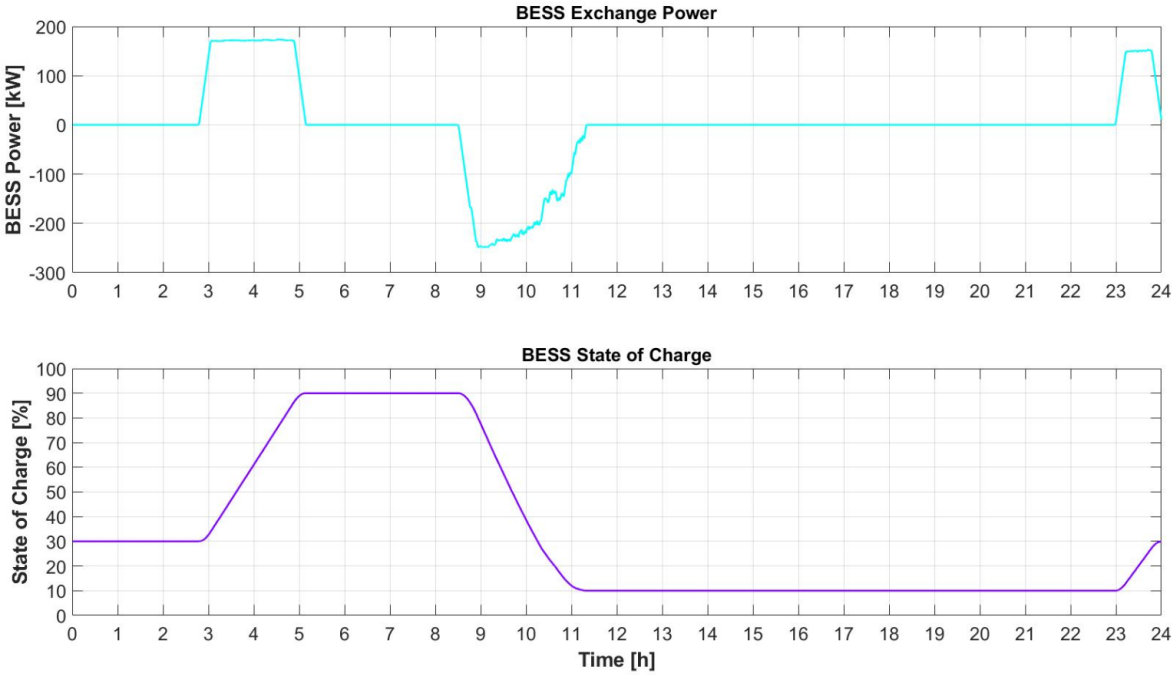

Figure 5.64 BESS Power and State of Charge Profile for Case 2C-2 (20-15-10 EV, Autumn)

5.2.7 Summary

Unbalance EVs distribution in the system scenarios has been simulated in three seasons PV profile. The proposed power management and BESS sizing successfully resolve the bus voltage and maximum transformer loading capacity issues. There are some impacts of the asymmetrical placement of EVs in the charger station. First, the longer charging period is required by BESS for increasing order EV distribution due to the maximum power that can be extracted from the grid. Normally, BESS will be charged only during the cheapest period, but because of high voltage drop happens when power drawn from the grid is too much, the power management system manages BESS to charge also during the next cheapest period. Second, high EV penetration at the end of feeder leads to larger discharging BESS power required during the beginning of EV charging process. High power that needs to be transferred to the end of the line causes severe bus voltage drop. To mitigate this issue, some of EV charging power demand is also supplied from BESS to alleviate the stress in the grid, so that the bus voltage is maintained at the safe margin.

Comparison of BESS maximum power and capacity for asymmetrical EV penetration in different seasons are presented in **Figure 5.65** and **Figure 5.66** accordingly. It is observed that different pattern of suggested BESS size occurs for different seasons because of different BESS location as shown in **Figure 5.67**. In case of winter, where BESS is located at the end of feeder, the same location with the normal symmetrical EV penetration case, the BESS size is higher for case with increasing order of EVs and lower for the decreasing order case. However, in case of summer, BESS is suggested to be placed at the middle bus for both cases of asymmetrical EV penetration. As a result, higher BESS size is required for both asymmetrical cases compared than the balance penetration case, even for the decreasing EV order case which is supposed to be lower than the requirement for symmetrical penetration. At the middle bus, shorter distance is taken to reach loads at the other bus compared than if the BESS is placed at the end bus. Another different pattern appears in case of autumn, where the BESS is suggested at the end of feeder for increasing EV order, while for decreasing EV order the BESS is placed at the middle of the line. This configuration leads to comparable maximum BESS power for both asymmetrical cases, but similar to the summer case, the BESS capacity for decreasing EV order case becomes higher than the normal balance EV penetration. In overall, the BESS location for asymmetrical EV penetration reacts differently for different PV power profile. **Figure 5.68** shows the comparison of BESS investment for different EV penetration and seasons. Higher investment is required for increasing order EV penetration compared than the decreasing EV order allocation.

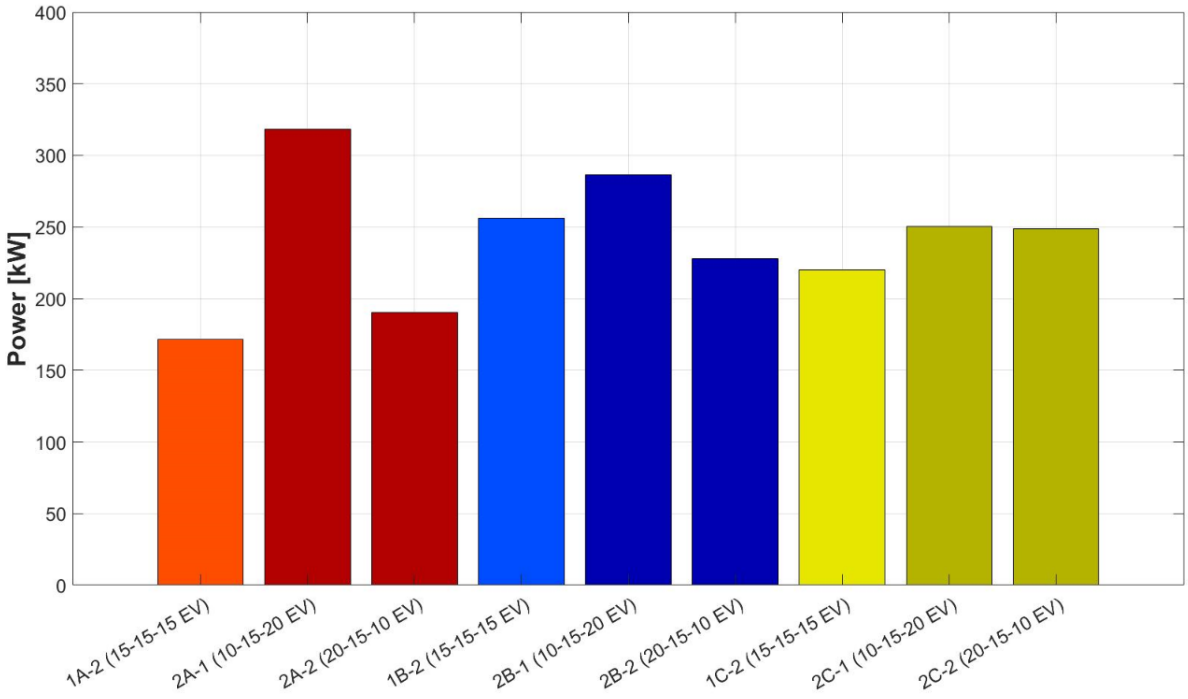

Figure 5.65 BESS Maximum Power for Case 2 (Unbalance EV Number)

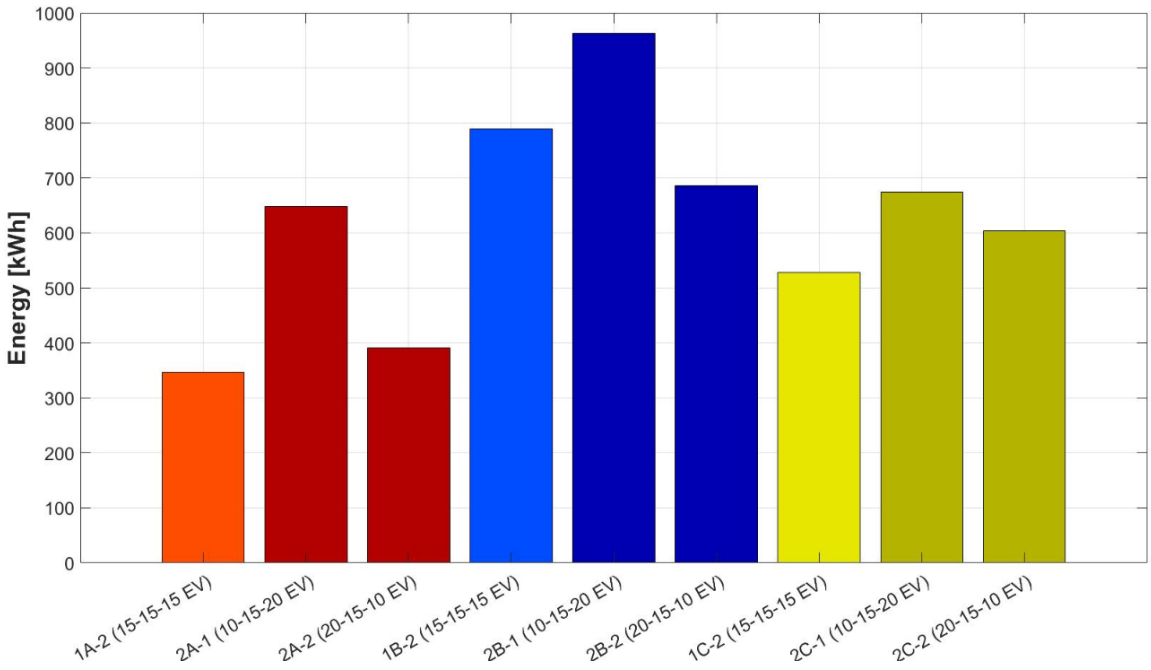

Figure 5.66 BESS Capacity Required for Case 2 (Unbalance EV Number)

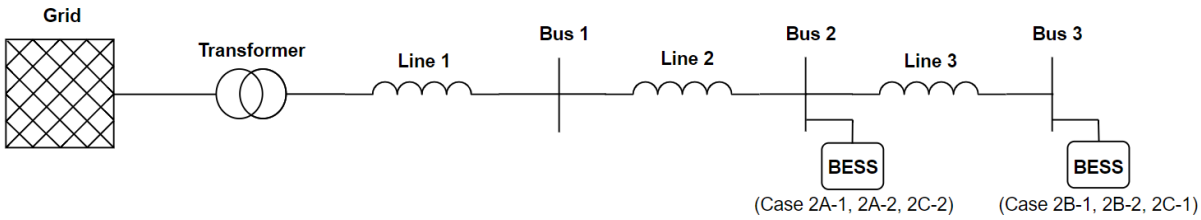

Figure 5.67 Optimal BESS Location for Case 2 (Unbalance EV Number)

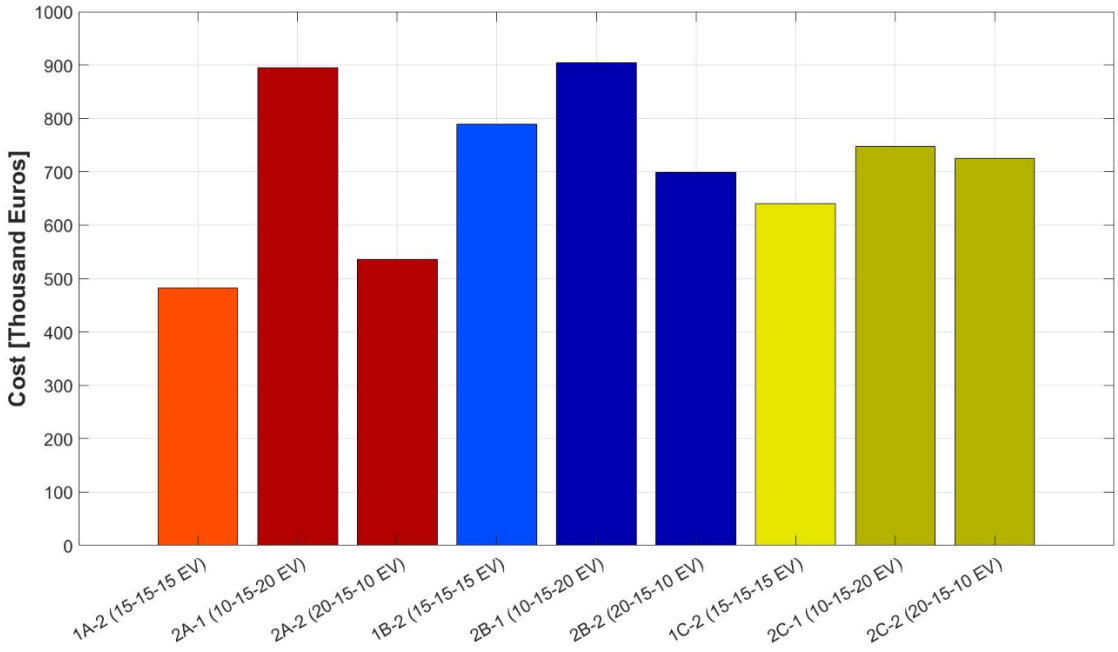

Figure 5.68 BESS Investment Cost for Case 2 (Unbalance EV Number)

The maximum transformer loading power of the system is presented in **Figure 5.69**. It is noticeable that for a case with higher BESS maximum power, less power stress occurs in the transformer. For example, in case of winter where the BESS is placed at the end of the feeder, maximum transformer utilization appears when the EVs are distributed in decreasing order which requires the least amount of BESS power. In contradict, least transformer loading happens in case of increasing order of EV distribution. Although the transformer loading differs for balance and unbalance EV distribution, the electricity cost need to be paid for both cases is almost the same as shown in **Figure 5.70**. This means that the net charging and discharging BESS power for all cases are similar despite of different BESS maximum power and capacity. However, the total cost of the system differs for all cases due to BESS investment contribution as shown in **Figure 5.71**. As expected, increasing order EV distribution ranks top in the total expenditure, then followed by balance allocation and last is the case of decreasing order.

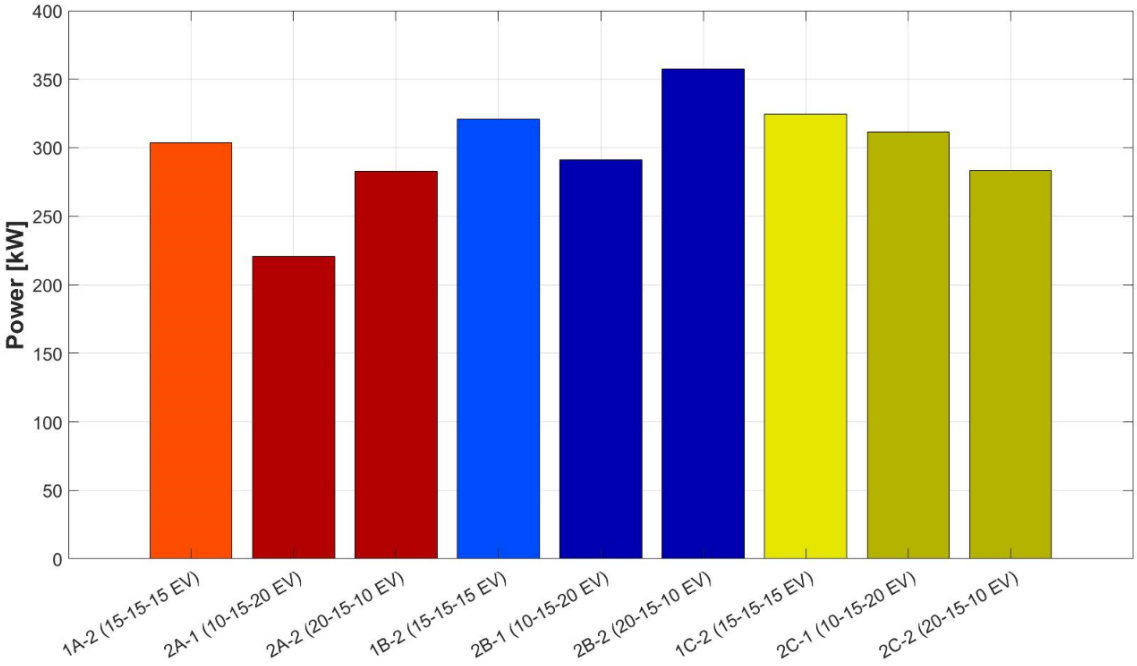

Figure 5.69 Maximum Transformer Loading Power for Case 2 (Unbalance EV Number)

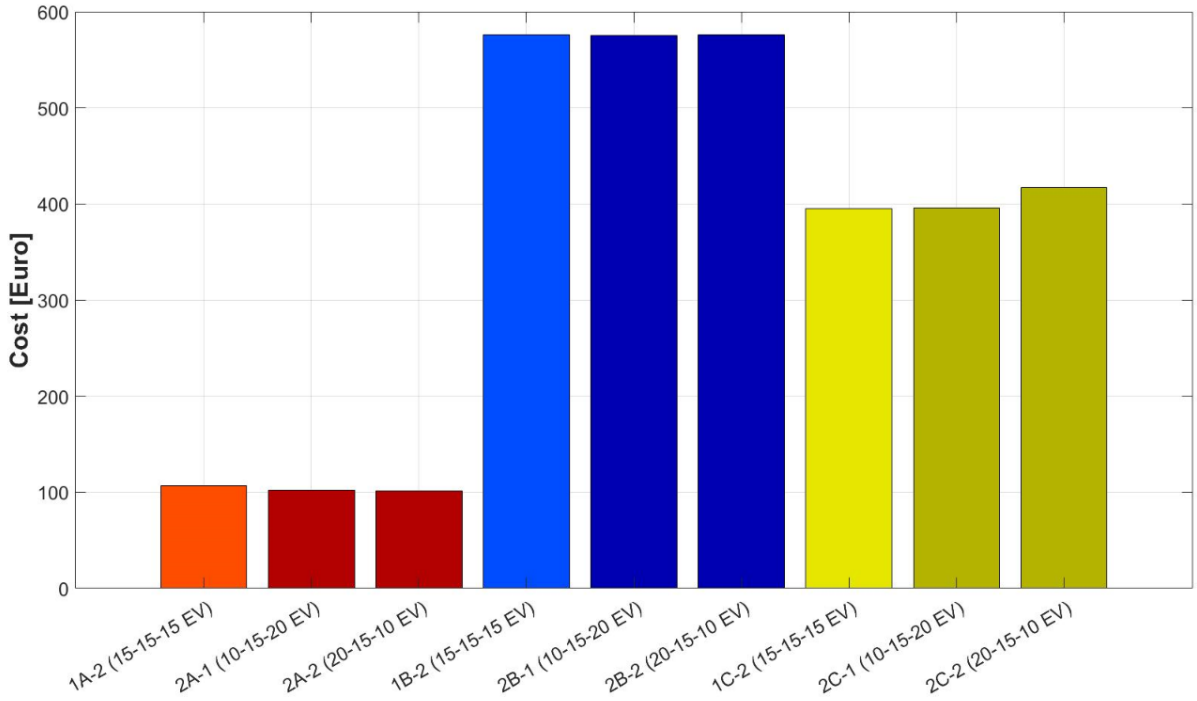

Figure 5.70 Electricity Cost for Case 2 (Unbalance EV Number)

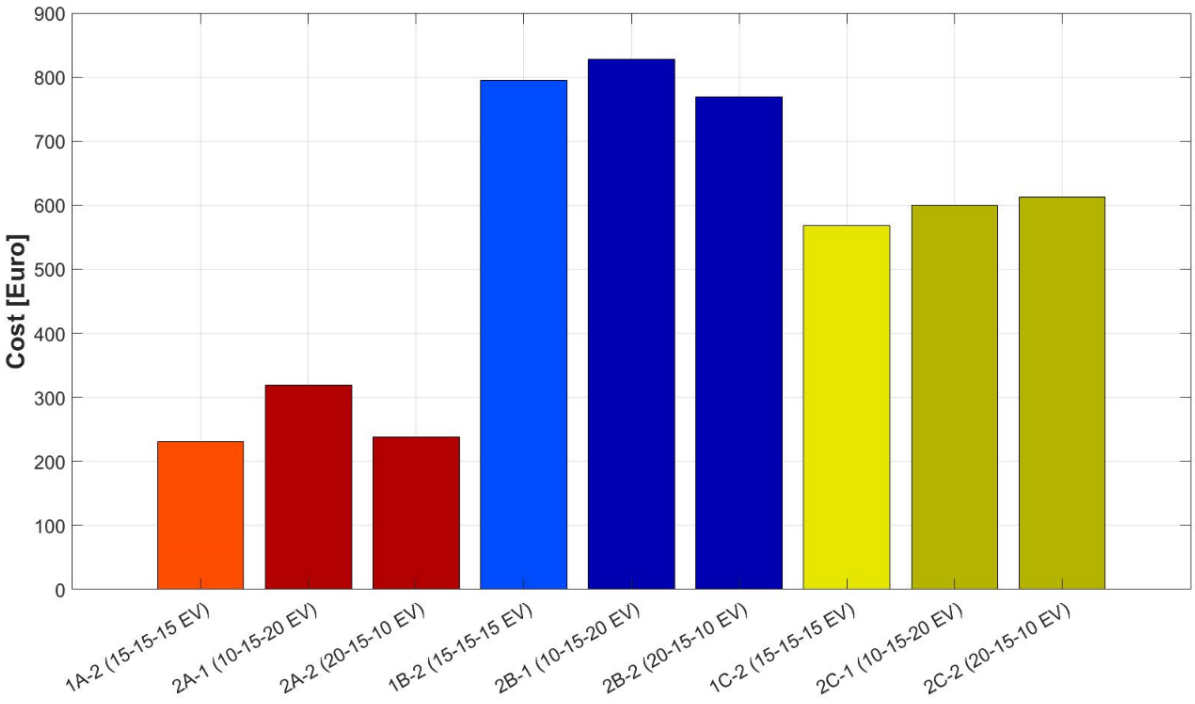

Figure 5.71 Total Cost for Case 2 (Unbalance EV Number)

5.3 Decentralized BESS

In this scenario, the proposed optimization model is given freedom to place BESS in all bus instead of only one BESS as occurred in previous simulations. The value of N^b in equation (4.1) is set to be three, which means the BESS can be installed in all of the bus. Decentralized BESS positioning is expected to give better system voltage profile and lower line losses compared to centralized BESS. Moreover, the impact to the cost involved will also be discussed in this section.

5.3.1 Case 3A (Summer)

In this section, PV power profile of summer season is adapted in decentralized BESS condition. Figure 5.72 presents the overall exchange power profile of the system. As usual, BESS is managed to charge during the lowest price period. Then, BESS is discharged during high demand of EV charging period. Last, BESS is recharged during the next cheapest electricity period. The different is two BESS is suggested to be located in the middle and end of the feeder in the system. However, different power and capacity sizing are advised. BESS in the furthest bus has much higher maximum power and energy compared than BESS in the middle of the system. This is because of more severe voltage drop appears at the end of the feeder. As response, more BESS power intervention occurs in the furthest bus. Visually, there is no significant change in bus voltage profile as seen in Figure 5.73 compared to the case of centralized BESS, presented in Figure 5.8. The

furthest bus voltage still reaches the lowest voltage limit allowed of 360 V, but there is shorter period of reaching the minimum limit during the first BESS charging period between 4-5 a.m. The BESS power and state of charge profile are presented in **Figure 5.74** and **Figure 5.75** respectively.

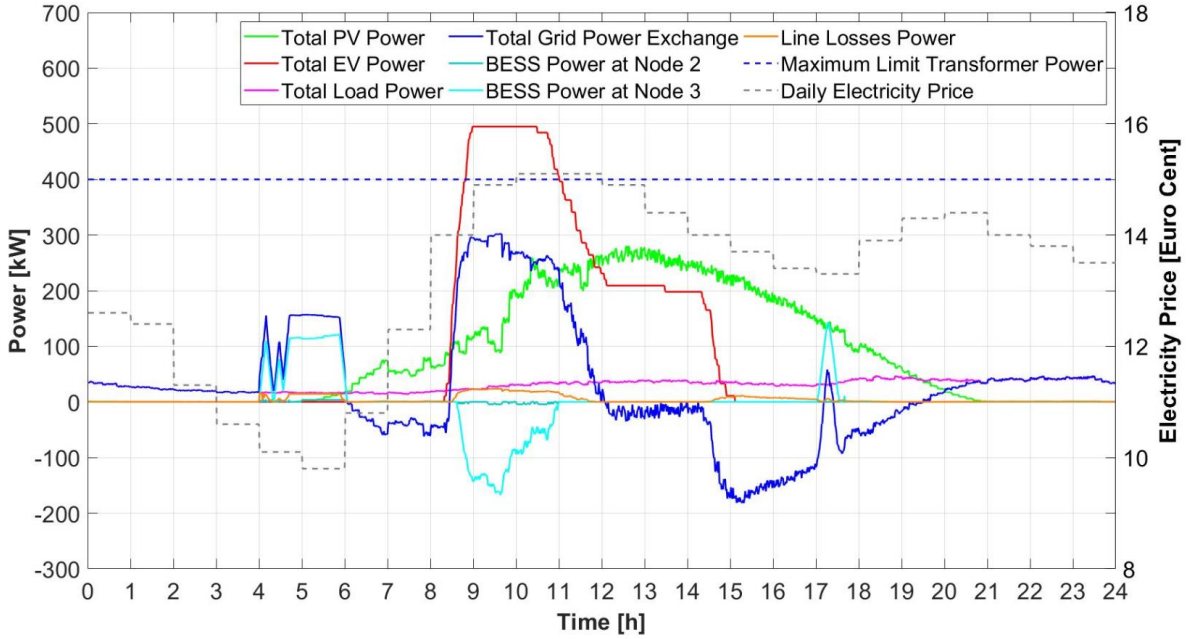

Figure 5.72 Power Exchange Profile of the Overall System for Case 3A (Decentralized, Summer)

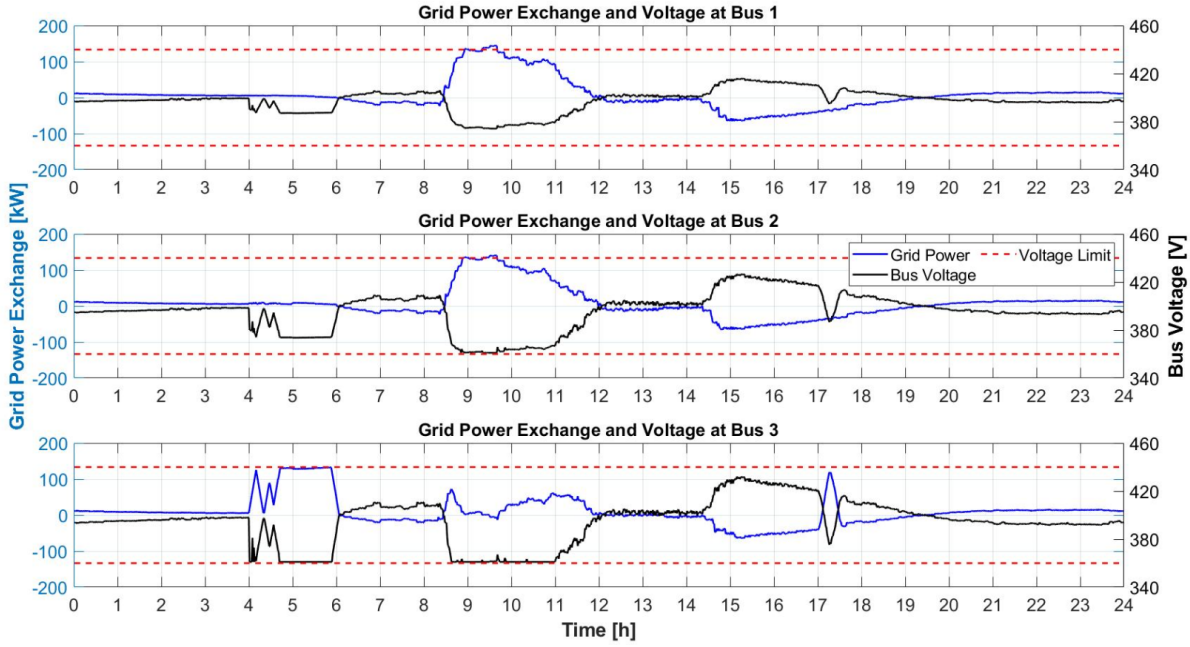

Figure 5.73 Voltage Profile at Different Bus of the System for Case 3A (Decentralized, Summer)

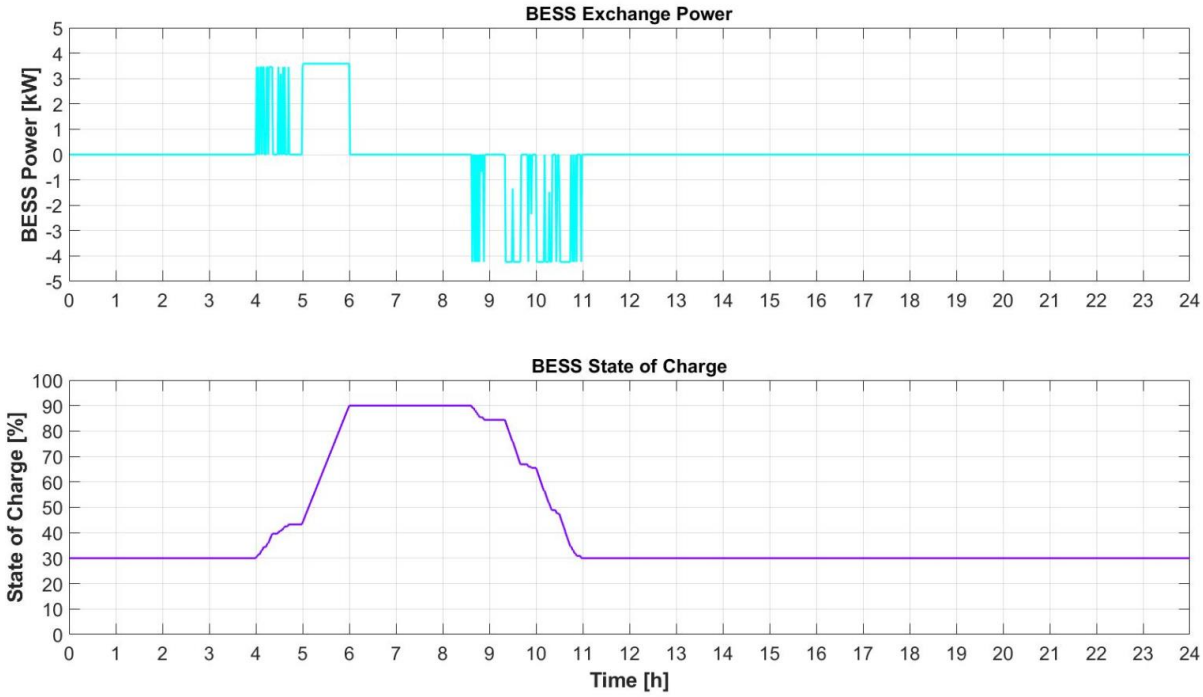

Figure 5.74 Power and State of Charge Profile for BESS in the middle bus in Case 3A (Decentralized, Summer)

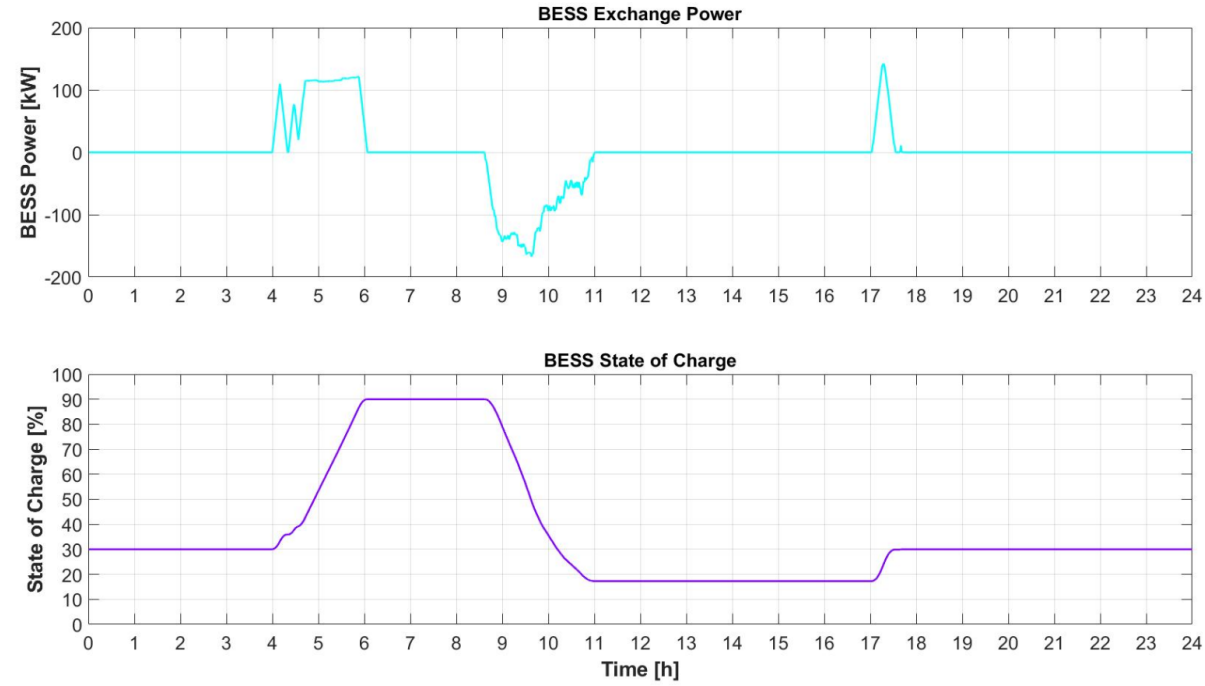

Figure 5.75 Power and State of Charge Profile for BESS in the end bus in Case 3A (Decentralized, Summer)

5.3.2 Case 3B (Winter)

In this case, the decentralized BESS approach is combined with winter PV profile. Overall system exchange power is illustrated in **Figure 5.76**. It is noticeable that more BESS charging power appears during the lowest electricity price period between 2-4 a.m. compared than the case of centralized BESS as presented in **Figure 5.22**. More BESS charging power can be extracted from the grid during the cheapest period can be possibly done by BESS in the middle of the system because of less severe voltage drop appears compared than the furthest bus. This condition leads to less electricity cost need to be paid due to shifting of previous not ideal BESS charging period between 12-1 a.m. to 2-4 a.m. which is the cheapest price period. This situation also appears in the second BESS charging period during the end of a day. Because of BESS instalment in the middle of the feeder, some charging energy which previously occurs in the second cheapest period between 10-11 a.m., now relocated by the BESS in the middle of the system to the lowest price period. In general, there is no significant impact, except the occurrence of small extra valley during the cheapest period in the first and second bus voltage as seen in **Figure 5.77**. BESS power and state of charge profile are shown in **Figure 5.78** and **Figure 5.79** correspondingly.

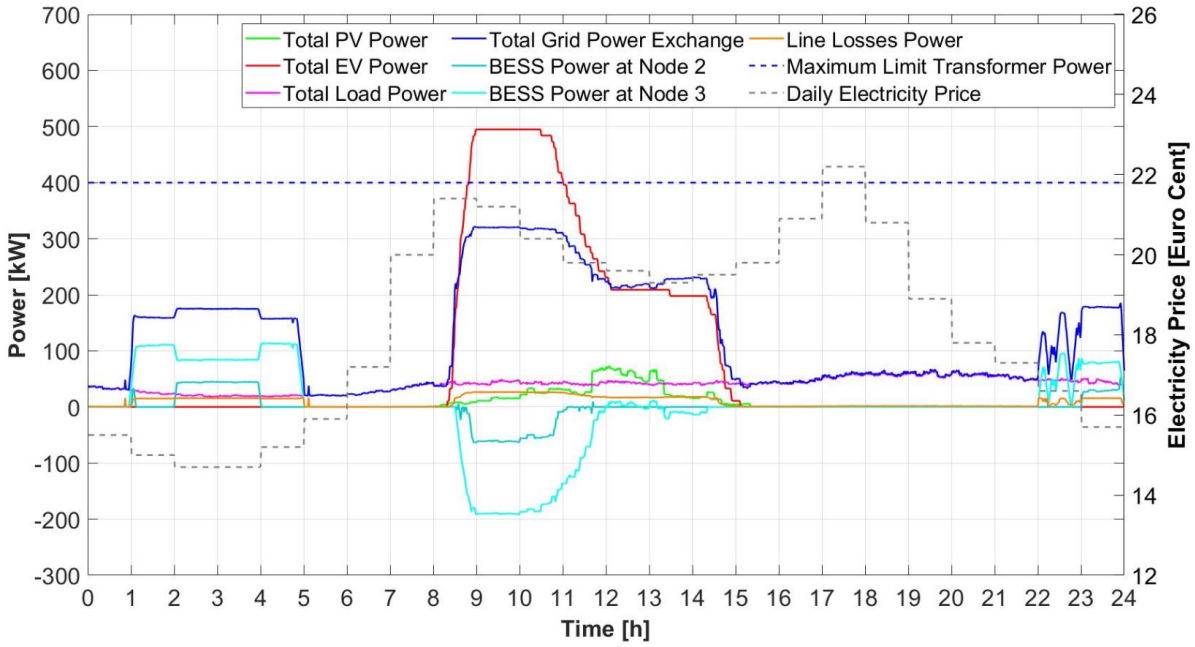

Figure 5.76 Power Exchange Profile of the Overall System for Case 3B (Decentralized, Winter)

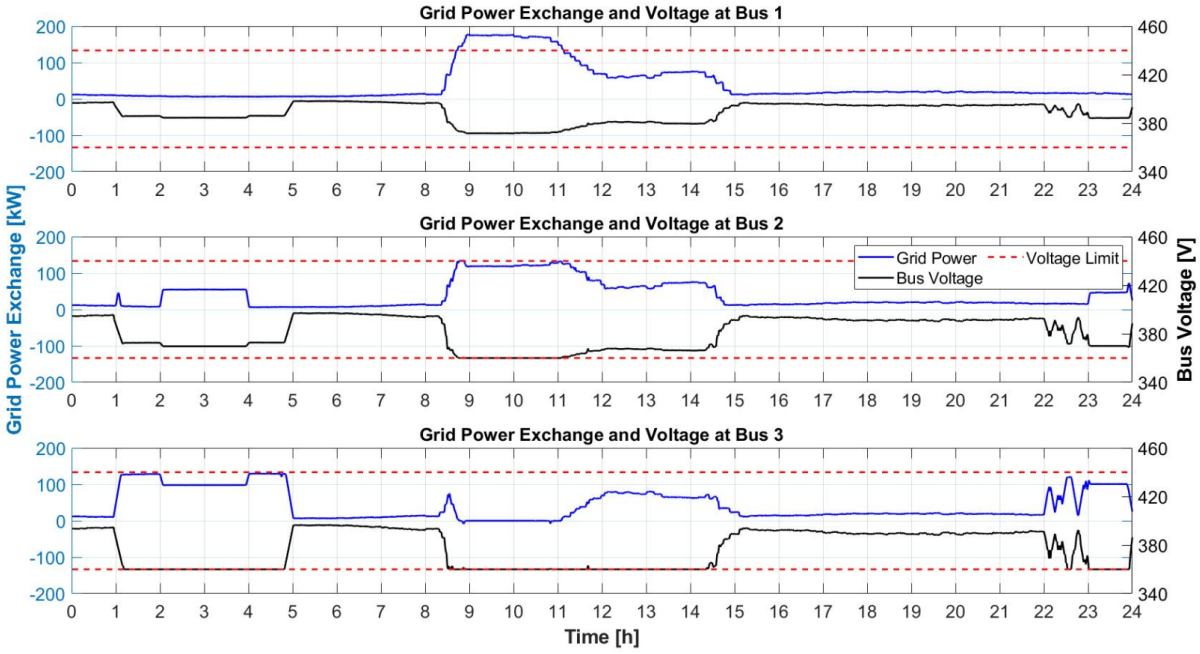

Figure 5.77 Voltage Profile at Different Bus of the System for Case 3B (Decentralized, Winter)

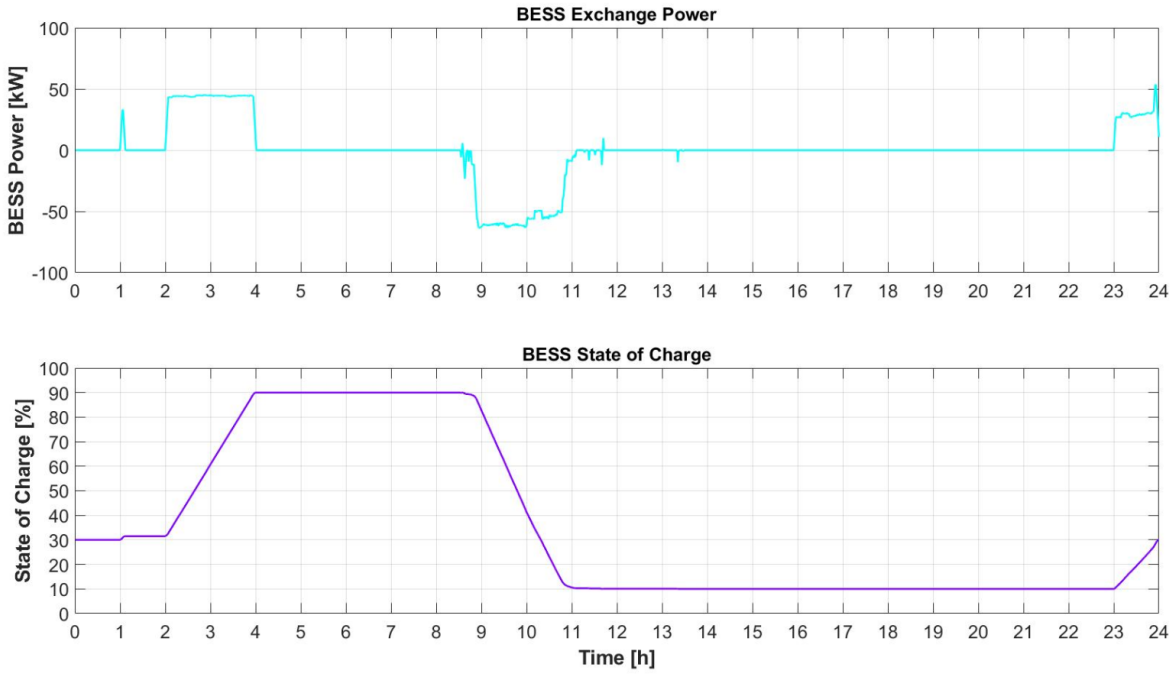

Figure 5.78 Power and State of Charge Profile for BESS in the middle bus in Case 3B (Decentralized, Winter)

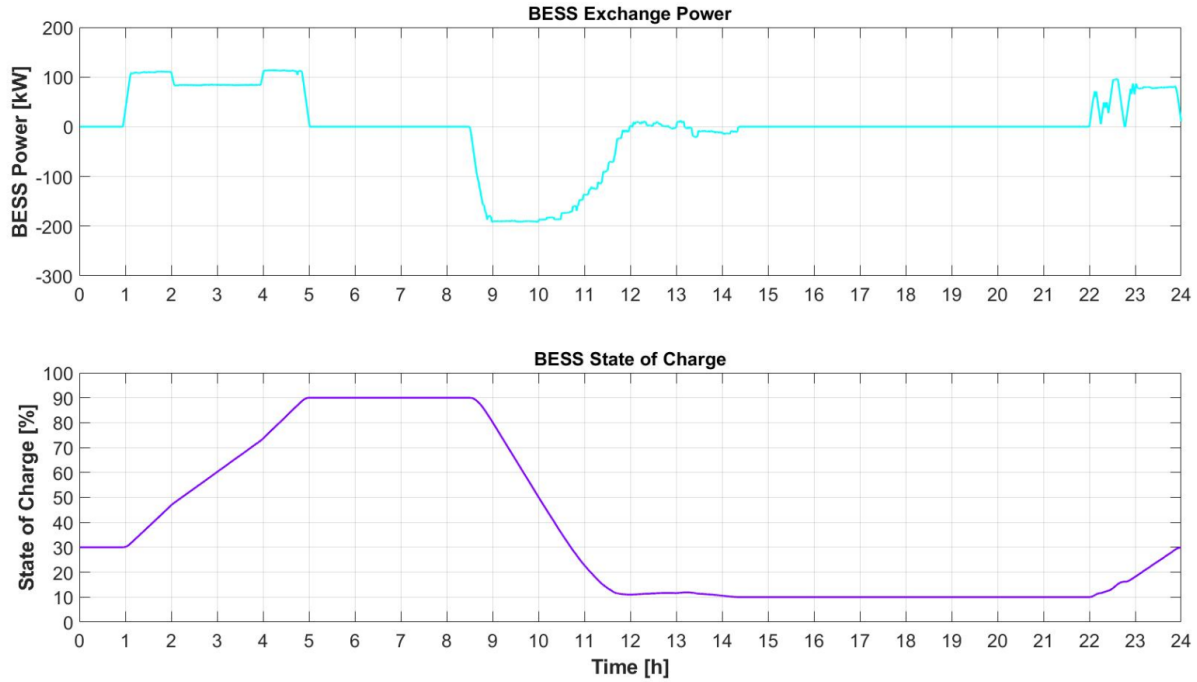

Figure 5.79 Power and State of Charge Profile for BESS in the end bus in Case 3B (Decentralized, Winter)

5.3.3 Case 3C (Autumn)

In this section, a combination of autumn PV profile and decentralized BESS is run into the simulation model. **Figure 5.80** shows the global exchange power of the system. Similar to the two previous decentralized cases, the power management shifts the unwanted BESS charging period during the second cheapest price to the lowest price period which is handled by BESS in the middle of the system. As a result, less money spent to buy electricity from the grid. Visually no substantial different appears in the bus voltage profile compared to the case of centralized BESS, an only slight shorter period of the voltage touching the minimum limit of 360 V during the first BESS charging period as seen in **Figure 5.81**. Specific look of BESS power and state of charge during daily operation are presented accordingly in **Figure 5.82** and **Figure 5.83**.

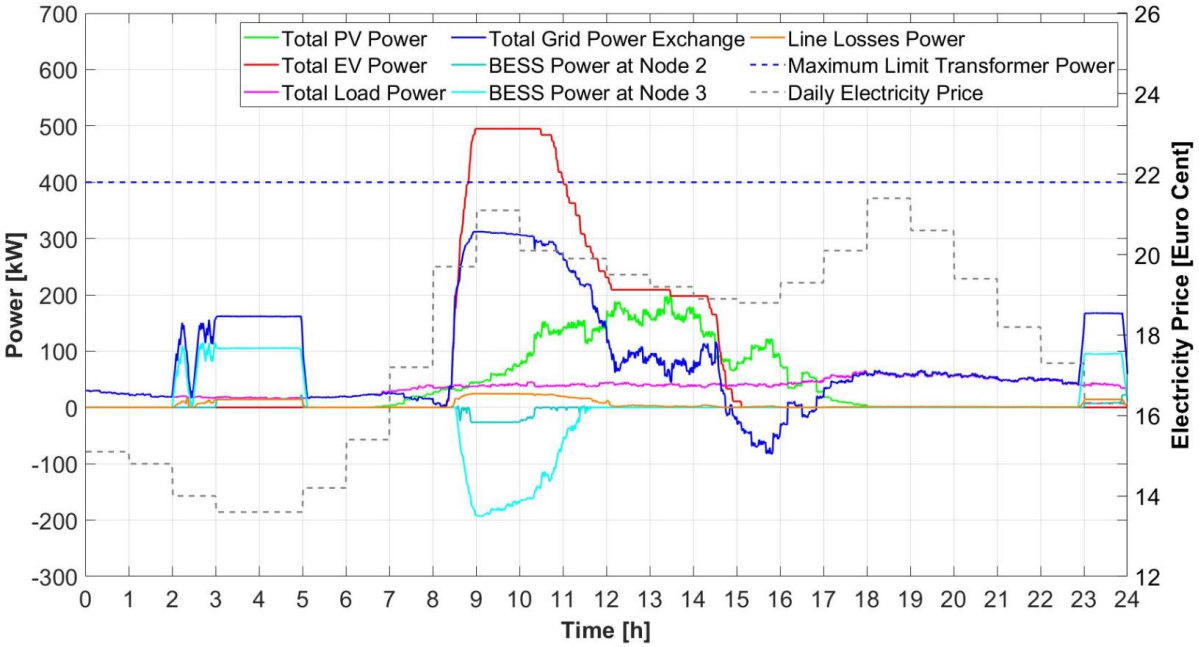

Figure 5.80 Power Exchange Profile of the Overall System for Case 3C (Decentralized, Autumn)

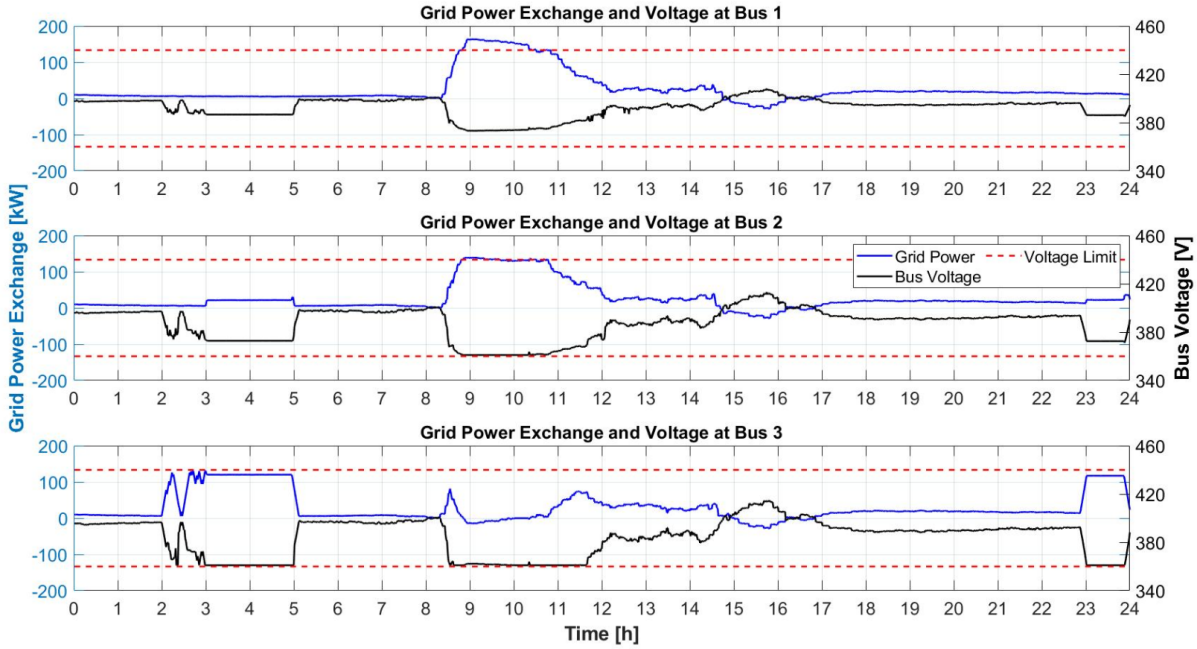

Figure 5.81 Voltage Profile at Different Bus of the System for Case 3C (Decentralized, Autumn)

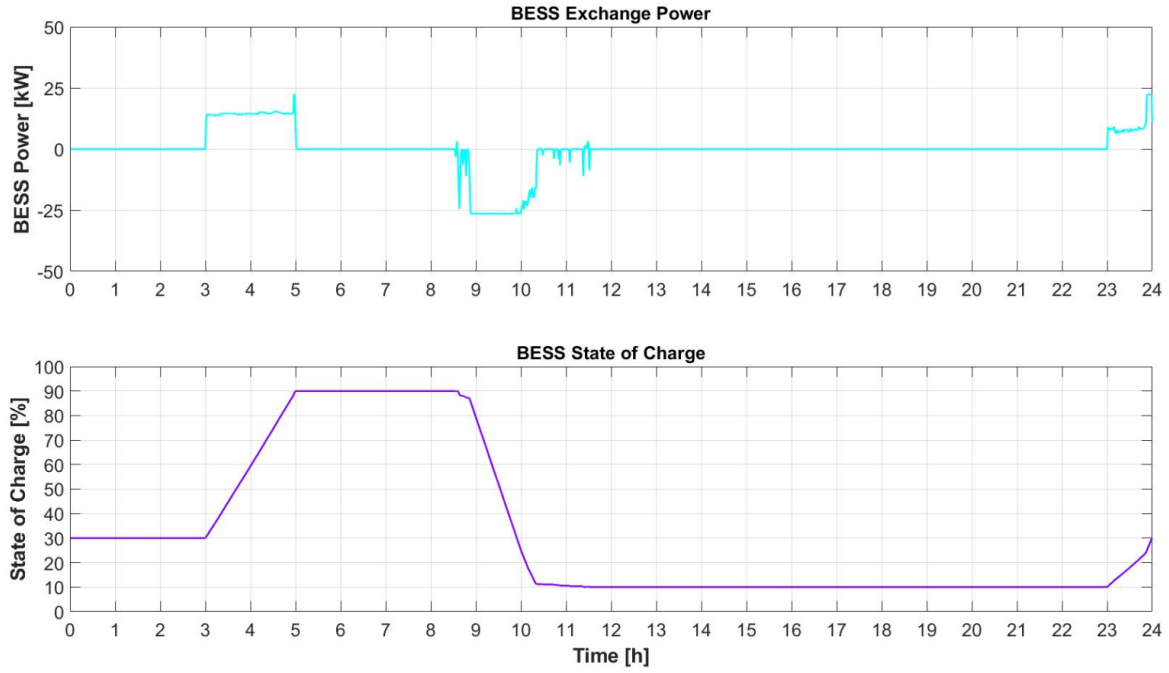

Figure 5.82 Power and State of Charge Profile for BESS in the middle bus in Case 3C (Decentralized, Autumn)

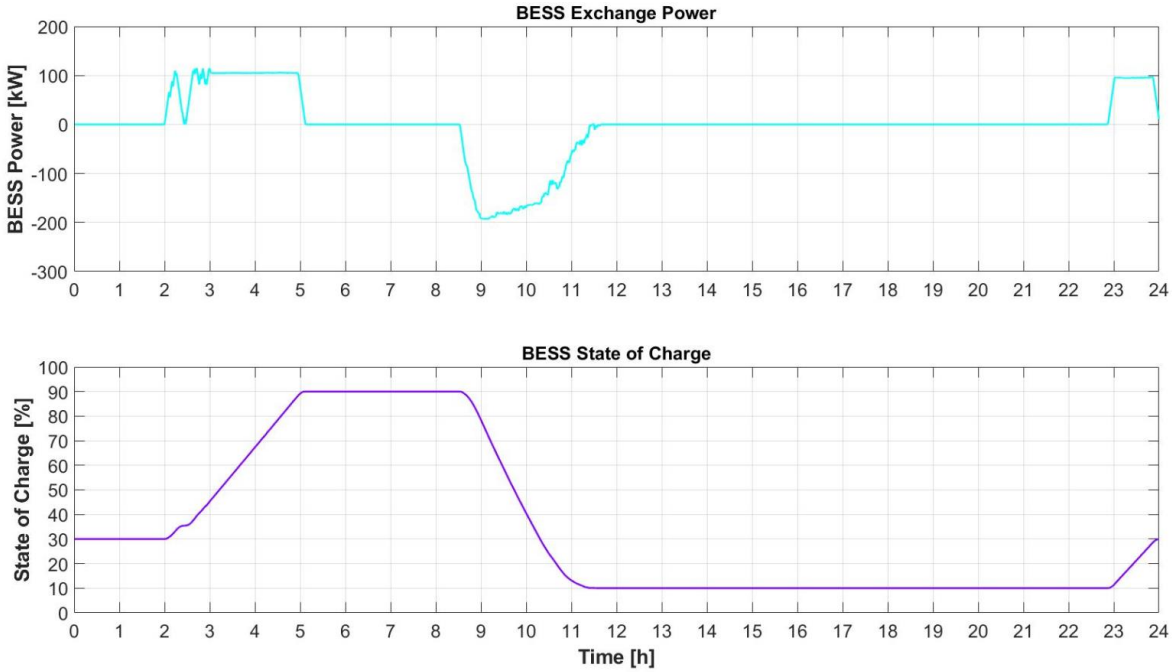

Figure 5.83 Power and State of Charge Profile for BESS in the end bus in Case 3C (Decentralized, Autumn)

5.3.4 Summary

Decentralized BESS approach has been implemented in this section through PV power profile of summer, winter, and autumn. The optimization solver is given freedom to place BESS in all the bus in the system instead of only one centralized BESS which is applied in the previous chapter. However, BESS only suggested being appeared in the middle and end of the feeder. It is not necessary to apply BESS in the frontest bus in the system because the least severe drop voltage occurs in that position. Moreover, asymmetrical BESS sizing is suggested for BESS in the second and third bus of the system. Much larger BESS maximum power and capacity are advised for the BESS in the furthest bus compared than BESS in the middle of the system as illustrated in **Figure 5.84** and **Figure 5.85**. This is logical because of the furthest bus will experience worst voltage drop and needs more support by BESS power to keep the bus voltage beyond the minimum voltage limit allowed. The power management shifts part of BESS charging period which previously also occurs during the second lowest electricity price period to the cheapest period which is now handled by the BESS in the middle of the system. This situation can be possibly done because of the middle bus experience less severe voltage drop, so that in total more power can be drawn from the grid during the cheapest period compared to centralized BESS which needs to spread the charging period to the next lowest price because of voltage limitation.

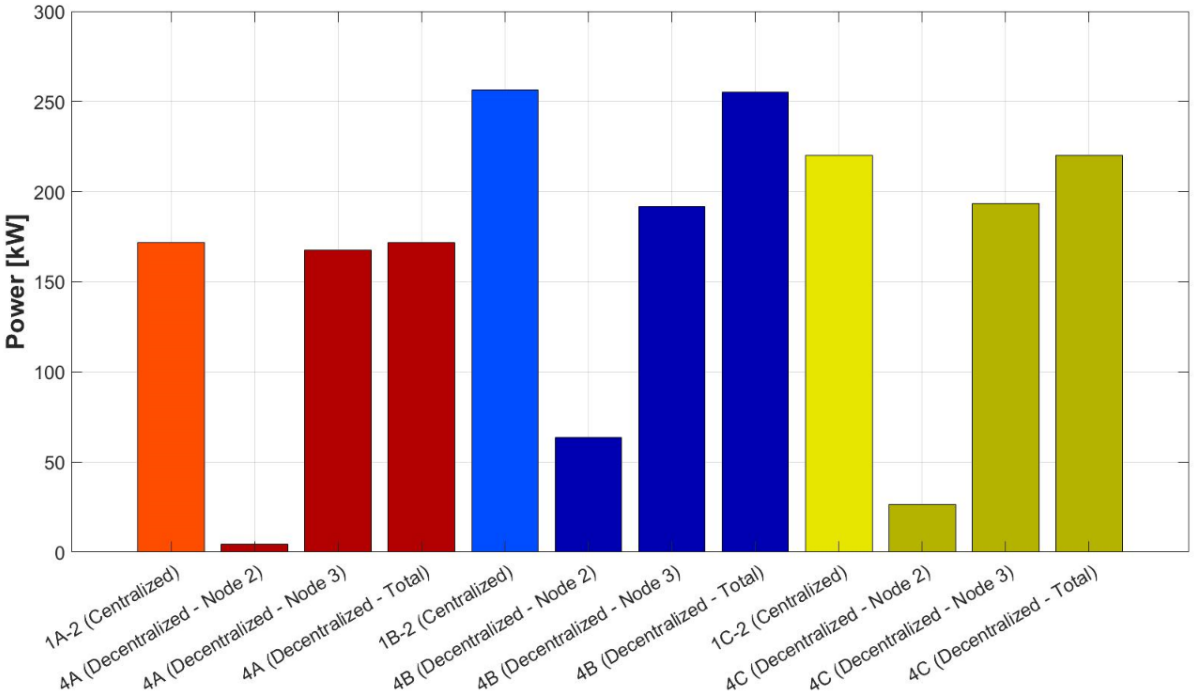

Figure 5.84 BESS Maximum Power for Case 3 (Decentralized BESS Location)

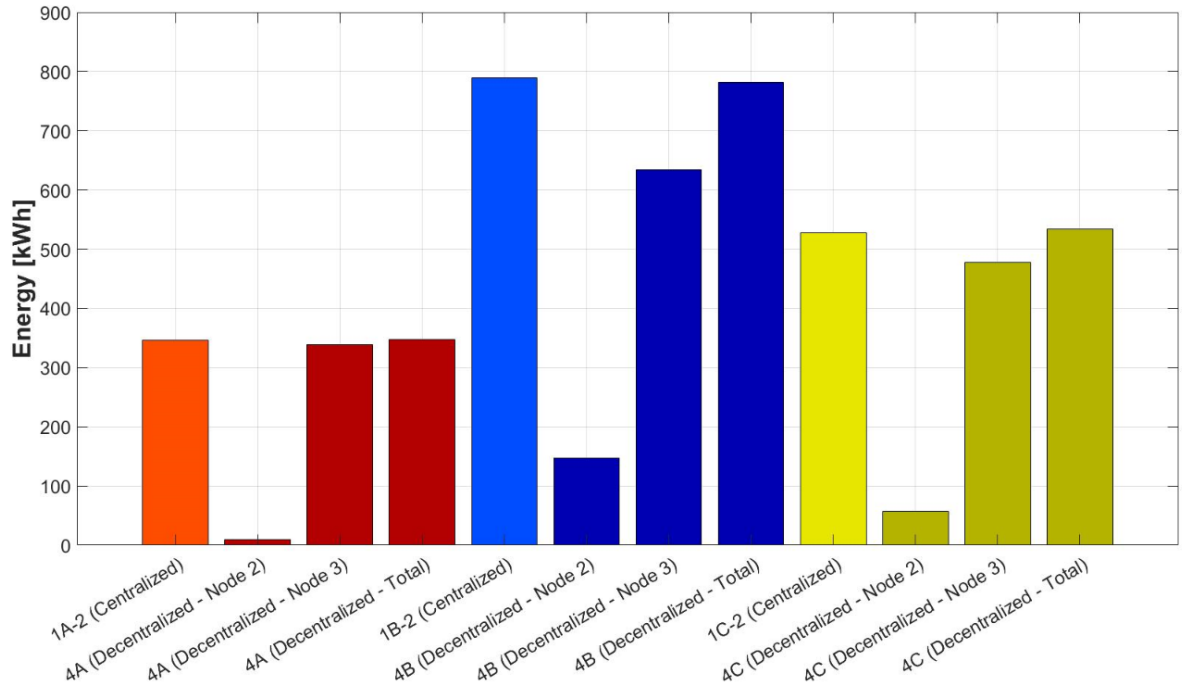

Figure 5.85 BESS Capacity Required for Case 3 (Decentralized BESS Location)

However, when the maximum power and capacity of the two BESS are summed up, the result is similar to the centralized BESS approach. As a consequence, the BESS investment cost of the centralized and decentralized BESS approach is almost the same as seen in **Figure 5.86**. The decentralized BESS approach is only slight cheaper compared to the centralized one.

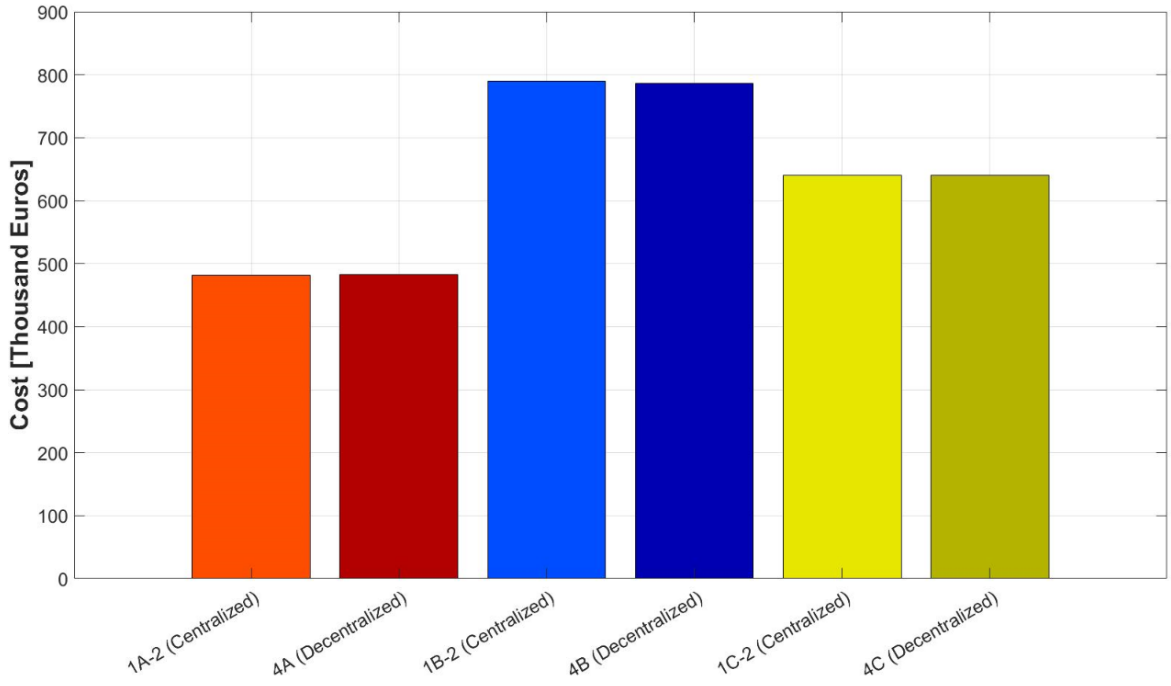

Figure 5.86 BESS Investment Cost for Case 3 (Decentralized BESS Location)

The BESS is suggested to be placed at the middle bus and furthest bus as illustrated in **Figure 5.87**, even though it is possible to be placed at the nearest bus from the transformer. BESS is prioritized to be placed at the bus with severe voltage condition which is the further from transformer, to make more significant impact for voltage mitigation and as a result less BESS is required to achieve less cost. Moreover, due to comparable BESS maximum power, the maximum transformer power of centralized and decentralized approach is also similar as shown in **Figure 5.88**. Furthermore, comparison of the electricity cost that needs to be paid by taking power from the grid is presented in **Figure 5.89**. Although the power management system has managed to shift unwanted BESS charging period during not the cheapest period, evidently no significant electricity cost reduction appears. Finally, the total cost comparison is displayed in **Figure 5.90**. In line with the BESS investment and electricity cost result, the total cost of the centralized and decentralized system is also analogous.

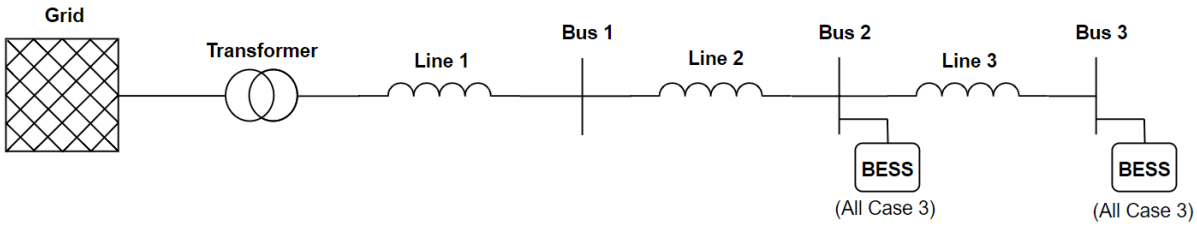

Figure 5.87 Optimal BESS Location for Case 3 (Decentralized BESS Location)

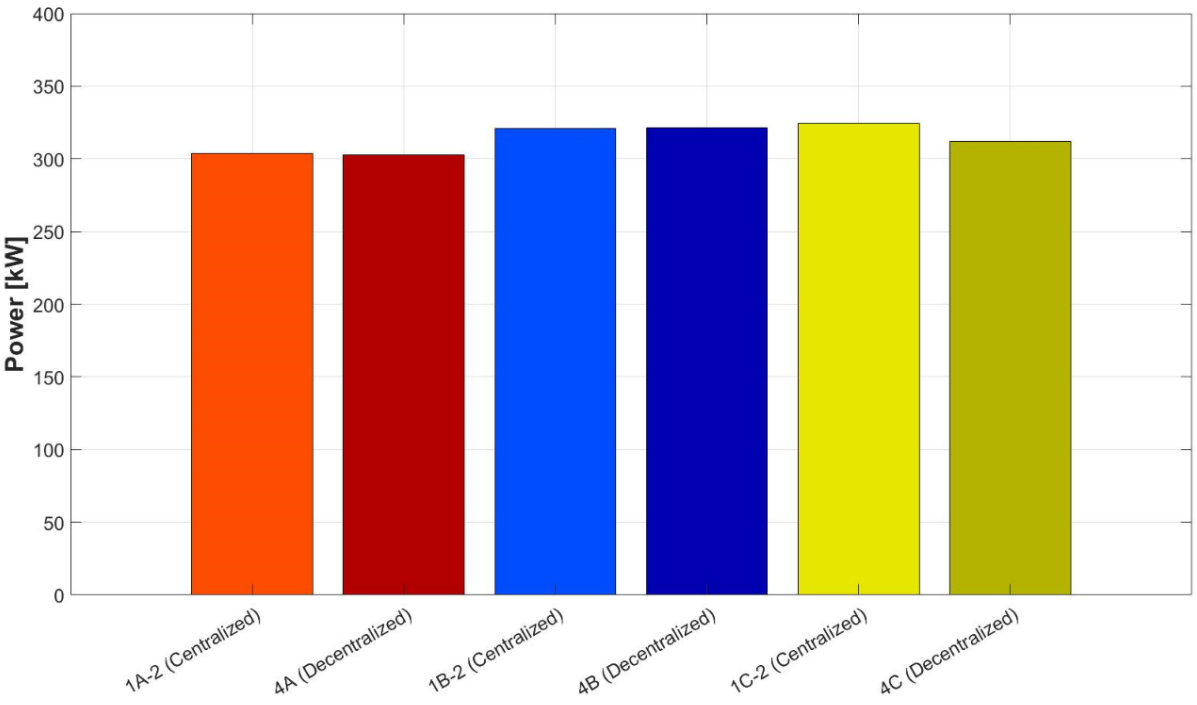

Figure 5.88 Maximum Transformer Loading Power for Case 3 (Decentralized BESS Location)

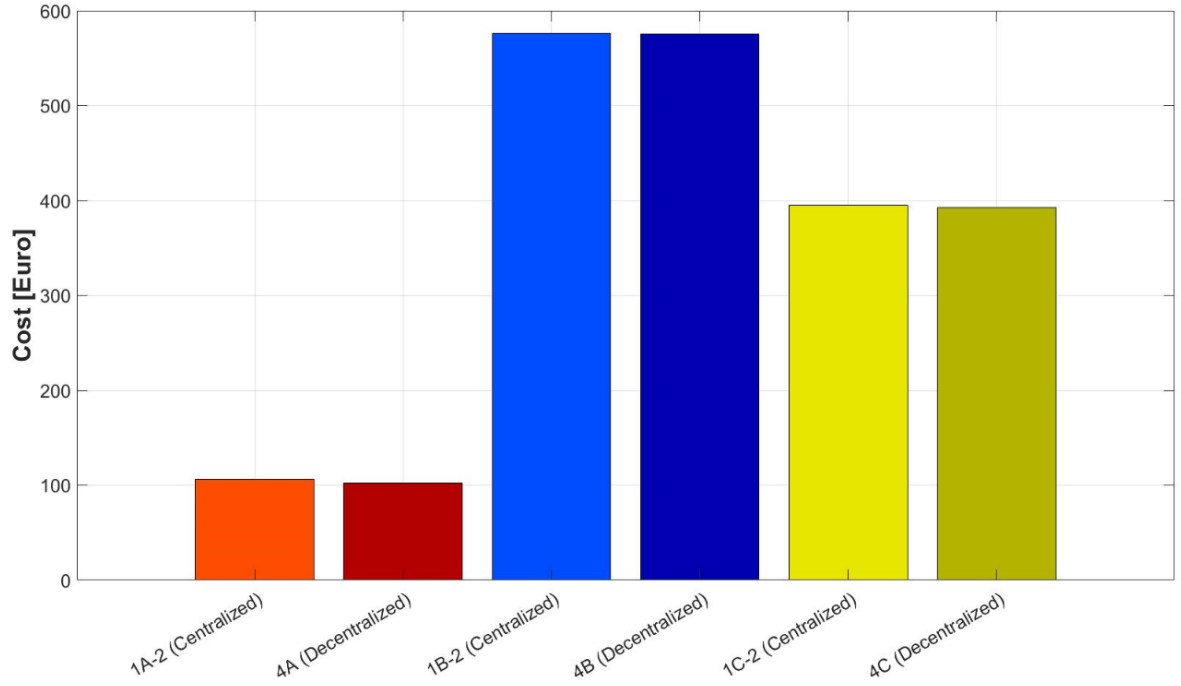

Figure 5.89 Electricity Cost for Case 3 (Decentralized BESS Location)

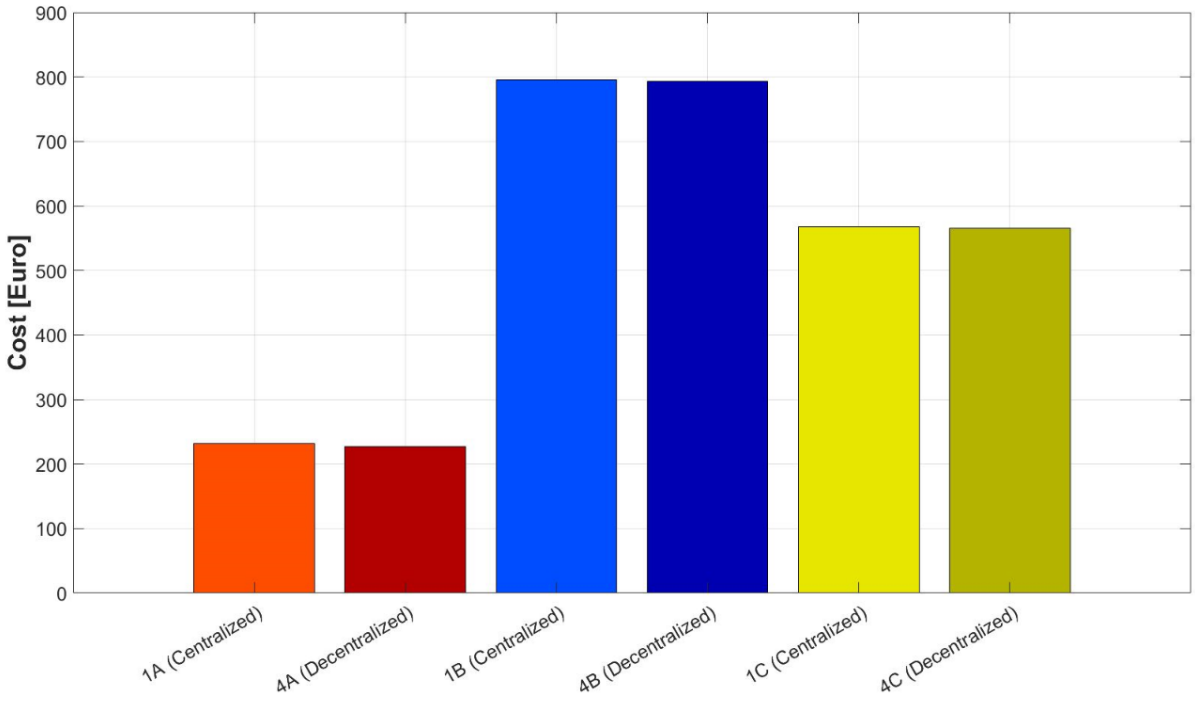

Figure 5.90 Total Cost for Case 3 (Decentralized BESS Location)

5.4 Different EV Charging Strategy

Although the proposed sizing methods and power management system seems fine, there is still an inefficiency PV usage due to uncontrolled EV charging scheme. EVs are directly charge as they arrive at the charger station which leads to a condition of inefficient use of PV power because the charging process is not being done during the peak PV power. The system is forced to draw more power from the grid to fulfil the power demand. In this section, three different EV charging methods are proposed to tackle the inefficiency issues in the system. First, the EV charging start is delayed until 10 a.m. to utilize more PV power during the day. Second, constant EV charging power during connection time in the EV charger station is deployed following equation **(5.1)**. Last, dynamic EV charging power controlled by the power management system is applied according equation **(5.1)** without subjection as the constant power case.

$$\left|P_{v,n,t}^{ch}\right| \leq 11\ kW \tag{5.1}$$

subject to:

$$P_{v,n,t+1}^{ch} - P_{v,n,t+1}^{ch} \leq 0$$

5.4.1 Case 4A-1 (Summer, EV Charging Period Shift)

In this scenario, summer PV profile is integrated with delayed EV charging strategy. All EVs charging are delayed from the normal direct uncontrolled case and all start from 10 a.m. in order to utilize more PV power which mostly occurs during the afternoon. The result of overall exchange power in the system is presented in **Figure 5.91**. More PV power utilization leads to less BESS intervention is required to keep the maximum transformer power and bus voltage between the safe margin compared to direct uncontrolled EV charging as seen in **Figure 5.8**. The BESS charging power during the first charging period is reduced because less BESS capacity is required. Then, BESS discharging power is also decreased because peak EV charging demand is already satisfied by more PV power during midday. Last, less energy is also needed to bring back BESS state of charge to the initial value. Moreover, better bus voltage profile is obtained as illustrated in **Figure 5.92** because of less grid power is needed to be drawn to charge BESS. Therefore, during the first BESS charging period, the voltage is not touching the minimum voltage allowed as happened in Case 1A-2. The BESS state of charge profile during daily operation is presented in **Figure 5.93**.

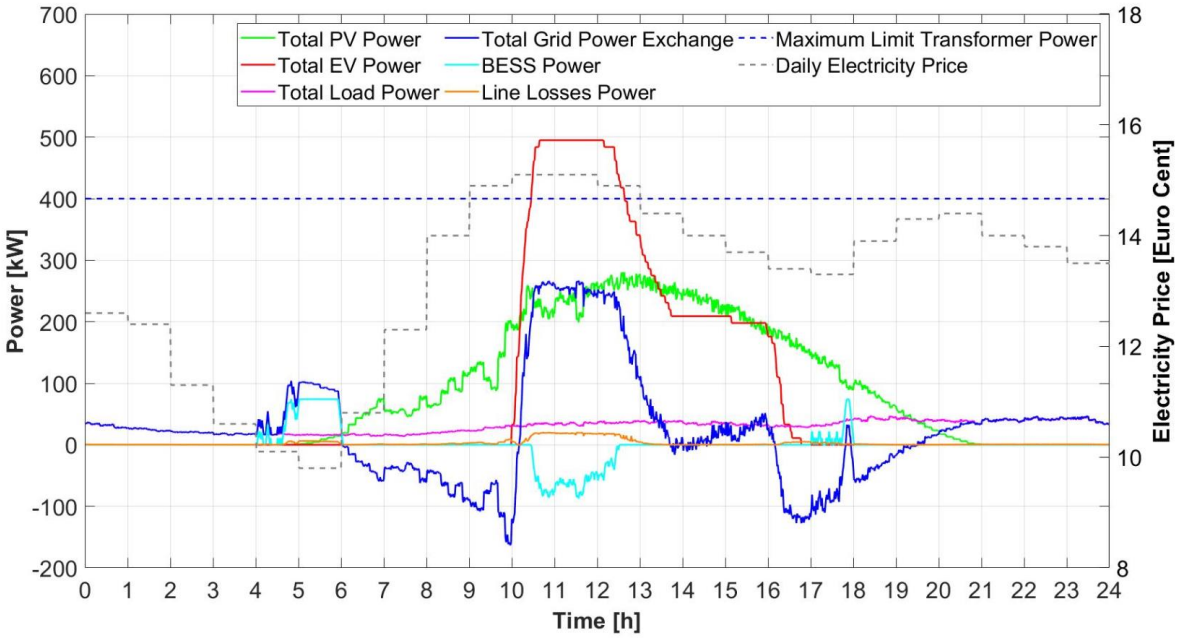

Figure 5.91 Power Exchange Profile of the Overall System for Case 4A-1 (EV Charging Period Shift, Summer)

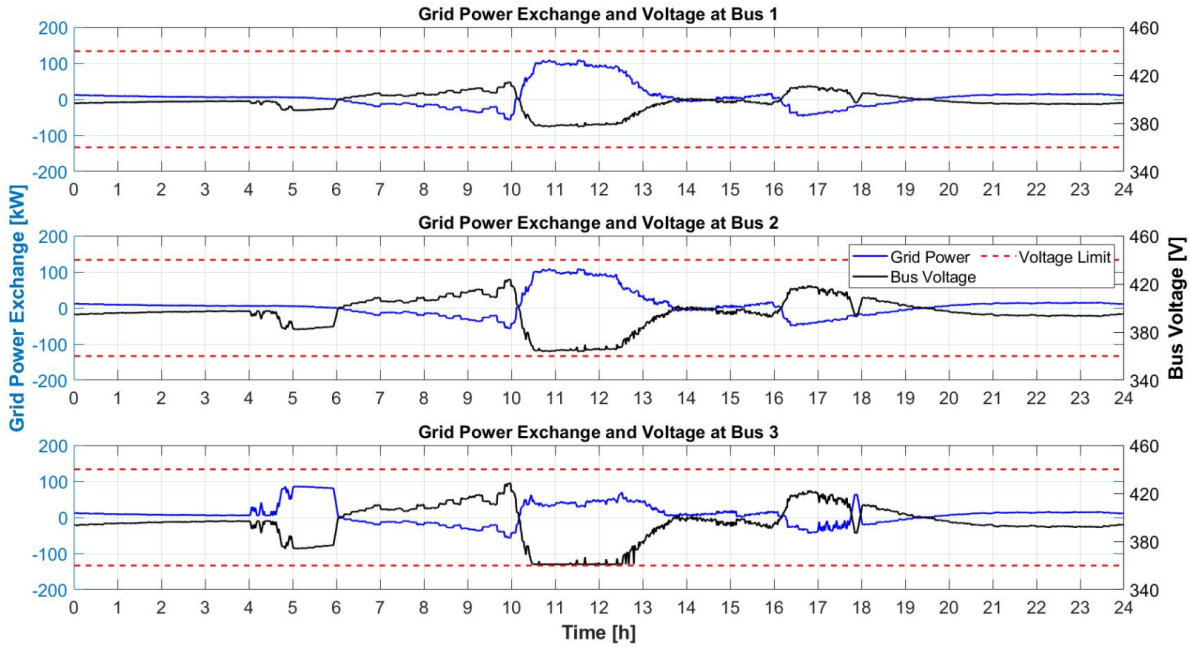

Figure 5.92 Voltage Profile at Different Bus of the System for Case 4A-1 (EV Charging Period Shift, Summer)

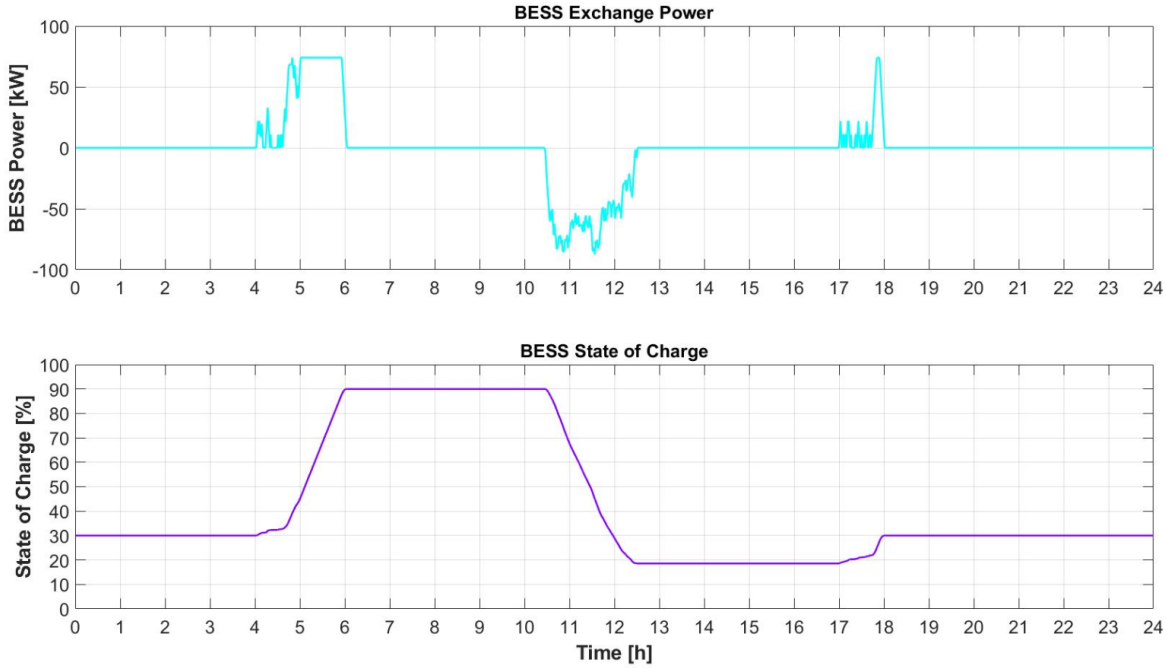

Figure 5.93 BESS Power and State of Charge Profile for Case 4A-1 (EV Charging Period Shift, Summer)

5.4.2 Case 4A-2 (Summer, Constant EV Charging Power)

In this case, the constant EV charging strategy is applied to the PV profile of summer. The power management system will determine the required constant EV is charging power depends on the energy difference between initial and full EV battery capacity and also remaining time between arrival and departure time of EV to the charger station. The lower EV residence time leads to the higher EV charging power required. **Figure 5.94** shows the overall exchange power in the system. It is noticeable that equal distributed EV charging power is applied between arrival and departure time of EV. As a result, no BESS is required, and less grid power is drawn to support EV charging compared to uncontrolled approach because of more PV power utilization. The peak EV charging power is reduced to be spread identically during the charging period. Furthermore, better bus voltage appears in the system as presented in **Figure 5.95**. The bus voltage never reaches the minimum voltage of 360 V which never happen in all previous simulations.

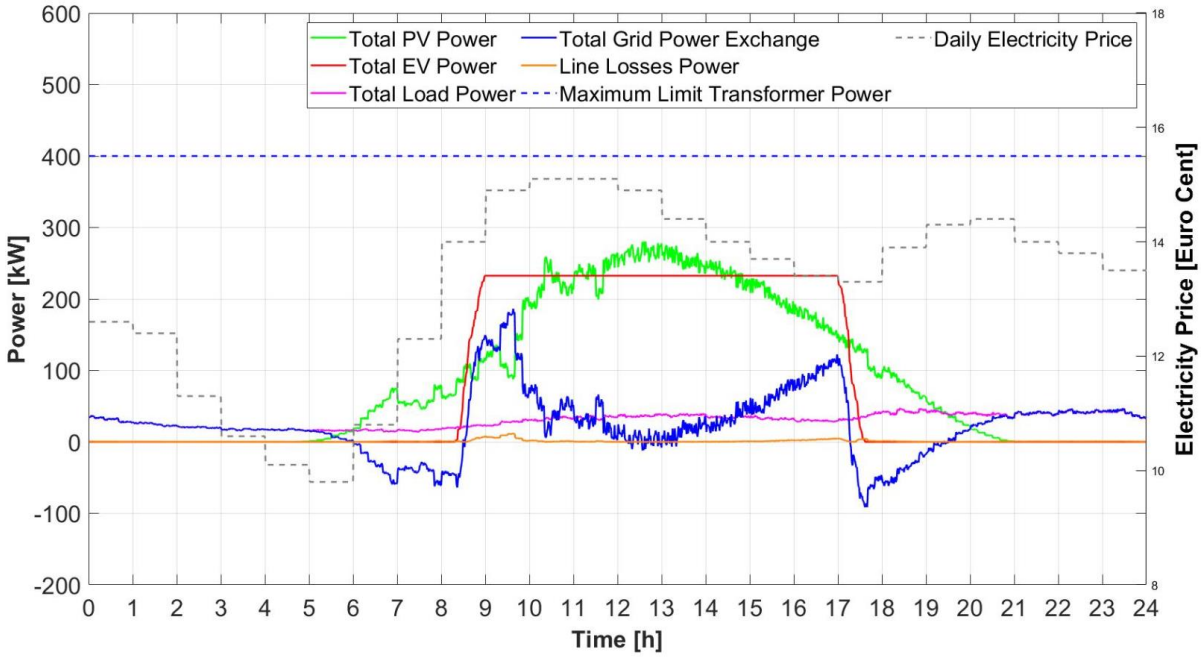

Figure 5.94 Power Exchange Profile of the Overall System for Case 4A-2 (Constant EV Charging, Summer)

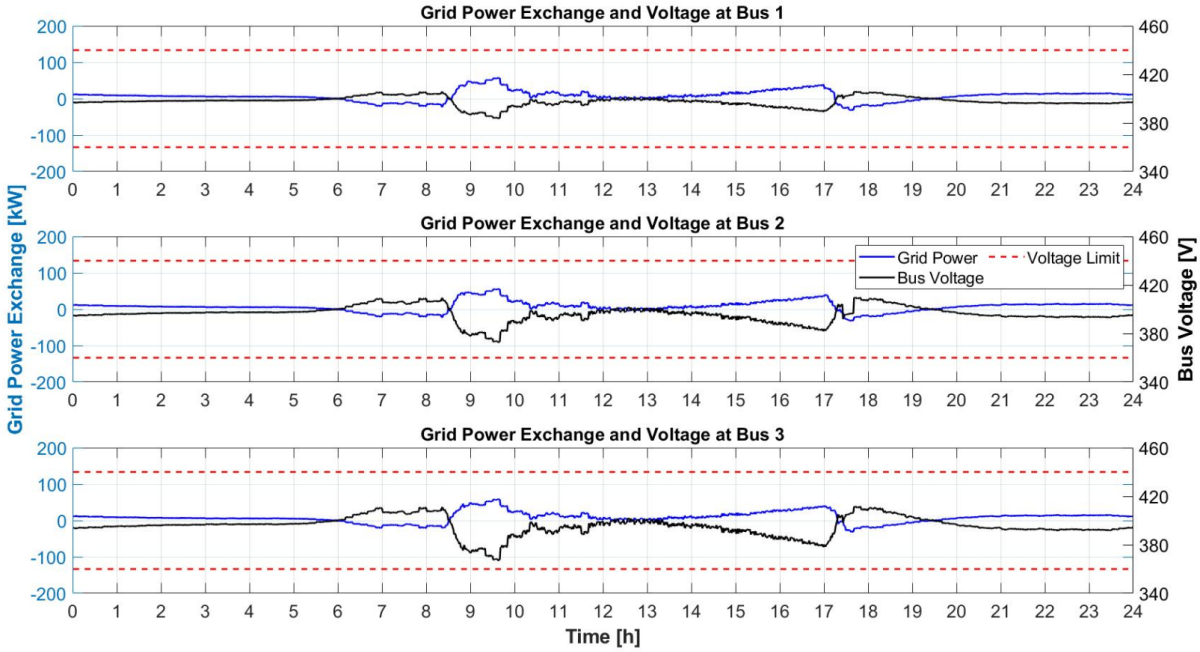

Figure 5.95 Voltage Profile at Different Bus of the System for Case 4A-2 (Constant EV Charging, Summer)

5.4.3 Case 4A-3 (Summer, Dynamic EV Charging Power)

In this section, the power management system is given freedom to determine the amount of EV charging power and scheduling between arrival and departure time to the charger station. The global exchange power of the system is illustrated in **Figure 5.96**. Similar to EV constant charging approach in the previous case, no BESS is suggested in the system due to its relatively high BESS price. **Figure 5.97** reveals different EV charging profile occurs at the different bus in the system. The power management system manages sequential peak EV charging period for every bus to distribute the voltage stress through the time. Moreover, EVs are prioritized to be mainly charged during low price period to decrease the electricity cost to be paid by drawing power from the grid. Furthermore, the power management system also delays the EV charging period during the highest electricity price at 10 a.m. to 12 p.m. to increase the revenue by selling PV power to the grid. However, because of most EVs charging are prioritized during the low price period, the bus voltage reaches the minimum voltage limit during high EV charging power demand as shown in **Figure 5.98**.

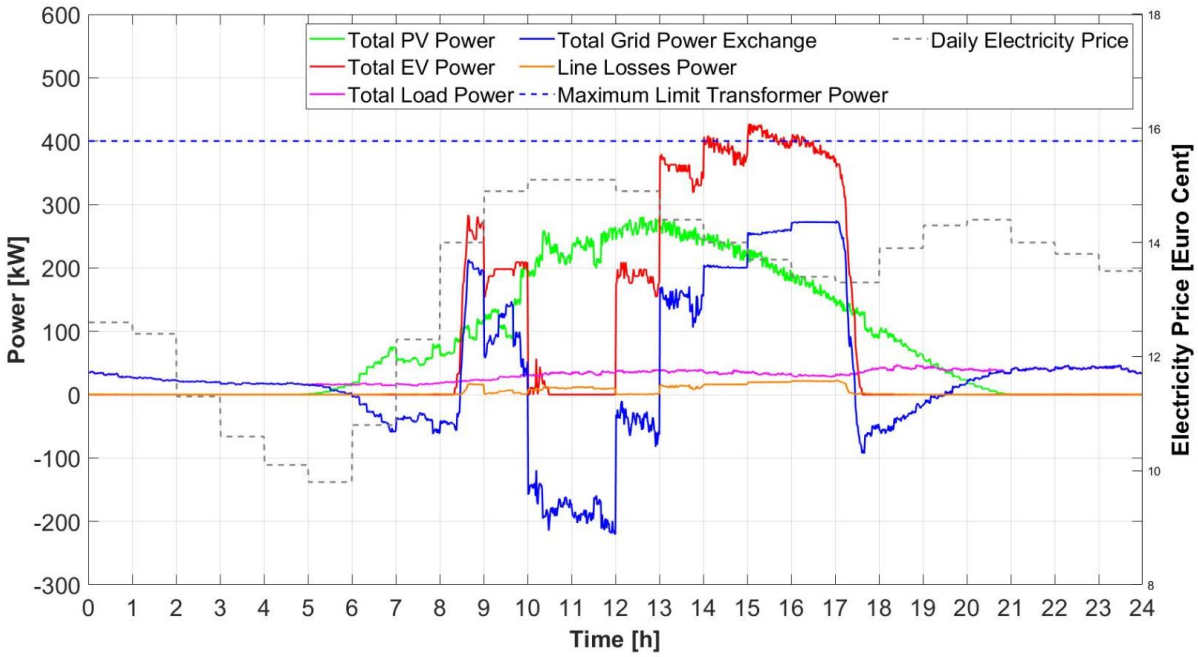

Figure 5.96 Power Exchange Profile of the Overall System for Case 4A-3 (Dynamic EV Charging, Summer)

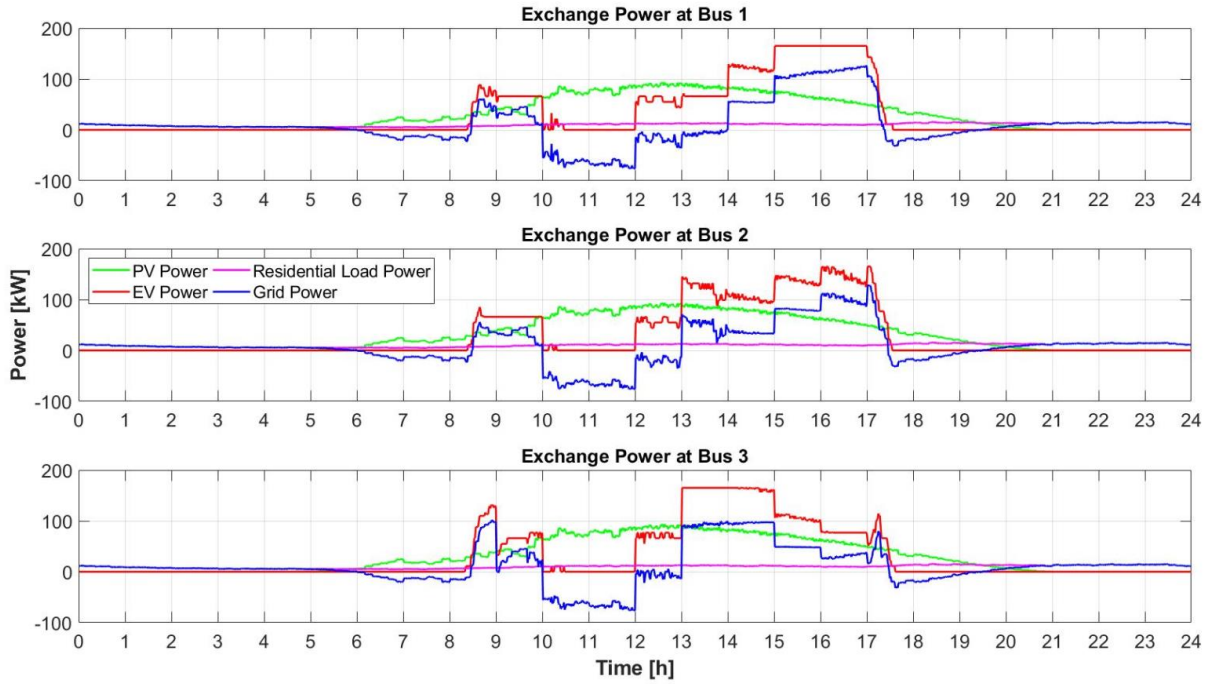

Figure 5.97 Power Exchange Profile of Each Bus for Case 4A-3 (Dynamic EV Charging, Summer)

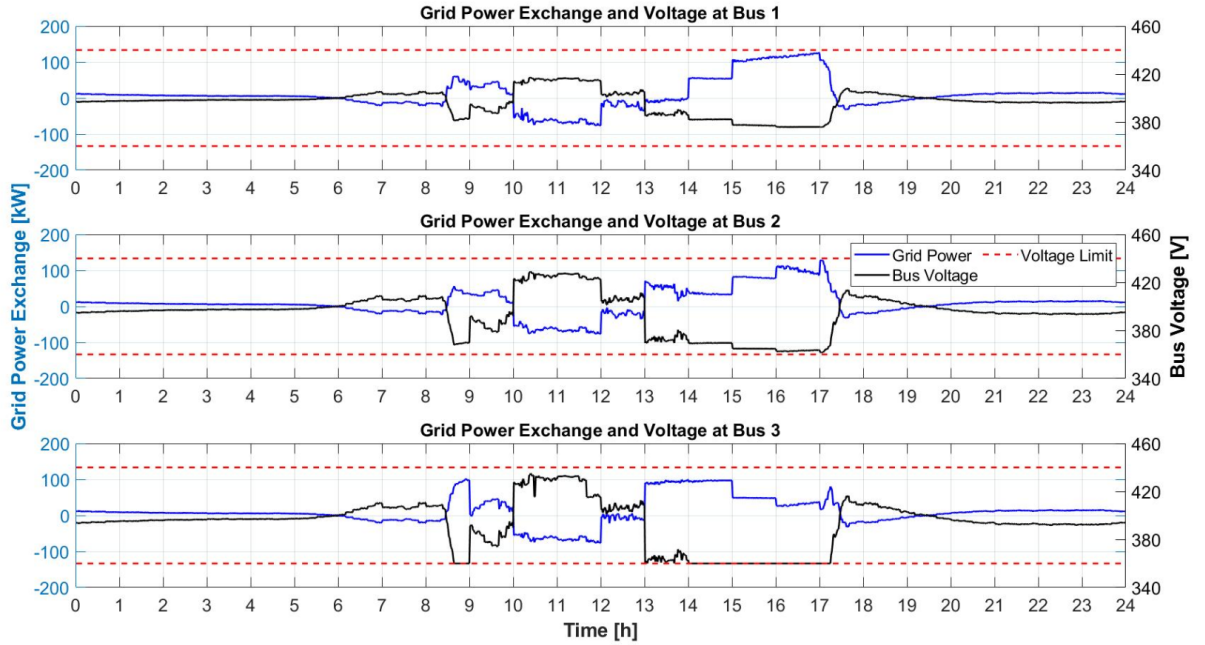

Figure 5.98 Voltage Profile at Different Bus of the System for Case 4A-3 (Dynamic EV Charging, Summer)

5.4.4 Case 4B-1 (Winter, EV Charging Period Shift)

In this case, deferred EV charging strategy is adopted in winter PV profile. The global system exchange power is presented in **Figure 5.99**. Contrast to result in summer simulation, in general, there is no significant change to the BESS operation in the system. The BESS is charging and discharging power amount and scheduling are similar to the direct uncontrolled charging schemes in Case 1B-2 as seen in **Figure 5.22**. BESS is still forced to spread its charging time also during not the cheapest period because of maximum grid power that can be drawn to satisfy the minimum voltage limit. This condition happens because of very low PV power is generated during the winter season. As a result, there is no PV power utilization addition as happened in Case 4A-1. Only a small amount of BESS power reduction appears during peak PV power production. Moreover, the bus voltage is maintained beyond the minimum voltage limit as shown in **Figure 5.100**. The daily BESS state of charge profile is illustrated in **Figure 5.101**.

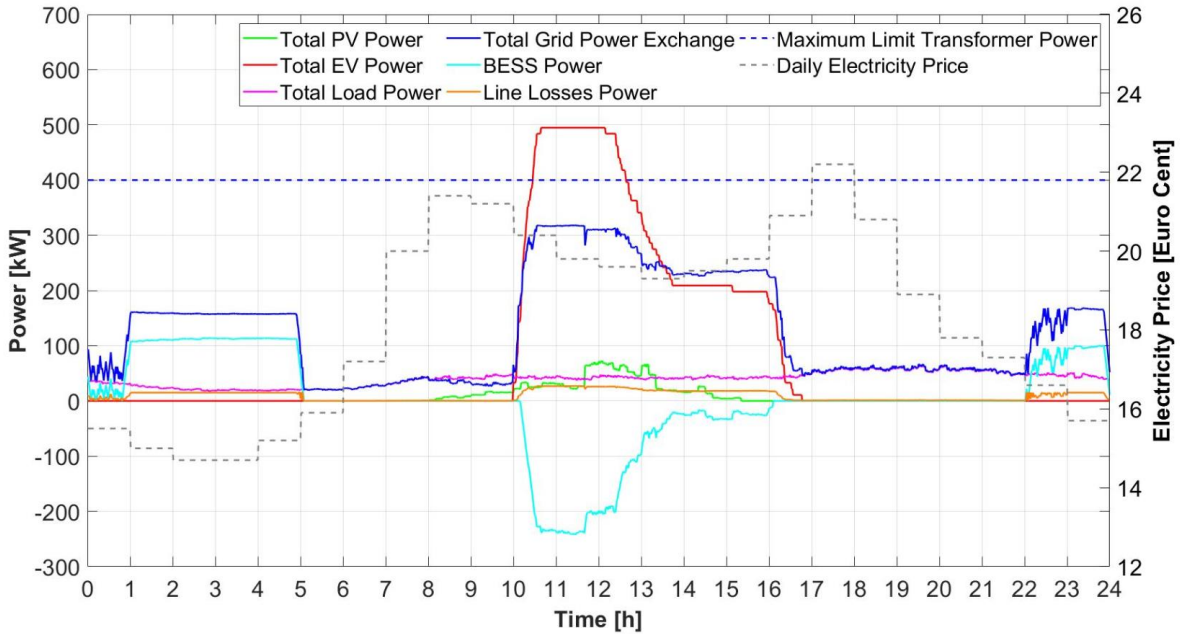

Figure 5.99 Power Exchange Profile of the Overall System for Case 4B-1 (EV Charging Period Shift, Winter)

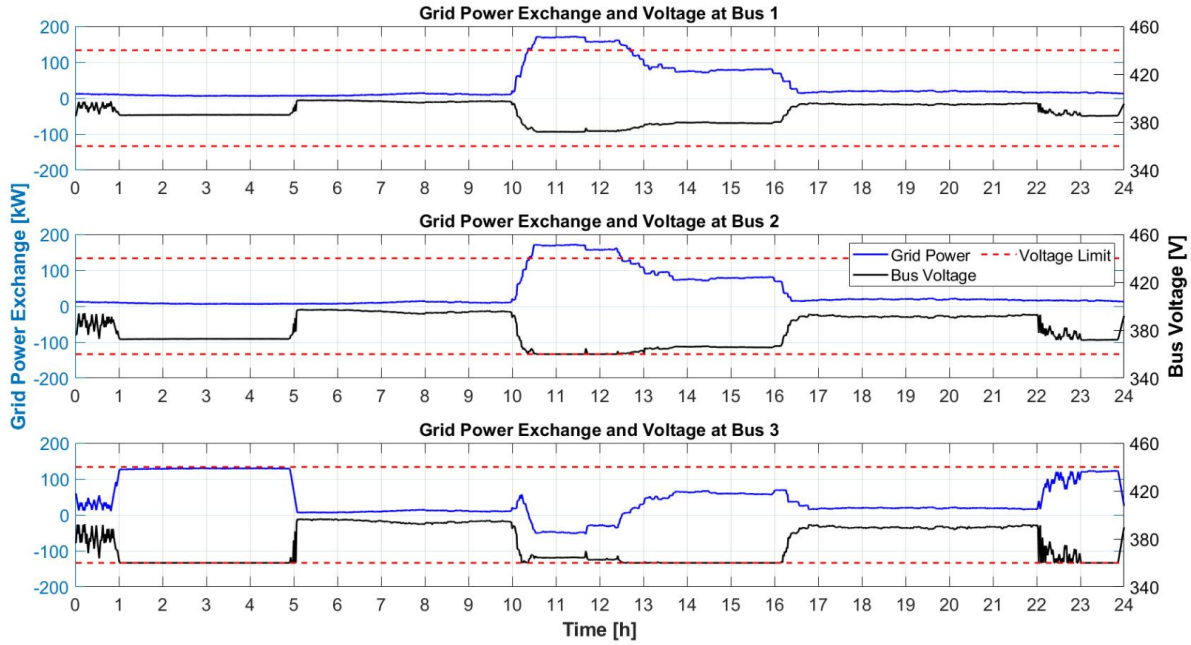

Figure 5.100 Voltage Profile at Different Bus of the System for Case 4B-1 (EV Charging Period Shift, Winter)

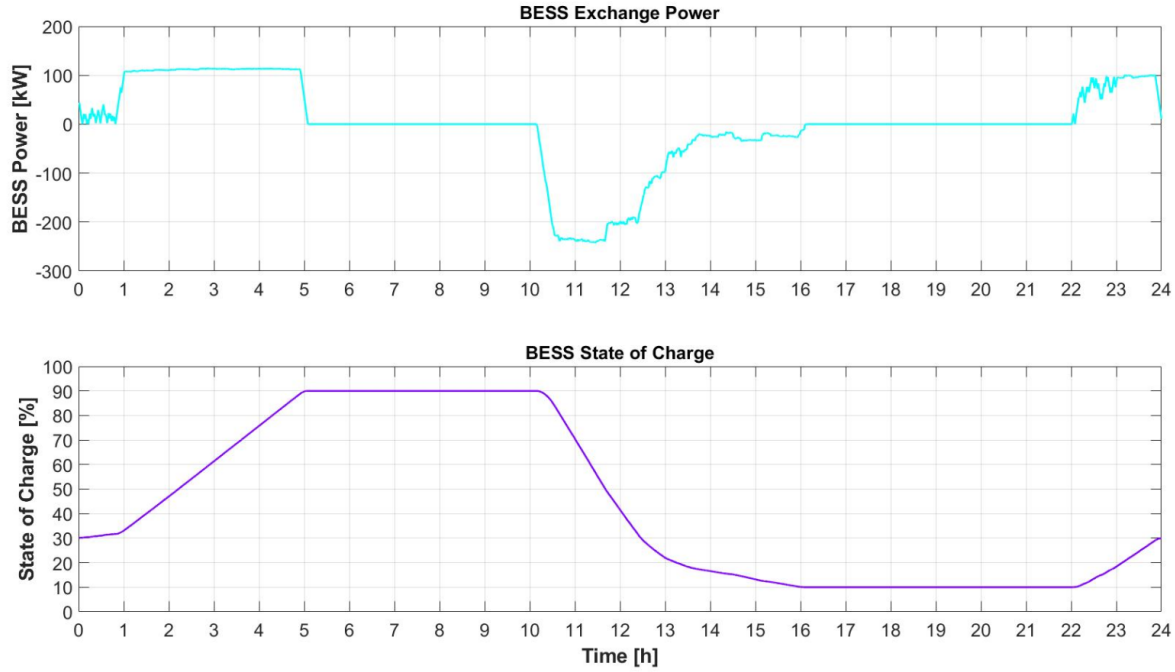

Figure 5.101 BESS Power and State of Charge Profile for Case 4B-1 (EV Charging Period Shift, Winter)

5.4.5 Case 4B-2 (Winter, Constant EV Charging Power)

In this section, the PV power profile of winter season is combined with constant EV charging strategy. The overall exchange of power in the system is shown in **Figure 5.102**. It is noticeable that less BESS charging and discharging energy is required to keep the system following the grid code limitation. First, BESS is charged only during the lowest electricity price period, 3 hours shorter compared to uncontrolled EV charging scheme in Case 1B-2 as illustrated in **Figure 5.22**. Besides, BESS maximum discharging power is highly reduced because of EV charging energy is distributed equally during EV residence time in the charger station. Last, shorter BESS recharging time is needed to gains back the state of charge to initial value due to less BESS capacity is required. The bus voltage and BESS state of charge are respectively presented in **Figure 5.103** and **Figure 5.104**.

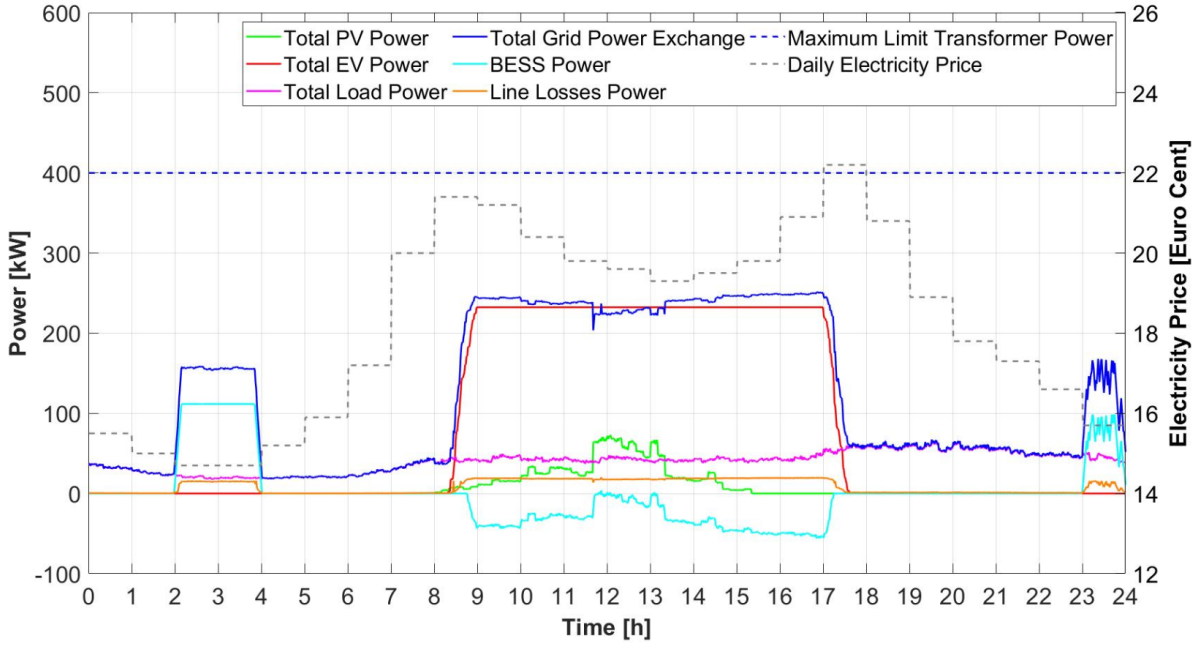

Figure 5.102 Power Exchange Profile of the Overall System for Case 4B-2 (Constant EV Charging, Winter)

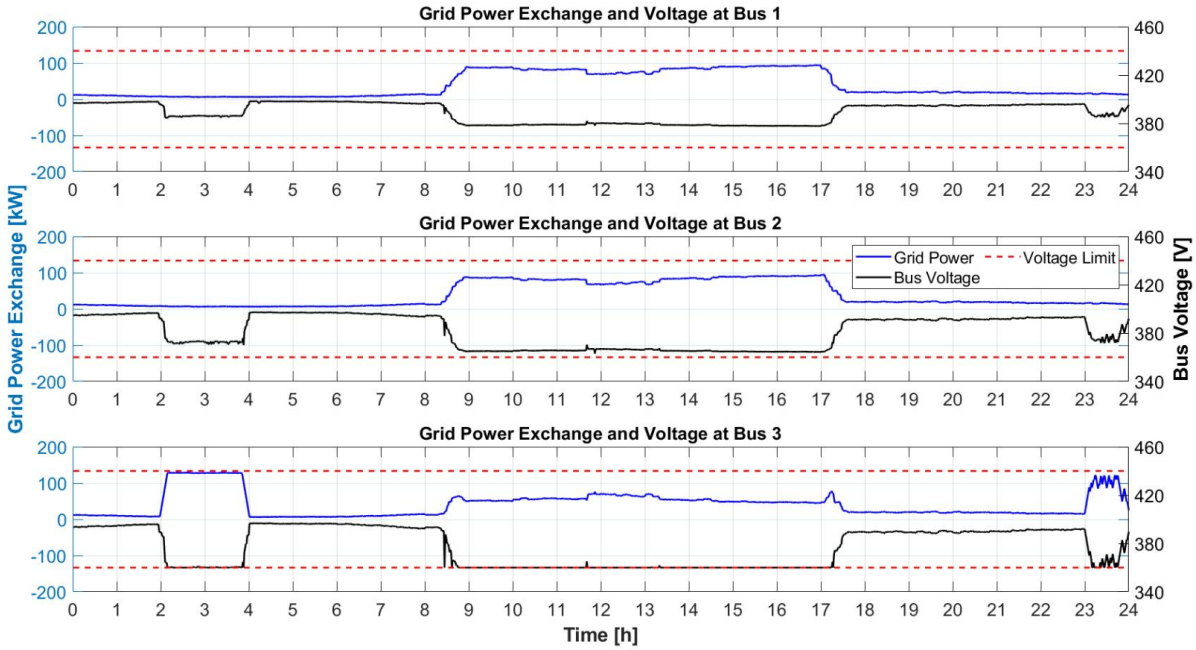

Figure 5.103 Voltage Profile at Different Bus of the System for Case 4B-2 (Constant EV Charging, Winter)

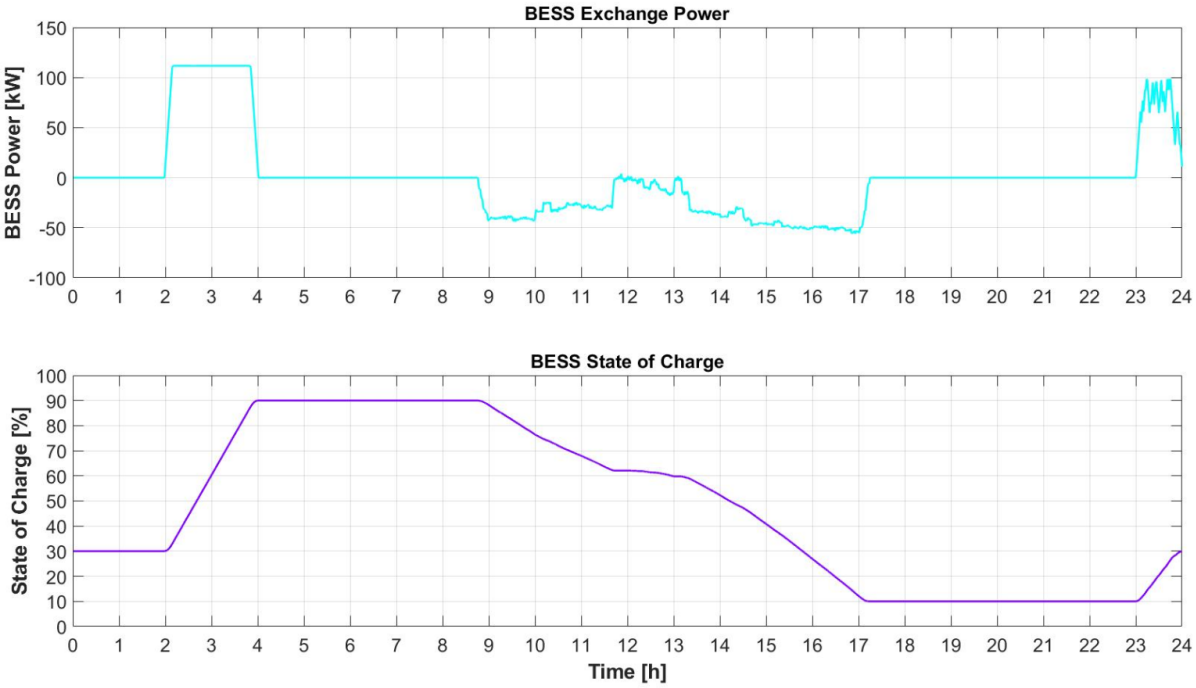

Figure 5.104 BESS Power and State of Charge Profile for Case 4B-2 (Constant EV Charging, Winter)

5.4.6 Case 4B-3 (Winter, Dynamic EV Charging Power)

In this scenario, variable EV charging power is implemented in winter PV power profile. **Figure 5.105** presents the overall exchange power of the system. Similar to the previous case, less BESS energy is required to keep the maximum transformer power and bus voltage stays in the safe margin. Initially, BESS is mainly charged during the lowest electricity period as preparation for high EV charging power demand period. Then, more EV charging power is delivered during low electricity price at 12 to 3 p.m. to minimize the electricity cost. Furthermore, the EV charging profile is controlled consecutively for different charging station as presented in **Figure 5.106**. EVs at the frontest bus is mainly charged during initial and end of EV residence time, while EVs at the middle bus are mostly charged during mid-day. Besides, EVs at the furthest bus is charged equally distributed during their connection time except during peak EV charging power at the second bus to keep the bus voltage not exceeding the minimum voltage limit allowed as seen in **Figure 5.107**. Last, all allowable BESS state of charge is explored to optimize the BESS utilization as illustrated in **Figure 5.108**.

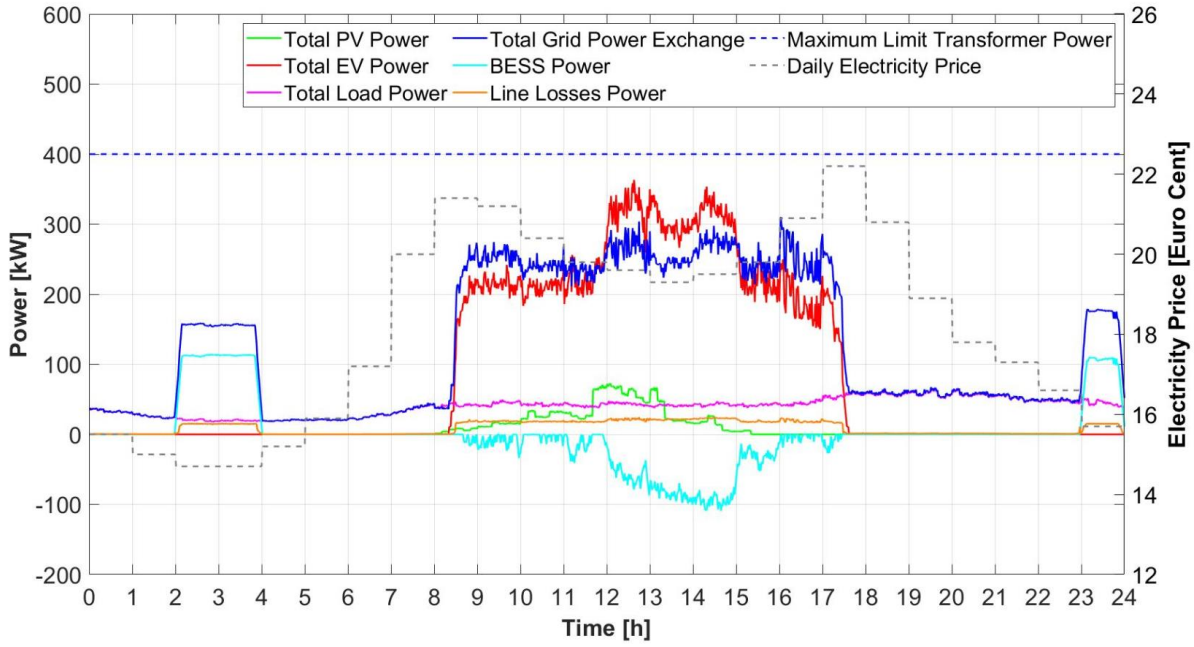

Figure 5.105 Power Exchange Profile of the Overall System for Case 4B-3 (Dynamic EV Charging, Winter)

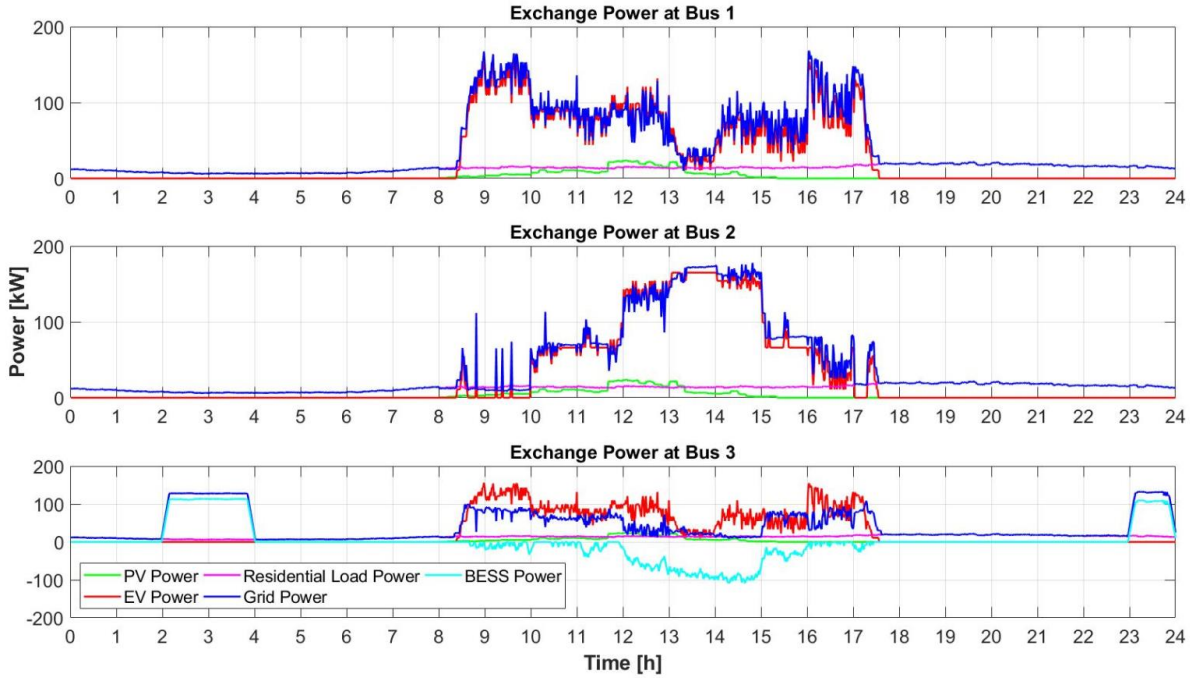

Figure 5.106 Power Exchange Profile of Each Bus for Case 4B-3 (Dynamic EV Charging, Winter)

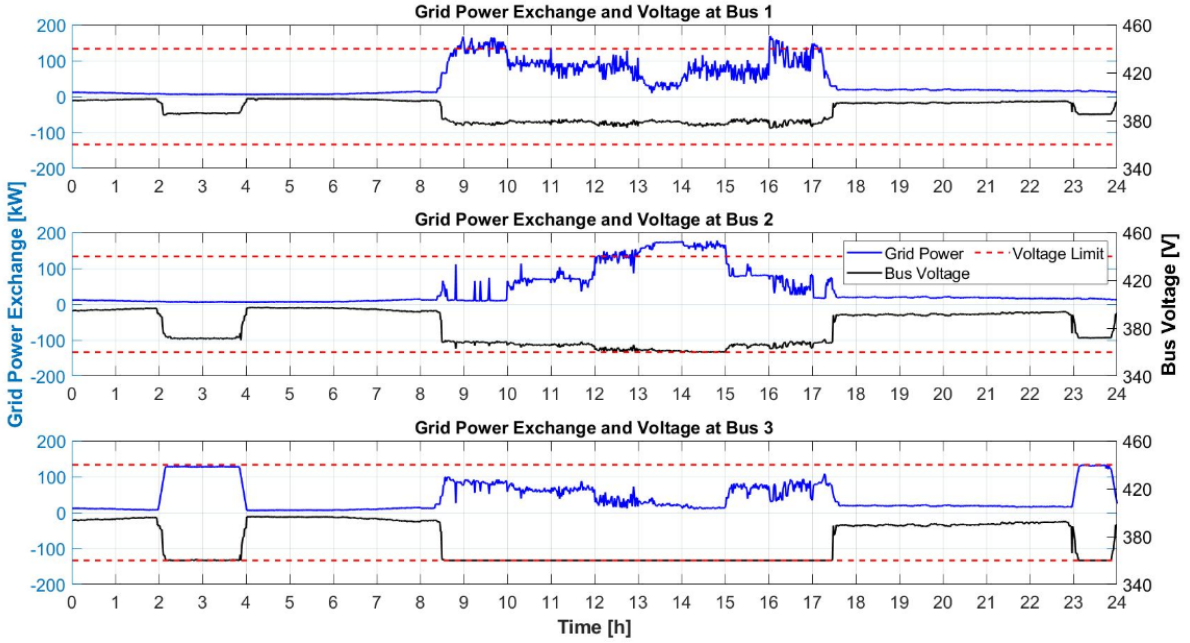

Figure 5.107 Voltage Profile at Different Bus of the System for Case 4B-3 (Dynamic EV Charging, Winter)

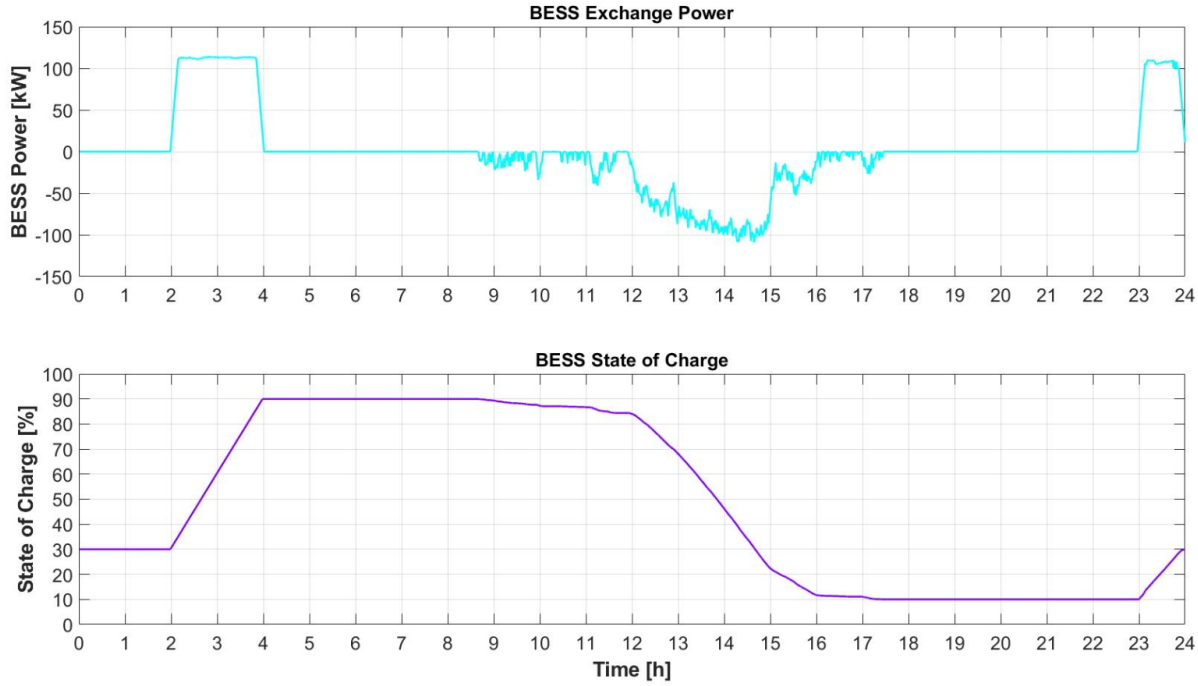

Figure 5.108 BESS Power and State of Charge Profile for Case 4B-3 (Dynamic EV Charging, Winter)

5.4.7 Case 4C-1 (Autumn, EV Charging Period Shift)

In this case, PV power profile during autumn is combined with postponed EV charging period method. The global overview of exchange power profile is illustrated in **Figure 5.109**. Less BESS energy is required to balance the system as indicated from shorter BESS charging period and lower BESS discharging power compared to ordinary direct uncontrolled EV charging strategy in Case 1C-2 as shown in **Figure 5.34**. Similar to Case 4A-1, higher PV power usage for EV charging is occurred due to the deferment. BESS is charged enough only during the lowest price to save the electricity cost. Later, less BESS power mitigation is required to reduce the stress in bus voltage during the mid-day. Detail of bus voltage and BESS state of charge profile are accordingly shown in **Figure 5.110** and **Figure 5.111**.

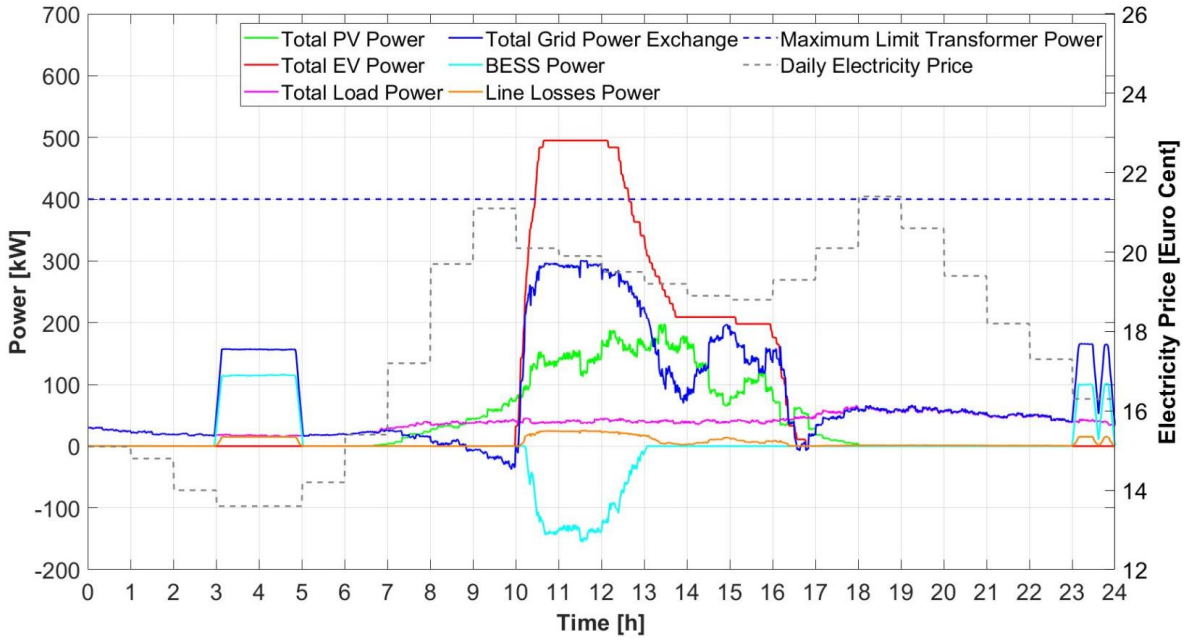

Figure 5.109 Power Exchange Profile of the Overall System for Case 4C-1 (EV Charging Period Shift, Autumn)

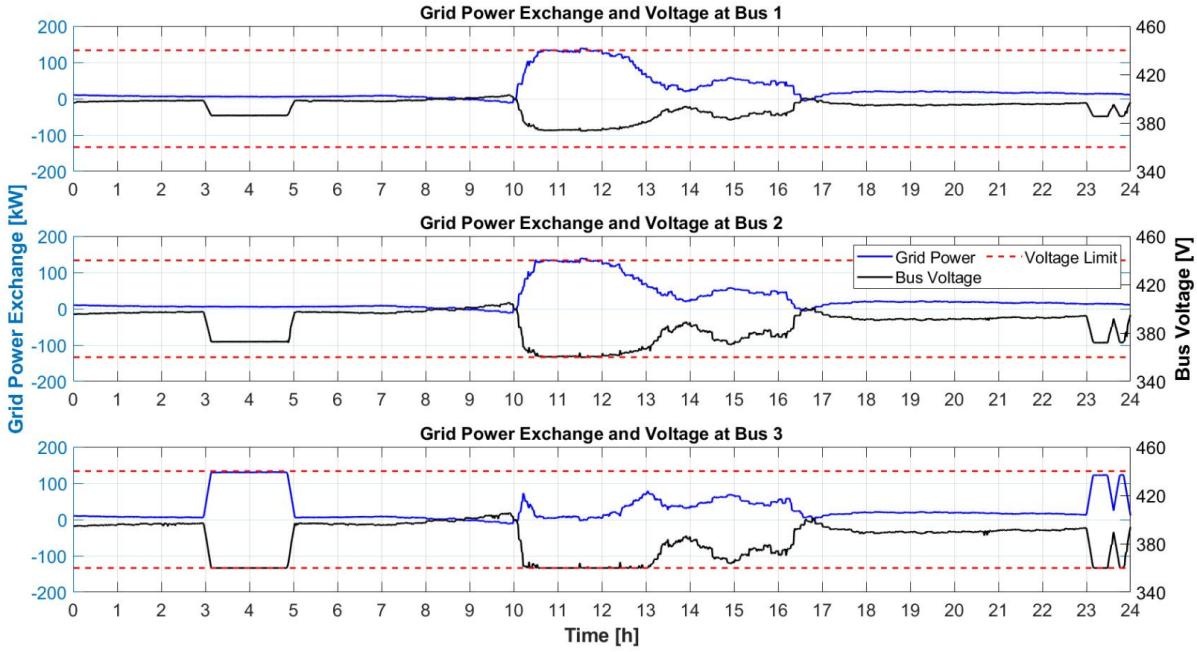

Figure 5.110 Voltage Profile at Different Bus of the System for Case 4C-1 (EV Charging Period Shift, Autumn)

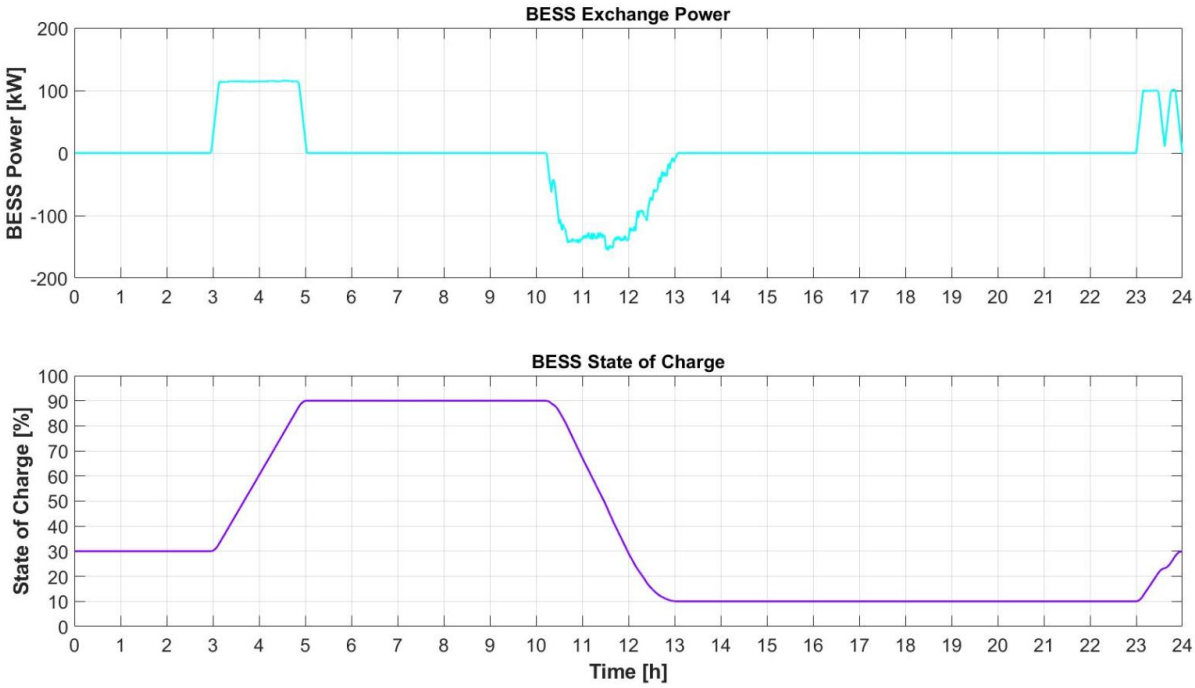

Figure 5.111 BESS Power and State of Charge Profile for Case 4C-1 (EV Charging Period Shift, Autumn)

5.4.8 Case 4C-2 (Autumn, Constant EV Charging Power)

In this case, the constant EV charging approach is implemented in autumn PV power profile. The overall exchange power of the system is presented in **Figure 5.112**. Different BESS power profile appears in this condition. There is no BESS recharging period during the end of the day. Less BESS energy is also required because of the EV charging power profile is distributed equally and maximize the PV power to reduce amount of power that needs to be drawn from the grid. Moreover, BESS is only required to keep the voltage above the minimum limit during the initial and end period of EV charging because of low PV power during the morning and late afternoon. Furthermore, BESS is also discharged during the highest electricity price period at 6 to 7 p.m. to gain more revenue by selling power to the grid. The bus voltage and BESS state of charge profile during daily operation are presented in **Figure 5.113** and **Figure 5.114** respectively.

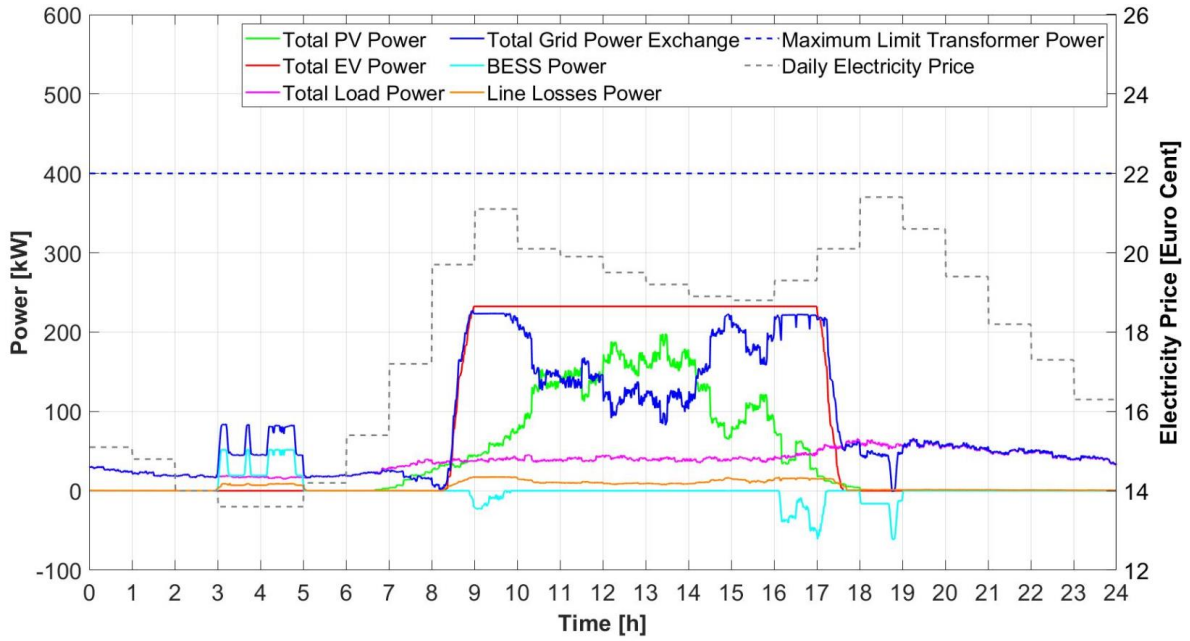

Figure 5.112 Power Exchange Profile of the Overall System for Case 4C-2 (Constant EV Charging, Autumn)

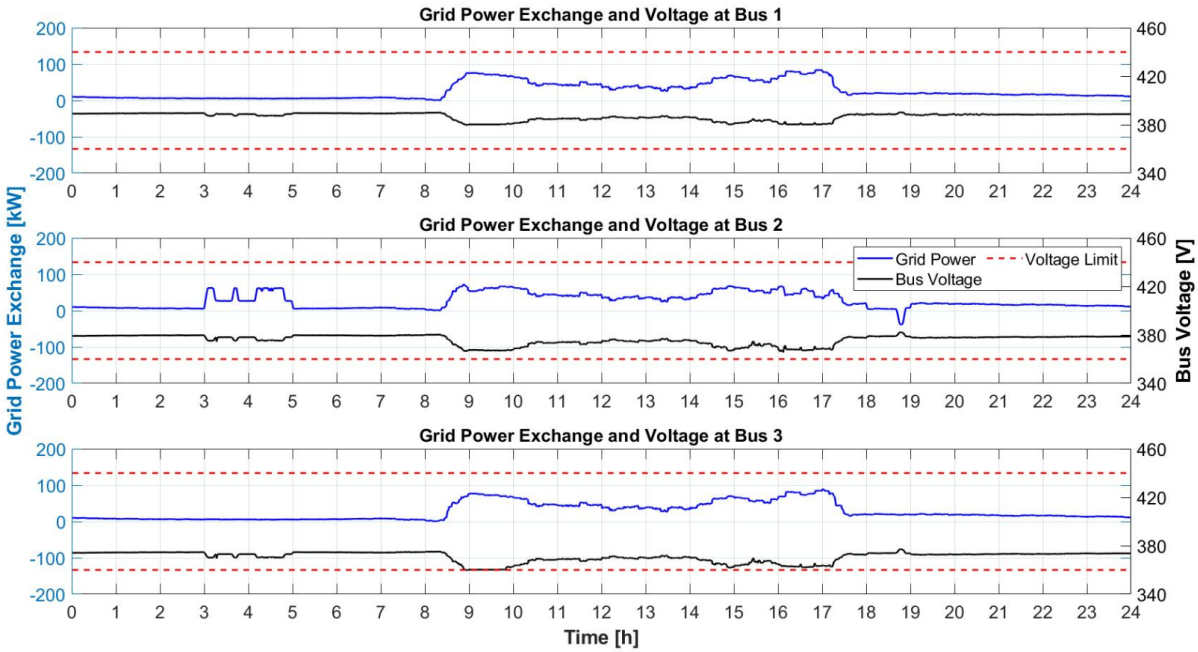

Figure 5.113 Voltage Profile at Different Bus of the System for Case 4C-2 (Constant EV Charging, Autumn)

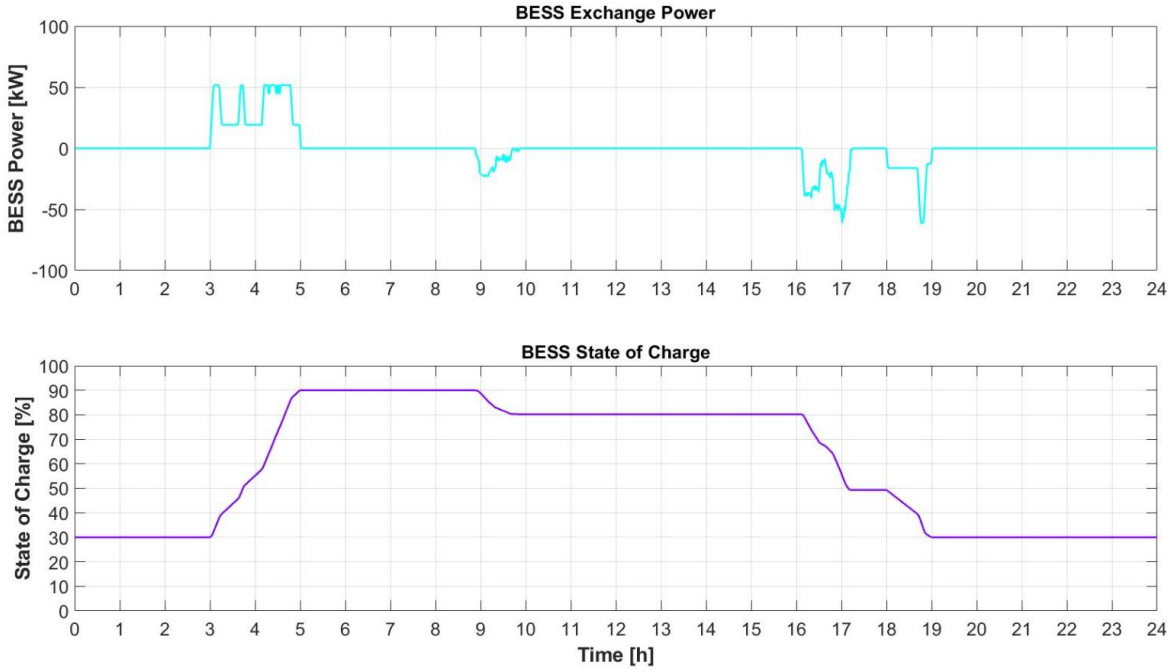

Figure 5.114 BESS Power and State of Charge Profile for Case 4C-2 (Constant EV Charging, Autumn)

5.4.9 Case 4C-3 (Autumn, Dynamic EV Charging Power)

In this scenario, autumn PV power profile is tested with flexible EV charging power which is controlled by the power management system. **Figure 5.115** shows the overall exchange power profile of the system. The power management system successfully manages the EV charging schedule so that no BESS is compulsory to be installed in the system. Similar to the two previous dynamic EV charging simulations, sequential EV charging scheduling is accomplished as illustrated in **Figure 5.116** and more charging power is mainly allocated during low electricity price period to keep the system following the grid code limitation and at the same time reduce the electricity cost. Moreover, to increase the revenue, the power management empties EV charging profile during the highest electricity price period at 9 to 10 a.m. and sell the excess PV power to the grid. Last, the bus voltage profile is kept in the safe margin allowed as presented in **Figure 5.117**.

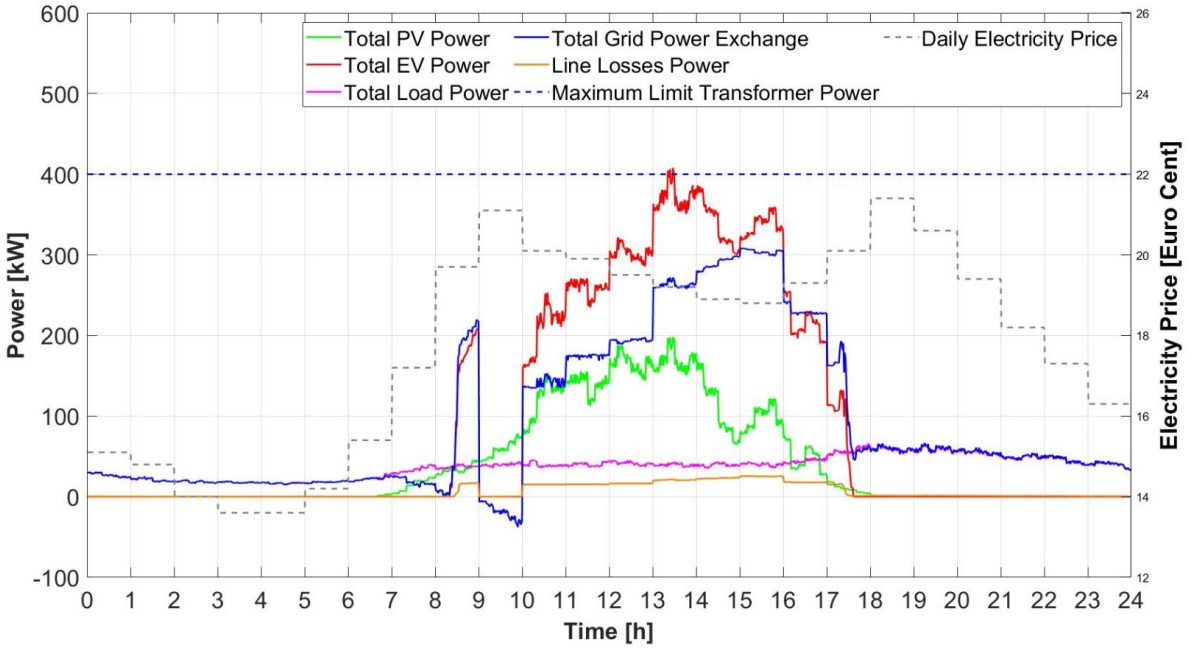

Figure 5.115 Power Exchange Profile of the Overall System for Case 4C-3 (Dynamic EV Charging, Autumn)

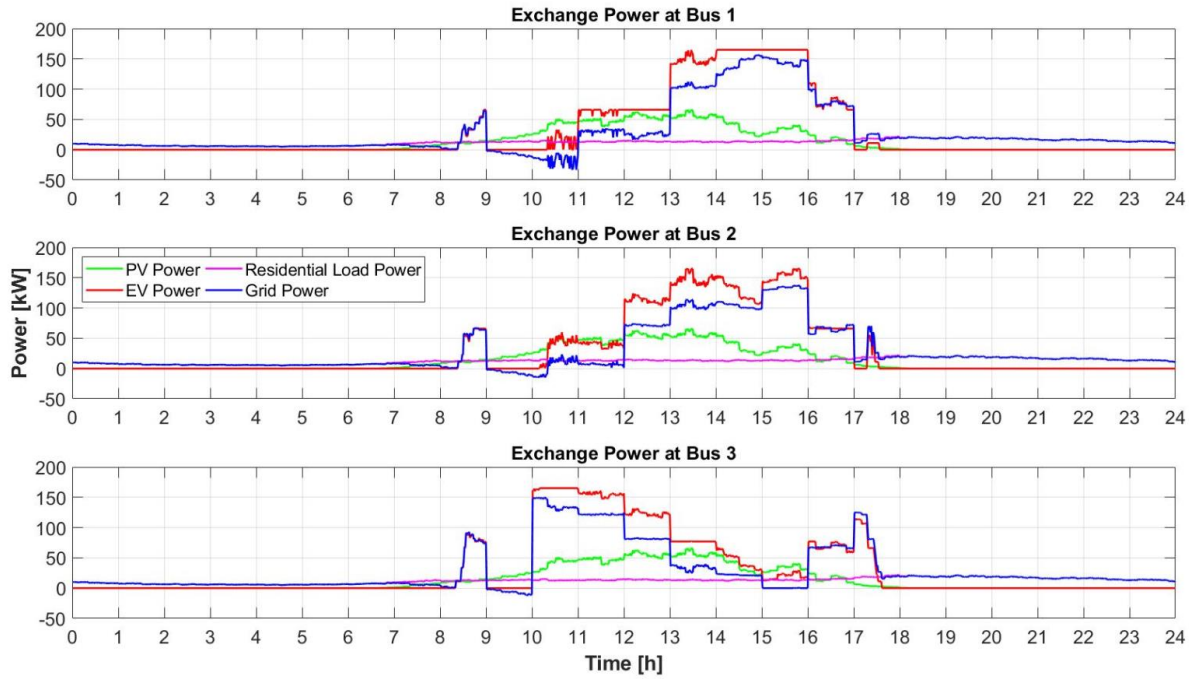

Figure 5.116 Power Exchange Profile of Each Bus for Case 4C-3 (Dynamic EV Charging, Autumn)

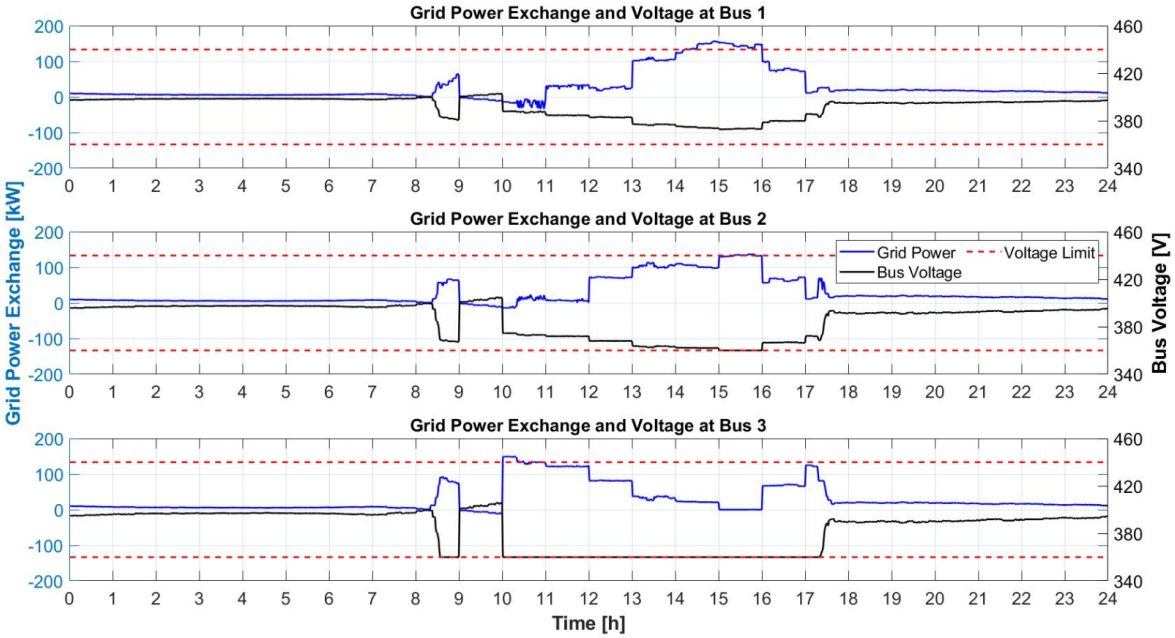

Figure 5.117 Voltage Profile at Different Bus of the System for Case 4C-3 (Dynamic EV Charging, Autumn)

5.4.10 Summary

Three different EV charging strategies have been proposed and tested in three different seasons of the year. First, the simplest method is by shifting the start of EV charging period to utilize more PV power. Second, EV charging power is equally distributed during connection time to the charger station. Third, smart variable EV charging is handled by the power management system.

In general, all three charging strategies have successfully reduced the urgency of BESS instalment. **Figure 5.118** and **Figure 5.119** present comparison of the BESS maximum power and capacity required for every EV charging strategy scheme. It is noticeable that less BESS mitigation is required and even no BESS is suggested during the summer season for constant and dynamic EV charging strategy because of the relatively high price of BESS investment. During winter, constant EV charging results to the least BESS capacity required, because the EV charging demand is distributed through all the charging period. A similar trend also appears on BESS investment as illustrated in **Figure 5.120**. The BESS placement is suggested in similar manner with the previous simulations, where the BESS is mainly located at the end of feeder as shown in **Figure 5.121**.

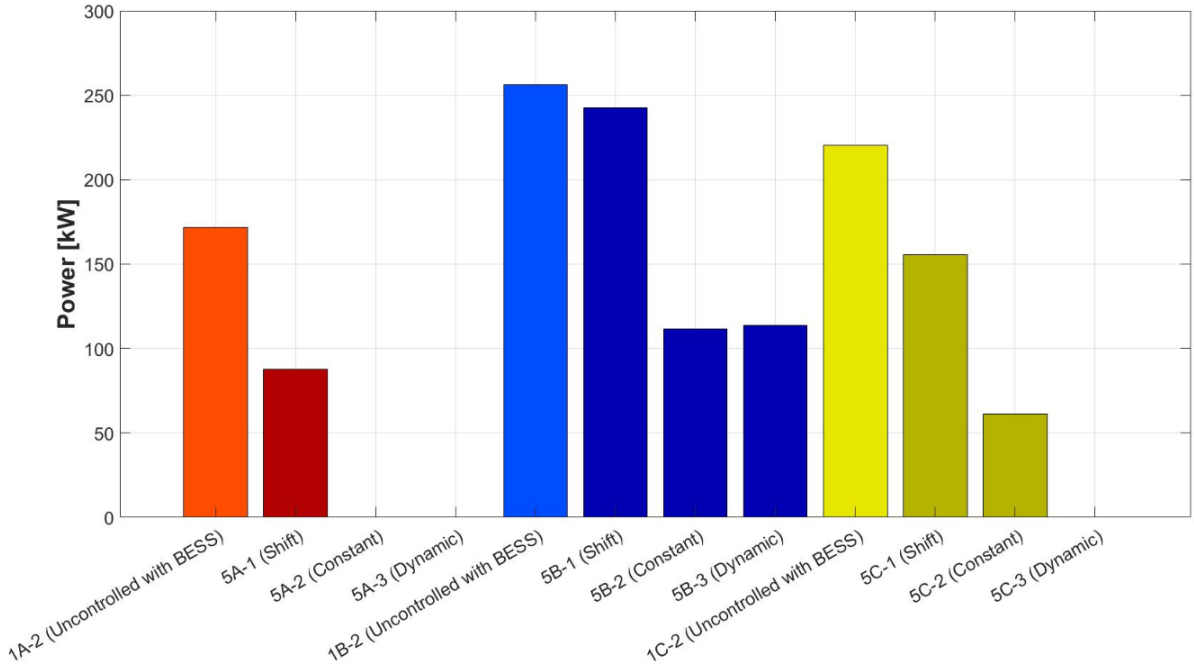

Figure 5.118 BESS Maximum Power for Case 4 (Different EV Charging Strategy)

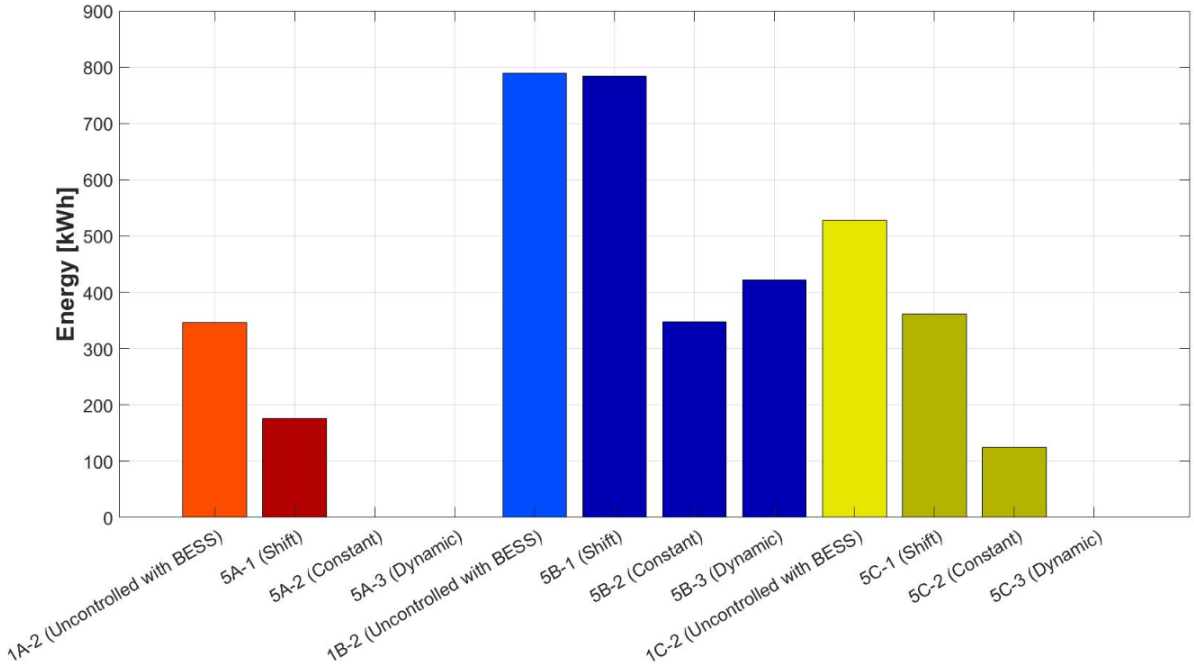

Figure 5.119 BESS Capacity Required for Case 4 (Different EV Charging Strategy)

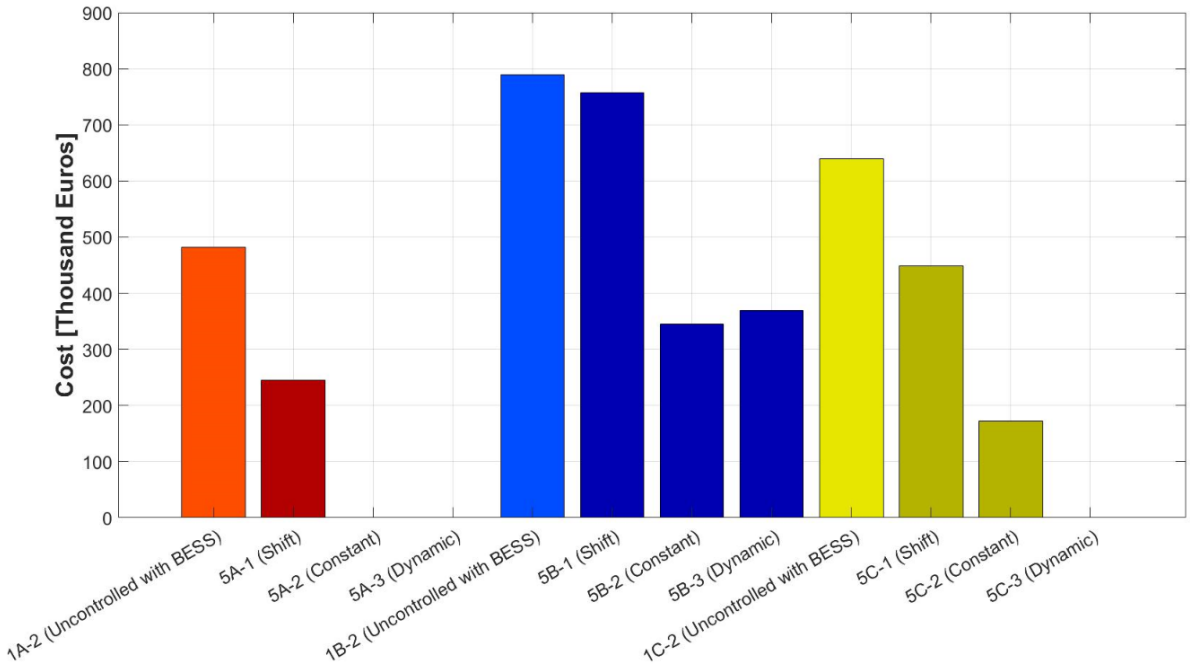

Figure 5.120 BESS Investment Cost for Case 4 (Different EV Charging Strategy)

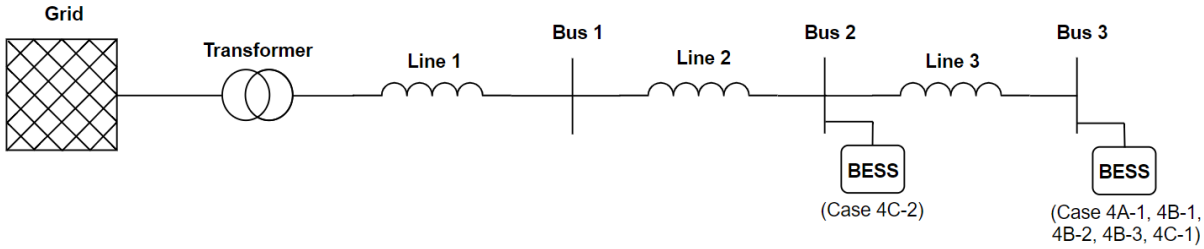

Figure 5.121 Optimal BESS Location for Case 4 (Different EV Charging Strategy)

Maximum transformer loading for every different EV charging strategy is shown in **Figure 5.122**. Constant EV charging has the most minimum transformer loading because of the EV charging power is distributed equally during EV residence time in the charger station. Lower transformer loading reduction also appears in case of the EV charging shifting and dynamic because of more utilization of PV power. Comparison of the electricity cost for different EV charging strategy is presented in **Figure 5.123**. The dynamic EV charging strategy has the lowest electricity cost. It proves that the smart charging successfully allocates EV charging scheduling mainly during low electricity price period. The complete total cost comparison is shown in **Figure 5.124**. The lowest total cost goes to the smart dynamic EV charging, then followed by the constant EV charging, next is the EV charging period shift approach, and last is the direct uncontrolled EV charging method.

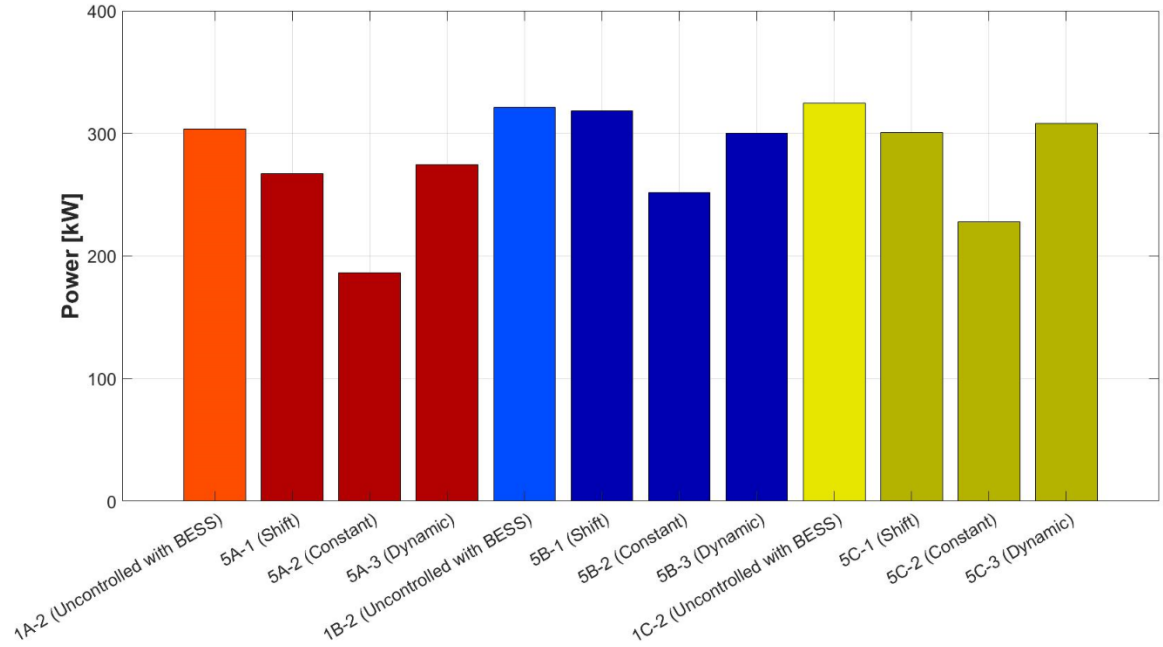

Figure 5.122 Maximum Transformer Loading Power for Case 4 (Different EV Charging Strategy)

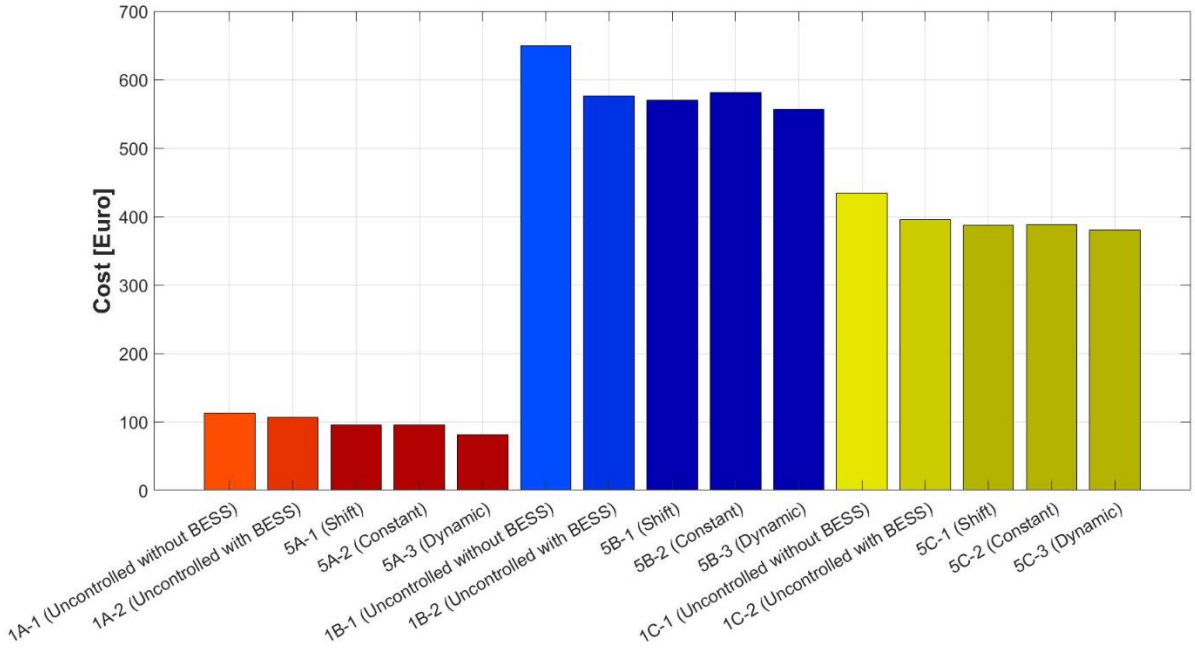

Figure 5.123 Electricity Cost for Case 4 (Different EV Charging Strategy)

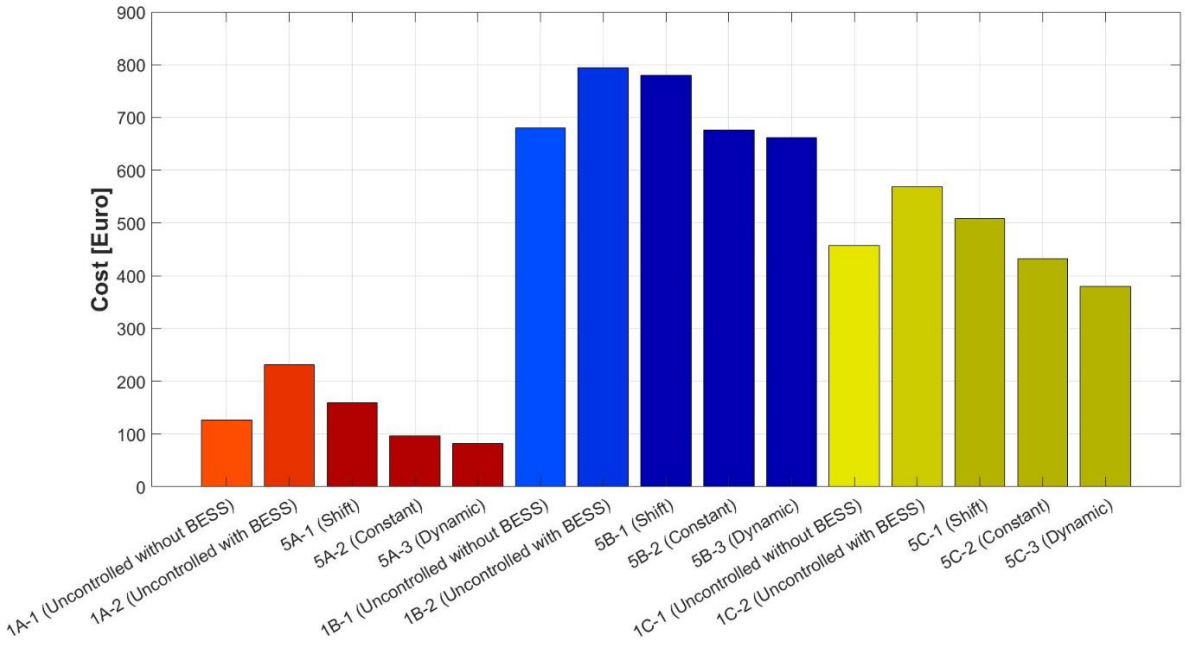

Figure 5.124 Total Cost for Case 4 (Different EV Charging Strategy)

6. Conclusions and Further Works

This chapter provides the summary of the thesis project. Research questions are answered as conclusions of all the results obtained in this study. Moreover, several recommendations are proposed to be conducted in the future work.

6.1 Conclusions

This section presents the summary of the thesis results about optimal battery sizing and location in addition of EV charging using PV power application by answering research questions that have been proposed.

1. **How to formulate the optimal battery sizing and location optimization along with the power management system of the EV-PV charging system in a low voltage distribution network?**

   First, the grid model, EVs parameters, and BESS characteristics that will be taken into the simulation are defined. Then, every subject characteristics and constraints are formulated in the mathematical equations form. Last, the objective function is constructed as the main target of the optimization. More detail answers will be given in sub research questions below.

a) How are the EVs properties modeled in the system?

This study considers EVs as the battery that needs to be charged fully at the departure time from the charger station. Ten most used EVs in the Netherlands are taken into account. EV arrival and departure time are randomized based on the previous research on EV charging pattern in the Netherlands. The battery charging efficiency is considered and implemented in the power balance equation. Energy balance equation is also constructed as an indicator of EV charging finish time. In the default direct uncontrolled charging scenario, EV charging power is set at a maximum power of 11 kW. Further details on other EV charging strategy will be covered in the research question 4.

b) How is the BESS characteristic modeled in the system?

The lithium-ion battery is considered in this study. The charging and discharging battery efficiency are applied to the power balance equation to differentiate the effect of those two processes. Besides, the charging and discharging power are limited to the maximum battery power which will be investigated in this study. Moreover, the energy balance equation is also formed as the basis for determining the battery state of charge and C-

rate. The battery SoC is set between 10 to 90%, while the C-rate is kept below 0.5. The size of The optimal BESS location is obtained by putting a binary variable at the power balance equation.

c) How is the low voltage distribution network model formed?

This study implements the low voltage CIGRE benchmark for the topology and line impedance value. The system consists of three buses connected in a radial network via a transmission line and connected to the large grid through a single stepdown transformer of 20/0.4 kV. Each bus consists of an EV charger station, residential load, PV system, and potential BESS installment in one of the three buses. The line impedance is represented in the Y bus matrix which is used in the power-voltage equation to determine the bus voltage. The bus voltage is kept between 360 to 440 V, following the European standard EN50160. Besides, the grid power drawn by the system is managed to be below the maximum transformer capacity of 400 kW.

(d) What is the objective function of the proposed optimization strategy?

The objective function is to minimize the total cost of the system. The cost is breakdown into three main categories, the BESS investment, grid reinforcement, and electricity cost. The BESS investment refers to the BESS maximum power and energy capacity which are suggested by the solver. The grid reinforcement cost subjects to the power addition required from the maximum transformer capacity. The electricity cost depends on the amount of energy bought from the grid and temporal electricity price.

2. How does the proposed optimization react with different EV number penetration and allocation?

(a) How does different EV number penetration affect the battery sizing and location along with the exchange power profile?

The battery power and energy size increase with the increment of EV number in every charger station as shown in **Figure 5.37** and **Figure 5.38** respectively. The result shows that the increment battery size is also increased in case of addition from 15 to 20 EVs compared to 10 to 15 EVs case. The BESS maximum power is increased ranging from 8.88-40.08%, while for BESS capacity 63.41-132.19%. Furthermore, the increased increment also occurs for the electricity cost from 13-66.38% as presented in **Figure 5.42**. As a result, the total cost increment of the system is also above the linearity from 18.59-62% as illustrated in **Figure 5.43.** For the BESS power management, longer and higher charging duration and power appear as the consequence of larger battery

capacity. This condition appears because of growing losses for more EV penetration causing more BESS and grid mitigation required. However, the power management will prioritize the charging process during the low electricity price period to minimize the system total cost. BESS is suggested to be placed at the furthest bus from the transformer. This condition happens due to the bus at the end of feeder suffers the most severe voltage drop because of the line impedance. As the consequence, BESS is placed at the furthest bus to give the most influential effect so that the battery size can be reduced compared if the BESS is placed in another bus to minimize the battery investment cost. No BESS is suggested in low EV penetration since there is no grid violation occurs and the BESS price is still relatively high.

(b) How does asymmetrical EV allocation at the charger station affect the battery sizing and location along with the exchange power profile?

In this project, two asymmetrical EV placement configurations are simulated. First, the number of EVs placed in the charger station is increasing from the nearest to the furthest bus (10-15-20 EVs). Second, in the opposite, the decreasing order of EVs penetration is distributed (20-15-10 EVs). The result shows that higher power and energy BESS capacity from 11.88-87.27% is required for increasing order of EV distribution as presented in **Figure 5.65** and **Figure 5.66**. More EVs located at the end of the feeder leads to larger voltage drop at the furthest bus. To tackle this issue, more BESS power mitigation is required to avoid the grid violation in the system. For decreasing EV order, the BESS size required depends on the BESS position. When BESS is located at the middle bus, more BESS size is needed compared to symmetrical penetration case and less size if BESS is suggested at the end of the feeder from -13.07-14.5%. The electricity cost of unbalance EV penetration varies from -5.02-5.49% as shown in **Figure 5.70**. Last, the total costs of asymmetrical penetration are ranging from -3.13-45.7% compared to balance EV allocation as illustrated in **Figure 5.71**.

3. What is the impact of decentralized BESS instalment compared to the centralized BESS?

In the decentralized case, the solver is given freedom to place more than one BESS in the system. However, the result shows that only two BESS are suggested at the middle and end of the feeder bus. A lot higher battery size is advised for the furthest bus because of more severe voltage drop occurs. No BESS is necessary to be located in the nearest bus due to insignificant voltage decrease. Nevertheless, when the two BESS size are summed up, the total size is comparable with the case of the centralized approach as shown in **Figure 5.84** and **Figure 5.85** with different of -0.91-1.12%. The

electricity cost of the decentralized case is slightly lower from 0.1-4.1% as presented in **Figure 5.89**. As a result, the total cost of decentralized case is only 0.21-1.77% lower than the centralized case as illustrated in **Figure 5.90**.

4. **How does different EV charging strategy affect the battery sizing and location along with the exchange power profile?**

   Besides of commonly used direct uncontrolled EV charging scheme, several EV charging strategies are proposed to investigate further potential reduction of the total cost. First, in the EV charging shift strategy, the initial charging process is delayed to utilize more PV power. As the result, less BESS capacity is required to compared to the direct uncontrolled EV charging scheme. Second, in the constant EV charging power case, the EV charging power is set at same value depends on the EV battery capacity and residence time at the charger station. Result shows that further BESS size reduction happens because the high EV charging load demand in previous uncontrolled scheme, is distributed equally during the connection time of EV at the charger station. Moreover, the transformer loading is also substantially reduced during EV charging period. Third, in the dynamic EV power scenario, the power management is allowed to freely manage the scheduling of EV charging. As a result, the proposed power management system manages the EVs to be mainly charged during low electricity price period. Furthermore, the PMS even delays the EV charging when the electricity price is high to give an opportunity for PV power to sell the electricity to the grid as extra revenue. The result shows that the dynamic EV charging strategy is successfully reducing further cost and becomes the lowest total cost among all the scenarios. In overall, implementation of controlled EV charging strategy has reduced the BESS size required from 5.39-100% for BESS maximum power and 0.58-100% for BESS capacity as illustrated in **Figure 5.118** and **Figure 5.119**. This means that for some cases, no BESS is required by conducting controlled EV charging. The electricity cost of the system is diminished by 0.89-23.51% as presented in **Figure 5.123**. Finally, the overall cost of the system is also decreased from 1.95-65.85% as shown in **Figure 5.124**.

6.2 Further Works

Several recommendations are suggested for the future works of optimal sizing and location of a battery energy storage system in a low voltage distribution network as follows:

1. Further details of the battery modelling can be applied in a distinct simulation program, for example, Simulink in Matlab software. The battery's voltage, current, and temperature can be considered to make the simulation becomes more realistic.
2. The proposed optimal battery sizing and placement with the power management system can also be implemented in a larger existing network, for example in the Dutch low voltage distribution network.
3. Longer simulation can be conducted for whole period of expected battery lifetime.
4. Another battery energy storage system services, such as frequency control and black start applications can implement the proposed optimization strategy.
5. Another optimization technique can be utilized as a performance comparison with the currently proposed optimization method.
6. Vehicle to Grid (V2G) technology can be adopted in the future work.
7. Grid Reinforcement to solve voltage violation can be implemented as comparison with BESS instalment in the future research.

Appendix A: Case 1 (Increasing EV Number)

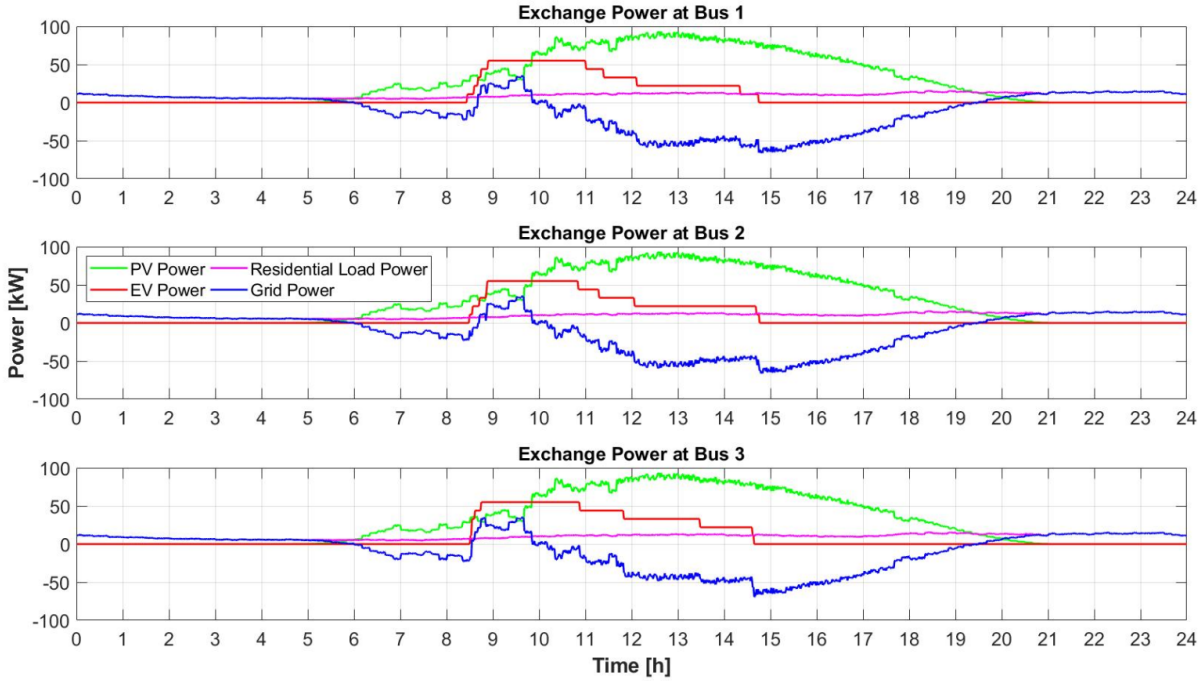

Figure A.1-A Power Exchange Profile of Each Bus for Case 1A-1 (5 EV, Summer)

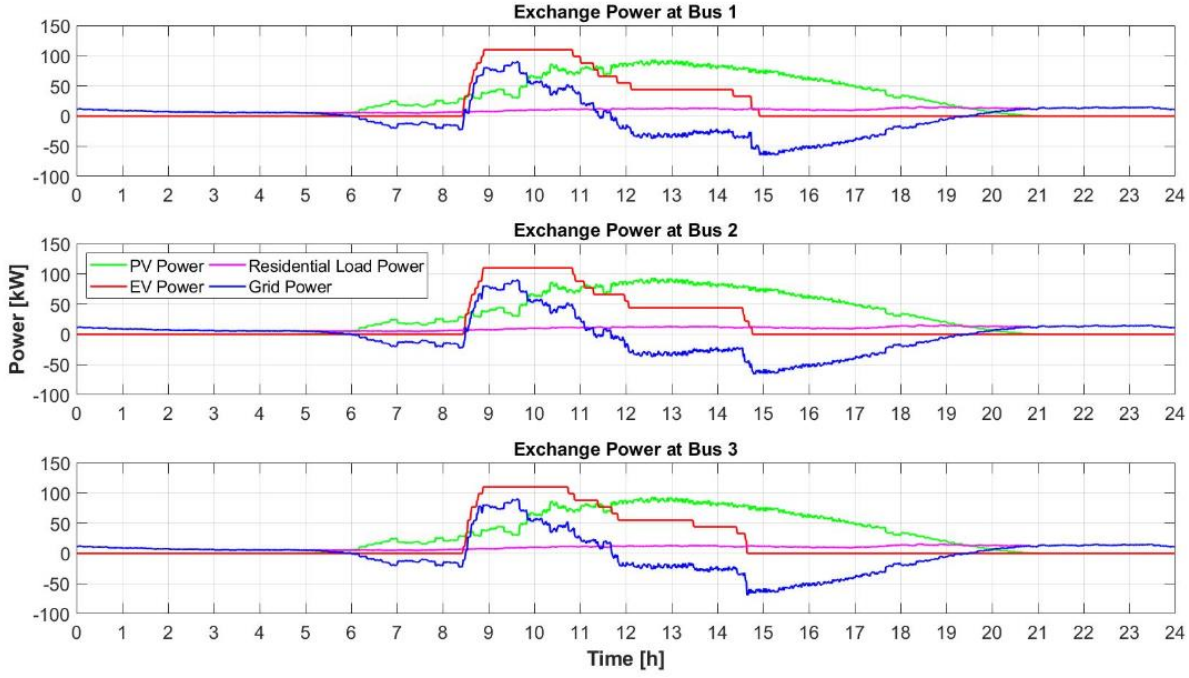

Figure A.2-A Power Exchange Profile of Each Bus for Case 1A-1 (10 EV without BESS, Summer)

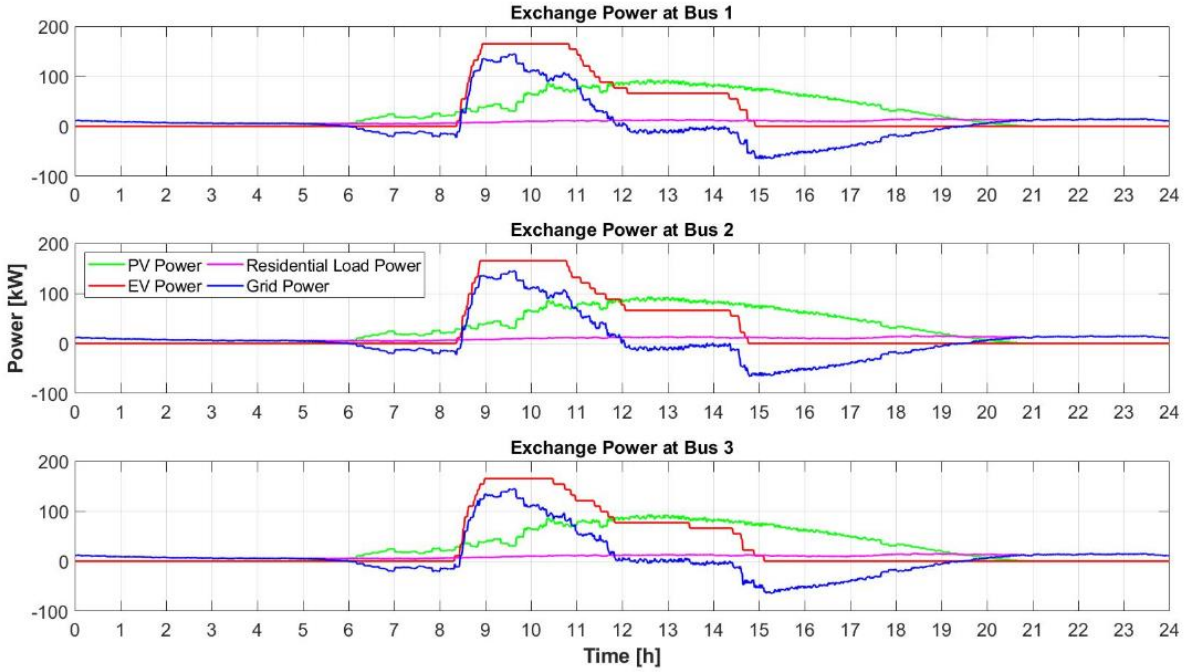

Figure A.3-A Power Exchange Profile of Each Bus for Case 1A-1 (15 EV without BESS, Summer)

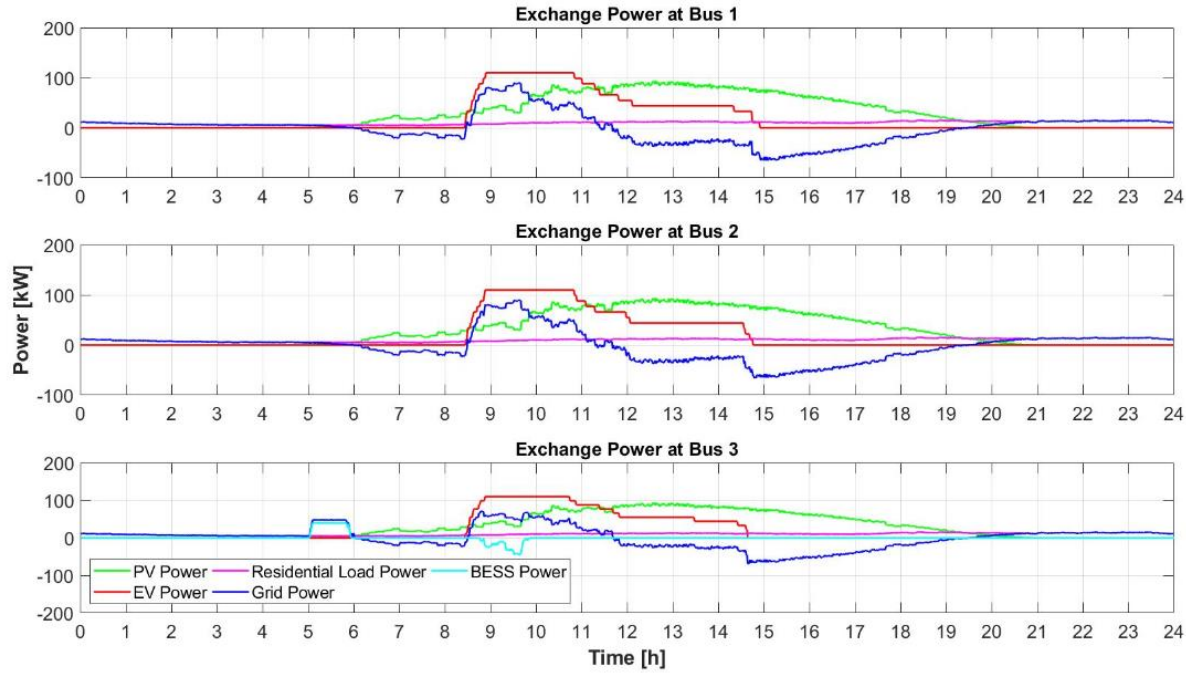

Figure A.4-A Power Exchange Profile of Each Bus for Case 1A-2 (10 EV with BESS, Summer)

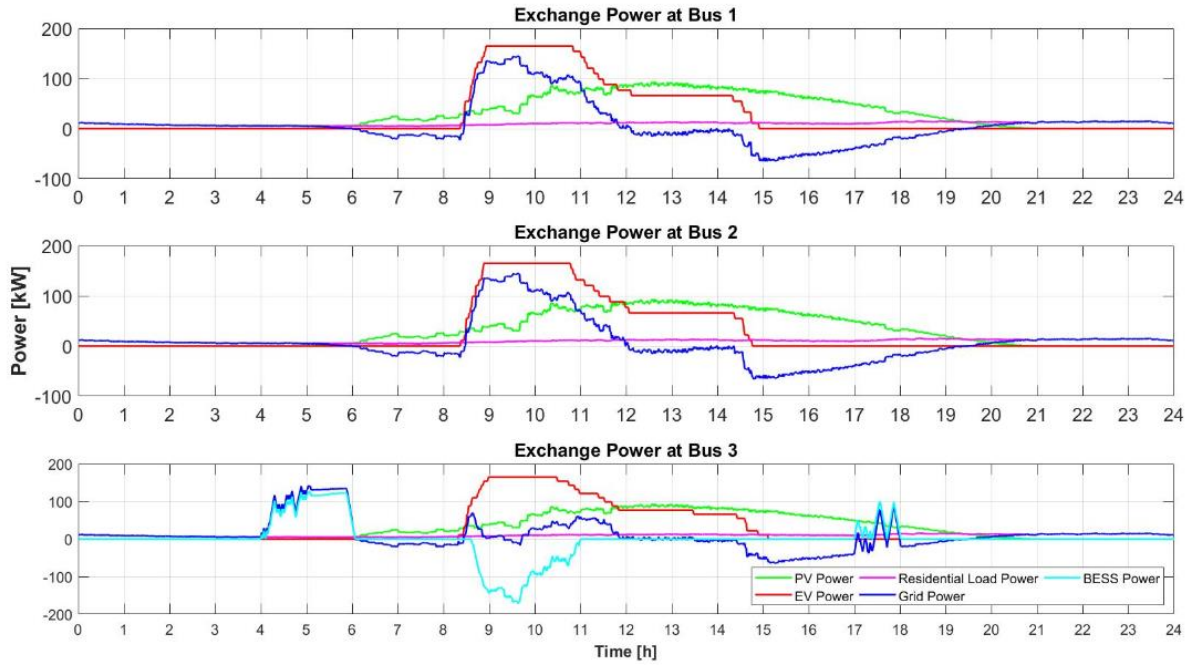

Figure A.5-A Power Exchange Profile of Each Bus for Case 1A-2 (15 EV with BESS, Summer)

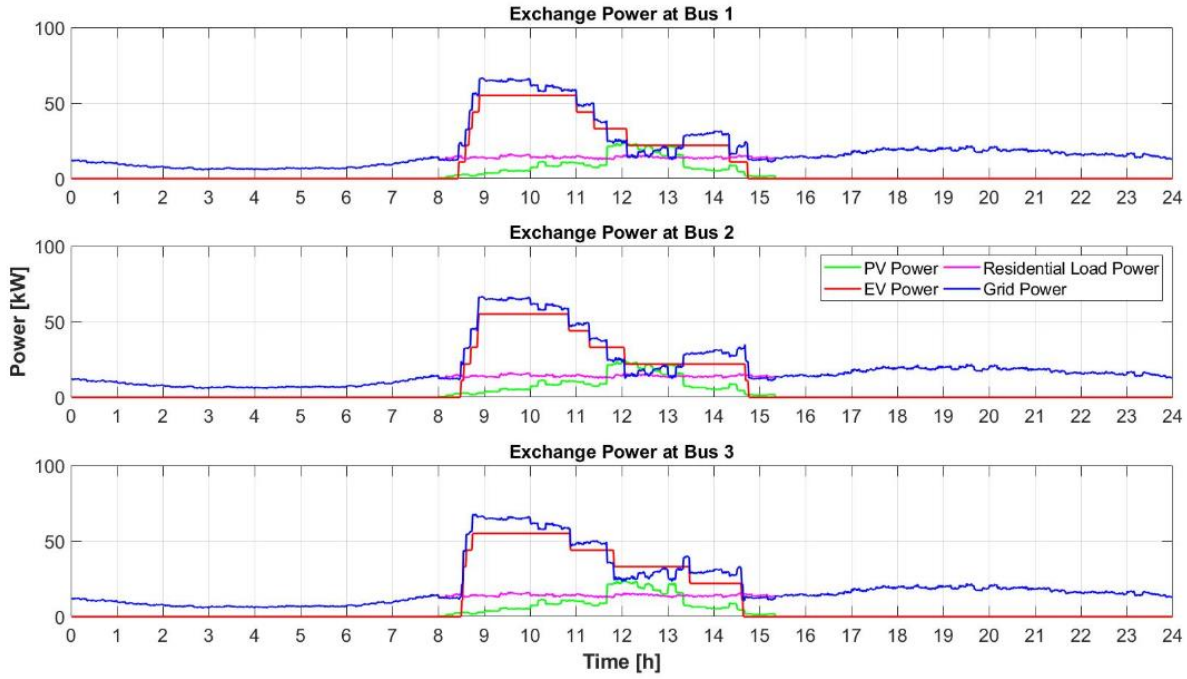

Figure A.1-B Power Exchange Profile of Each Bus for Case 1B-1 (5 EV, Winter)

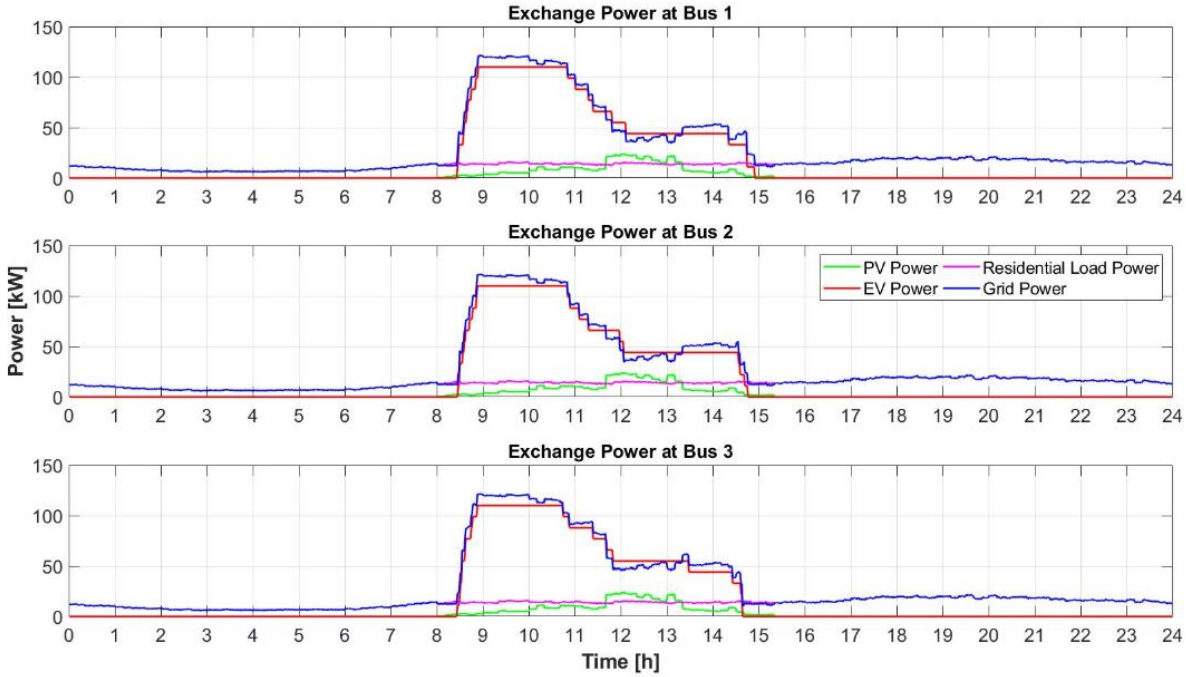

Figure A.2-B Power Exchange Profile of Each Bus for Case 1B-1 (10 EV without BESS, Winter)

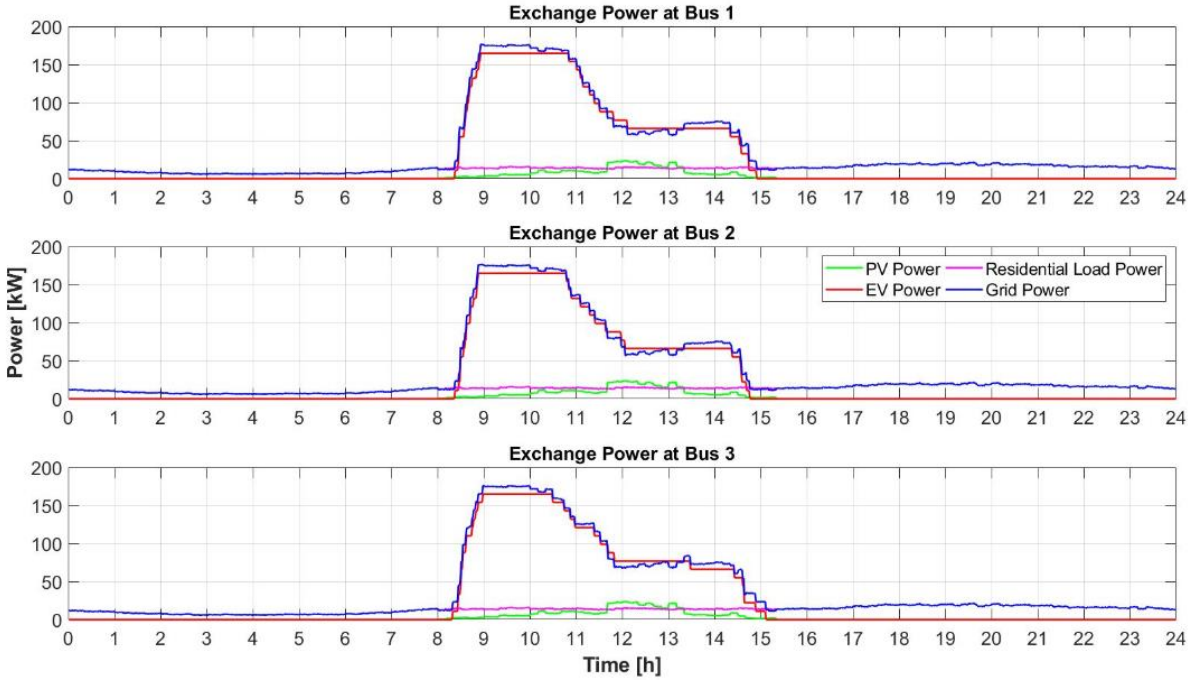

Figure A.3-B Power Exchange Profile of Each Bus for Case 1B-1 (15 EV without BESS, Winter)

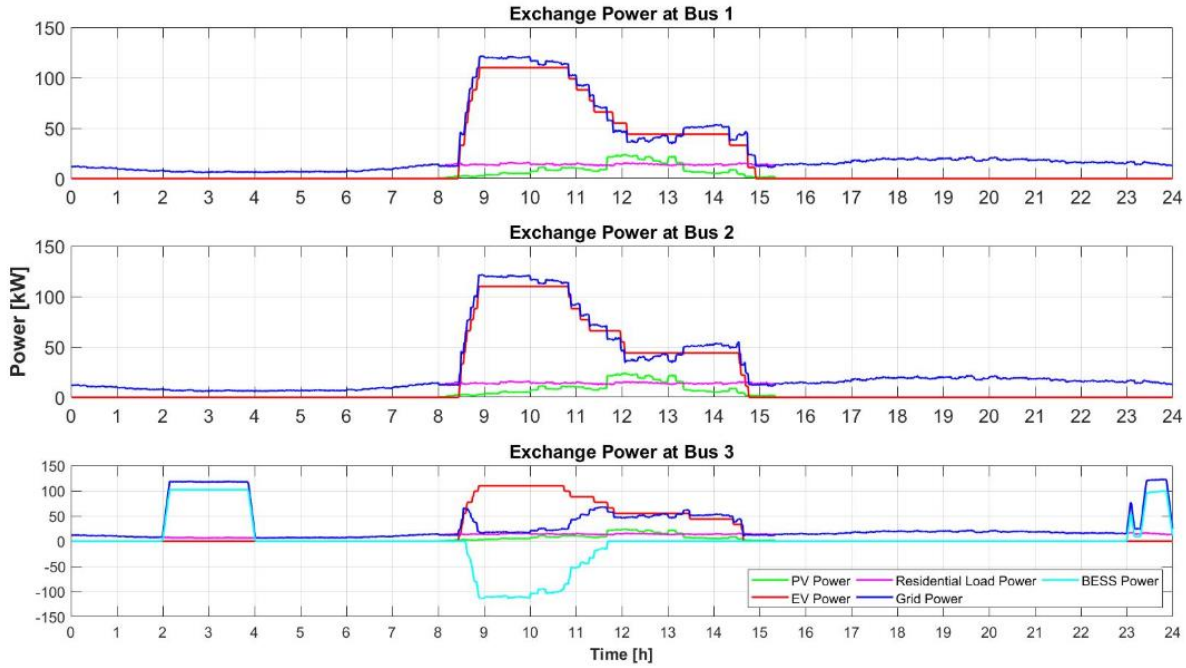

Figure A.4-B Power Exchange Profile of Each Bus for Case 1B-2 (10 EV with BESS, Winter)

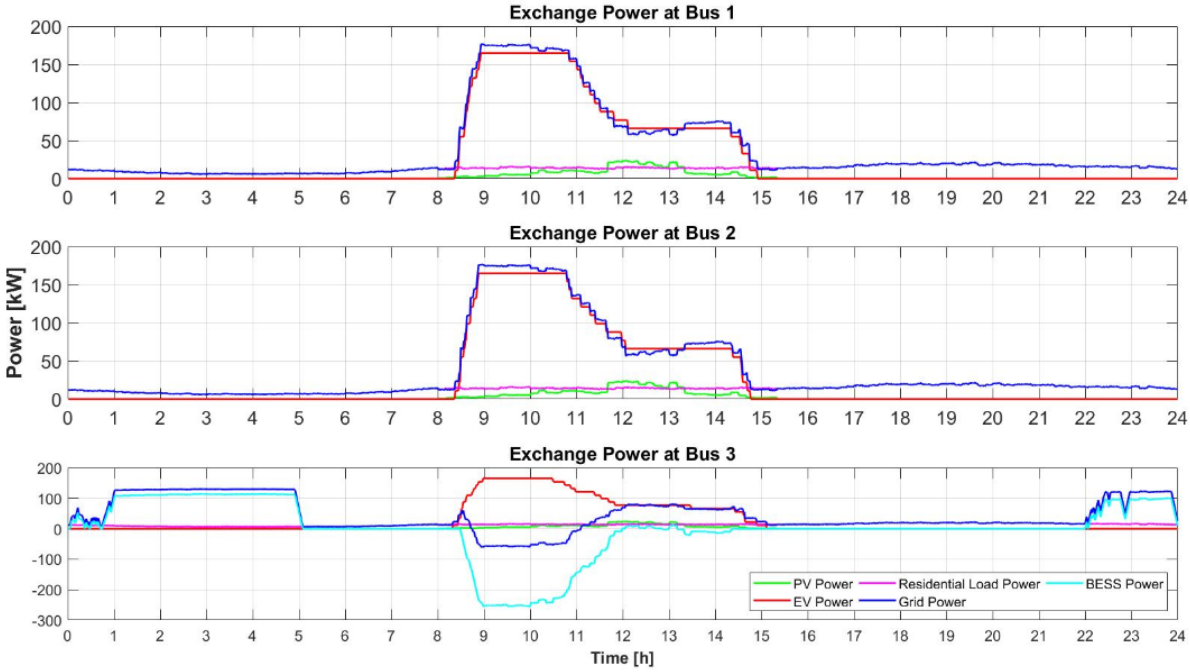

Figure A.5-B Power Exchange Profile of Each Bus for Case 1B-2 (15 EV with BESS, Winter)

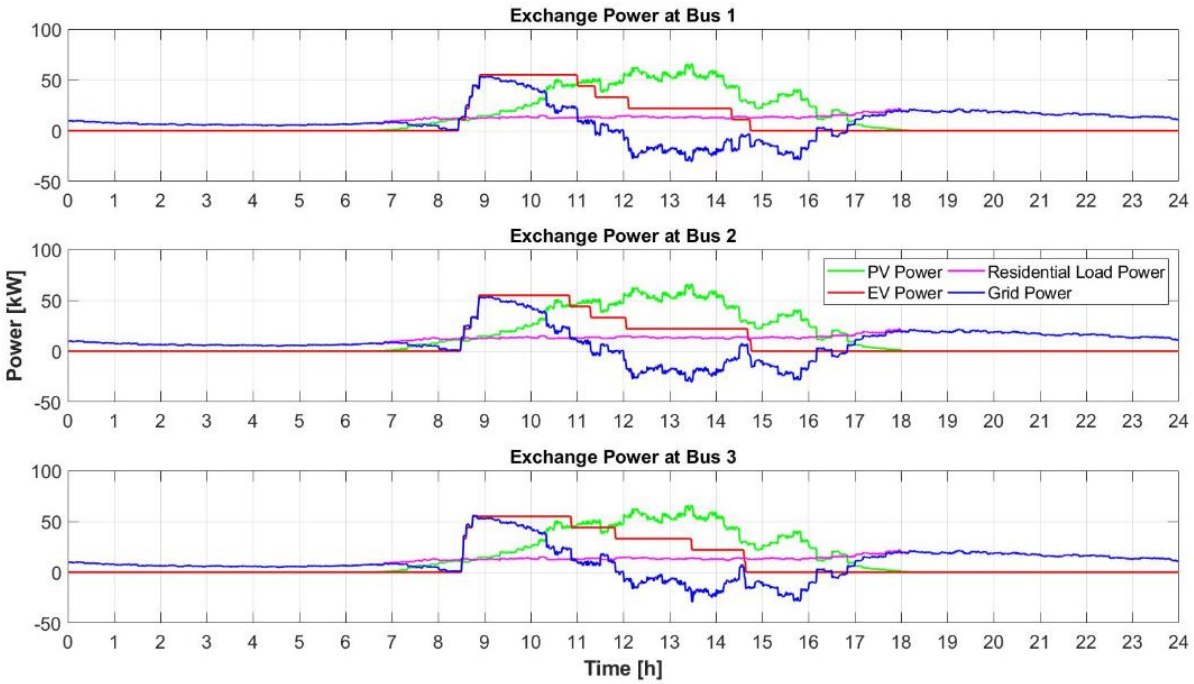

Figure A.1-C Power Exchange Profile of Each Bus for Case 1C-1 (5 EV, Autumn)

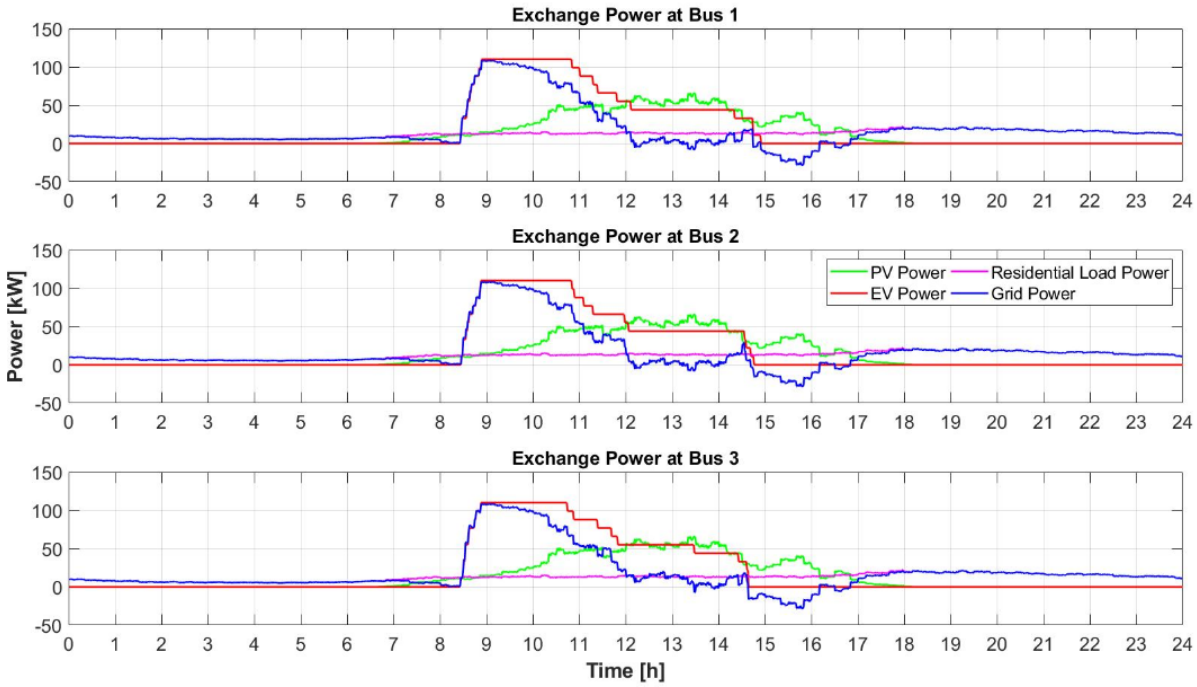

Figure A.2-C Power Exchange Profile of Each Bus for Case 1C-1 (10 EV without BESS, Autumn)

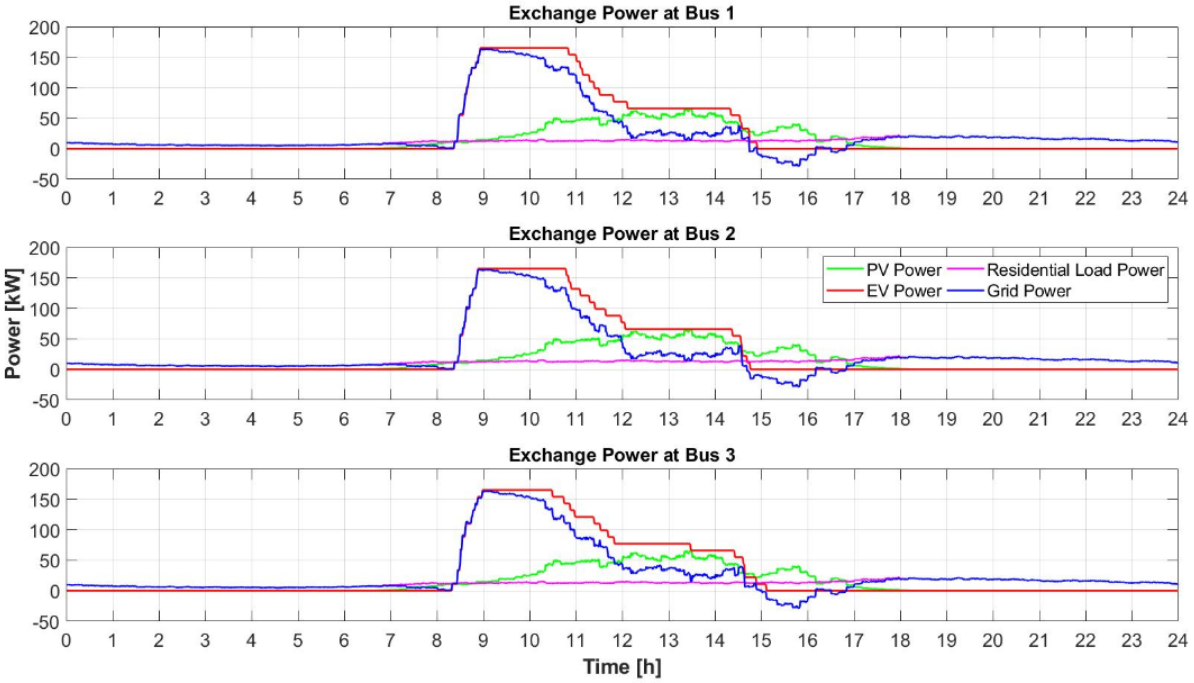

Figure A.3-C Power Exchange Profile of Each Bus for Case 1C-1 (15 EV without BESS, Autumn)

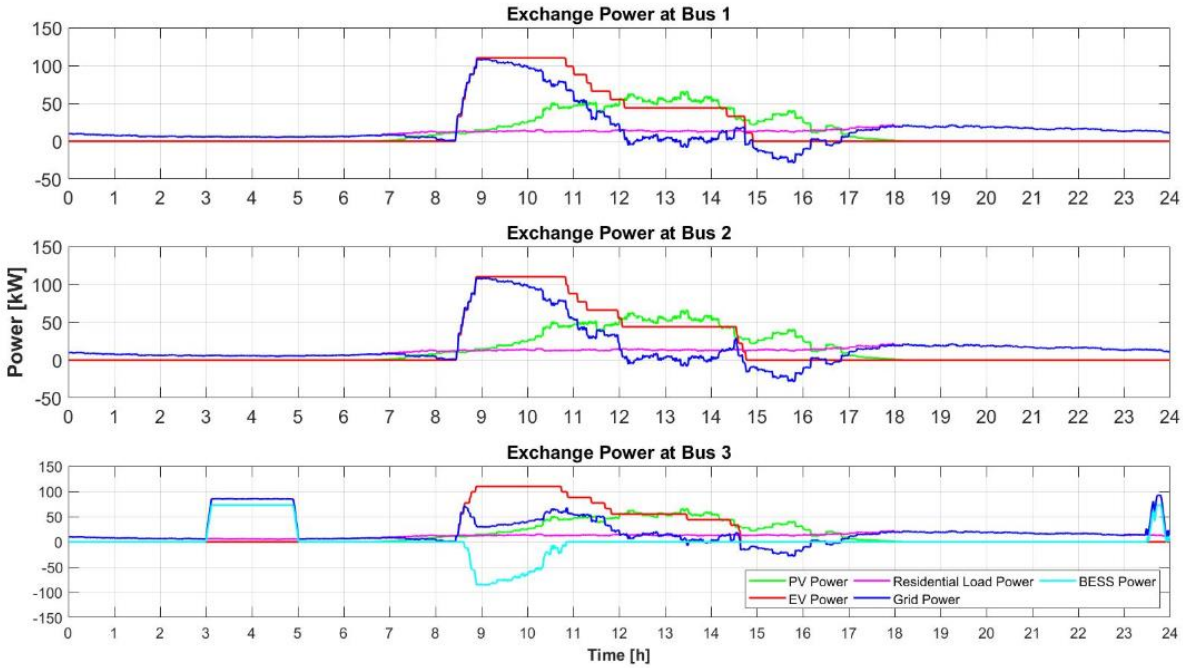

Figure A.4-C Power Exchange Profile of Each Bus for Case 1C-1 (10 EV with BESS, Autumn)

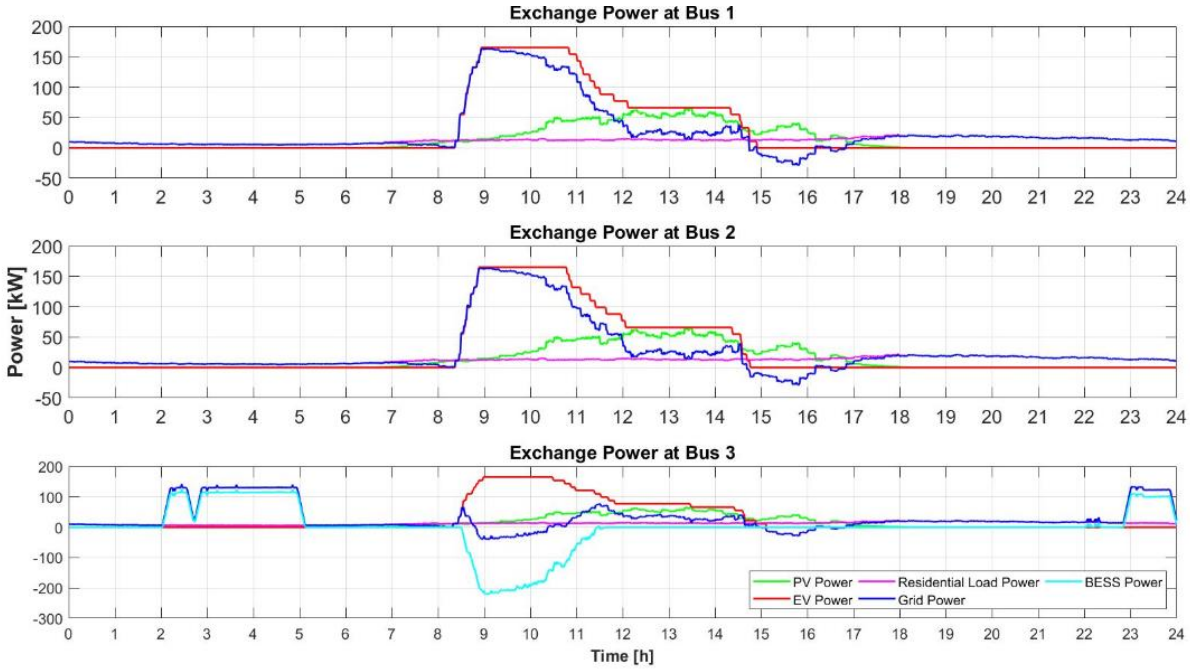

Figure A.5-C Power Exchange Profile of Each Bus for Case 1C-1 (15 EV with BESS, Autumn)

Appendix B: Case 2 (Unbalance EV Number)

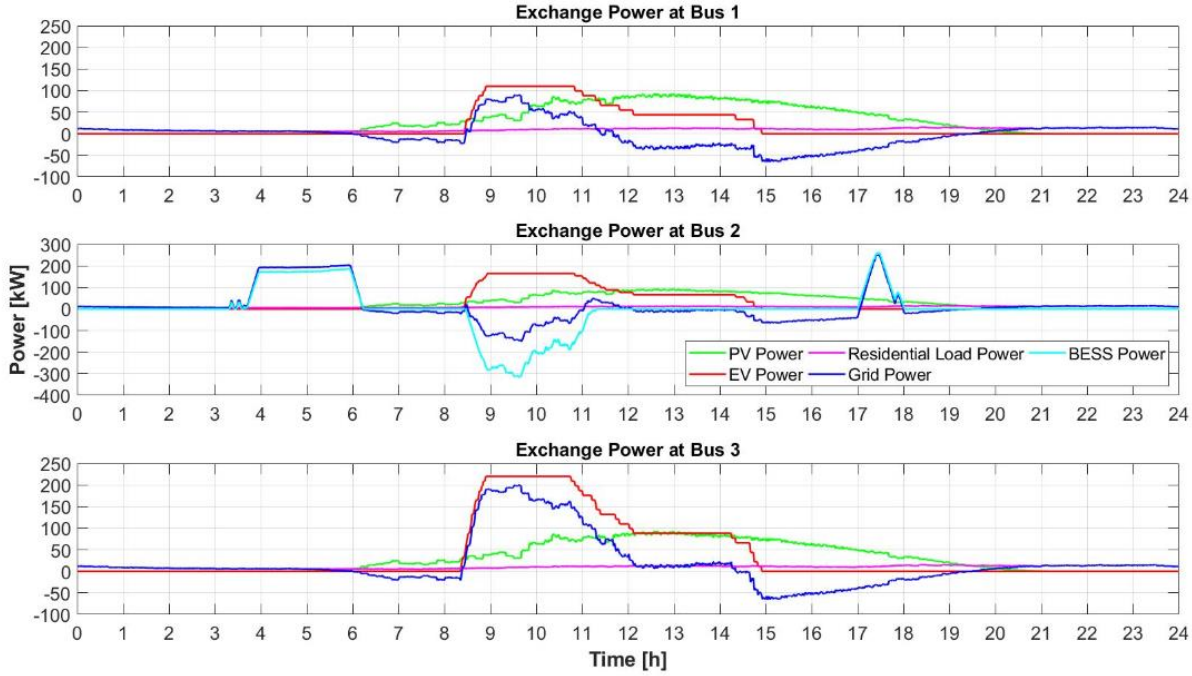

Figure B.1-A Power Exchange Profile of Each Bus for Case 2A-1 (10-15-20 EV, Summer)

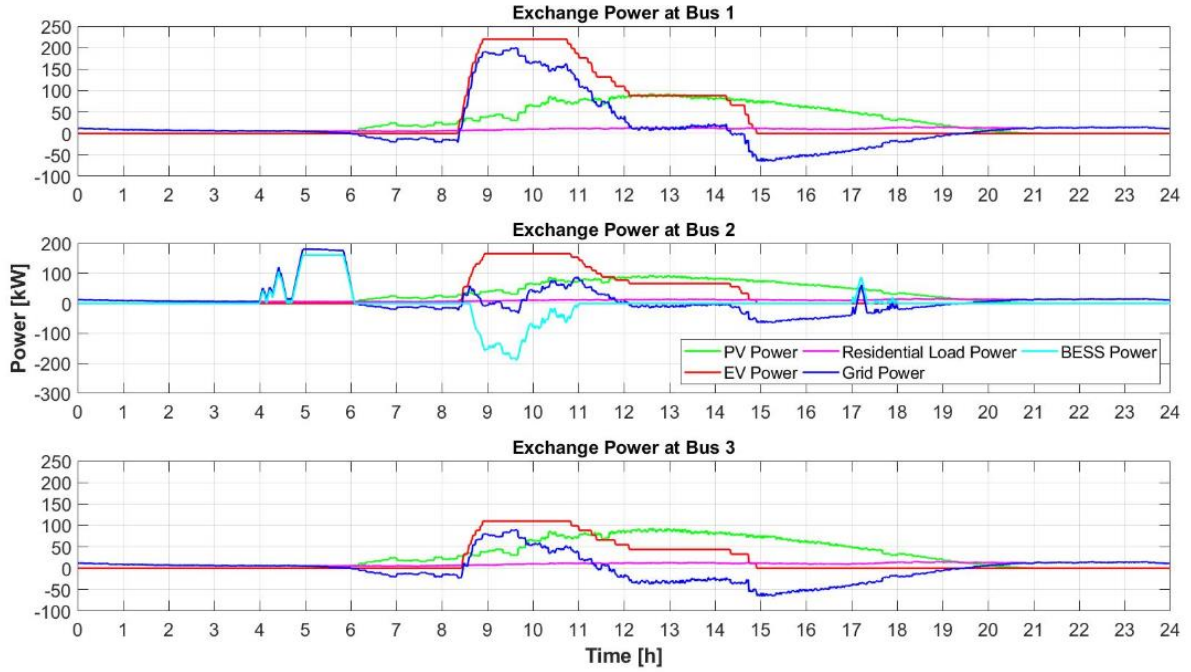

Figure B.2-A Power Exchange Profile of Each Bus for Case 2A-2 (20-15-10 EV, Summer)

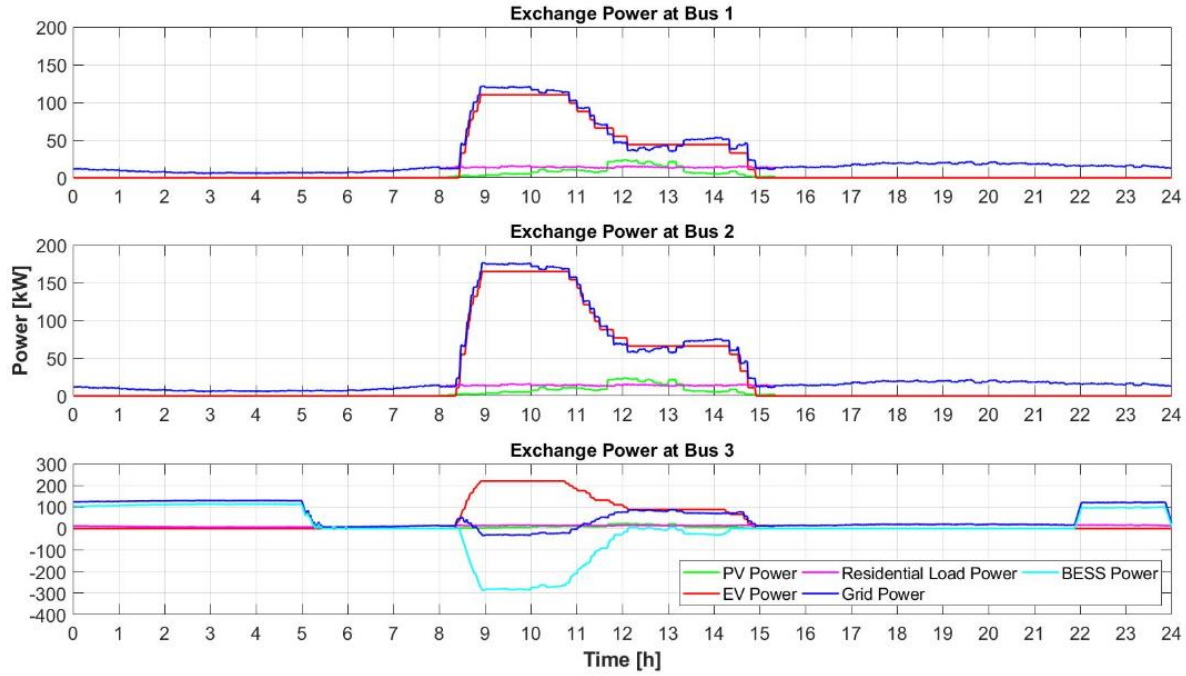

Figure B.1-B Power Exchange Profile of Each Bus for Case 2B-1 (10-15-20 EV, Winter)

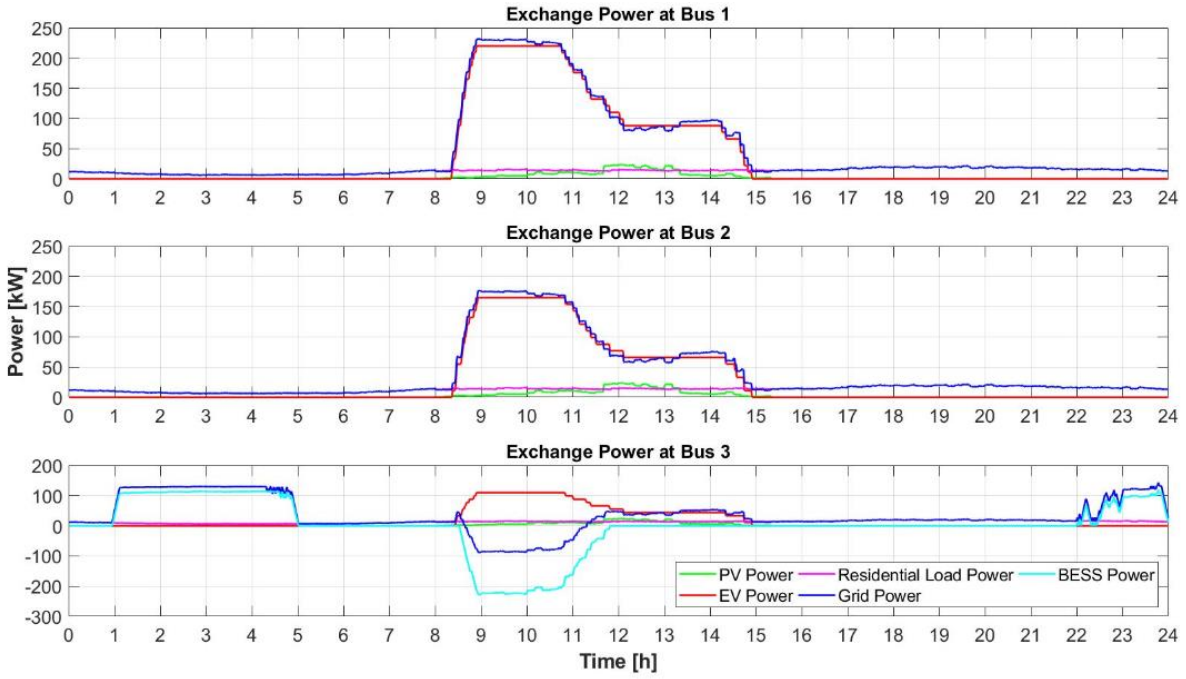

Figure B.2-B Power Exchange Profile of Each Bus for Case 2B-2 (20-15-10 EV, Winter)

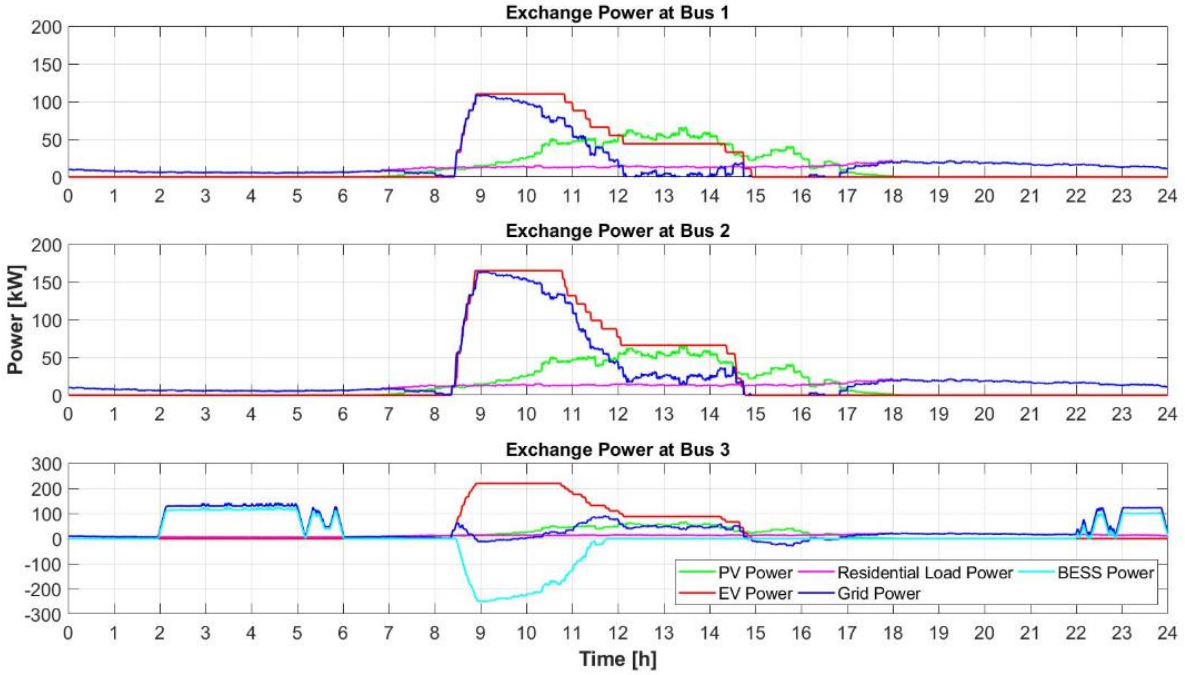

Figure B.1-C Power Exchange Profile of Each Bus for Case 2C-1 (10-15-20 EV, Autumn)

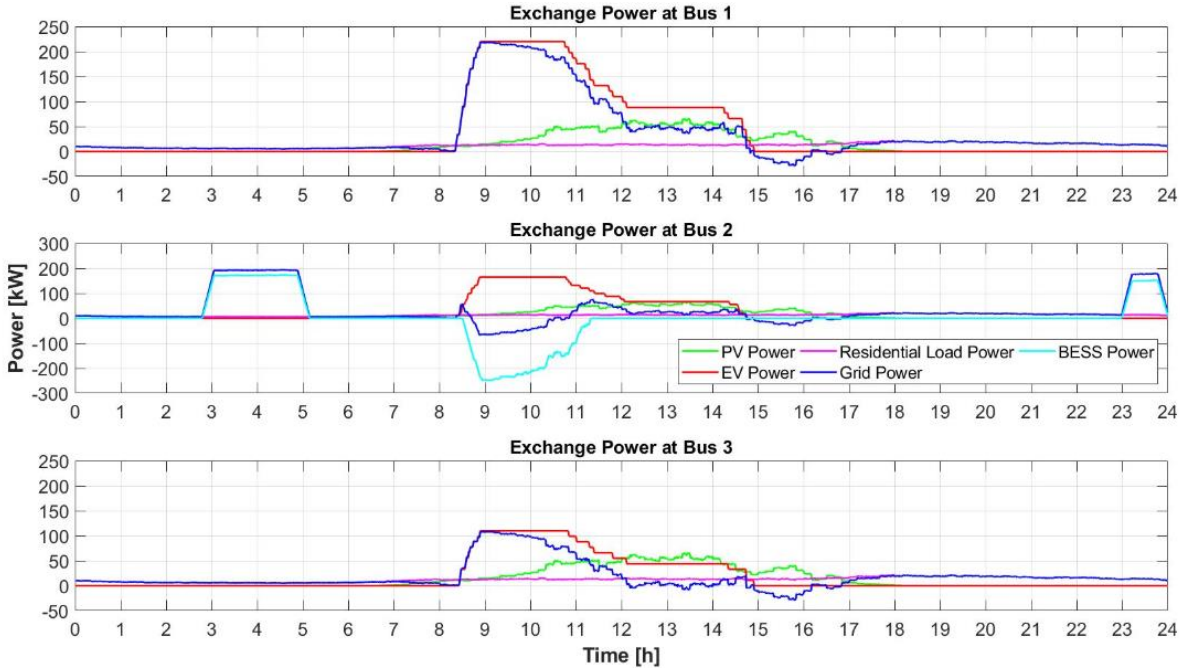

Figure B.2-C Power Exchange Profile of Each Bus for Case 2C-2 (20-15-10 EV, Autumn)

Appendix C: Case 3 (Decentralized BESS)

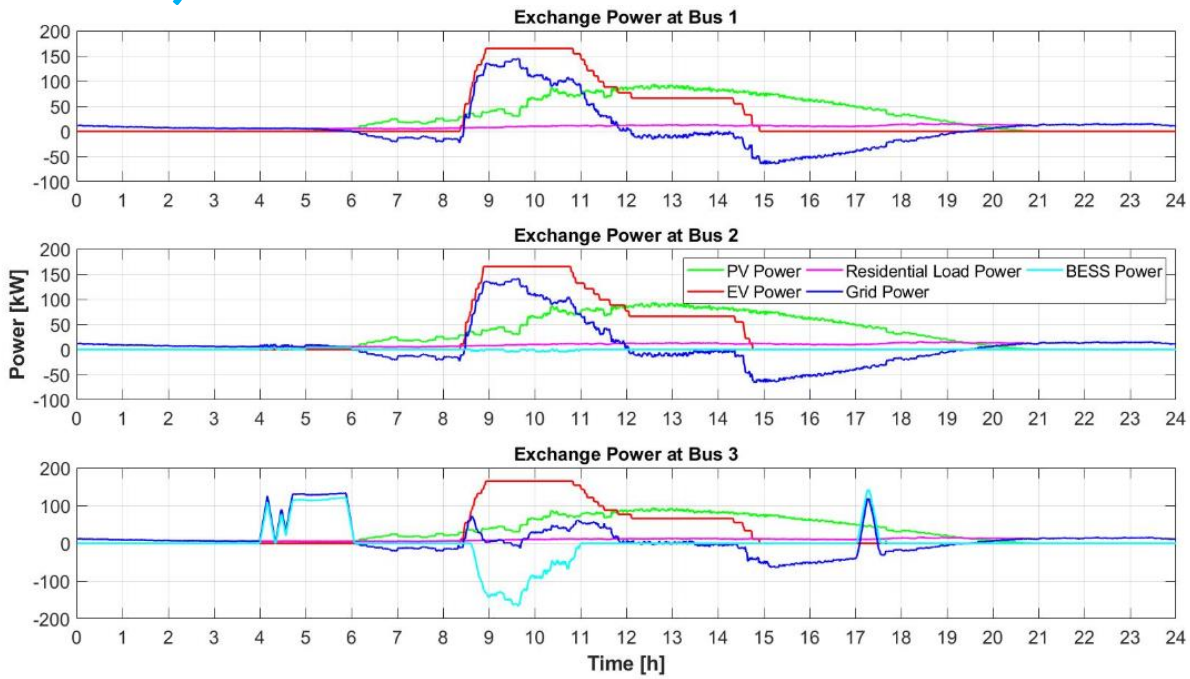

Figure C.1-A Power Exchange Profile of Each Bus for Case 3A (Decentralized, Summer)

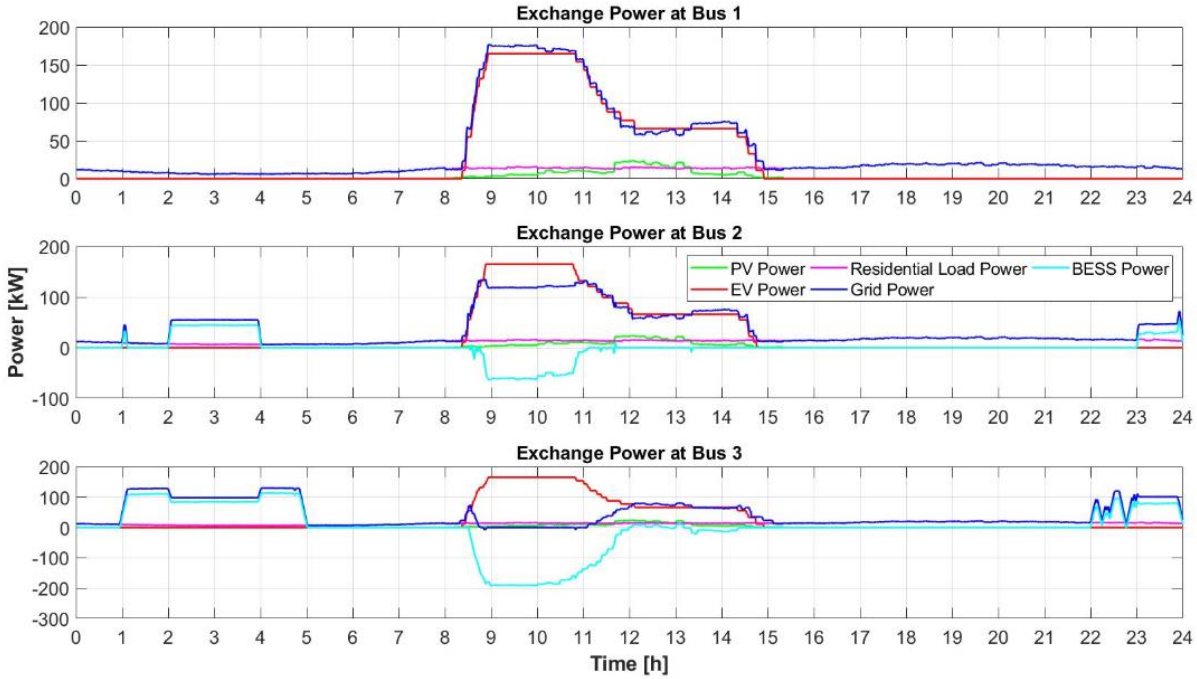

Figure C.1-B Power Exchange Profile of Each Bus for Case 3B (Decentralized, Winter)

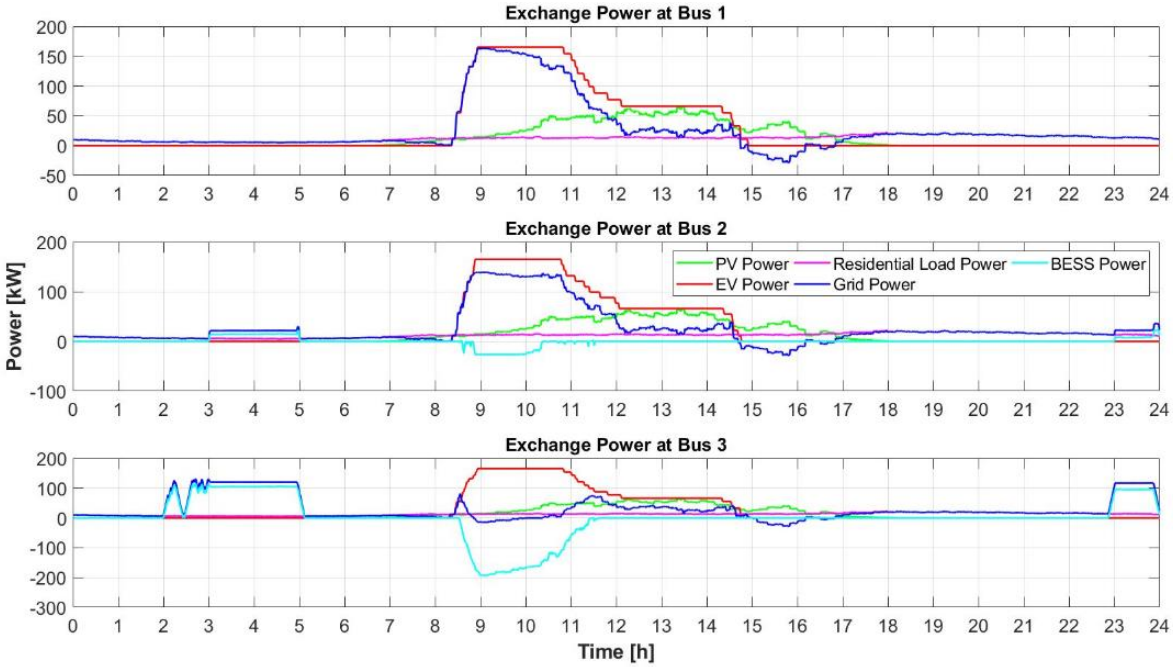

Figure C.1-C Power Exchange Profile of Each Bus for Case 3C (Decentralized, Autumn)

Appendix D: Case 4 (Different EV Charging Strategy)

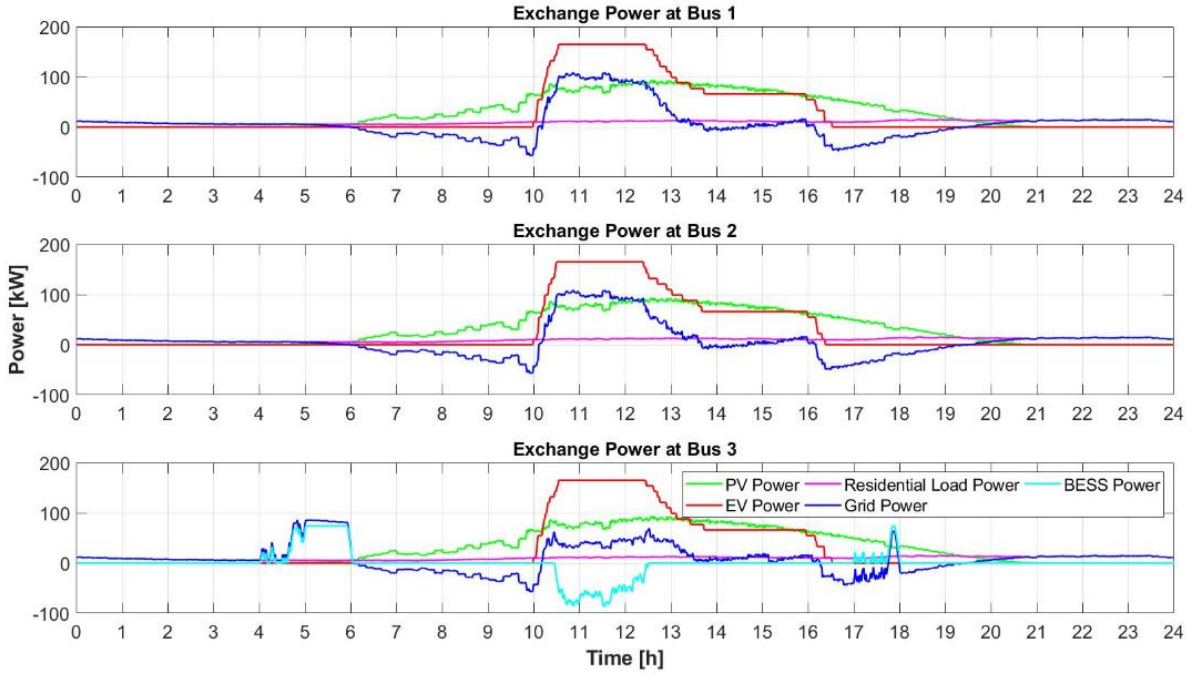

Figure D.1-A Power Exchange Profile of Each Bus for Case 4A-1 (EV Charging Period Shift, Summer)

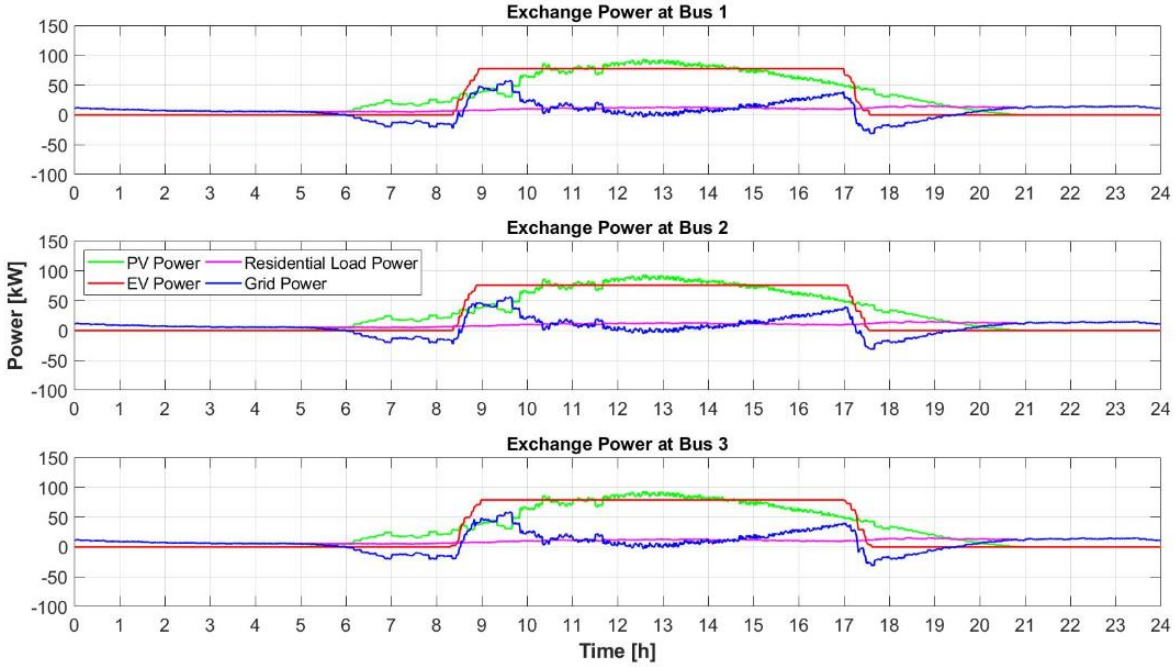

Figure D.2-A Power Exchange Profile of Each Bus for Case 4A-2 (Constant EV Charging, Summer)

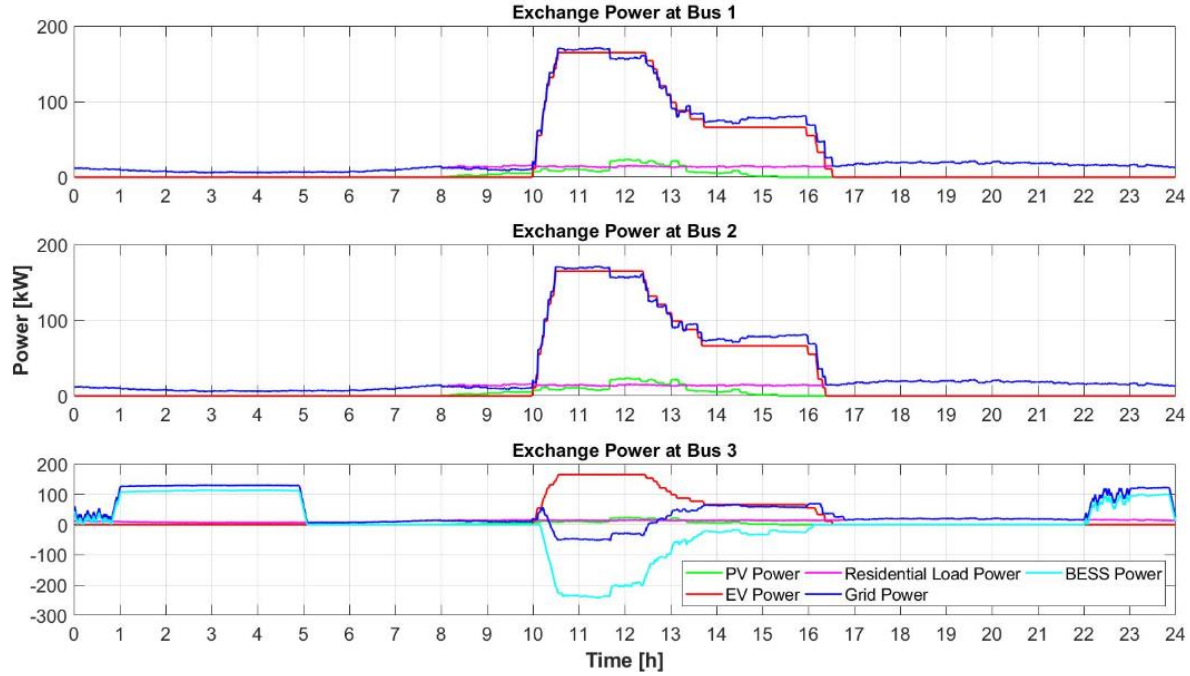

Figure D.1-B Power Exchange Profile of Each Bus for Case 4B-1 (EV Charging Period Shift, Winter)

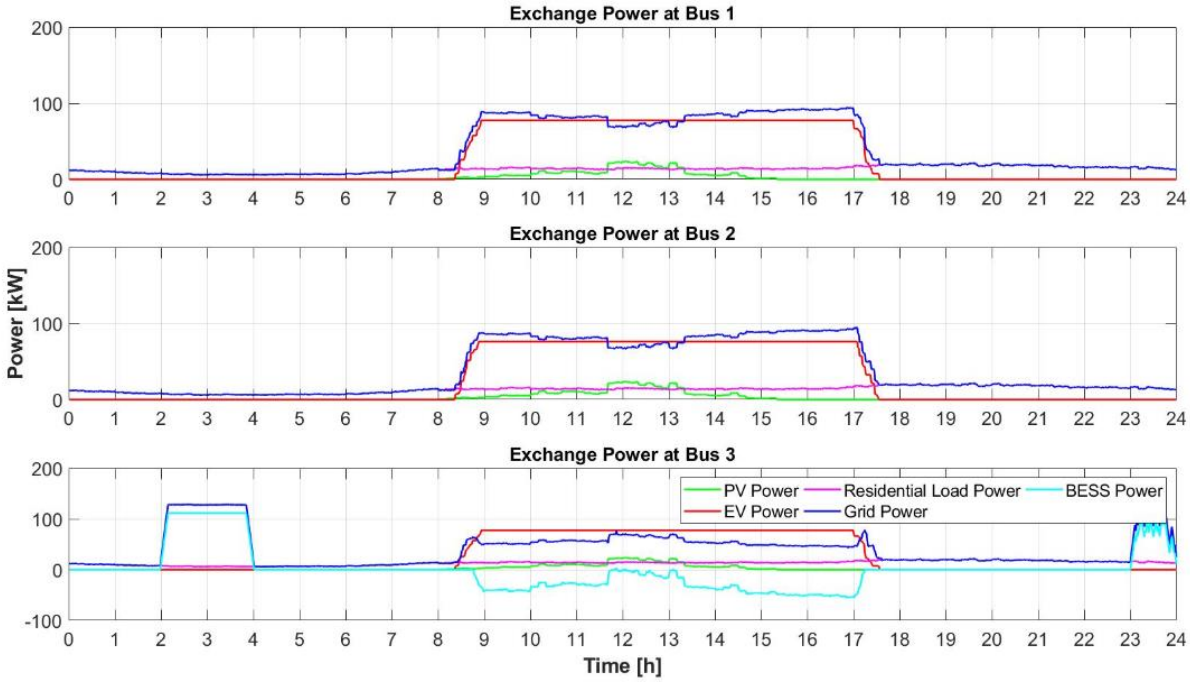

Figure D.2-B Power Exchange Profile of Each Bus for Case 4B-2 (Constant EV Charging, Winter)

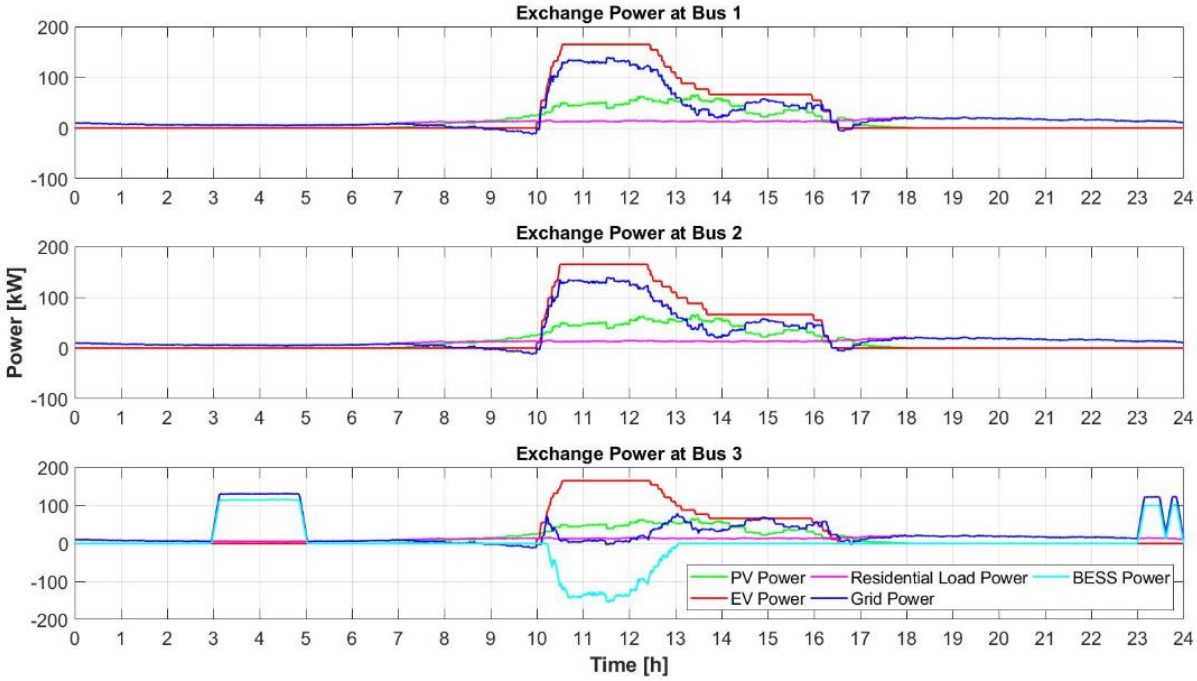

Figure D.1-C Power Exchange Profile of Each Bus for Case 4C-1 (EV Charging Period Shift, Autumn)

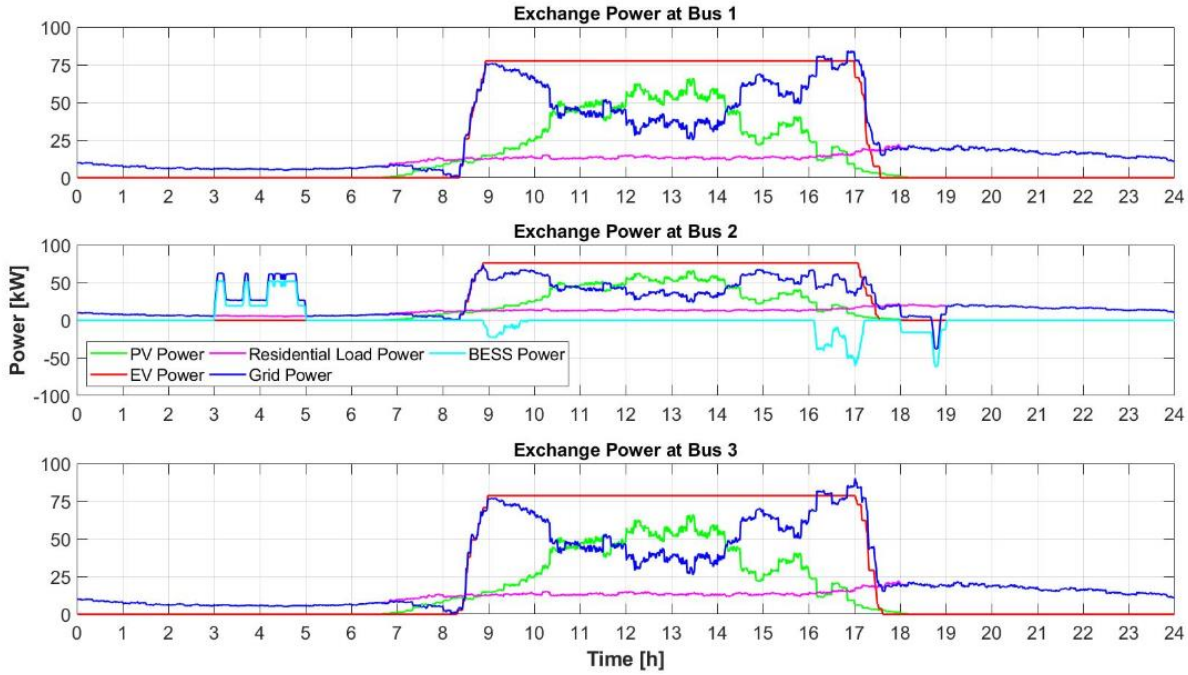

Figure D.2-C Power Exchange Profile of Each Bus for Case 4C-2 (Constant EV Charging, Autumn)

Appendix E: Technical Comparison

	Case Study	BESS Max Power (kW)	BESS Capacity (kWh)	BESS Position (Bus)	Maximum Transformer Power (kW)	
					Grid Only	Grid with BESS
Summer	no EV	-	-	-	46.398	46.398
	5 EV	-	-	-	111.154	111.154
	10 EV	47.116	95.346	3	304.563	246.536
	15 EV	171.765	346.174	3	542.208	303.833
	20 EV	346.373	928.583	3		346.343
	10-15-20 EV	318.253	648.264	2		220.568
	20-15-10 EV	190.256	391.472	2		282.543
	Decentralized	4.238	8.846	2		302.630
		167.504	338.629	3		
		171.742	347.475	(total)		
	15 EV Shift	87.525	176.147	3		266.872
	15 EV Constant	-	-	-		186.311
	15 EV Dynamic	-	-	-		274.733

	Case Study	BESS Max Power (kW)	BESS Capacity (kWh)	BESS Position (Bus)	Maximum Transformer Power (kW)	
					Grid Only	Grid with BESS
Winter	no EV	-	-	-	65.808	65.808
	5 EV	-	-	-	216.596	216.596
	10 EV	114.097	318.26	3	431.242	282.122
	15 EV	256.207	788.876	3	715.655	321.117
	20 EV	410.943	1765.432	3	1233.144	351.361
	10-15-20 EV	286.648	962.394	3		291.089
	20-15-10 EV	228.131	685.807	3		357.457
	Decentralized	63.497	147.632	2		321.176
		191.765	634.092	3		
		255.262	781.724	(total)		
	15 EV Shift	242.409	784.324	3		318.228
	15 EV Constant	111.692	347.132	3		251.513
	15 EV Dynamic	113.754	421.245	3		300.401

	Case Study	BESS Max Power (kW)	BESS Capacity (kWh)	BESS Position (Bus)	Maximum Transformer Power (kW)	
					Grid Only	Grid with BESS
Autumn	no EV	-	-	-	64.70	64.70
	5 EV	-	-	-	170.60	170.60
	10 EV	86.005	174.478	3	375.299	267.414
	15 EV	220.289	527.675	3	636.472	324.513
	20 EV	373.487	1104.847	3	1178.17	344.058
	10-15-20 EV	250.38	674.747	3		311.570
	20-15-10 EV	249.055	604.186	2		283.130
	Decentralized	26.424	56.471	2		312.306
		193.505	477.119	3		
		219.929	533.59	(total)		
	15 EV Shift	155.566	361.638	3		300.866
	15 EV Constant	61.13	124.684	2		227.700
	15 EV Dynamic	-	-	-		308.382

Appendix F: Cost Comparison

	Case Study	BESS Investment Cost		Electricity Cost (Euro)		Grid Reinforcement Cost (Euro)		Total Cost Per Day (Euro)	
		Initial Investment (Thousand Euros)	Per day Cost (Euro)	Grid Only	Grid with BESS	Grid Only	Grid with BESS	Grid Only	Grid with BESS
Summer	no EV	-		-209.851		-		-209.851	
	5 EV	-		-100.592		-		-100.592	
	10 EV	132.309	36.249	0.591	2.831	-		0.591	39.080
	15 EV	481.973	132.047	112.392	106.542	13.932	-	126.324	238.589
	20 EV	1031.855	282.700	290.309	279.100	50.322	-	340.631	561.800
	10-15-20 EV	894.802	245.151		102.479		-		347.630
	20-15-10 EV	535.947	146.835		101.194		-		248.029
	Decentralized	482.259	132.126		102.230		-		234.356
	15 EV Shift	245.530	67.269		95.481		-		162.750
	15 EV Constant	-			95.894		-		95.894
	15 EV Dynamic	-			81.490		-		81.490

	Case Study	BESS Investment Cost		Electricity Cost (Euro)		Grid Reinforcement Cost (Euro)		Electricity Cost (Euro)	
		Initial Investment (Thousand Euros)	Per day Cost (Euro)	Grid Only	Grid with BESS	Grid Only	Grid with BESS	Grid Only	Grid with BESS
Winter	no EV	-		140.847		-		140.847	
	5 EV	-		292.733		-		292.733	
	10 EV	343.117	94.005	455.863	434.313	3.061	-	458.924	528.318
	15 EV	789.772	216.376	649.576	576.173	30.926	-	680.502	792.549
	20 EV	1396.784	382.681	975.571	739.517	81.625	-	1057.197	1122.198
	10-15-20 EV	904.353	247.768		575.587		-		823.355
	20-15-10 EV	698.905	191.481		576.223		-		767.704
	Decentralized	785.756	215.276		575.605		-		790.881
	15 EV Shift	757.102	207.425		569.652		-		777.077
	15 EV Constant	345.135	94.558		581.317		-		675.875
	15 EV Dynamic	369.110	101.126		556.437		-		657.563

	Case Study	BESS Investment Cost		Electricity Cost (Euro)		Grid Reinforcement Cost (Euro)		Electricity Cost (Euro)	
		Initial Investment (Thousand Euros)	Per day Cost (Euro)	Grid Only	Grid with BESS	Grid Only	Grid with BESS	Grid Only	Grid with BESS
Autumn	**no EV**	-		-22.359		-		-22.359	
	5 EV	-		120.823		-		120.823	
	10 EV	241.628	66.199	268.011	260.903	-		268.011	327.102
	15 EV	639.895	175.314	434.174	395.045	23.168	-	457.342	570.359
	20 EV	1139.558	312.208	719.882	546.626	76.239	-	796.122	858.834
	10-15-20 EV	746.801	204.603		395.993		-		600.596
	20-15-10 EV	725.432	198.748		416.735		-		615.483
	Decentralized	640.611	175.510		392.492		-		568.002
	15 EV Shift	449.027	123.021		387.086		-		510.107
	15 EV Constant	171.917	47.100		388.588		-		435.688
	15 EV Dynamic	-			380.201		-		380.201

Bibliography

[1] United Nations Environment Programme, *Global Status Report 2017; Towards a zero-emission, efficient, and resilient buildings and construction sector*. 2017.

[2] D. J. Santini, “Electric Vehicle Waves of History: Lessons Learned about Market Deployment of Electric Vehicles,” *Electr. Veh. â€“ Benefits Barriers*, pp. 35–62, 2011.

[3] I. E. A. International and E. Agency, “Global EV Outlook 2018,” 2018.

[4] M. Messagie, F. S. Boureima, T. Coosemans, C. Macharis, and J. Van Mierlo, “A range-based vehicle life cycle assessment incorporating variability in the environmental assessment of different vehicle technologies and fuels,” *Energies*, vol. 7, no. 3, pp. 1467–1482, 2014.

[5] E. A. M. A. ACEA, “Overview of tax incentives for electric vehicles in the EU,” *ACEA - Eur. Automob. Manuf. Assoc.*, no. January, pp. 2016–2019, 2017.

[6] RVO, “Electric transport in the Netherlands,” p. 40, 2017.

[7] National Enterprise Agency, “Electric passenger cars and charging points in The Netherlands Analysis of 2017,” no. January, pp. 3–6, 2018.

[8] Solar Power Europe, “Global Market Outlook for Solar Power 2018-2022,” 2018.

[9] ENTSOE, “Installed Capacity per Production Type in the Netherlands,” 2018. [Online]. Available: https://transparency.entsoe.eu/generation. [Accessed: 19-Sep-2018].

[10] International Renewable Energy Agency (IRENA), *Electricity storage and renewables: Costs and markets to 2030*, no. October. 2017.

[11] P. Robson and D. Bonomi, “Growing The Battery Storage Market 2018: Exploring four key issues,” *Energy Storage World Forum*, no. January, 2018.

[12] J.-M. Durand, M. J. Duarte, and P. Clerens, “Joint EASE/EERA recommendations for a European Energy Storage Technology Development Roadmap Towards 2030,” *Int. Energy Storage Policy Regul. Work.*, p. 108, 2017.

[13] D. Xu, T., Wang, W., Gordin, M. L., Wang, D. and Choi, “Lithium-ion batteries for stationary energy storage,” *J. Miner. Met. Mater. Soc.*, vol. 62, pp. 24–30, 2010.

[14] J. Luo, X., Wang, J., Dooner, M. and Clarke, “Overview of current development in electrical energy storage technologies and the application potential in power system operation,” vol. 137, pp. 511–536, 2015.

[15] R. Díaz-González, F., Sumper, A., Gomis-Bellmunt, O. and Villafáfila-Robles, “A review of energy storage technologies for wind power applications,” vol. 16, pp. 2154–2171, 2012.

[16] US DOE/EPRI, *Electricity Storage Handbook in Collaboration with NRECA*. 2015.

[17] US DOE, “Global Energy Storage Database. United States Department of Energy.

Office of Electricity & Energy Reliability," 2017. [Online]. Available: http://www.energystorageexchange.org/projects.

[18] M. M. Thackeray, "Spinel Electrodes for Lithium Batteries', Journal of the American Ceramic Society," vol. 82, no. 12, pp. 3347–3354, 2004.

[19] K. Chen, C. H., Liu, J., Stoll, M. E., Henriksen, G., Vissers, D. R. and Amine, "Aluminum-doped lithium nickel cobalt oxide electrodes for high-power lithium-ion batteries," *J. Power Sources*, vol. 128, no. 2, pp. 278–285, 2004.

[20] V. L. Krause, L. J., Jensen, L. D. and Chevrier, "Measurement of Li-Ion Battery Electrolyte Stability by Electrochemical Calorimetry," *J. Electrochem. Soc.*, vol. 164, no. 4, pp. A889–A896, 2017.

[21] S. J. Stan, A.-I., Swierczynski, M., Stroe, D.-I., Teodorescu, R. and Andreasen, "Lithium ion battery chemistries from renewable energy storage to automotive and back-up power applications — An overview," pp. 713–720, 2014.

[22] J. Scrosati, B. and Garche, "Lithium batteries: status, prospects and future," *J. Power Sources*, vol. 195, no. 9, pp. 2419–2430, 2010.

[23] P. B. Soto, F. A., Ma, Y., Martinez de la Hoz, J. M., Seminario, J. M. and Balbuena, "Formation and Growth Mechanisms of Solid- Electrolyte Interphase Layers in Rechargeable Batteries," *Chem. Mater.*, vol. 27, no. 23, pp. 7990–8000, 2015.

[24] K. Chen, Z., Belharouak, I., Sun, Y.-K. and Amine, "Titanium-Based Anode Materials for Safe Lithium-Ion Batteries," *Adv. Funct. Mater.*, vol. 23, no. 8, pp. 959–969, 2013.

[25] ISEA, "Technology Overview on Electricity Storage. Overview on the potential and on the deployment perspectives of electricity storage technologies," 2012.

[26] G. Nitta, N., Wu, F., Lee, J. T. and Yushin, "Li-ion battery materials: present and future', Materials Today," vol. 18, pp. 252–264, 2015.

[27] H. C. Hesse, M. Schimpe, D. Kucevic, and A. Jossen, *Lithium-ion battery storage for the grid - A review of stationary battery storage system design tailored for applications in modern power grids*, vol. 10, no. 12. 2017.

[28] H. C. Truong, C.N.; Naumann, M.; Karl, R.C.; Müller, M.; Jossen, A.; Hesse, "Economics of Residential Photovoltaic Battery Systems in Germany: The Case of Teslas Powerwall," *Batteries*, vol. 2, no. 14, 2016.

[29] M. Mehrabankhomartash, M. Rayati, A. Sheikhi, and A. M. Ranjbar, "Practical battery size optimization of a PV system by considering individual customer damage function," *Renew. Sustain. Energy Rev.*, vol. 67, pp. 36–50, 2017.

[30] R. Tisseur, F. De Bosio, G. Chicco, M. Fantino, M. Pastorelli, and P. Di Torino, "Optimal Scheduling of Distributed Energy Storage Systems by Means of ACO Algorithm."

[31] D. Q. Hung and N. Mithulananthan, "Community Energy Storage and Capacitor

Allocation in Distribution Systems," *21st Australas. Univ. Power Eng. Conf. (AUPEC),* pp. 1–6, 2011.

[32] V. Kalkhambkar, R. Kumar, and R. Bhakar, "Optimal Sizing ofPV-Battery for Loss Reduction and (Nor)," *IEEE Int. Conf. Recent Adv. i*, vol. ICRAIE-201, 2014.

[33] T. Kerdphol, R. N. Tripathi, T. Hanamoto, Khairudin, Y. Qudaih, and Y. Mitani, "ANN based optimized battery energy storage system size and loss analysis for distributed energy storage location in PV-microgrid," *2015 IEEE Innov. Smart Grid Technol. - Asia (ISGT ASIA)*, pp. 1–6, 2015.

[34] Y. Zhang, A. Lundblad, P. E. Campana, F. Benavente, and J. Yan, "Battery sizing and rule-based operation of grid-connected photovoltaic-battery system: A case study in Sweden," *Energy Convers. Manag.*, 2017.

[35] Y. Zhang, P. E. Campana, A. Lundblad, and J. Yan, "Comparative study of hydrogen storage and battery storage in grid connected photovoltaic system: Storage sizing and rule-based operation," *Appl. Energy*, vol. 201, pp. 397–411, 2017.

[36] J. Zhuang, G. Shen, J. Yu, T. Xiang, and X. Wang, "Micro-grid energy storage location and sizing optimization method based on demand response," *Proc. - 2016 Int. Conf. Intell. Transp. Big Data Smart City, ICITBS 2016*, no. 4, pp. 517–520, 2017.

[37] B. J. Abdelhak, E. Najib, H. Abdelaziz, F. Hnaien, and F. Yalaoui, "Optimum sizing of hybrid PV/wind/battery using Fuzzy-Adaptive Genetic Algorithm in real and average battery service life," *2014 Int. Symp. Power Electron. Electr. Drives, Autom. Motion, SPEEDAM 2014*, pp. 871–876, 2014.

[38] K. Khalid Mehmood, S. U. Khan, S.-J. Lee, Z. M. Haider, M. K. Rafique, and C.-H. Kim, "Optimal sizing and allocation of battery energy storage systems with wind and solar power DGs in a distribution network for voltage regulation considering the lifespan of batteries," *IET Renew. Power Gener.*, vol. 11, no. 10, pp. 1305–1315, 2017.

[39] V. Kalkhambkar, R. Kumar, and R. Bhakar, "Joint optimal sizing and placement of renewable distributed generation and energy storage for energy loss minimization," *2017 4th Int. Conf. Adv. Comput. Commun. Syst.*, pp. 1–9, 2017.

[40] M. Gitizadeh and H. Fakharzadegan, "Battery capacity determination with respect to optimized energy dispatch schedule in grid-connected photovoltaic (PV) systems," *Energy*, vol. 65, pp. 665–674, 2014.

[41] F. Marra *et al.*, "EV charging facilities and their application in LV feeders with photovoltaics," *IEEE Trans. Smart Grid*, vol. 4, no. 3, pp. 1533–1540, 2013.

[42] P. Fortenbacher, A. Ulbig, and G. Andersson, "Optimal Placement and Sizing of Distributed Battery Storage in Low Voltage Grids Using Receding Horizon Control Strategies," *IEEE Trans. Power Syst.*, vol. 33, no. 3, pp. 2383–2394, 2018.

[43] J. Hill and C. Nwankpa, “Battery Energy Storage Dispatch Analysis within the Storage Placement Problem,” *2017 Ieee Int. Symp. Circuits Syst.*, pp. 2512–2515, 2017.

[44] P. Fortenbacher, M. Zellner, and G. Andersson, “Optimal Sizing and Placement of Distributed Storage in Low Voltage Networks,” 2015.

[45] A. K. Barnes, J. C. Balda, A. Escobar-Mejia, and S. O. Geurin, “Placement of energy storage coordinated with smart PV inverters,” *2012 IEEE PES Innov. Smart Grid Technol. ISGT 2012*, pp. 1–7, 2012.

[46] E. Grover-Silva, R. Girard, and G. Kariniotakis, “Optimal sizing and placement of distribution grid connected battery systems through an SOCP optimal power flow algorithm,” *Appl. Energy*, vol. 219, no. August, pp. 385–393, 2018.

[47] D. Karadimos, A. Karafoulidis, D. Doukas, P. Gkaidatzis, D. Labridis, and A. Marinopoulos, “Techno-Economic Analysis for Optimal Energy Storage Systems Placement Considering Stacked Grid Services,” 2017.

[48] H. Nazaripouya, Y. Wang, P. Chu, H. R. Pota, and R. Gadh, “Optimal sizing and placement of battery energy storage in distribution system based on solar size for voltage regulation,” *2015 IEEE Power Energy Soc. Gen. Meet.*, pp. 1–5, 2015.

[49] Z. Qing, N. Yu, Z. Xiaoping, Y. You, and D. Liu, “Optimal siting & sizing of battery energy storage system in active distribution network,” *2013 4th IEEE/PES Innov. Smart Grid Technol. Eur. ISGT Eur. 2013*, no. 2012, pp. 1–5, 2013.

[50] S. B. Karanki, D. Xu, B. Venkatesh, and B. N. Singh, “Optimal location of battery energy storage systems in power distribution network for integrating renewable energy sources,” *2013 IEEE Energy Convers. Congr. Expo.*, pp. 4553–4558, 2013.

[51] S. B. Karanki and D. Xu, “Optimal capacity and placement of battery energy storage systems for integrating renewable energy sources in distribution system,” *2016 Natl. Power Syst. Conf.*, pp. 1–6, 2016.

[52] T. Kerdphol, Y. Qudaih, and Y. Mitani, “Battery energy storage system size optimization in microgrid using particle swarm optimization,” *IEEE PES Innov. Smart Grid Technol. Eur.*, pp. 1–6, 2014.

[53] I. Biswas, V. Dash, and P. Bajpai, “Sizing optimization of PV-FC-Battery system with hybrid PSO-EO algorithm,” *2012 Annu. IEEE India Conf. INDICON 2012*, pp. 869–874, 2012.

[54] C. D. Rodriguez-Gallegos *et al.*, “Placement and Sizing Optimization for PV-Battery-Diesel Hybrid Systems,” *2016 Ieee Int. Conf. Sustain. Energy Technol.*, pp. 83–89, 2016.

[55] P. Belotti, C. Kirches, S. Leyffer, J. Linderoth, and J. Luedtke, “Mixed-Integer Nonlinear Optimization,” 2012.

[56] M. R. Bussieck and A. Pruessner, “Mixed-Integer Nonlinear Programming,” vol.

20007, no. 1, pp. 1–7, 2003.

[57] M. Hunting, “The AIMMS Outer Approximation Algorithm for MINLP,” *Paragon Decis. Technol*, no. November, pp. 1–9, 2011.

[58] X. Li, A. Sundaramoorthy, and P. I. Barton, “Nonconvex generalized benders decomposition,” *Optim. Sci. Eng. Honor 60th Birthd. Panos M. Pardalos*, vol. 9781493908, pp. 307–331, 2014.

[59] V. Eronen, “On extended cutting plane and algorithms α ECP,” pp. 1–45, 2013.

[60] I. E. Grossmann, J. Viswanathan, A. Vecchietti, R. Raman, and E. Kalvelagen, “GAMS/DICOPT: A discrete continuous optimization package,” *Math. Methods Appl. Sci*, vol. 11, pp. 649–664, 2001.

[61] S. Papathanassiou, H. Nikos, and S. Kai, “A benchmark low voltage microgrid network,” *Proc. CIGRE Symp. power Syst. with dispersed Gener.*, no. April, pp. 1–8, 2005.

[62] N. DiOrio, A. Dobos, and S. Janzou, “Economic Analysis Case Studies of Battery Energy Storage with SAM,” *Natl. Renew. Energy Lab. Denver, CO, USA*, no. November, 2015.

[63] D. W. van der Meer, “Advancing sustainable transportation by charging EVs with PV power at the workplace,” 2016.

[64] RVO, Netherlands Enterprise Agency, “Statistics Electric Vehicles in the Netherlands,” no. May, pp. 2–5, 2018.

[65] J. C. Spoelstra, “Charging behaviour of Dutch EV drivers,” 2014.

[66] K. Jager, O. Isabella, A. H. M. Smets, R. A. C. M. M. van Swaaij, and M. Zeman, “Solar Energy Fundamentals, Technology and Systems,” *Delf Univ. Technol.*, pp. 1–420, 2014.

[67] B. Asare-Bediako, W. L. Kling, and P. F. Ribeiro, “Future residential load profiles: Scenario-based analysis of high penetration of heavy loads and distributed generation,” *Energy Build.*, vol. 75, pp. 228–238, 2014.

[68] ENTSOE, “Day-ahead Prices,” 2018. [Online]. Available: https://transparency.entsoe.eu/transmission-domain/r2/dayAheadPrices. [Accessed: 10-Aug-2018].

[69] Isabelle Vlasman, “Developing smart charging strategies for large-scale integration of photovoltaics and electric vehicles,” 2017.

[70] Eurelectric, *Application guide to the european standard en 50160 on voltage characteristics of electricity supplied by public distribution systems*. 1995.